UNIVERSITEIT VAN PRETORIA
UNIVERSITY OF PRETORIA
YUNIBESITHI YA PRETORIA

Profiling of rough terrain

by

Carl Martin Becker

Submitted in partial fulfilment of the requirements of the degree

Master of Engineering

in the

Department of Mechanical and Aeronautical Engineering
Faculty of Engineering, Built Environment and Information Technology

University of Pretoria
Pretoria

October 2008

UNIVERSITEIT VAN PRETORIA
UNIVERSITY OF PRETORIA
YUNIBESITHI YA PRETORIA

Profiling of rough terrain

Candidate: Carl Martin Becker

Supervisor: Prof. P.S. Els

Department: Mechanical and Aeronautical Engineering

Degree: Master of Engineering

Abstract

In the automotive industry one of the methods used in accelerating the design, testing and development of a system or a vehicle is the use of virtual vehicle simulations. The simulations cut costs in the form of fewer prototypes required for actual testing and accelerated fault finding in the design of a system.

The simulation results are very dependent on the model used for the simulation and the inputs to the system. Feasible results can often be obtained with a simplified model if the correct input data is supplied to the simulation.

In South Africa, the commercial, military and off-road vehicle industries mainly use the test tracks at the Gerotek Test Facilities for ride comfort and durability tests over repeatable terrains. Terrain profiles of these tracks are not available and cannot be measured using commercially available inertial profilometers due to the severe roughness of the terrain.

This study concentrates on obtaining the input data in the form of the terrain profile used for vehicle simulations and field tests in which a vehicle is driving on rough terrains. The input data is referred to as the profile of the terrain and the profiled terrains are the actual terrains used for testing.

Three different methods are used in measuring the profile of the terrain namely a mechanical profilometer, photogrammetry and a 3-D scanner using a laser displacement sensor. These methods are evaluated by profiling the same section of the Belgian paving and calculating the Displacement Spectral Densities. The most efficient method is used to profile additional terrains.

The terrain profiles thus obtained is used as input to an existing off-road vehicle simulation model built in MSC Adams View. This model has previously been verified over discrete obstacles where excellent correlation with experimental results was obtained. Comparison between simulated and measured results over the terrains profiled in this study also gives good correlation, establishing further confidence in the measured terrain profiles.

Keywords: road profiling, rough roads, displacement spectral densities, profilometer, vehicle simulations

UNIVERSITEIT VAN PRETORIA
UNIVERSITY OF PRETORIA
YUNIBESITHI YA PRETORIA

Profiel opmeting van rowwe terrein

Kandidaat: Carl Martin Becker

Studieleier: Prof. P.S. Els

Departement: Meganiese en Lugvaartkundige Ingenieurswese

Graad: Magister in Ingenieurswese

Opsomming

In die voertuigindustrie is voertuigsimulasies, een van die metodes wat gebruik word om die ontwerp, toets en ontwikkeling van ‘n stelsel of ‘n voertuig te versnel. Die simulasies is meer koste-effektief om dat minder prototipes benodig word vir die werklike toets van die stelsel of voertuig en ontwerpsdefekte vinniger opgespoor kan word.

Die simulasieresultate is afhanklik van die model wat gebruik word asook die insette na die model. Bruikbare resultate kan dikwels verkry word met ‘n vereenvoudigde model, indien die korrekte insetdata aan die simulasie verskaf word. Aan die ander kant kan komplekse modelle, met foutiewe insetdata, nooit goeie antwoorde lewer nie.

In Suid-Afrika, word die Gerotek toetsfasiliteit se toetsbane deur die kommersiële, militêre en die 4x4 voertuigindustrie gebruik vir hoofsaakllik ritgemak- en leeftydstoetse oor herhaalbare terrein. Terreinprofiele van die toetsbane is nie beskikbaar nie en kan nie gemeet word met die beskikbare kommersiële traagheidsprofilometers nie, as gevolg van die hoë rofheid van die bane.

Die studie konsentreer op die verkryging van insetdata, in die vorm van die terreinprofiel wat gebruik word vir voertuigsimulasies en terreintoetse waar ‘n voertuig op rowwe terrein bestuur word. Die insetdata word na verwys as die terreinprofiel, waar die saamgestelde profiel van die terrein die werklike toetsterrein weerspieël.

Drie verskillende metodes word gebruik om die profiel van die terrein te meet naamlik, ’n meganiese profilometer, fotogrammetrie en ‘n 3-D laser aftaster. Die metodes word geëvalueer deur die profiel van dieselfde seksie van die Belgiese plaveisel te bepaal en die verplasingspektraaldigtheid te bereken. Die mees doeltreffende metode word gebruik om saamgestelde profiele van addisionele terreine op te stel.

Die terreinprofiele wat verkry is word gebruik as ‘n inset tot ’n bestaande simulasiemodel van ’n vierwielaangedrewe veldry (heg-en-steg) voertuig, in MSC Adams View. Die model is voorheen gevalideer oor diskrete hindernisse, waar uitstekende ooreenstemming met eksperimentele resultate verkry is. ‘n Vergelyking tussen gesimuleerde en gemete resultate oor die saamgestelde profiel terrein, in die studie, lewer ook bevredigende resultate wat verdere vertroue vestig in die meting van die terreinprofiele.

Sleutelwoorde: Padprofiele, rowwe terrein, profilometer, voertuig simulasies, verplasingspektraaldigtheid

Acknowledgements

- To God for all that He enables us to achieve
- My family and friends for their continued support
- Professor P.S Els for his exceptional guidance and for believing in me
- Barend Swart and Harold Fry from CAD Mapping cc
- Pro Mapping cc
- Everyone who lent a helping hand.

Contents

List of Figures

List of Tables

List of symbols

• English letters and symbols

A = Roughness coefficient

C = Unit vector in the XY plane of measured length l

C = Capacitance [Farad]

c = Damper rate

d = Diameter [m]

d = Distance along road [m]

F = Frequency variable

f = Frequency [Hz]

f_c = Cut-off frequency [Hz]

g = Gravitational acceleration [9.81 m/s^2]

H = Height [m]

k_s = Spring rate

k_t = Tyre spring rate

L = Length [m]

m_s = sprung mass

m_u = unsprung mass

n = Number of points in the profile

n = Road index

R = Resistance [ohm]

R_{xx} = Autocorrelation function

r = Radius [m]

S_{xx} = Power spectral density

S_z = Vertical displacement spectral density

T = End time

t = Time [seconds]

v = Velocity [m/s]

X = Fourier transform

x = Road height [mm]

x = X component of measured length L [m]

X,Y = Measured point

y = Error in the vertical direction of the profile

y = Y component of measured length L [m]

z = Vertical resolution [mm]

- **Greek symbols**

α = Angle [Degrees]

β = Angle [Degrees]

γ = Angle [Degrees]

Δ = Difference

δ = Change in distance [m]

φ = Spatial frequency [cycles/m]

θ = Angle [Degrees]

ϑ = Angle [Degrees]

τ = Change in time [seconds]

τ = Time constant of RC filter [seconds]

ω = Angular frequency [rad/s]

• Abbreviations

3-D	Three – Dimensional
$4S_4$	4 State Semi-Active Suspension System
ADAMS	Automatic Dynamic Analysis of Mechanical Systems (Computer Software)
APL	Longitudinal Profile Analyzer, APL in French
ASTM	American Society for Testing and Materials
CCD	Charged-Coupled Device
CSIR	Council for Scientific and Industrial Research
DGPS	Differential Global Positioning System
DSD	Displacement Spectral Density
FFT	Fast Fourier Transform
FM	Frequency Modulation
GIS	Geographic Information System
GPS	Global Positioning System
HSP	High Speed Profilometer

INS	Inertial Navigation System
IMU	Inertial Measuring Unit
IRI	International Roughness Index
ISO	International Organization for Standardization
IVP	Integrated Vision Products
LF	Left Front
LR	Left Rear
MIT	Massachusetts Institute of Technology
mW	milliWatt
PGC	Photo Ground Control
PSD	Power Spectral Density
RDF	Road Definition File
RF	Right Front
RMS	Root Mean Square
RMSE	Root Mean Square Error
RR	Right Rear
RTK	Real Time Kinematic
RQI	Road Quality Index
SCEOS	Sheffield Centre for Earth Observation Science
TIN	Triangle Network
TINA	Tina Is No Acronym
UMTRI	University of Michigan Transportation Research Institute
UTK	University of Tennessee, Knoxville
UV	Ultraviolet
VTMS	Vehicle Terrain Measurement System

1. Introduction

In the fast evolving world we live in, time and money are two very important factors in the development of any system and more advanced technologies need to be developed in less time. Thus methods, which enable us to accomplish these new goals more rapidly, are essential.

In the automotive industry one of the methods used in accelerating the design, testing and development of systems and vehicles is the use of virtual vehicle simulations. Time is used more effectively when the simulations are run after hours and saves actual testing time. The simulations cut costs in the form of fewer prototypes required for actual testing and accelerated fault finding in the design of a system.

Simulation results are very dependent on the model used for the simulation as well as the inputs to the system. Viable results are often obtainable with a simplified model if the correct simplifications and assumptions are made together with accurate input data supplied to the simulation. This study concentrates on obtaining the input data, in the form of the terrain profile, used for vehicle simulations in which a vehicle is driving on rough terrains.

Thoresson (2003) developed and validated a mathematical model of the Land Rover Defender 110 used by the University of Pretoria as their test vehicle. The development of the 4 State Semi-Active Suspension System ($4S_4$) was done by Els (2006) at the University of Pretoria and was implemented on the same Land Rover Defender 110. Rollover tests and simulations have been completed by Uys (2007) with the mathematical model developed by Thoresson with the addition of the $4S_s$ suspension characteristics. Ride comfort simulations over the Belgian paving at the Gerotek Test Facilities completed by Thoresson did not correlate with the actual field tests, while correlation for the other obstacles were excellent. The conclusion was made that the Belgian paving data used in the simulations was imprecise and lead to the necessity of accurate profile information of the actual off-road terrains used in simulations and field tests.

The question of why measure actual roads when one can just generate a random road with the same Road Quality Index (RQI) or road roughness from the International Road Index (IRI) may be asked. The main reason why actual road information was required for this study remains for simulation verification and correlation with actual field tests. Each random road generated for a simulation differs and one was not able to execute and compare field tests on the same road. Off-road terrains are often not random and very little data on off-road terrains are available.

The main objective of this study is to obtain accurate profiles of actual off-road terrains used for vehicle testing at the Gerotek Test Facilities west of Pretoria, South Africa (Gerotek Test Facilities, 2007). The severe roughness of these terrains prevents the use of existing profilometers available in South Africa.

The terrains are cast in concrete, kept in good condition and are only used for testing and not driven on continuously. These terrains are used as the benchmark for testing by many commercial, military and off-road vehicle developers. From these profiles realistic three dimensional (3-D) models are generated. The 3-D models are then used in virtual vehicle simulations. This is done in order to correlate the response of the vehicle in virtual simulations with real life tests.

Three different methods are considered in measuring the profile of the terrain. The first method is a mechanical measuring device nick named the Can-Can Machine, the second method utilizes Photogrammetry and the third method is a laser which scans a section of the terrain at a time. These methods are evaluated by profiling the same section of the Belgian paving at the Gerotek Test Facility (Gerotek Test Facilities, 2007) and calculating the Displacement Spectral Densities. The most efficient method is used to profile more terrains used for actual testing and in turn used in simulations. Simulations assist in the development and improvement of vehicle suspension systems and set-ups. The results from the simulations are correlated with actual tests done on the same terrain using a previously validated MSC.ADAMS/VIEW model of a Land Rover Defender 110, Thoresson (2003) and Els (2006).

A brief literature overview concerning on-road and off-road profilometers used in the past and present, together with statistics and profile characterisation methods are presented in paragraph 2. The development, working principals, testing and calibration of suitable equipment of three different profilometers are discussed in paragraph 3. In paragraph 4 simple obstacles are profiled and evaluated. The profiling of 3-dimensional rough roads are presented, discussed and characterized in paragraph 5. In paragraph 6 off-road simulations and results are presented and discussed. Conclusions drawn from the study together with recommendations for future work are presented in the final paragraph.

2. Literature survey

Realistic terrain representation is the key to successful physics-based simulations of all-terrain, all-season vehicle performance, (Shoop et.al., 2004). The use of 3-D tyre models in simulations are increasing and thus 3-D road profiles are required. In 3-D simulations the road is sometimes modelled as separate left and right surfaces to reduce the number of elements in contact with the tyre, as it reduces the solver duration.

Imine et.al (2003) describes a profilometer as an instrument used to produce a series of numbers related in a well-defined way to a true profile. Gorsich et.al. (2003) states that road profilometers typically has errors caused by gyro errors and errors caused by ultrasonic devices. Low frequency trends in the data were often removed using a high pass filter. Other errors were caused by the dynamics of the vehicle carrying the profilometer and the road profilometer itself. Some road profilometers only take a one-dimensional trace (or two traces) of the three-dimensional surface of the road. This removes all the lateral variation in the data, and assumes every time a vehicle drives along the road or terrain, it drives along exactly the same path. On a typical test course, different paths mean different road profiles and possibly much different reliability and durability results. The fact that different paths mean different road profiles embraces the requirement for accurate full 3-D terrain profiles for valid simulation results.

In the above references, no indication was provided to which profilometer had been used in obtaining data on roads. Concrete and asphalt roads are also referred to as smooth or normal roads due to the fact that these roads are extensively smoother than the off-road terrains which need to be profiled for the current study.

2.1. Road profilometers

The following paragraphs describe different profilometers and profiling methods employed in recording the profiles of concrete or asphalt roads.

2.1.1. High Speed Profilometers (HSP)

The Council for Scientific and Industrial Research (CSIR) is one of the largest research, technology and innovation institutions in Africa. In profiling a road the CSIR utilizes a High Speed Profilometer (HSP), as seen in Figure 1 (Anon, 2005).

The HSP can collect accurate information relating to the longitudinal and transverse variations of a road surface relatively quickly. The HSP measures:

- Longitudinal profiles in both wheel tracks at 250 mm intervals;
- Transverse profiles spanning both wheel tracks (lane occupied by vehicle) at regular intervals down to 1,5 m;
- Geographic coordinates by means of GPS accurately to within one metre;
- Longitudinal gradients.

The HSP is a sophisticated instrument using modern laser and optical technology and it can test at speeds up to 120 km/h.

Figure 1: The HSP of the CSIR (Anon, 2005).

The same type of equipment used by the CSIR is used in the United States of America, which also just profiles the wheel tracks of the vehicle used to transport the profilometer. An assessment of profilometer performance for construction quality control was done by the University of Michigan Transportation Research Institute (UMTRI), (Karamihas and Gillespie, 2002). The assessment was performed on four sites: (1) moderately rough asphalt of typical surface texture, (2) new longitudinally tined concrete, (3) moderately rough broom-finished concrete and (4) new transversely tined concrete. Four broad classes of profilometers participated in the assessment. They were as follows: Static, Walking-speed, Lightweight Inertial and High-speed Inertial Profilometers.

The Walking-speed and Lightweight Inertial Profilometers fundamentally work on the same principals as the High-speed Inertial Profilometers. The Inertial Profilometer will be discussed in paragraph 2.1.2.

Figure 2 and Figure 3 show the difference between the longitudinally tined concrete and the transversely tined concrete respectively. It is clear that these surfaces are considered rough when one's hand is brushed over it. The intension of the present study is to profile off-road terrains, where the range of the vertical displacement on the road can vary from 10 mm up to 150 mm.

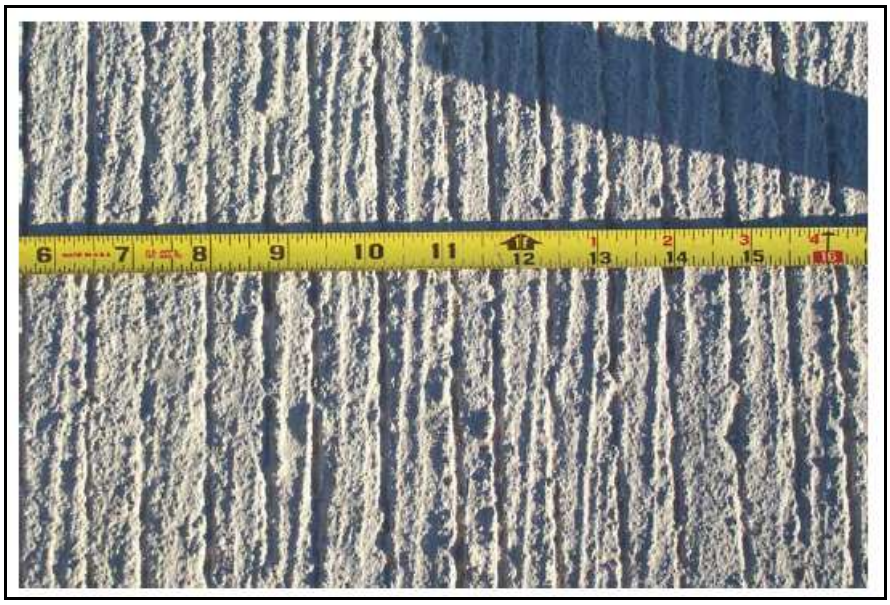

Figure 2: Longitudinally tined concrete, direction of travel from bottom to top (Karamihas and Gillespie, 2002).

Figure 3: Transversely tined concrete, direction of travel from left to right (Karamihas and Gillespie, 2002).

2.1.2. Inertial Profilometer

General Motors Research Laboratories made a breakthrough in the 1960's when they developed the Inertial Profilometer. This made high-speed profiling possible for monitoring large road networks (Spangler, 1964).

According to Spangler (1964) an Inertial Profilometer utilizes an accelerometer which measures the vertical response of the vehicle travelling on the road. The profilometer was capable of measuring and recording road surface profiles at speeds ranging from 16 to 112 km/h. The vertical body motion (Inertial reference) was obtained by the double integration of the response measured by the accelerometer.

The relative displacement between the pavement surface and the vehicle body was measured with a non-contact light (laser) or acoustic measuring system (Infrared or ultrasonic sensor) and was mounted on the vehicle body together with the accelerometer. Figure 4 shows a schematic drawing by Imine and Delanne (2005) of an Inertial Profilometer.

The pavement elevation profile was obtained by subtracting the output from the height sensor from the absolute motion of the vehicle body (Kulakoski et.al., 1986).

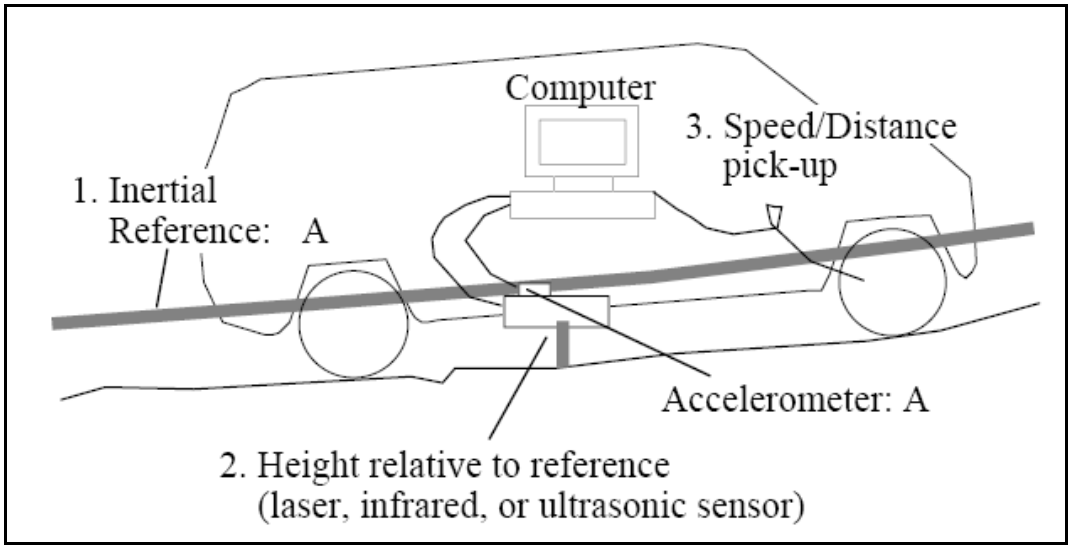

Figure 4: Schematic drawing of an Inertial Profilometer by Imine and Delanne (2005).

Imine and Delanne (2005) removed the noise in the acceleration signal by filtering the signal with a low-pass filter. A high-pass filter was then used to eliminate the low-frequency component and constant generated by the integration of the acceleration signal.

As stated previously the Lightweight Profilometer and the Walking Profilometer were variations on the High Speed Profilometers but they were essentially based on the principals of the High Speed Profilometer. Karamihas and Gillespie (2002) indicated that Lightweight Inertial Profilometer and High Speed Inertial Profilometer measurements were supposed to have the same meaning. This was very important for several reasons: (1) High Speed Profilometers were often used to audit measurements made by Lightweight Profilometers for smoothness specifications, (2) High Speed Profilometers may be used for measurements of smoothness of pavements that were under warranty, and (3) studies of roughness progression from cradle to grave often rely on measurements by both types of Inertial Profilometer. Examples of these profilometers can be seen in Figure 5 and Figure 6 respectively.

Figure 5: International Cybernetics Corporation Lightweight Profilometer, profiling moderately rough asphalt (Karamihas and Gillespie, 2002).

Figure 6: Walking Profilometer (Karamihas and Gillespie, 2002).

2.1.3. Longitudinal Profile Analyser

The Longitudinal Profile Analyser (Figure 7), also known in French as APL has been developed by The Roads and Bridges Central Laboratory (Imine and Delanne, 2005). The system includes one or two signal-wheel trailers towed by a car at a constant speed. A data acquisitioning system was utilised to record the data. An oscillating beam holding the measuring wheel was supported by a chassis and a suspension and damping system ensures that the wheel was in permanent contact with the pavement.

Vertical movement of the wheel results in angular travel of the beam, measured with respect to the horizontal arm of an inertial pendulum, independently of movements of the towing vehicle.

An angular displacement measurement was made with the use of an angular displacement transducer associated with the pendulum. The electrical signal was amplified and recorded by the data acquisitioning system. Rolling surface undulations in a range of 100 mm were recorded, for wavelengths in ranges from 0.5 to 20 m or 1 to 50 m, depending on the speed at which the chassis was towed.

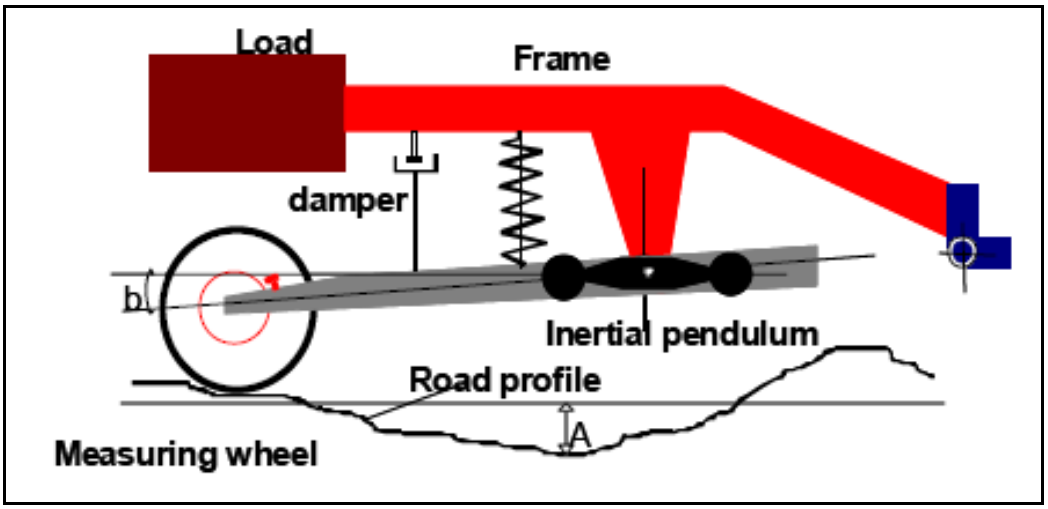

Figure 7: Longitudinal Profilometer Analyser (Imine and Delanne, 2005).

Imine and Delanne (2005) proved that the Longitudinal Profilometer Analyser gave a very precise measurement of the profile elevation. Rough measurements had to be processed to get a good estimate of the road profile.

2.2. Off-road Profilometers

The following methods were used in obtaining profiles for off-road terrains which were sometimes referred to as rough roads. These methods may also be used on normal/smooth roads.

2.2.1. Rod and Level

The rod and level are familiar surveying tools. This method is called “static” because the instruments are stationary when the elevation measures are taken (Sayers and Karamihas, 1998).

The elevation reference is provided by the level, the readings from the rod provide the height relative to the reference and a tape measure locates the individual elevation measurements. The method is shown in Figure 8.

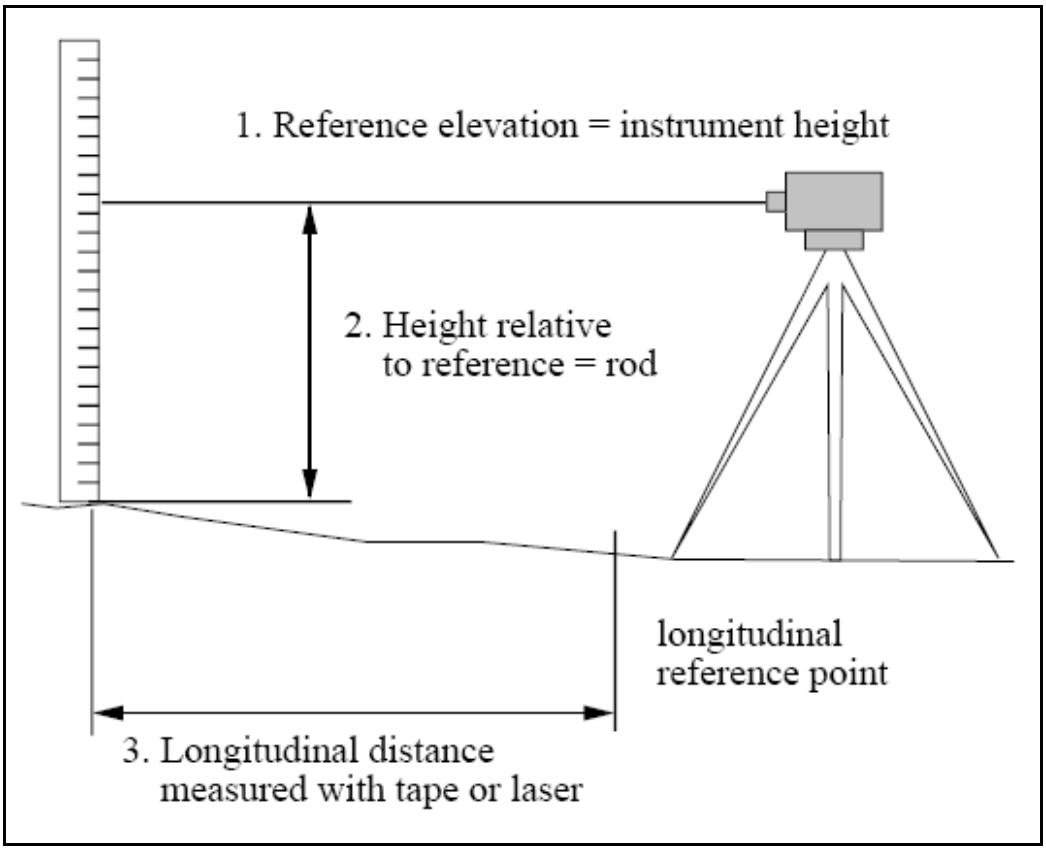

Figure 8: Visual representation of the Rod and Level Profilometer (Sayers and Karamihas, 1998).

This method is generally used for laying out a road. The requirements for obtaining a profile measure that is valid for computing roughness differ in that the elevation measurements need to be taken at close intervals of 250 mm or less (Sayers and Karamihas, 1998). This can be a very time consuming exercise and are much more stringent than necessary for normal surveying. The ASTM Standard E1364 provides guidelines for measuring profiles with a static method (ASTM E1364 – 95, 2005).

2.2.2. The Dipstick

In the Little Book of Profiling (Sayers and Karamihas, 1998), the Dipstick, see Figure 9, is described as a device developed and patented by the Face Company. The device is faster than the rod and level method in measuring profiles of roads suited for roughness analysis. It includes a battery-powered computer which automatically records data and performs the arithmetic needed to produce a profile.

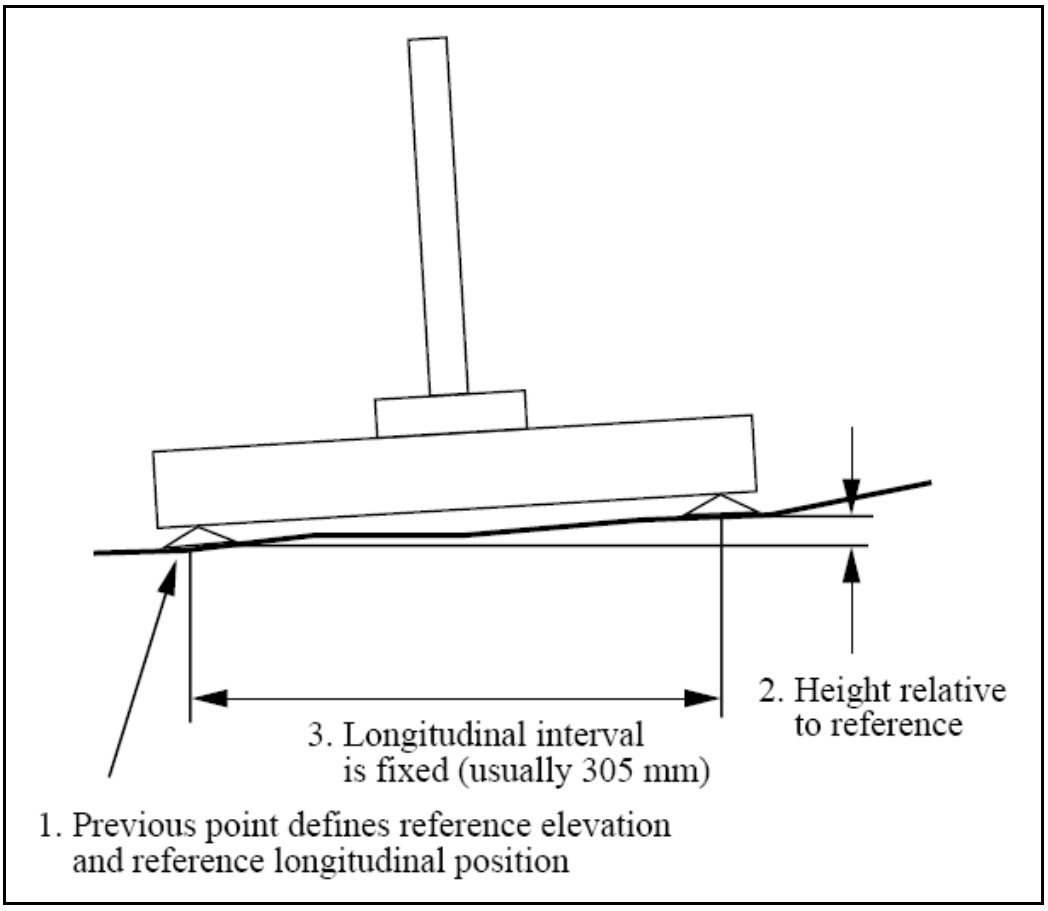

Figure 9: A basic representation of the Dipstick (Sayers and Karamihas, 1998).

The device is “walked” along the line being profiled. It contains a precision inclinometer that measured the difference in height between supports. The base on which these supports were mounted were normally spaced 305 mm apart. A line along the ground was profiled as follows: lean the device forward so that all of its weight is on the leading foot, raising the rear foot slightly off the ground. Pivot the device 180˚ about the leading foot, locating the other foot (formerly behind the leading foot) in front, along the line being profiled. The sensor was constantly monitored by the computer. When the computer senses that the instrument has stabilized, it automatically records the change in elevation and beeps; this signals that the next step may be taken.

The reference elevation in this design was the value calculated for the previous point. The height relative to the reference was deducted by the angle of the device relative to gravity, together with the spacing between its supports. The longitudinal distance of the profile was calculated by multiplying the number of measures made with the known spacing of the supports.

The profiles obtained with the Dipstick and the profiles obtained with the Rod and Level typically correspond to one another if the value of the first elevation (the initial reference) was set to match the elevation used in the Rod and Level profile.

2.2.3. Vehicle Terrain Measurement System

The Vehicle Terrain Measurement System (VTMS), (Kern, 2007), consists of four major components: a scanning laser, an inertial navigation system, a data acquisition system and a power management system. The use of these components allows this system to record the measured profile and to place the profile in global coordinates. These components are mounted on the rear of the host vehicle as shown in Figure 10. The VTMS is capable of measuring profiles both on-road and off-road.

The scanning laser is mounted 2 m above the profiled terrain and scans the terrain surface over a width of 4 m. The spacing between sequential points in the grid is approximately 5 mm, however the spacing is not uniform. This is due to the scanning laser operating by directing a laser beam at a rotating prism. The rotation of the prism causes the reflection of the laser beam to the terrain to be in equally spaced angles across the width of the scan. This causes the spacing in the centre of the path to be about 3.3 mm and 6.6 mm on the outside of the path. A second cause is that the lateral position depends on the vertical position of each point.

Figure 10: Vehicle Terrain Measurement System mounted on host vehicle (Kern, 2007).

The positioning system used in the VTMS is a Differential Global Positioning System (DGPS). The DGPS produces global positioning with an accuracy of 20 mm for a longitudinal distance traveled up to 10 km. Thus the final accuracy of the Vehicle Terrain Measurement System is confined to the 20 mm accuracy of the DGPS. The DGPS consists of two units, the base unit which is stationary and the unit mounted in the host vehicle, which contribute to the accuracy obtained. The DGPS signal is then combined with the IMU measurements in a Kalman filter to produce the final prediction of the orientation and position of the host vehicle.

2.2.4. Profilometers used in South Africa for profiling off-road terrain

Zaayman (1988) developed a tool for measuring and characterizing the profiles of rough terrain surfaces. A workable measuring device was created which would need only minor modifications for it to be applicable to a large variety of terrains. The measuring device was complete with software which was developed to give a set of profile heights for the measured terrain. The profile characterization software calculated the power spectral density of the profile as well as the roughness constant.

The system comprised of hardware components linked to measurement instrumentation and software. The hardware consisted of a two wheeled cart which had a small single wheel following the left hand track of the vehicle and a wheel-set following the right hand track of the vehicle (see Figure 11). The wheel-set was constructed in such a way that there were always at least two wheels following the ground in the track profile. The pivot movement of the wheel-set with respect to the cart frame was measured by a potentiometer giving as output the angle α between the wheel-set frame and the cart frame. A proximity switch was mounted on the wheel-set, with a notched plate attached to one of the wheels, thus a pulse was generated every time the notched plate passed the proximity switch during movement.

This gave the sloped distance which the cart had covered. In order to ensure that the wheel constantly turned, even though it might not have be in contact with the ground, the front and rear running wheels were connected by a chain and sprocket system.

A gyroscope mounted on the cart frame measured the pitch angle θ and roll angle β which the frame made with the absolute horizontal plane as it moved behind the towing vehicle. The values of θ, β and α were recorded every time a pulse occurred in the signal of the proximity switch. The output signals from every transducer were stored on an FM tape recorder.

The coordinates were then converted to only the value of the height, y, at equally spaced horizontal distances. The result was an array of height values,

y, starting at horizontal distance x = 0 which could be plotted to form the profile of the road.

The smallest obstacle the concept could measure with reasonable accuracy was a half round obstacle with the radius equal to the radius of the wheel (37 mm).

The speed of the tow vehicle could not be kept at a low enough speed for rough terrains. Too high towing speed resulted in the proximity switch generating pulses too fast and the pulses could be missed during analogue to digital conversion of the time data. The higher towing speed also generated unwanted vibrations and movement of the measuring device.

This concept worked better for the profiling of tarred roads where the amplitude of the longitudinal displacement of the surface was small in comparison with those found on off-road terrains. The concept also only measured a single line on the road travelled.

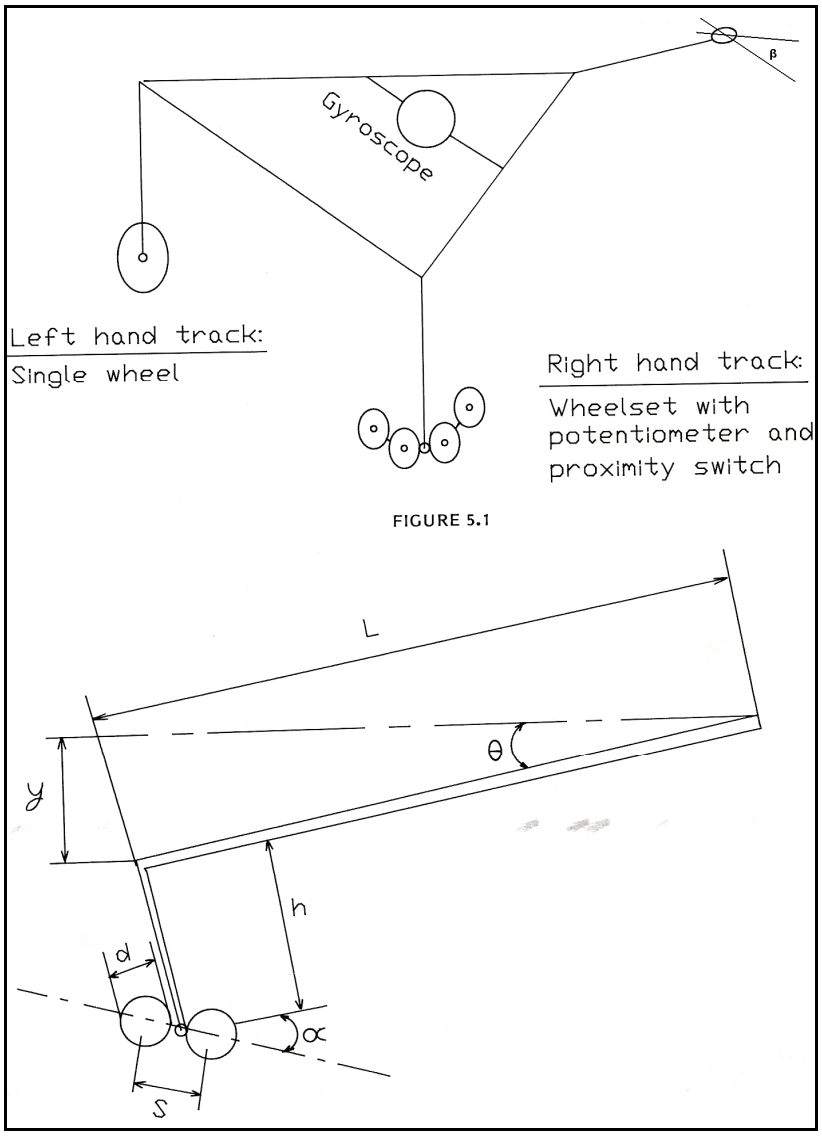

Figure 11: Zaayman's description of his concept (Zaayman, 1988).

2.3. Stereo Vision Measurement System

The experimental stereo vision system of the Sheffield Centre for Earth Observation Science (SCEOS) as described by McDonald et.al. (2000) comprises of two CCD cameras, a mount and a frame grabber connected to a computer (see Figure 12). It is possible to measure the position of an object by placing the object in view of both cameras. The cameras are focused on the object and the images are recorded. The simultaneous recording of the images are done with the use of the TINA software tool as described by Pollard et.al. (1989). The edge detection algorithm, as described by Canny (1986), is used to detect the position of the edges for each of the two images. The calibration process, which is done with a calibration tile, yields sixty-four

constraints on the seven camera parameters which include a translation vector, three angles of rotation and a focal length. The software uses the information on the edges of the images along with the camera parameters obtained from the calibration to rectify the stereo images to a parallel camera configuration.

The edge features in the rectified images are then correlated to determine the relative positions of the pixels in each image. The positions of the correlated pairs of pixels in the rectified image are then triangulated to determine the position of the particular points on the soil surface with reference to the position of the left camera. To aid the correlation procedure, which can become confused when noisy images are used, a laser stripe generator is used to produce one distinct line in the pair of images.

The best way to measure a soil surface is to take several sets of stereo images offset by a known amount; a mosaic of the images can then be used to produce useful measurements of the soil profile at the required resolution. The movement of the cameras and laser are constrained to one dimension to ease the alignment process. This is done by mounting the CCD camera and laser diode on a linear scanner. The movement of the system is regulated by a computer controlled stepper motor over a length of three metres. The accuracy of the profilometer is dependent on the resolution of the CCD camera, the integrity of the reference and soil images, the alignment and the positional accuracy of the linear scanner.

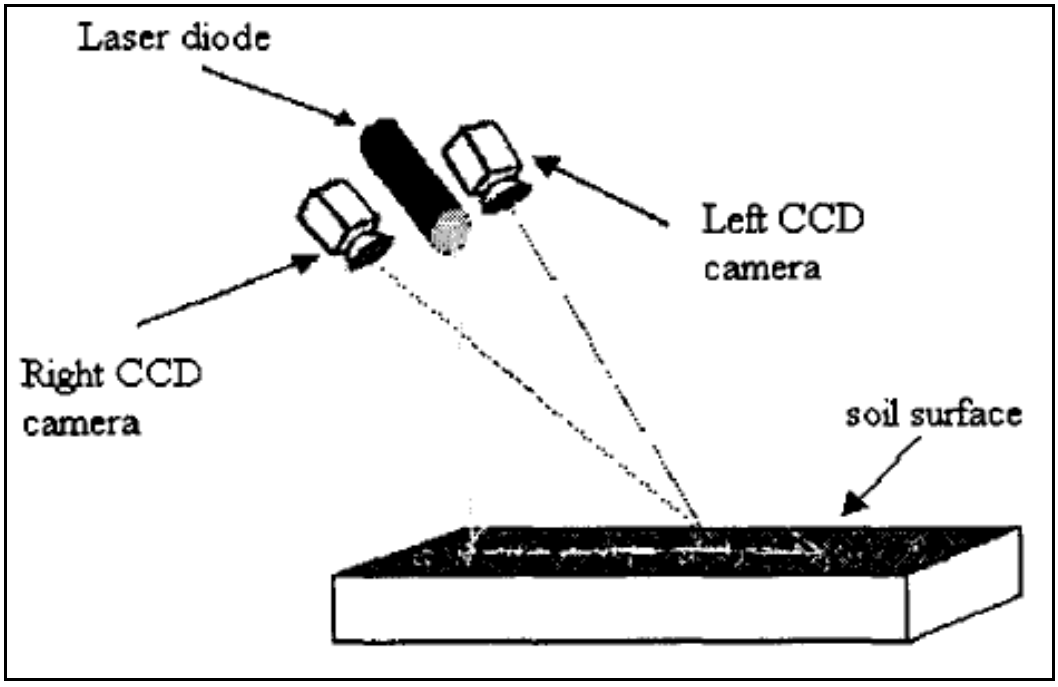

Figure 12: A schematic view of the Stereo Vision Measurement System (McDonald et.al., 2000).

2.4. Aerial Photography

Man's ability to see in three dimensions is a result of having two eyes that record slightly different images of the objects around him. These two slightly different images are fused by the brain to give an impression of depth.

An essential feature of aerial photography for mapping purposes is that it must be possible to view an optical model of the terrain in three dimensions. If the photographic sequence is arranged so that a portion of the terrain between the two camera stations is recorded on successive exposures, two slightly different views of the same area of terrain, called the 'overlap', are recorded on the photographic emulsion. If the pair of photographs, also known as stereo pairs, is viewed under suitable conditions, an optical model of the area of overlap will be seen in relief. The condition to be satisfied is for each eye to have a slightly different view of the same area of terrain; this can be achieved if the left eye only views the left photograph and the right eye views only the right photograph of the overlap (see Figure 13) (Ritchie et.al., 1991).

A three-dimensional, or stereoscopic, image of the terrain cannot be created from aerial photographs unless the conditions, as described above, are reproduced in their taking. The dimension of height not only enhances the interpretation of many features but also allows the photogrammetrist the possibility of measuring heights within the stereoscopic model, using only a minimal amount of ground-derived information. Normally four known height points are required for one overlap. Figure 14 describes the overlap requirements for complete photographic coverage.

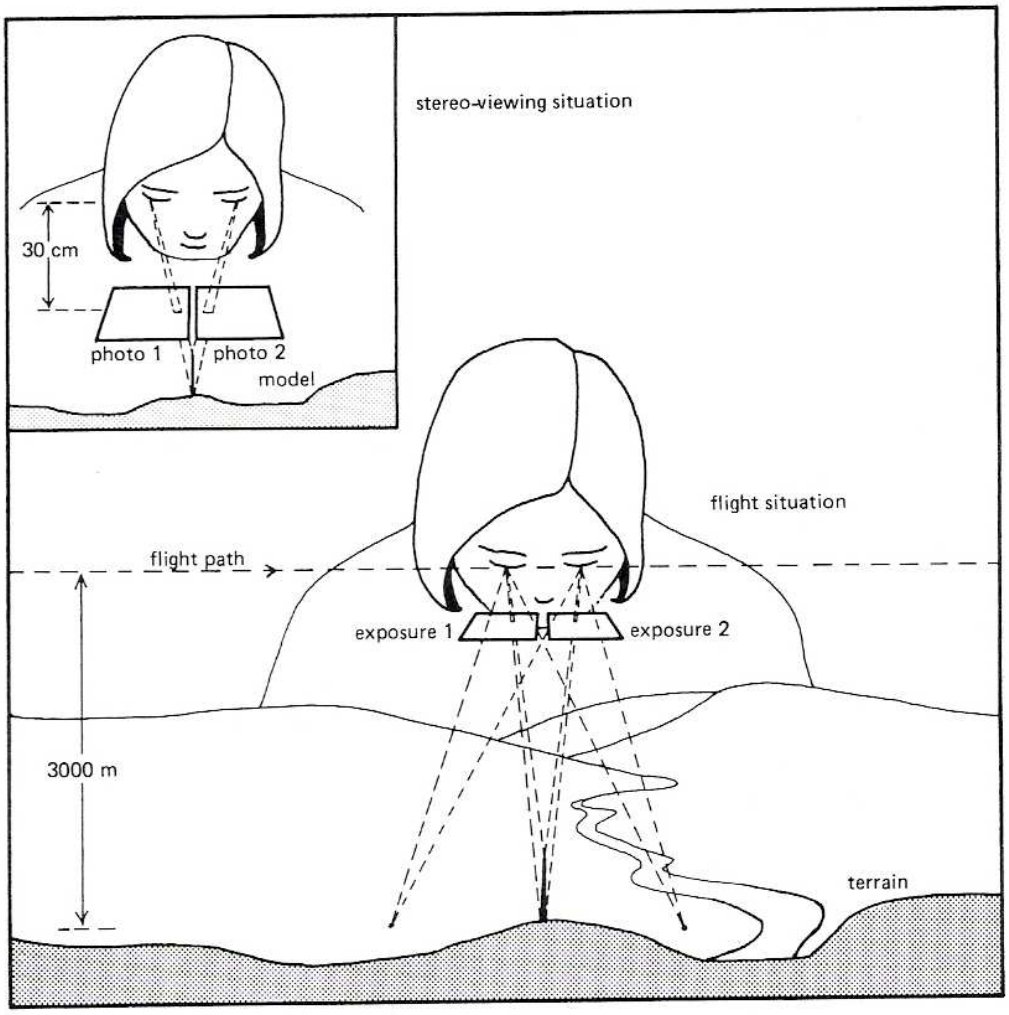

Figure 13: Giant eye-base described by Ritchie in Surveying and mapping for field scientists (Ritchie et.al., 1991).

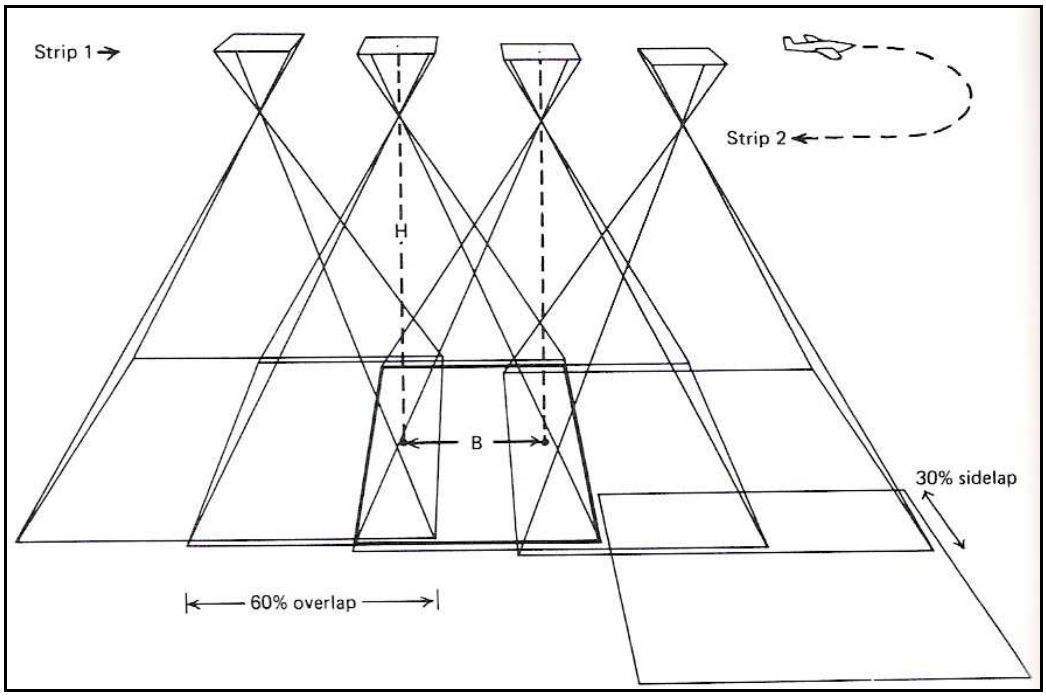

Figure 14: Overlap requirements for complete photographic coverage and stereoscopic viewing described by Ritchie (1991).

2.5. Stereoscopes

The simplest, and least expensive, piece of equipment for viewing the three-dimensional image from overlapping photographs is the lens stereoscope. It consists of a pair of lenses mounted on a frame, which is supported over the photographs by thin metal legs. Figure 15 shows two examples of stereoscopes.

When the lens stereoscope is set up, the distance from the lens to the photograph is equal to the focal length of the lenses, so that the photographic image will appear sharp in the focal plane of the lenses. The image appears enlarged, usually 2x to 2.5x. The photographs are arranged below the lenses so that the appropriate eye is viewing the same detail in the appropriate photograph at the same time. It is necessary to place one photograph on top of the other so that the separation of corresponding images is about the same as the lenses separation. This limits the portion of the photograph that can be viewed at any time. The portability of the lenses stereoscope makes it suitable for use in the field.

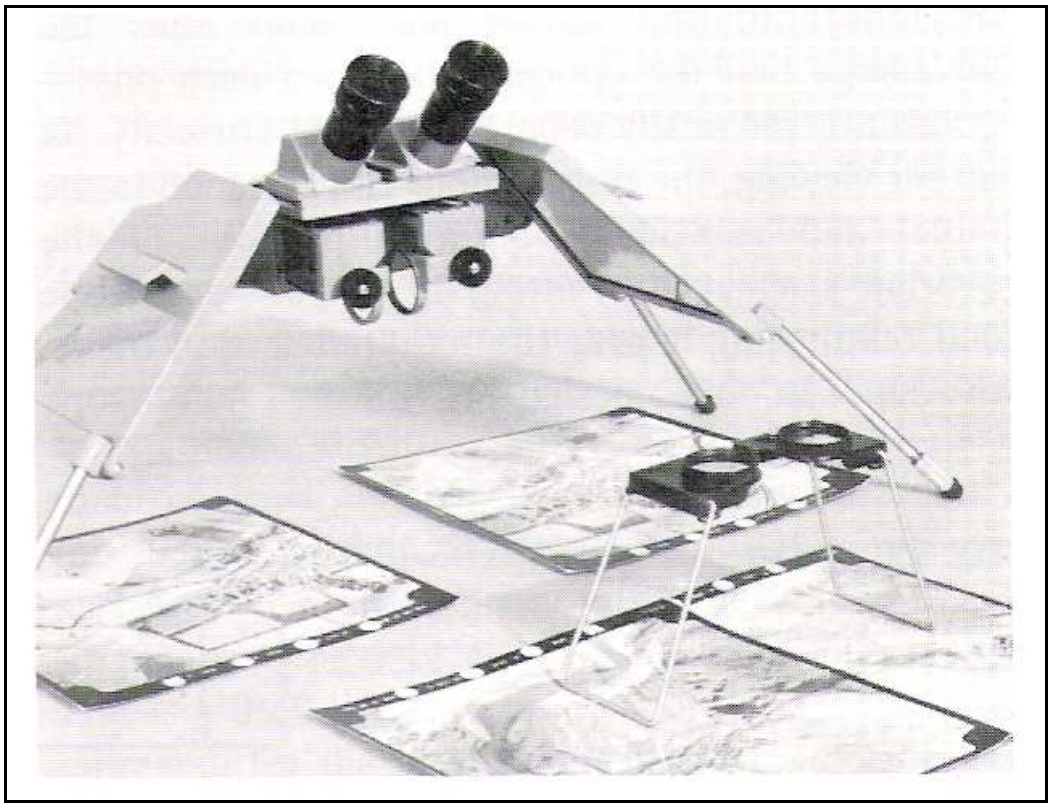

Figure 15: Mirror stereoscope and lens stereoscope (Ritchie et.al., 1991).

2.6. Laser Displacement Scanners

Several groups have been studying the best way to acquire 3-D models of real world environments. Research efforts generally fall into one of two categories: image-based methods, where the 3-D geometry is inferred from 2-D images; and the laser range-based approach, where the 3-D geometry is measured directly through laser range scanners.

Image-based methods have been around the longest and have been used for many 3-D modelling tasks. The standard method for developing large-scale terrain models is with the use of stereo techniques with aerial imagery to develop coarse models of the ground below, as described in Paragraph 2.3 to 2.5.

The MIT City Scanning Project uses spherical cameras and Geographic Information System (GIS) localization to develop models of the environment around them. In general, these techniques give results that have centimetre-to metre-level accuracy. Other laser sensor platforms are available which produce geo-referenced imagery but they produce data that is not suitable for close-range mapping, (Antone and Teller, 2000).

The University of Tennessee, Knoxville (UTK) developed a Mobile Scanning System which is more flexible in the types of environments and structures that can be digitized when compared to methods utilizing aerial terrain scanning. Their system combines laser range scanners, high resolution video cameras, a Global Positioning System (GPS) and an Inertial Navigation System (INS) to measure the system's position and orientation. The instrumentation is mounted on a vehicle and the terrain is digitized to provide a geometrically accurate 3-D model of the terrain as the vehicle is driving, an example of the vehicle is shown in Figure 16. The system uses a downward looking laser range scanner to digitize the terrain.

Figure 16: UTK's Mobile Scanning System consisting of a vehicle, laser range scanner, GPS, INS and high-resolution video camera (Grinstead et.al., 2005).

The Mobile Scanning System acquires data in real-time but processes the data offline. A typical terrain model can consist of over 200 000 geometry profiles, 1 million position and orientation measurements and 20 000 high resolution colour images. A rough estimation of the storage capacity required for the raw data alone exceeds 10 gigabytes.

The micro-scale system utilizes an Integrated Vision Products (IVP) Ranger to acquire high-resolution, high-accuracy 3-D models of roads and other surfaces. The measuring principle of IVP Ranger to acquire 3-D shapes is based on the method called laser triangulation, or sheet-of-light range imaging. The object is illuminated from one direction with a laser line projector and viewed with the camera from another. The illumination angle, the viewing angle, and the baseline between the illuminator and the camera define the triangulation geometry, from which the camera calculates the 3-D shape. The micro-scale system is capable of measuring the geometry very densely

(approximately 1 mm between data points) with an accuracy on the order of 5 mm, at the cost of having a very limited field-of-view and a high amount of raw data to process (Grinstead et.al., 2005).

2.7. Road Profile statistics

An extensive amount of work has been conducted by, amongst others, Sun et.al. (2005), Gorsich et.al. (2003) and Rouillard et.al. (2001) on obtaining statistical information on actual roads. Statistical models of each test terrain at the US Army's Aberdeen Test Centre have been created to establish and quantify the roughness of each course. The assumptions of linearity, normality and stationarity are usually made about a time series in order to create proper models for course elevations. Stationarity means that the variation of the course is uniformly rough along the length of the course. Linearity is essential for a relatively simple representation of the series. Normality is a common assumption used to build statistical models.

Sun et.al. (2005) tested stationarity by comparing the mean and the variance for the different segments of the data. A previous study indicated that the Belgian Block data is linear and Gaussian but not stationary.

The statistics are also used when random roads are generated from a given Road Quality Index (RQI) or road roughness from the International Road Index (IRI). Each random road generated for a simulation differs and one is not able to execute and compare field tests on the same road. Off-road terrains are often not random and very little data on off-road terrains are available. The focus of this study is on the off-road terrains at the Gerotek Test Facilities (Gerotek Test Facilities, 2007), whose profiles are not known. The emphasis on the present study is not on obtaining statistics of the profiles, but rather real terrain profiles for the use in simulations.

2.8. Displacement Spectral Densities (DSD)

The roughness of a test course can be specified with the use of the Root Mean Square elevation (RMS) in the time domain or a Displacement Spectral Density (DSD) in the frequency domain (Gorsich et.al., 2003), and the roughness of a terrain is characterized according to the ISO 8608 standard, ISO (1995). The RMS of the vertical displacement of the profile and the square root of the area under the displacement spectral density should result in the same value.

The Power Spectral Density (PSD) of a signal describes how the power of a signal or a time series is distributed in the frequency domain. The same can be done for the displacement; consequently the Displacement Spectral

Density of a signal describes how the displacement of a signal or a time series is distributed in the frequency domain.

The ISO 8608 standard, ISO (1995), is an international standard which specifies a uniform method of reporting measured vertical road profile data for either one-track or multiple-track measurements. It applies to the reporting of measured vertical profile data taken on roads, streets and highways and on off-road terrain. The standard provides general guidance for the use of road profile statistical data for simulation studies and for related studies such as evaluation of comfort, suspensions and road profiles. The ISO standard supplies one with different road classifications, these classifications are supplied in the form of class limits for the Displacement Spectral Densities for different classes of roads. The classes range from a class-A road which is a smooth road to a class-H road which is a very rough terrain. The classes are presented on a graph as shown in Figure 17.

The earliest motivation for performing Displacement Spectral Density calculations on road profiles was their usefulness in vehicle dynamics. However, many researchers noted that the Displacement Spectral Density would also be a convenient way to classify road roughness and deterioration, (Andren, 2006).

The estimated Displacement Spectral Density is formed by taking the Fast Fourier Transform (FFT) of a window of the now one-dimensional processed profile. Windowing the data on a segment of the road profile data allows multiple estimated Displacement Spectral Densities to be formed and averaged to increase the accuracy of the final Displacement Spectral Density. The windowing is typically done with a Hanning window. Changing the window sizes can also greatly vary the final Displacement Spectral Density estimate Gorsich et.al. (2003).

The Displacement Spectral Density of a random road, plotted on a log-log scale, formulates a straight line and may be described by the power function.

$$S_z = A\varphi^{-n}$$

Where S_z is the vertical displacement spectral density (mean vertical displacement) ^{2} / (frequency band), n is the road index, A is the roughness coefficient at a spatial frequency of 1 cycle/m and φ is the spatial frequency measured in cycles/metre (cycles/m), Uys et.al. (2007). The road index parameter is calculated with a spatial frequency window from 0.05 cycles/m to 10 cycles/m.

The ISO 8606 standard (ISO, 1995) specifies that for off-road profiles the reported spatial frequency range for φ should be from 0.05 cycles/m (wavelength = 20 m) to 10 cycles/m (wavelength = 0.1 m).

Hall (1998) indicated that the lower value of φ = 0.05 cycles/m was accepted since the vehicle speed over off-road/ rough terrain was normally much less

than the case for on-road terrains. The upper spatial frequency limit of φ = 10 cycles/m was consistent with the length of the tyre contact patch.

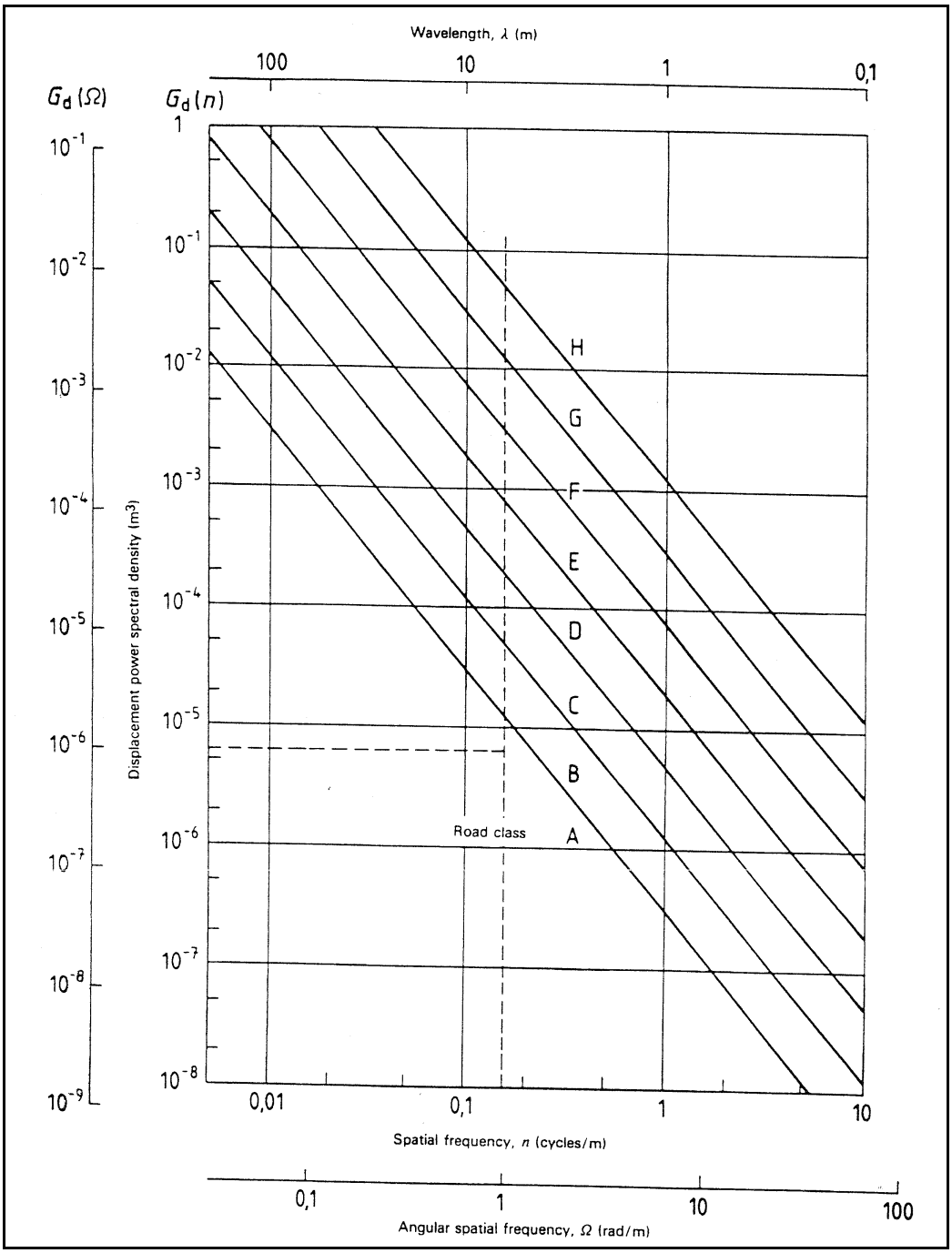

Figure 17: ISO 8606 road classification, (ISO, 1995).

Road profiles are usually considered to be a random process $x(d)$, where x is the road height and d is the distance along the road. As the vehicle travels along the road with a velocity v, the random process $x(d)$ is converted to a

random process in the time domain $x(t)$, which is the input to the vehicle suspension via the tyre. The process $x(d)$ is generally described in terms of its Displacement Spectral Density as a function of the frequency in either radians or cycles per unit distance. A stationary zero mean random process $x(t)$ with dimensions of distance (m) can be characterized by its autocorrelation function:

$$R_{xx}(\tau) = \langle x(t)\, x(t-\tau) \rangle = \lim_{T \longrightarrow \infty} \frac{1}{T} \int_0^T x(t)\, x(t-\tau)\, dt \qquad [\text{m}^2]$$

where $\langle x(t)\, x(t-\tau) \rangle$ is the time averaging operation.

If f is the frequency variable in cycles per second or more commonly known as Hz, the 'double side' Displacement Spectral Density $S_{xx}(f)$ is the Fast Fourier Transform of the autocorrelation function $R_{xx}(\tau)$.

$$S_{xx}(\tau) = \int_{-\infty}^{\infty} R_{xx}(\tau) e^{-j2\pi f \tau} d\tau \qquad [\text{m}^2/\text{Hz}]$$

The Displacement Spectral Density has the property that if the integral is calculated over all of the frequencies, the mean square value of $x(t)$ is determined.

A road profile $x(d)$, with d being the distance along the road, can be characterized by the autocorrelation function $R_{xx}(\delta) = \langle x(d)\, x(d-\delta) \rangle$, where $\langle x(d)\, x(d-\delta) \rangle$ is now a distance averaging operation. The Displacement Spectral Density of the road profile , $x(d)$ which is still determined with the use of the Fast Fourier Transform of the autocorrelation function, $R_{xx}(\delta)$, is then expressed in terms of a frequency variable F in cycles per metre (Davis and Thompson, 2001).

$$S_{xx}(F) = \int_{-\infty}^{\infty} R_{xx}(\delta) e^{-j2\pi F \delta} d\delta \qquad [\text{m}^3/\text{cycle}]$$

Another valid method for calculating the Displacement Spectral Density was described by Zaayman (1988). In this method the Displacement Spectral Density $S_{xx}(\delta)$ of the road was calculated by dividing the squared Fast Fourier Transform X_δ of the road profile $x(d)$ by twice the step in frequency ΔF .

$$S_{xx}(F) = \frac{\left|X_\delta(F)\right|^2}{2\Delta F}$$

The squared Fast Fourier Transform is equivalent to the Fast Fourier Transform of the road profile X_δ multiplied with the complex conjugate of X_δ.

$$\left|X_\delta(F)\right|^2 = X_\delta X_\delta^*$$

This method used in calculating the Displacement Spectral Density is accurate and is used for calculating the Displacement Spectral Densities of the measured profiles in this study.

2.9. International Roughness Index (IRI)

Sayers and Karamihas (1998) provide information about measuring and interpreting road profiles. They also provide a very descriptive interpretation of the International Roughness Index (IRI). Almost every automated road profiling system includes software to calculate a statistic called the International Roughness index (IRI).

The IRI was the first widely used profile index where the analysis method was intended to work with different types of profilometers. IRI is defined as a property of the true profile and therefore it can be measured with any valid profilometer. The analysis equations were developed and tested to minimize the effects of some profilometer measurement parameters such as sample interval.

The IRI is calculated by simulating a quarter-car model, known as the Golden car, driving on the measured profile at 80 km/h. The absolute suspension travel of the quarter-car is added together and divided by the length of the input profile. The result of the absolute suspension travel divided by the length of the input profile produces the IRI value.

Let T be time it takes a vehicle to traverse a pavement section of length L at a constant speed of v = 22.22 m/s. The IRI is defined by the average of the absolute value of $\dot{z}_s(t)$ over time $T = n\Delta t$, ie. (Sun, 2001)

$$IRI = \frac{1}{L}\int_0^T \left|\dot{z}_s(t)\right| dt = \frac{1}{vn\Delta t}\sum_{i=0}^{n}\left|\dot{z}_s(t_i)\right|\Delta t = \frac{1}{vn}\sum_{i=0}^{n}\left|\dot{z}_s(t_i)\right|$$

The IRI summarizes the roughness qualities that impact vehicle response and is most appropriate when a roughness measure is desired that relates to: overall vehicle operating cost, overall ride quality, dynamic wheel loads and overall surface condition. The standard IRI values for different road surfaces are tabulated in Table 1.

Road Surface	IRI (m/km)
Superhighways	0.25 - 1.9
New pavements	1.45 – 3.3
Older pavements	2.2 – 5.75
Maintained unpaved roads	3.4 – 9.9
Damaged pavements	4 – 10.9
Rough unpaved roads	8 - 20

Table 1: IRI values for different roads.

Figure 18 shows IRI ranges represented by different classes of road.

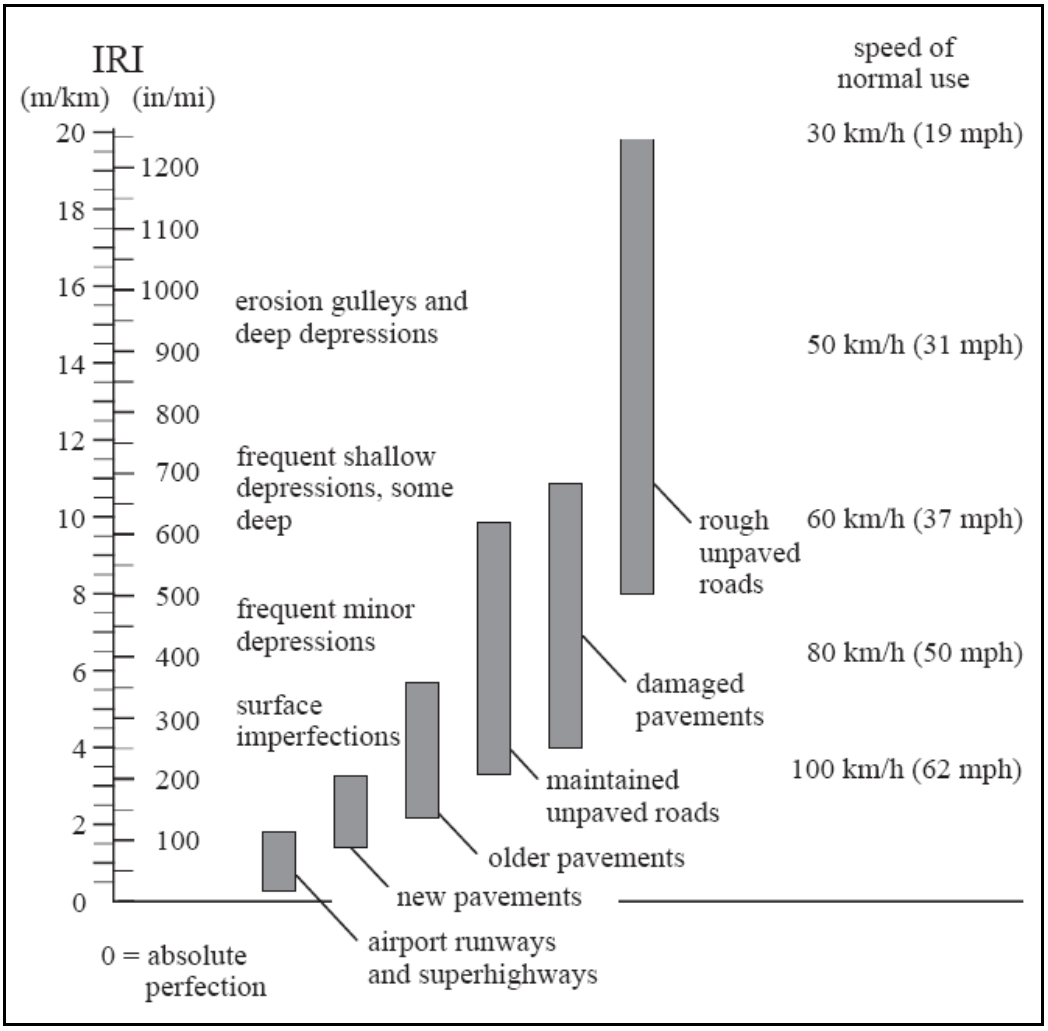

Figure 18: IRI ranges representing different classes of road (Sayers and Karamihas, 1998).

The Golden car quarter-car model used in calculating the IRI is just what its name implies: a model of one corner (or quarter) of a car as indicated in Figure 19. The model includes one tyre, represented with a vertical spring, the

mass of the axle supported by the tyre, a suspension spring and damper and the mass of the body supported by the suspension for that tyre. The quarter-car model was tuned to maximize correlation with response-type road roughness measuring systems. The Golden car parameters give the quarter-car a behaviour typical of most highway vehicles with one exception: the damping is higher than most cars. This keeps the IRI from "tuning in" to certain wavelengths and degrading correlation with other vehicles.

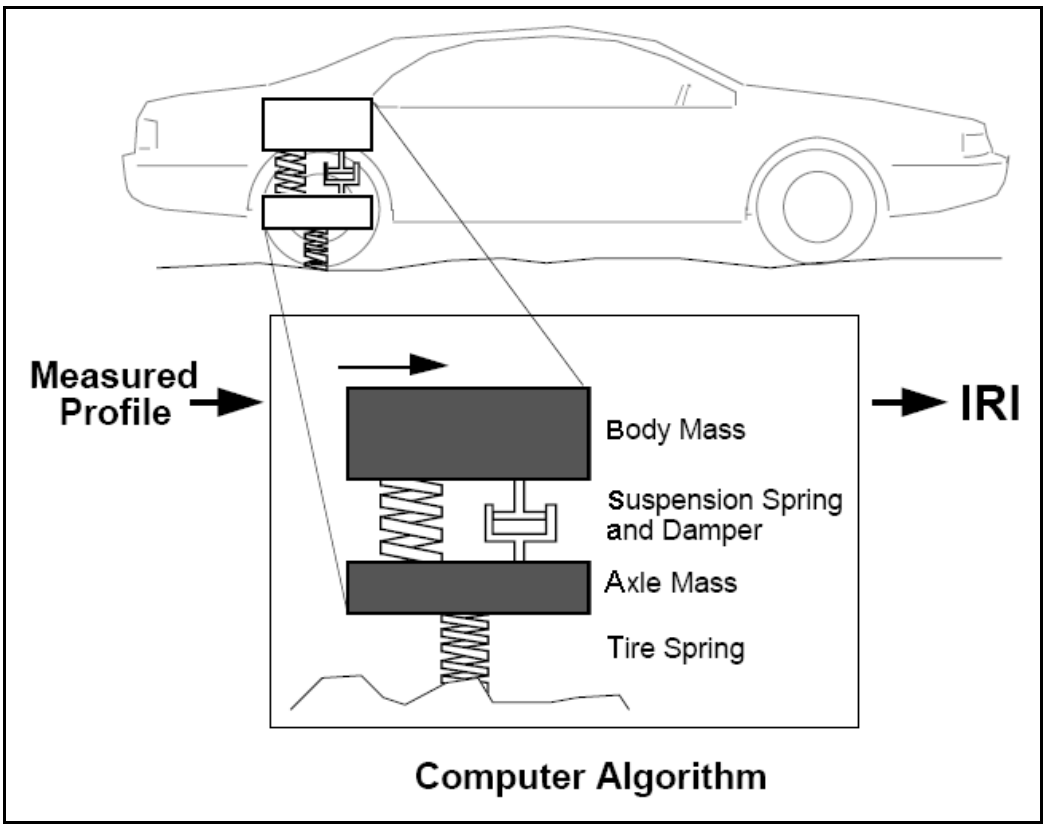

Figure 19: Golden car, IRI quarter-car model (Sayers and Karamihas, 1998).

2.10. Summary on literature survey

From the literature study the following conclusions were drawn and the proceedings of the study were consequently adapted.

The High Speed Profilometer, Inertial profilometer, Lightweight profilometer, Walking profilometer and Longitudinal Profilometer Analyser could not be used in our application since they only profile the longitudinal and transverse profiles in the wheel tracks of the vehicle used and a 2-D model of the road could be generated. The HSP was also designed to profile concrete roads and asphalt roads at high speeds. The HSP was also restrained by a lower operation speed limit of 12 km/h. In some instances this lower operating speed limit was a too high travelling speed for some of the off-road terrains

which were required to be profiled. Also the vehicle which the HSP is mounted is not suitable for some of the terrains.

The Rod and Level and the Dipstick methods may be used if a single line profile of the terrain were to be used in simulations but would be too time consuming to measure a 3-D profile of the terrain.

The use of 3-D tyre models in simulations are increasing and thus 3-D road profiles are required. In 3-D simulations the road is often modelled as separate left and right surfaces to reduce the number of elements in contact with the tyre, as it reduces the solver duration. The resolution of the Vehicle Terrain Measurement System is very high and not required due to the simulations programs not being able to process the amount of data and the higher resolution does not affect the vertical response of the model if a 3-D tyre model is used. Some tyre models are capable of handling complete 3-D contact. If more data is recorded than required every second or third data point may be used, thus one is still able to use very high resolution data. A higher resolution road profile may have an effect on the vertical response of the model if a point contact is used in the model. When a 3-D tyre model is used in a simulation the mesh size of the road profile used for the simulation should not be larger than half the contact patch of the tyre. Thus one is able to use a road profile with a mesh size smaller or equal to 100 mm in the direction of travel. The biggest problem with their system is the cost of the system and the system's capability is limited to the vehicle on which the system is mounted.

Photogrammetry and stereo techniques with aerial imagery is a possible option in profiling rough terrains. No literature was obtained where actual rough terrains were profiled with the use of Photogrammetry but it remains an option worth investigating for the profiling rough terrains.

Laser scanning platforms are very accurate systems but the accuracy is compromised by the Global Positioning System when the 3-D model is placed in a global coordinate system. These systems have colossal raw data bundles and require state of the art computers for effective data processing. The laser scanning platforms are highly-priced and way beyond the resources for this study. The Laser scanning platforms are widely available however the vertical height required in order to profile a 100 m section of a terrain may compromise the obtainable resolution of the profile.

The terrain is classified with the use of a Displacement Spectral Density of the terrain which is an effective method in determining the roughness of the terrain. Terrains are classified in eight different types of roads ranging from a class-A road, which is a very smooth road up to a class-H road, which is an extremely rough terrain and only intended with the use of an off-road vehicle. The IRI is also a valid method used in comparing profiles of different terrains as well as comparing the same terrain profile, profiled with different profilometers.

It is important to know the orientation of the profilometer when a terrain is profiled because the terrain is profiled relative to the profilometer. Most of the terrains used for testing by the University of Pretoria have a known horizontal reference with a fixed height around the terrain. The known horizontal reference is in the form of a level surface around each terrain. The constant reference simplifies the method used to obtain the orientation of the profilometers.

For the present study three profilometers are constructed with the known level reference in mind. The first profilometer is a mechanical profilometer on three wheels, each moving on the known level reference. The second profilometer profiles a terrain with the use of Photogrammetry and the third profilometer utilize a laser which is mounted in a gimball.

3. Test Equipment

In this paragraph the three profiling methods proposed in this study for obtaining profiles of rough terrains are described. The development, working principals, testing and calibration of suitable equipment is discussed. Individual tests were conducted on each method to validate the profile obtained.

It is required that the profilometers are capable of the following;

- Profile rough terrain (vertical displacements > 25 mm).
- The mesh size of the profiled road may not be larger than half the contact patch of the tyre. Thus the mesh size is required to be smaller or equal to 100 mm in the direction of travel for typical tyre sizes.
- Effective profiling with minimal resources required.
- Minimum profile width of 2.5 m.
- Profile terrain with vertical accuracy < 5 mm.
- Profilometer must be light weight and easily transported.
- The cost of the profilometer should be kept to a minimum.
- The profiling speed < 6km/h, a fast walking speed.

In the light of these requirements, three concepts have been chosen for further investigation and development namely:

1. A mechanical profiler using arms pivoted to a reference frame on one side with small wheels on the ends in contact with the ground, nicknamed the Can-Can machine (see paragraph 3.1).

2. Photogrammetry using a digital camera mounted on a tripod above the terrain (see paragraph 3.2).

3. A laser displacement scanner mounted in a gimball that is rotated by two stepper motors (see paragraph 3.3).

3.1. Can-Can Machine

The Can-Can Machine is a mechanical measuring device which profiles a terrain by measuring angles. When you drag your hand over a surface, the surface may be smooth or rough; the movement of your fingers gives you a feel for the profile of the surface. If an obstacle is in the way, your fingers simply bend at the top knuckle and move over the obstacle. Another explanation could be if you are sitting on a wheeled office chair with your legs kept firm with your heals on the floor. When the chair is pulled backwards your heals will follow the profile of the floor by pivoting your legs at the knees. This is the principle behind the operation of the Can-Can Machine.

The Can-Can Machine is a light weight, right angle triangular structure with a wheel on each corner of the structure (see Figure 20). The two rear wheels are mounted 4.5 metres apart and the front wheel is used to steer the structure. The rear wheel track width of 4.5 meters facilitates the profilometer in utilizing the smooth and level zero reference surfaces on either side of the profiled terrain on the Gerotek suspension track. A 12 Volt wiper motor is mounted on the frame of the wheel and a chain is used to drive the wheel. A 5 amp adjustable voltage regulator (LM338K) is used to build a speed control to adjust the profiling speed. The speed control can adjust the speed from standing still to 1 km/h, a slow walking pace. Figure 21 shows the wiring diagram of the speed control. The speed of the profilometer is low to eliminate any dynamic effects of the profilometer.

A Crossbow tilt sensor is mounted on the rear beam and provides the orientation of the rear beam in both pitch and roll directions. The rear beam is designed for a maximum deflection of 3 mm at the centre of the beam with all the required equipment mounted on the beam.

Figure 20: The Can-Can Machine on the Fatigue track at Gerotek.

Thirty arms are mounted 100 mm apart on the rear beam of the structure and they follow the profile of the terrain (see Figure 22). The thirty arms allow the Can-Can Machine to profile a 3 meter wide section of the terrain. Each arm has a 30 mm nylon wheel at the one end which is in contact with the terrain. Nylon wheels are used since the nylon wheels were found to have a lower tendency to bounce on the terrain than rubber wheels.

The displacement at the tip of the arm is calculated by measuring the angle at the pivot point. The angles are measured with the use of high precision single turn potentiometers. The potentiometers are mounted inline with the pivot point of the arms. The arms and potentiometers are attached to one another with plastic tubing to compensate for some misalignment (see Figure 23). The arms are all bent with the same curve and at the same angle. This is done to

allow the wheels to move over a large obstacle without the arms coming into contact with the obstacle.

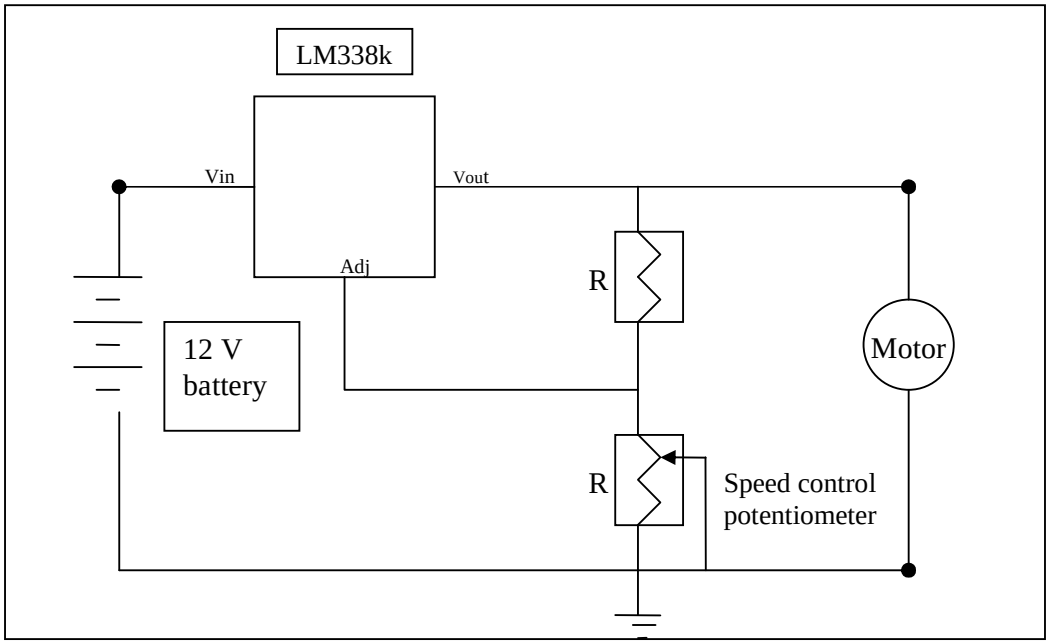

Figure 21: Wiring diagram of speed control for the Can-Can profilometer.

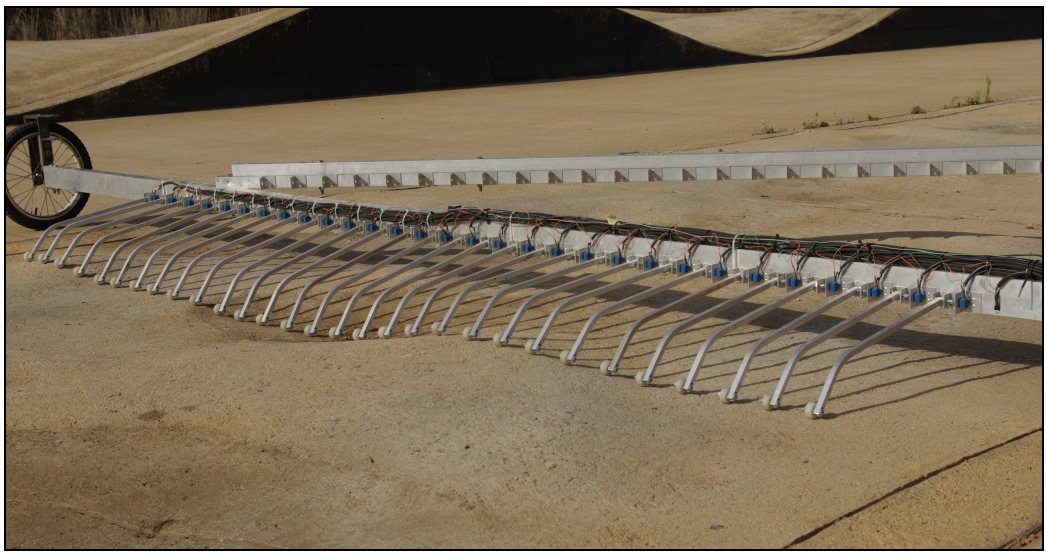

Figure 22: Thirty arms mounted on the rear beam of the Can-Can.

The potentiometers used on the Can-Can Machine are good quality Bourns 93R cermet track 10kΩ linear 16 mm, 2 Watt single turn potentiometers which have a 10% tolerance, 5% linearity and a temperature coefficient of 150. A LM 7805 5 Volt voltage regulator is used in supplying a regulated 5 Volts to all of the potentiometers. Figure 24 shows the wiring diagram of the LM 7805 which supplies a regulated 5 Volt to each potentiometer.

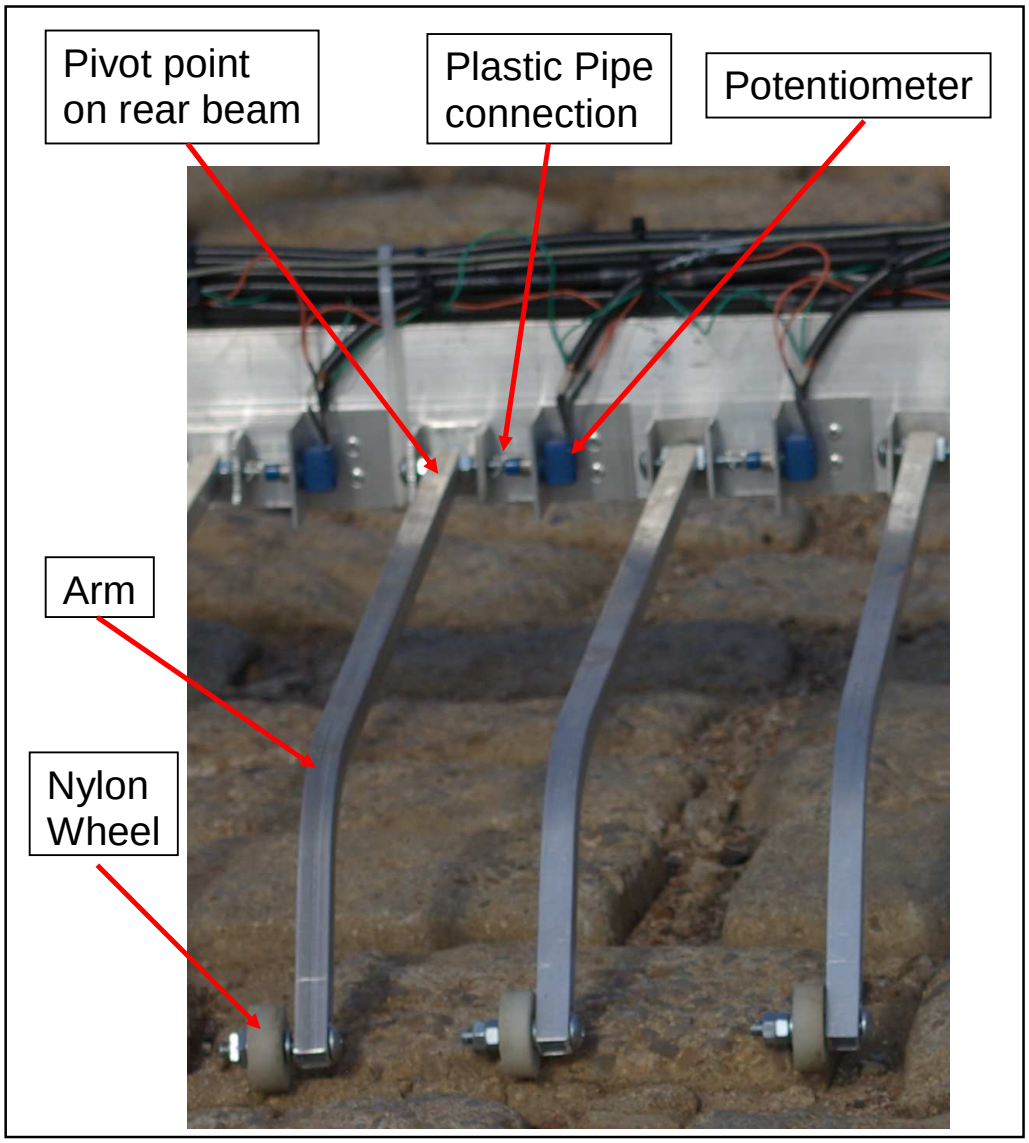

Figure 23: Close up of the arms and the potentiometers.

Although high precision linear potentiometers are used, as a check every fifth potentiometer is calibrated to determine the voltage output in relation to the rotation of the potentiometer due to the arm movement, the average of the calibrated potentiometers are used as the calibration factor for all the potentiometers. This is done because all of the potentiometers were purchased from the same supplier and were from the same production consignment. The calibration is done with the use of a dividing head, which is generally used on a milling machine. The chuck of the dividing head rotates once for every 40 revolutions of its side wheel. The rotating end of the potentiometer is placed in the chuck, the base of the potentiometer is kept static and the chuck is rotated. The voltage output of the potentiometer is measured for every two revolutions of the side wheel (every 9˚) (see Figure 25).

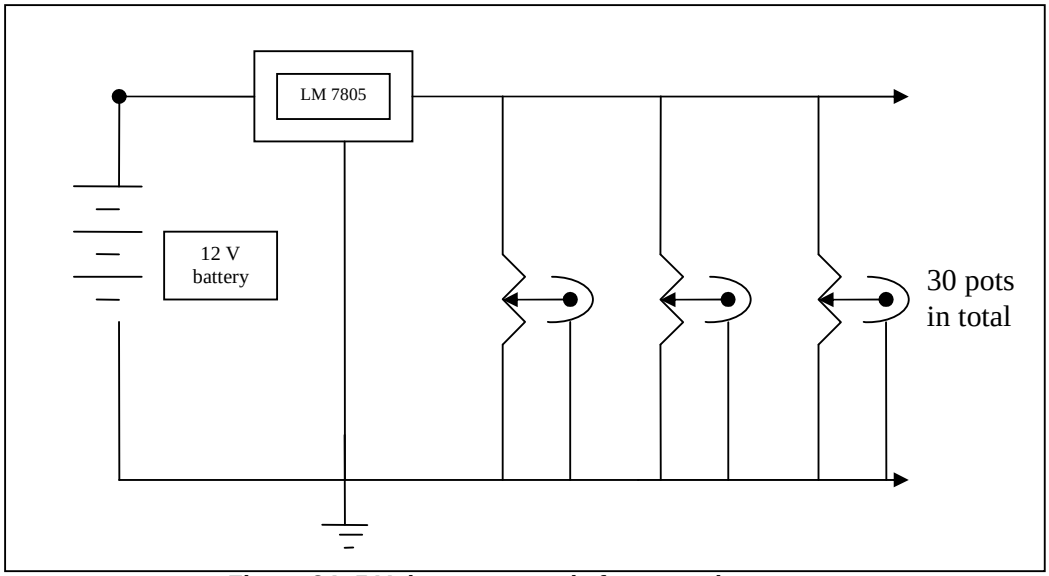

Figure 24: 5 Volt power supply for potentiometers.

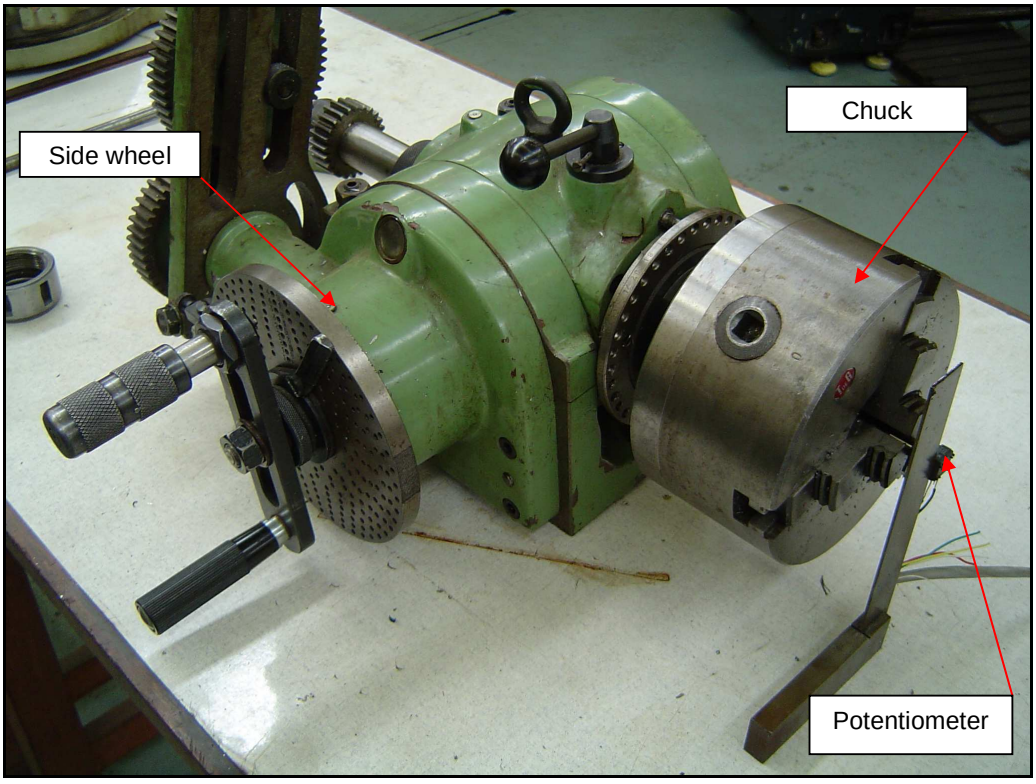

Figure 25: Calibration of potentiometers with the use of a dividing head.

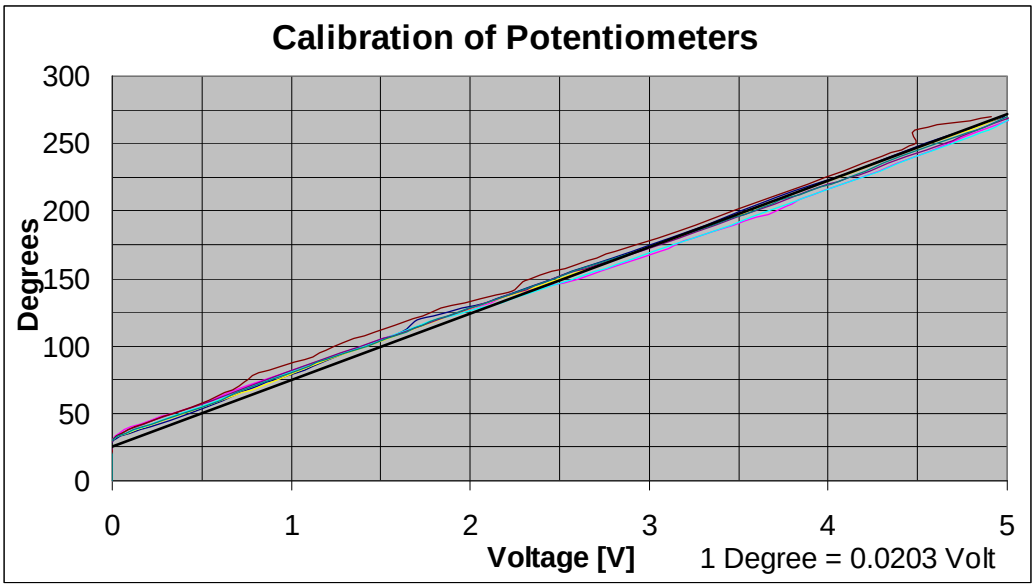

Figure 26: Calibration graph of potentiometers.

The degrees and measured voltage output are plotted to determine the voltage calibration value (see Figure 26). The gradient of the line in the figure is equal to the calibration value of the potentiometers, which is 49.156˚/Volt. This indicates that for every 49.15 degrees of rotation the output voltage of the potentiometer changes with one volt. The calibration graph also indicates that the potentiometers are linear.

A 5 volt, 12-bit resolution (4096 or 2^{12} steps), Analogue to Digital converter is used to convert the analogue values to digital format which is in turn recorded on a data logging computer. The resolution of the converter is determined by dividing the voltage amplitude of the converter by the converter bit size minus 1.

$$\frac{Voltage\_amplitude}{(bit\_size-1)} = \frac{(-5 \rightarrow 5Volts)}{(2^{12}-1)}$$
$$= \frac{10}{4095}$$
$$= 0.00244V$$

Thus the resolution of the potentiometers is calculated by multiplying the potentiometer calibration value with the converter resolution, which results in the following potentiometer resolution;

$$49.156^{\circ}/V * 0.00244V = 0.12^{\circ}$$

The length of the arms, L, from the contact point on the terrain to the pivot point is 470 mm. With the angle resolution, θ, of the potentiometers known it is

possible to calculate the obtainable resolution of the concept in the vertical direction, z.

$$\begin{aligned} z &= L\sin\theta \\ &= 470\sin 0.12^{\circ} \\ &= 0.98mm \end{aligned}$$

This indicates that the combination of the potentiometers and the analogue to digital converter has a resolution of 0.98 mm.

As the profilometer moves forward the tips of the arms move over the terrain causing the arm to pivot on the potentiometer. This arc motion at the tip of the arm causes an adjustment on the potentiometer equal to θ degrees (see Figure 27).

The potentiometer gives a different voltage output as the angle θ varies and is recorded by the converter. The variation in the potentiometer voltage output is used to calculate θ, which in turn enables the computation of the point (X, Y) as follows:

$$\theta_0 = \sin^{-1}\left(\frac{197}{L}\right)$$
$$\beta = \theta + \theta_0$$
$$X = -L\cos\beta$$
$$Y = -L\sin\beta + 197\left(ground\_reference\right)$$

The horizontal ground reference, θ_0, is determined with the wheels at the end of the arms horizontally in line with the pivot point after which the zero reference , θ_z, is determined. The zero reference is the constant height of 197 mm at which the potentiometers are mounted on the rear beam from the ground. With this array of points calculated, the programme written in Matlab is able to plot the terrain in three dimensions as required. In order to keep X to a minimum, the rear beam is mounted as low as possible with sufficient clearance for the rough terrain to pass below the beam. A Matlab programme is written to plot the recorded data and can be used to plot any recorded section of a terrain.

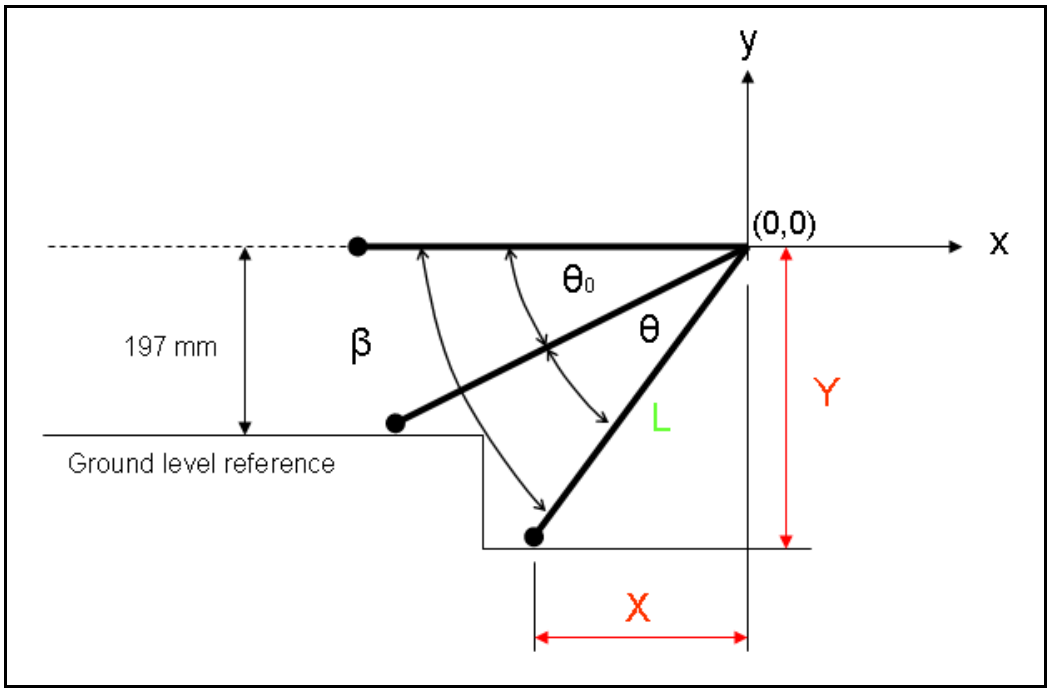

Figure 27: Description of the arm movement.

To measure the global X position of the pivot point, a digital encoder is designed and built in-house (see Figure 28). The encoder is mounted on the driving wheel and digitally triggers the data acquisitioning system with the use of two slotted opto-couplers. Data from the potentiometers and the tilt sensor are therefore recorded at constant horizontal distance intervals. The two slotted opto-couplers are mounted at an offset which enables the system to detect whether the Can-Can is moving forwards, backwards or standing still. The encoder has 120 triggers per revolution of the wheel, which gives a trigger every 10.18 mm of horizontal movement. The use of the encoder enables the data acquisitioning system to operate according to the operating speed of the Can-Can Machine, thus the system samples faster if the Can-Can Machine is operating at a faster speed and slower if the Can-Can is moving slowly. The encoder has two continuous potentiometers which rotate with the encoder without slip. The output of the continuous potentiometers indicates whether the opto-couplers are operating correctly.

When the encoder triggers, the data acquisitioning system samples 10 points on each channel in quick succession and saves the average of the 10 points. This average filters the electrical noise from the data and provides a smoother, more accurate profile.

The terrains profiled on the Suspension track at the Gerotek Test Facilities have level and smooth concrete sections on both sides of the terrain which provide a fixed reference for the profilometer.

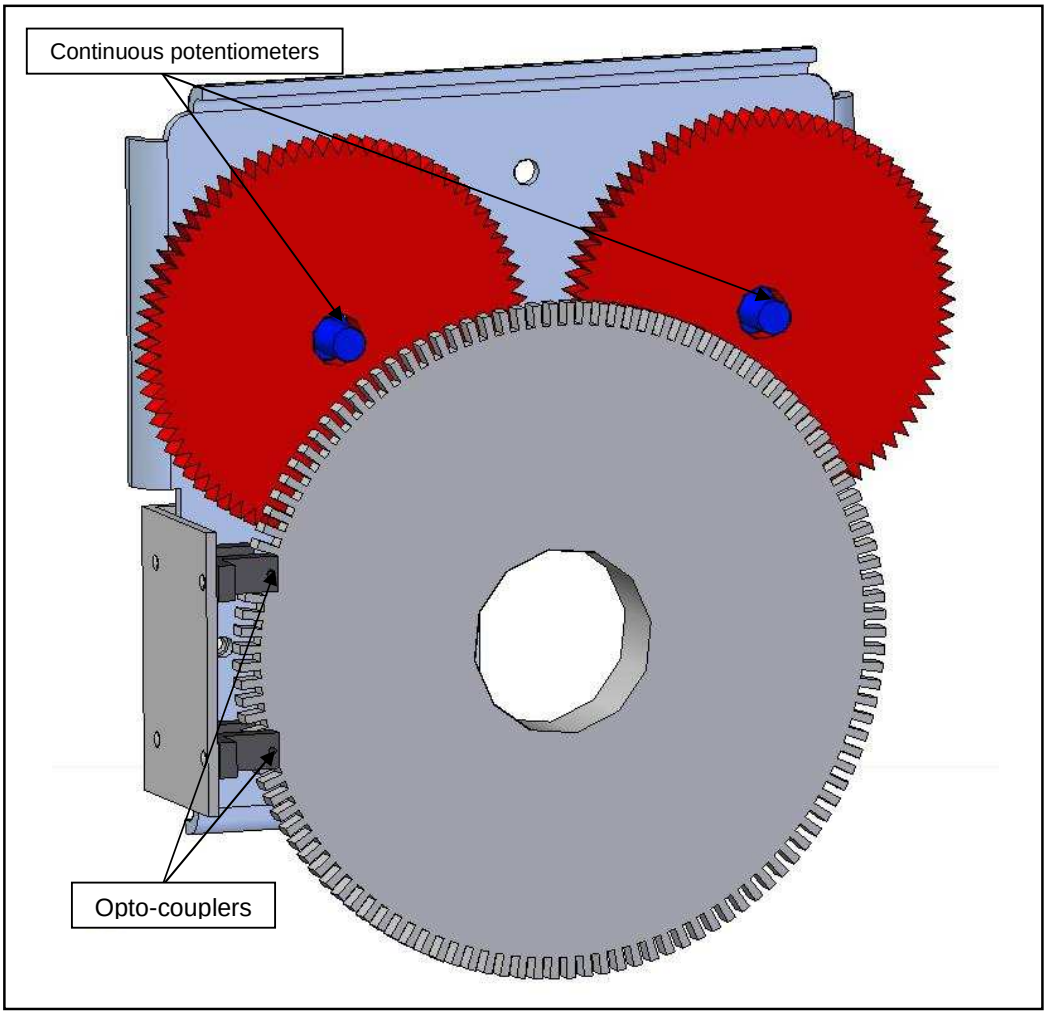

Figure 28: Encoder used to trigger data acquisitioning system.

The other terrains profiled with the Can-Can Machine require fixed references due to the fact that the whole structure of the profilometer moves over the rough terrain. The fixed reference is obtained with the use of a tilt sensor, surveying equipment and two straight beams on which two of the three wheels move.

A Crossbow CXTA02 tilt sensor is mounted in the middle of the rear beam and is used to determine the orientation of the Can-Can Machine in both pitch and roll. The certificate of conformance can be seen in Appendix A. This type of tilt sensor is based on an accelerometer and therefore calculates the tilt angle based on the gravity vector. It is therefore only accurate at low frequencies and the frequency range in which it gives acceptable accuracy had to be determined. Thus tests were conducted to determine the maximum frequency at which the tilt sensor can operate. The tilt sensor was mounted at 43 degrees on an actuator as shown in Figure 29.

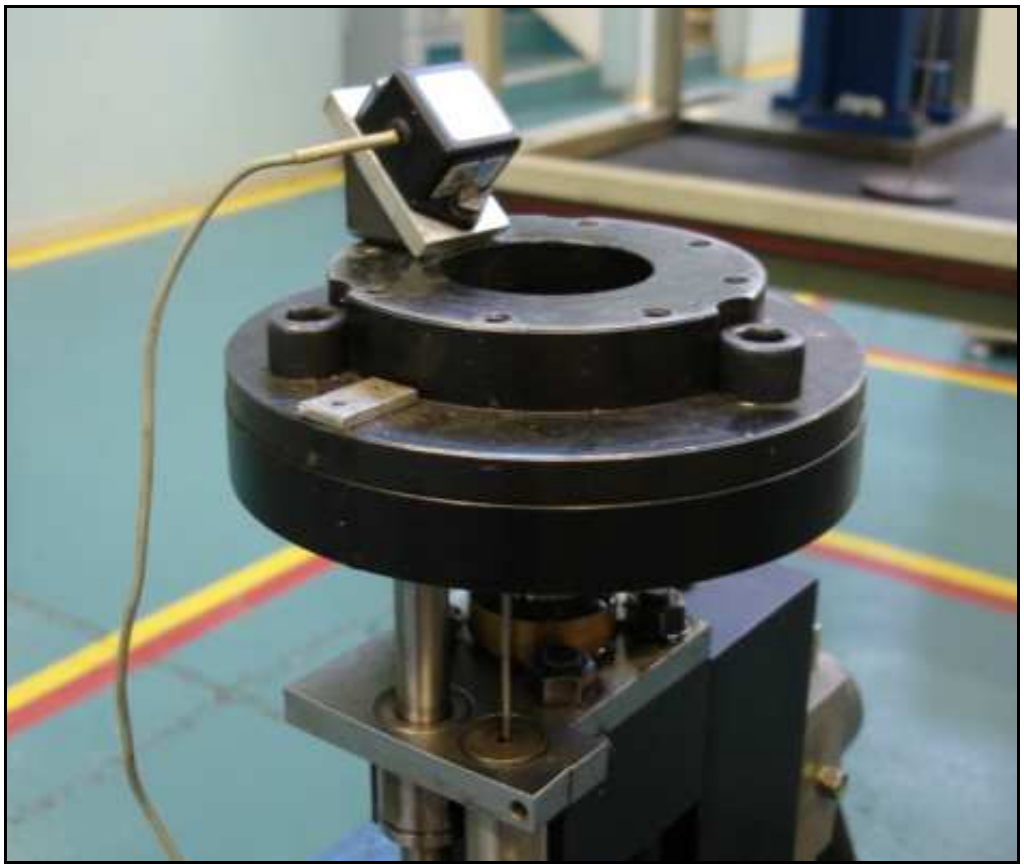

Figure 29: Crossbow tilt sensor mounted on an actuator at 43 degrees.

A 0 to 1 Volt random signal with a frequency content from 0 to 4 Hz was generated to excite the actuator over a period of 600 seconds. The response of the tilt sensor to the random input can be seen in Figure 30. The top graph in Figure 30 shows the input signal to the actuator. The middle graph shows the measured response from the tilt sensor and indicates significant noise of up to 4° superimposed on the true 43° orientation. The bottom graph shows the Fast Fourier Transform (FFT) of the tilt sensor's response.

It can be seen from the FFT graph in Figure 30 that the tilt sensor has a natural frequency between 2 and 3 Hz. The response of the tilt sensor was filtered with a 0.1 Hz low-pass RC filter. A 0.1 Hz low-pass RC filter was used due to the fact that the Can-Can Machine moves very slowly and the assumption was made that frequencies higher than 1 Hz will not be generated when the Can-Can Machine is profiling a terrain. The wiring diagram of the simple passive RC filter is shown in Figure 31.

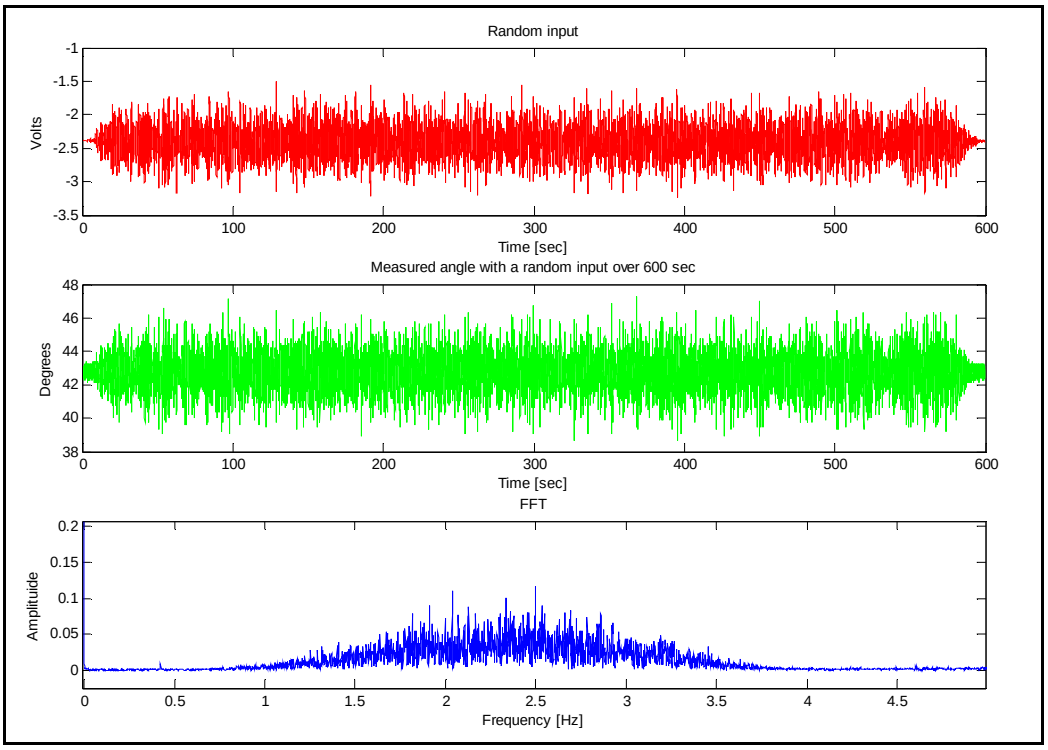

Figure 30: Response of tilt sensor to a random input.

The time constant of the filter, τ, is calculated as follows;

$$\tau = RC$$
$$with$$
$$R = 1M\Omega$$
$$C = 1.5\mu F$$
$$thus$$
$$\tau = (1e6)(1.5e-6)$$
$$= 1.5\,\text{sec}$$

The cut-off frequency, f_c, of the RC filter is calculated as follows;

$$f_c = \frac{1}{2\pi RC}$$
$$= 0.106Hz$$

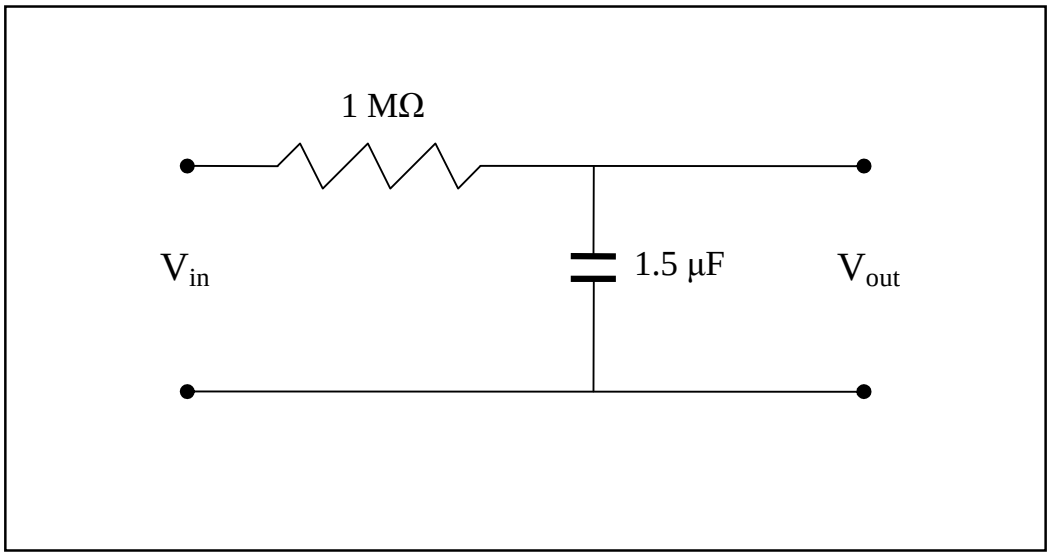

Figure 31: 0.1 Hz RC Filter.

The top graph in Figure 32 shows the FFT of the tilt sensor's response and the applied low-pass RC filter. The bottom graph shows the difference between the raw data and the filtered data from the tilt sensor's response. It is clear that the low-pass RC filter has a dramatic improvement on the measuring capability of the tilt sensor and thus the decision is made that the tilt sensor is capable of providing steady measurements for determining the orientation of the Can-Can Machine when profiling a terrain.

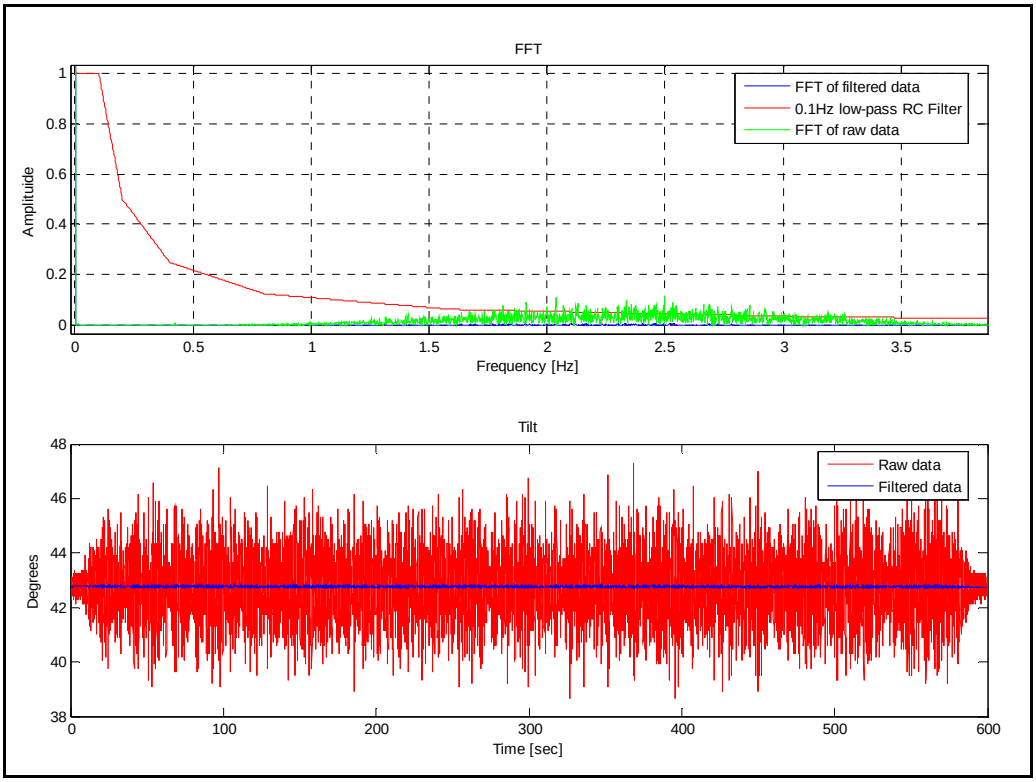

Figure 32: 0.1 Hz Low-pass filtered response of tilt sensor to a random input.

3.1.1. Test sections for Can-Can Machine

To verify correct operation and accuracy, the Can-Can Machine is tested in three different ways. The first method is used to test and investigate the accuracy of the arm movement. The profilometer was used to profile a 55 mm flat-top bump on a flat surface. The actual profile of the bump and the profile from the Can-Can Machine are shown in Figure 33.

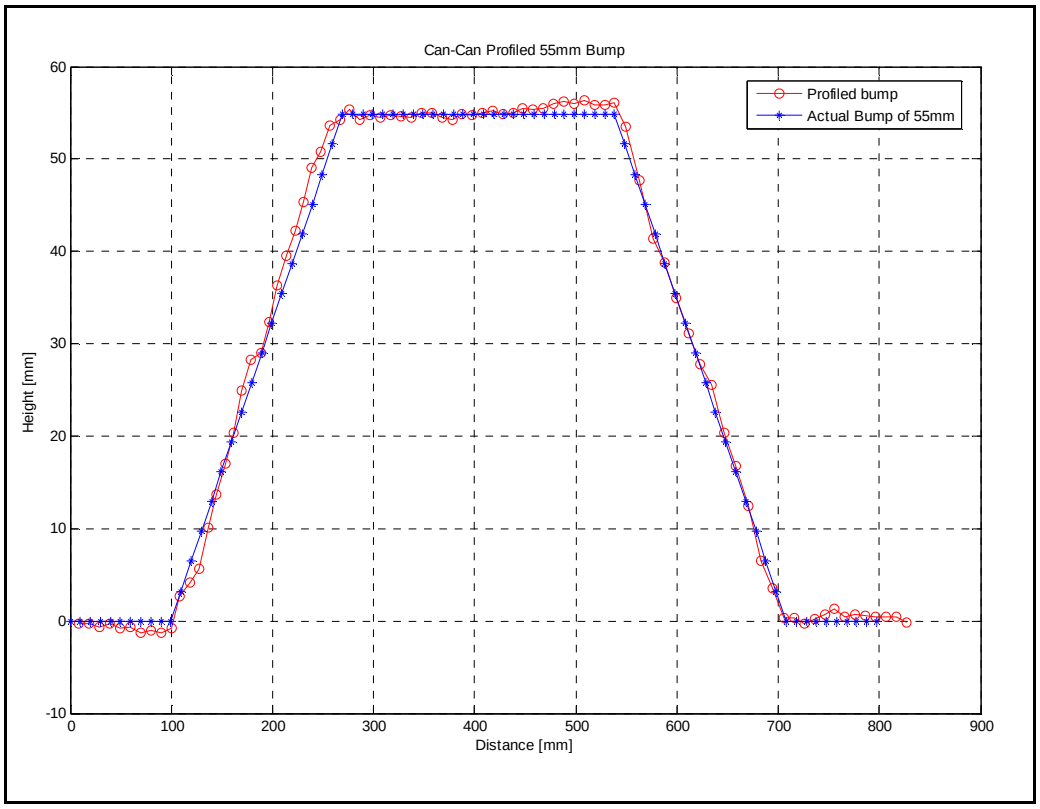

Figure 33: 55 mm flat-top bump profiled with Can-Can Machine.

The blue line in the figure is the actual profile of the bump and the red line is the bump profiled with the Can-Can Machine. The RMS value of the profile is 36.2 mm and the RMS value of the actual bump is 37.7 mm. The Root Mean Square Error (RMSE) represents the difference between the actual profile of the bump and the Can-Can profiled bump. The RMSE is given by the following formula:

$$RMSE = \sqrt{\frac{\sum_{i=1}^{n}\left(y_{i-actual} - y_{i-Can-Can}\right)^2}{n-1}}$$

Where:

y is the error in the vertical direction of the profile
n is the number of points in the profile.

The RMSE in the vertical direction is calculated at 2.73 mm. The difference in the profiles at the top of the bump is due to the small wheels at the end of the arms, which have a diameter of 30 mm. This error may be decreased with the use of even smaller wheels at the tips of the arms which is used to follow the profile of the terrain. Smaller wheels are not used simply because if even smaller wheels are used more noise will be present in the profile. Another contributing factor in not using smaller wheels on the profiling arms is that the wheels on the arms of the profilometer are smaller than the actual vehicle's wheels by a factor of 25 and the high frequencies measured by the smaller wheels will not have an effect on the response of the vehicle in the simulations. The corners at the top of the actual bump have a small radius and can be seen if the actual bump is plotted with a finer resolution.

The second test performed on the Can-Can Machine is profiling a flat concrete surface when one of the profilometer's wheels is moving over a 105 mm flat-top bump. The purpose of this test is to determine if the tilt sensors can be used to successfully eliminate the effects of roll and pitch of the main beam if the three wheels of the Can-Can Machine move over rough obstacles.

The measured profile is adjusted with the use of the orientation of the profilometer as measured with the tilt sensor. The top graph of Figure 34 shows the profile with the effect of the orientation of the Can-Can Machine added to the measured profile. The bottom graph shows the profile of the flat measure concrete surface without the orientation of the profilometer added. It can be seen in the top graph of Figure 34 that the concrete surface is flat but not exactly horizontal, which is indeed the case with the surface used for this test. Figure 35 shows the difference in the two profiles obtained in Figure 34 and illustrates the importance of the addition of the orientation of the profilometer to the measured profile.

The difference in the profiles increases to the one side because only the left wheel of the Can-Can Machine moved over the 105 mm flat-top bump. It is clear that even with the addition of the tilt sensor the profile of the flat surface is still not exactly flat. The RMSE calculated from a zero reference was 17.87 mm. Figure 36 shows the tilt sensor data added to the measured profile. It can be seen that when the profilometer moves too fast over a big obstacle the tilt sensor does not stabilize. This is due to the 0.1 Hz low-pass RC filter applied to the tilt sensor data which has a time constant of 1.5 seconds. The black line in Figure 36 indicates that the tilt sensor did not stabilize and did not profile a flat top bump. In this case the tilt sensor should be a mirror image of the blue line which is the raw profile. This can be corrected by profiling at a lower speed when the profilometer needs to move over large obstacles, which in turn will also decrease the RMSE.

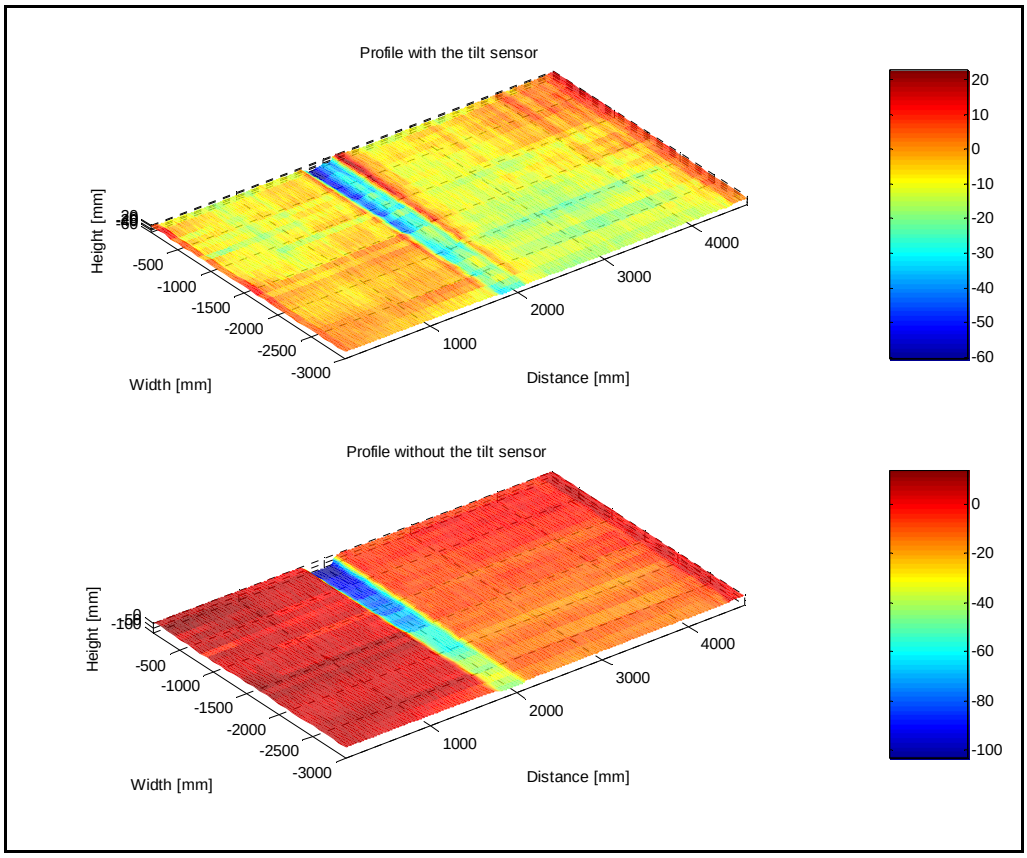

Figure 34: Profile of flat concrete surface.

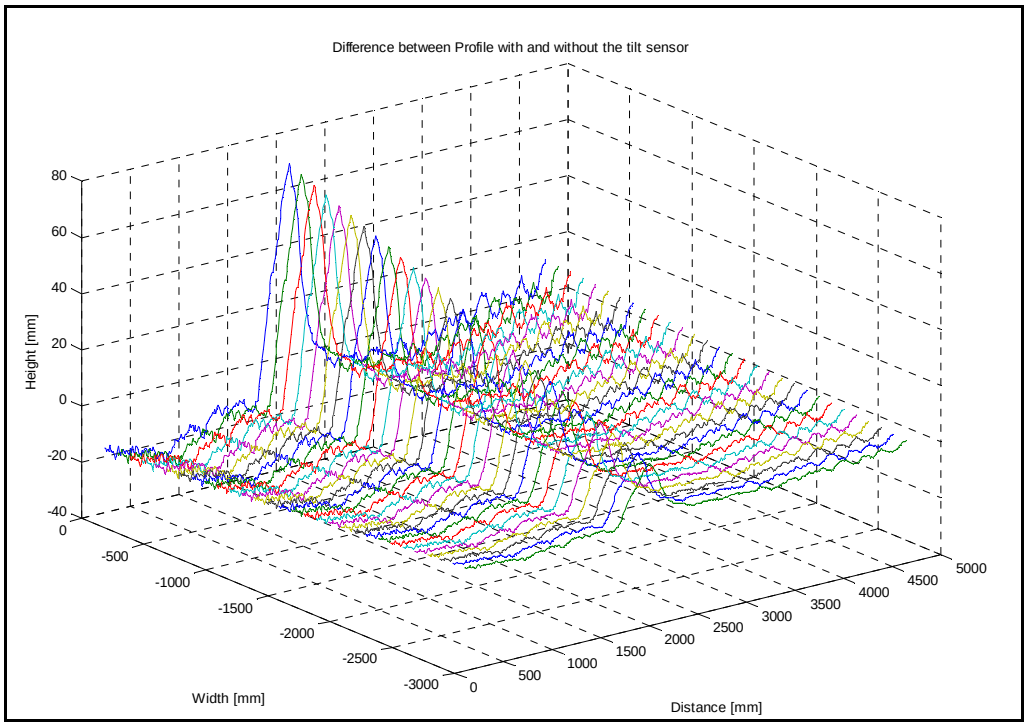

Figure 35: Difference in the profile of the flat concrete surface with and without the orientation of the profilometer.

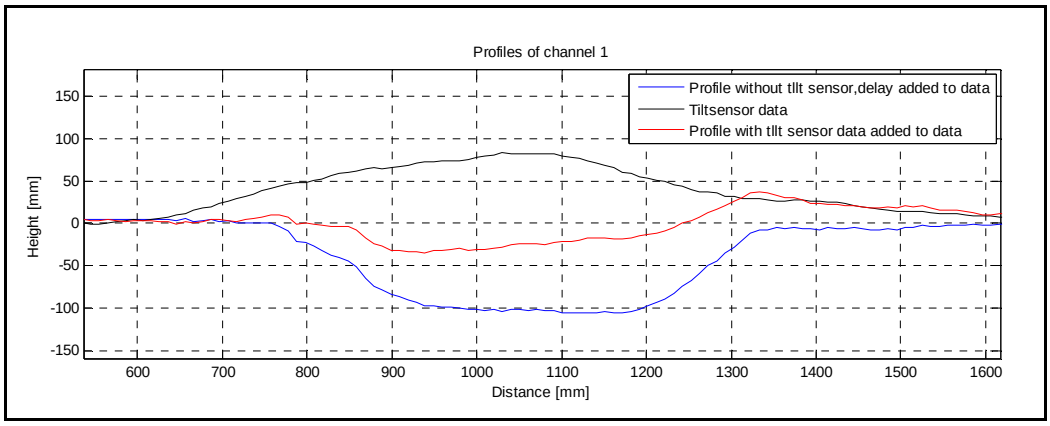

Figure 36: Profile of channel 1 for flat test section with Can-Can Machine.

The third test conducted on the Can-Can Machine is a test that assesses the profile of test bumps profiled with the wheels of the profilometer also moving slowly over obstacles. Figure 37 shows the actual test section in which the Can-Can Machine profiled from left to right. Figure 38 shows the profiled test section. The top figure indicates the profile corrected using the tilt sensor data while the bottom figure indicates the uncorrected profile. The test section layout is as follows, the profilometer profiles a flat section with the left wheel of the profilometer moving over a 105 mm flat-top bump, and then a 55 mm flat-top bump is profiled without the profilometer moving over any obstacle. After the 55 mm bump is profiled the profilometer's left wheel moves over a 105 mm flat-top bump whilst profiling a 55 mm flat-top bump. Excellent results are achieved with the Can-Can Machine moving slowly over the obstacles in this test.

Figure 39 shows the different profiles of channel 1. This channel profiled the two 105 mm flat-top bumps just after the left wheel of the profilometer moved over them. The black line in Figure 39 is the tilt sensor data and it is clear that the slower profiling speed produces an accurate profile of the profiled terrain due to the fact that the tilt sensor data resembles the flat-top bump. The error in the profiled terrain is no more than 10%.

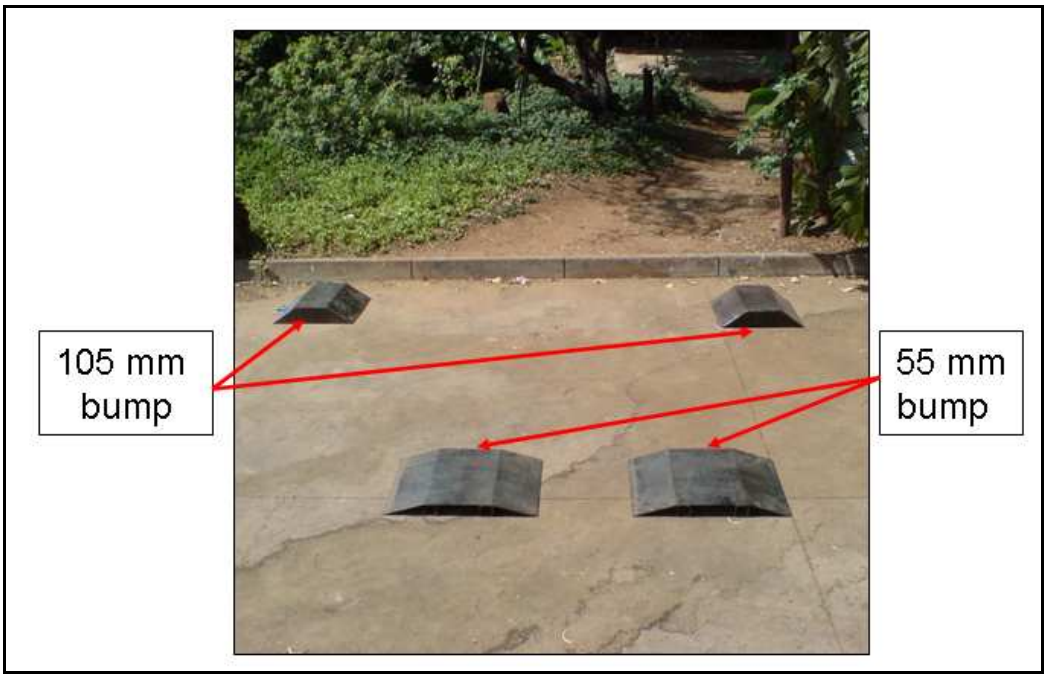

Figure 37: Final test section for Can-Can Machine.

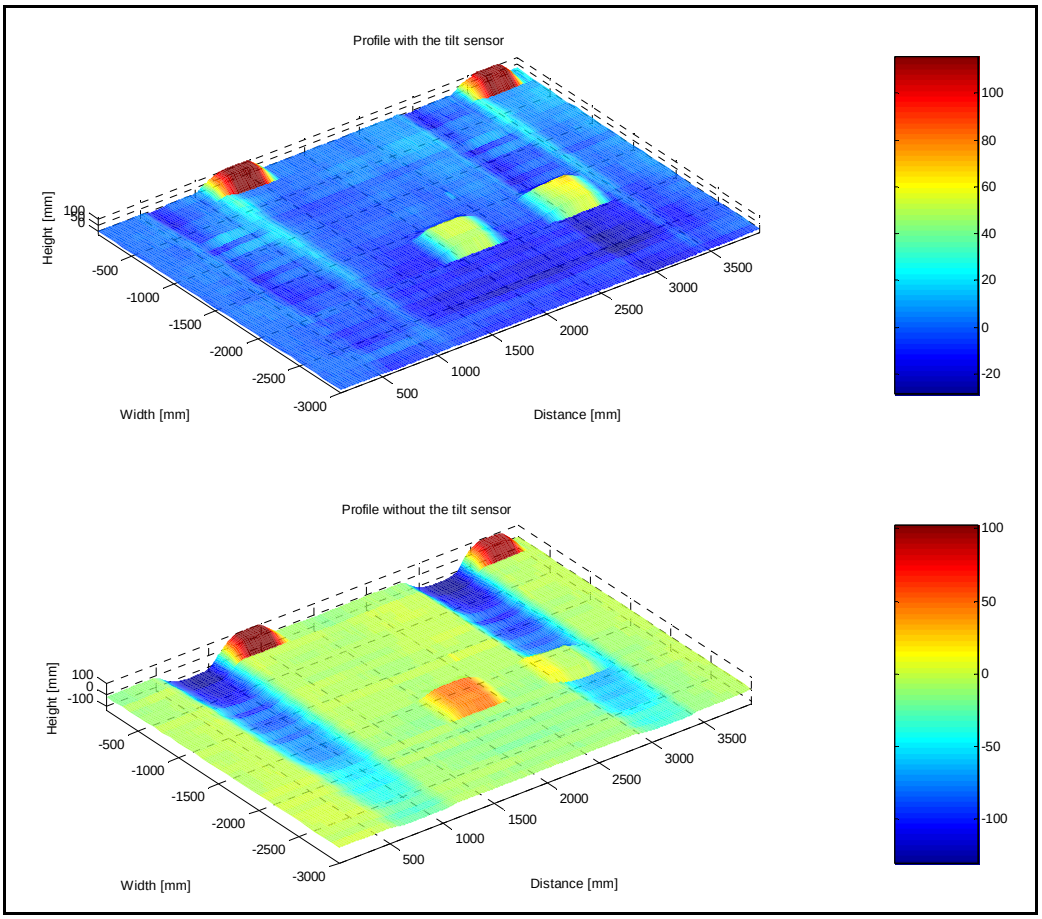

Figure 38: Profile of final test section for Can-Can Machine.

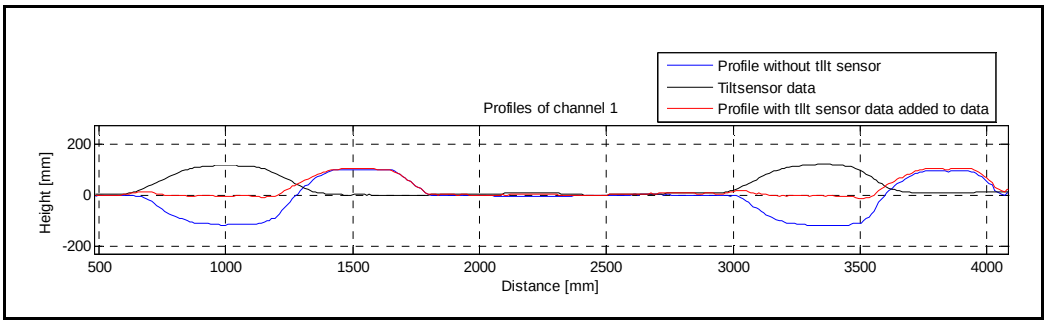

Figure 39: Profiles from channel 1 for final test section with Can-Can Machine.

The results obtained from the third test indicate that the Can-Can Machine is an accurate rough road profilometer which is not resource intensive and is capable of profiling any road surface. If very rough terrain is profiled the most accurate profile will be obtained by profiling the terrain as slowly as possible. The overall accuracy of the Can-Can Machine was found to be in the order of 5 mm (or less than 10% compared to the exact profile) when the profilometer moved over large obstacles.

3.2. Photogrammetric Profiling

Photogrammetric profiling basically consist of taking overlapping photographs of the terrain from a suitable height, perpendicular to the terrain, using a calibrated camera. Targets on the terrain with accurately known coordinates are included in the photographs and are used for orientation and absolute reference. This technique is regularly employed for generating contour maps from aerial photographs. The question to be answered here is whether it could be used to measure much smaller profiles using a camera mounted much closer to the terrain.

The photogrammetry and mapping for the present study were implemented thanks to CAD MAPPING cc. Paragraph 3.2.1 to 3.2.5 describe the procedure followed by CAD MAPPING cc in obtaining the profile captured on the photographs. Paragraph 3.2.6 describes the test section employed to validate the use of photogrammetry to capture the profile of a rough road at such a low vertical height from the ground.

3.2.1. Camera calibration

An in-house camera calibration was done with the use of the calibration grid as seen in Figure 40. The calibration grid is a pattern of dots specifically designed for the calibration software. Each position on the grid is assigned a calibration value to determine the lens distortions, focal length and size of the

image (see attached calibration certificate in Appendix A). Camera calibration is a method for accurately determining values for a camera's parameters. Once a camera is calibrated, it will provide accurate measurements necessary for photogrammetry.

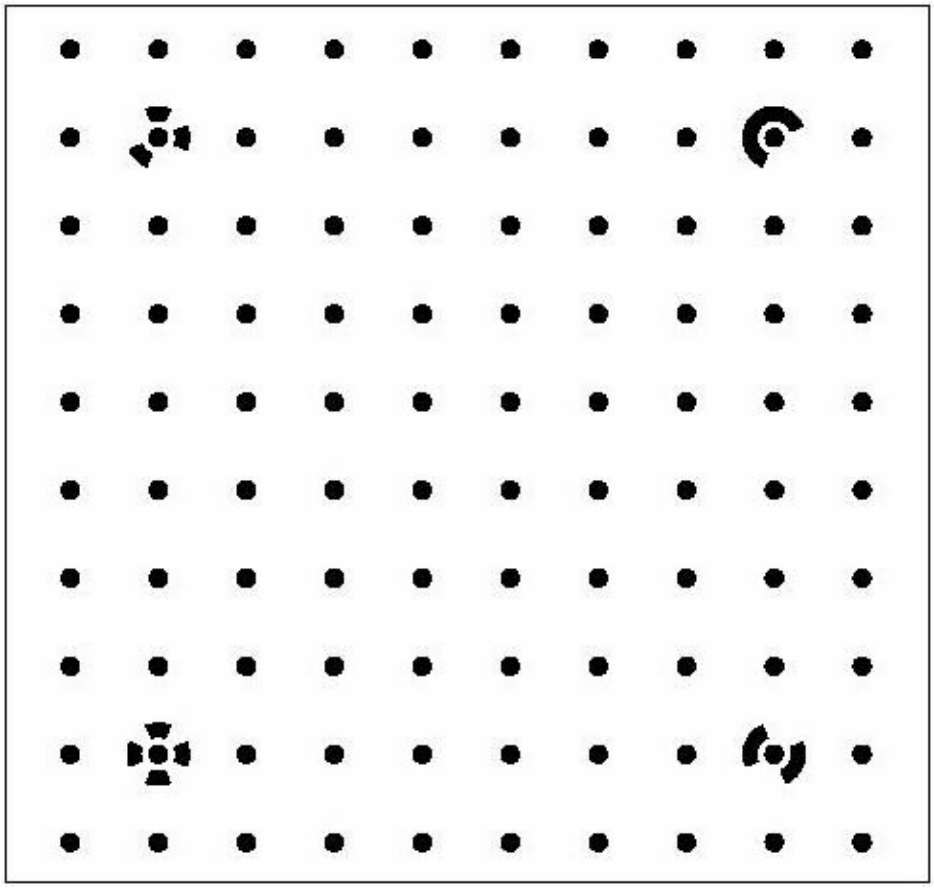

Figure 40: Calibration grid used for camera calibration.

3.2.2. Ground control

Pre-determined control points were marked with the use of targets along the terrain to be mapped and surveyed using a Total Station provided by the Topographical Department of The University of Pretoria and Pro Mapping cc (see Figure 41). Coordinates in a local system were obtained. A Total Station was used because the DGPS could only provide an accuracy of 12 mm on the position of the points surveyed, as where the Total Station was able to obtain a 3 mm accuracy. This accuracy was required to obtain exploitable results with the use of photogrammetry and gave an overall accuracy of 2 mm to 5 mm on the profile.

Figure 41: Ground control points surveyed using a Total Station.

3.2.3. Mapping

After the camera was calibrated and the control points were surveyed, photographs of the test section were captured with a standard off-the-shelf 5 mega pixel Sony Cyber Shot Digital camera. The lens of the digital camera was a Carl Zeiss lens with 3 x optical zoom which is equivalent to a 35 mm photography lens. For the test section the camera was placed in a custom build cradle as shown in Figure 42. The cradle was suspended 2 m above the ground between two vehicles with the use of a rope and pulley system. The imagery was subjected to further analysis using a digital photogrammetric workstation (see Figure 43).

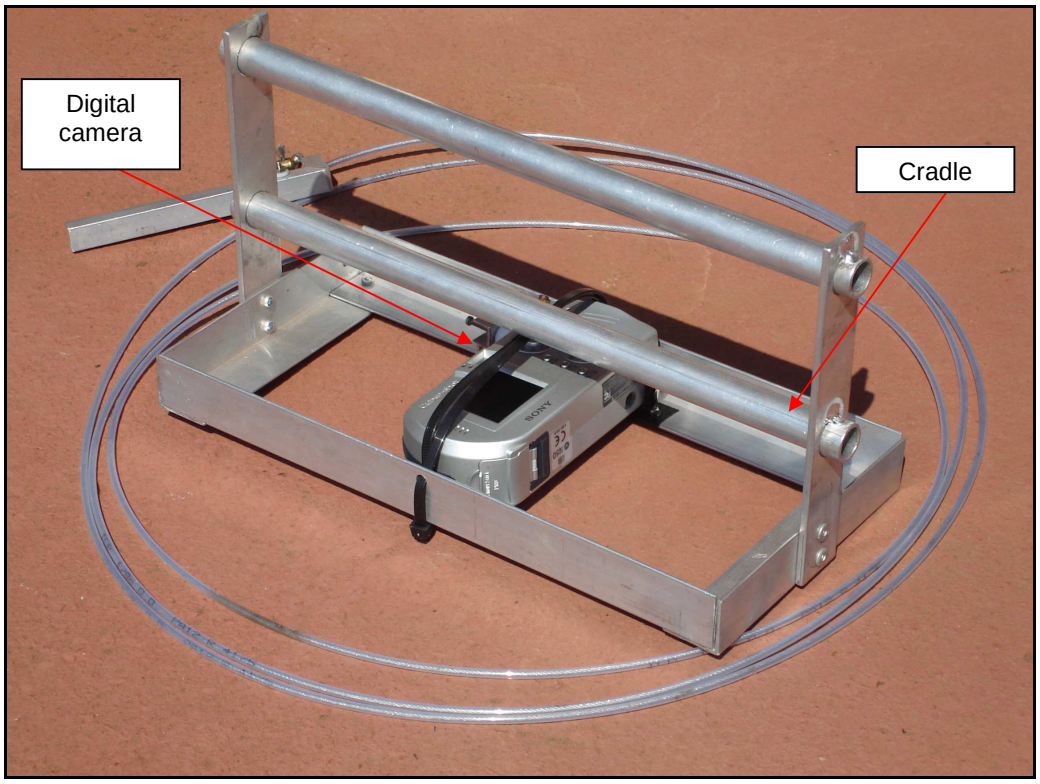

Figure 42: Cradle used for photogrammetry test section.

Figure 43: Digital photogrammetric workstation.

3.2.4. Triangulation inner orientation

An inner orientation was measured by observing the corners of each image as fiducial marks. The reference values for the physical position of the fiducial marks were obtained from the calibration certificate.

3.2.5. Aerial Triangulation

Aerial triangulation is a combined procedure used to determine the transformation from image coordinates to model and then ground coordinates. The routine enables users to observe Photo Ground Control (PGC) points and relative points, which were revered to as Von Gruber positions, in the stereo pairs along the entire strip (see Figure 44). These measurements were then used to determine perspective centre coordinates and exterior orientation angles. The observations can be used in a Bundle Block adjustment. The results determined by the Bundle Block can then be used in the absolute orientation of the stereo pairs.

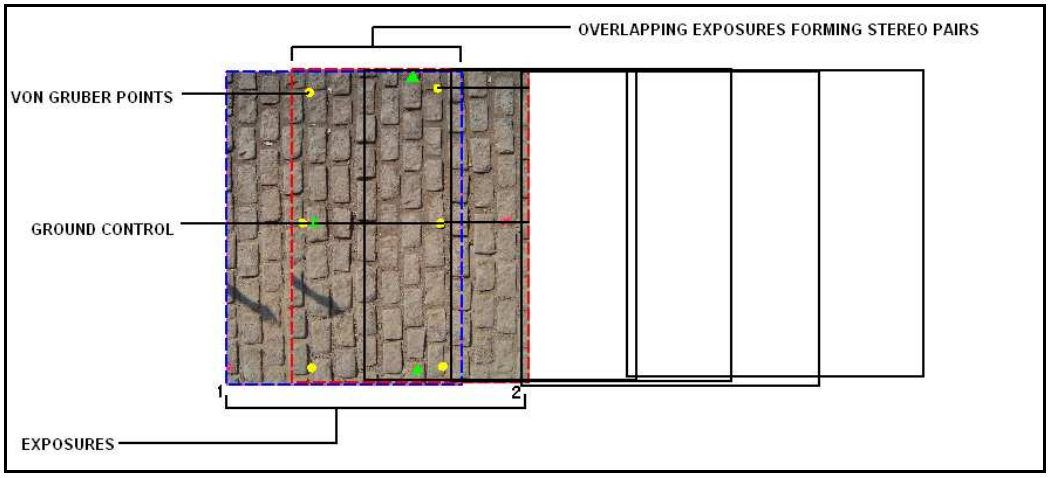

Figure 44: Stereo pairs, von Gruber points and ground control.

Break lines are read to determine the Triangle Network (TIN).The triangles provide three-dimensional information for surface creation and modelling. An example of the break lines and triangles are shown in Figure 45.

Break lines

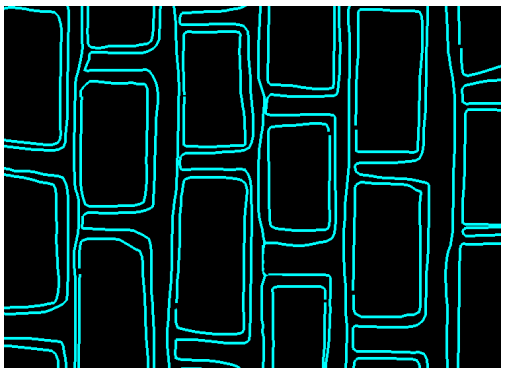

Triangles

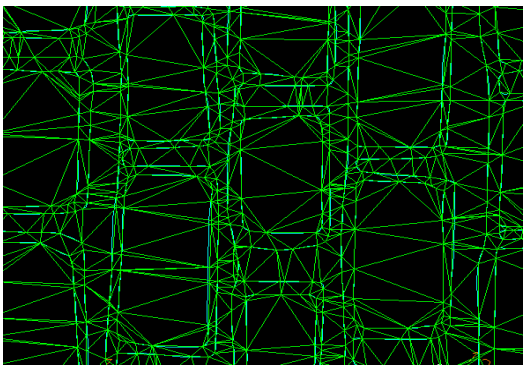

Figure 45 (a) and (b): Example of break lines and triangles.

3.2.6. Test section for photogrammetry

To determine if photogrammetry could be used for profiling obstacles at a close range an indicative experiment was conducted. A test section for photogrammetry was set up and contained objects such as a bucket, a book, a tennis ball and a bottle.

A typical photograph, as used for photogrammetry, is shown in Figure 46. Old compact discs were used as the control points. These points were measured and used to model the test section.

The procedure as described in paragraph 3.2.1 to 3.2.5 was put into process and a model of the test section was created. The data points were used in Matlab to plot a top view of the test section as well as a three dimensional model. The top view can be seen in Figure 47. A remarkable resemblance between the photograph captured from above and the top view of the model was obtained together with an accuracy of 10 mm. The photograph taken of the test section, shown in Figure 48 compares well the model in Figure 49.

The model of the bottle does not really match the actual bottle. This is due to the height ratios of the camera to the ground and the top of the bottle to the camera. An example in normal photogrammetry with the same problem would be the modelling of a very high and slender building at a rather low flying altitude. This problem does not occur with the bucket because of the cross sectional area of the bucket almost equalling the height. The large ball and small cube seen in Figure 48 were not part of the model in Figure 49.

The results from the test section were satisfactory and it was decided to proceed with the profiling of the Belgian paving at the Gerotek test facilities, utilizing this concept. This is described later in paragraph 5.

Figure 46: Top view of test section as captured with digital camera.

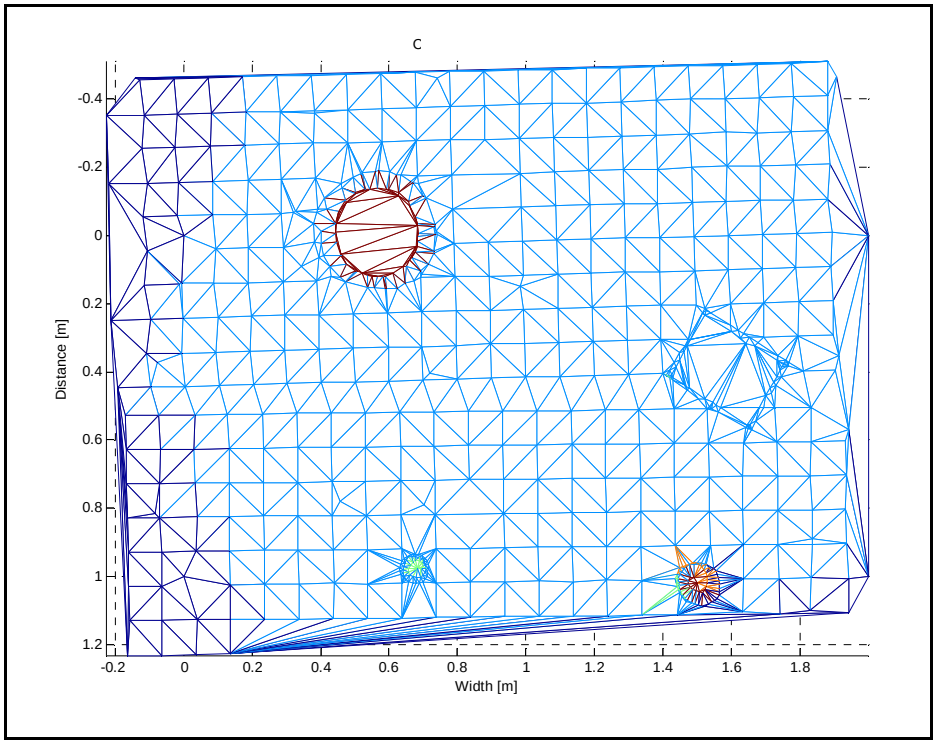

Figure 47: Model of top view for test section.

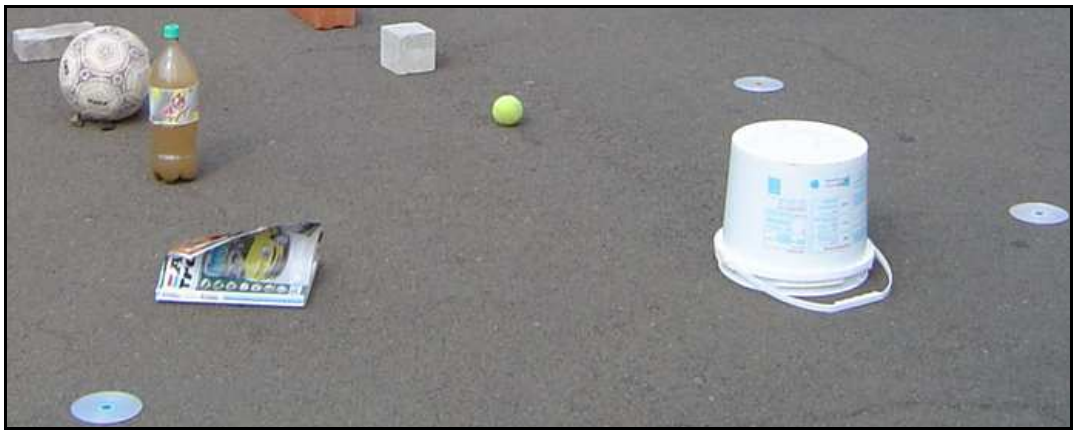

Figure 48: Three-dimensional view of test section.

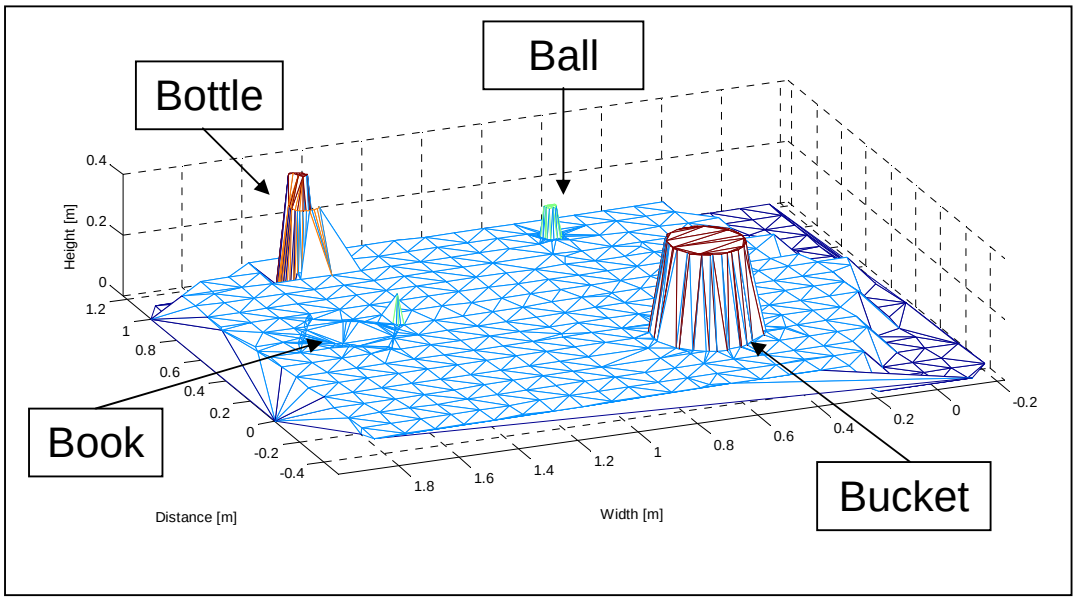

Figure 49: Three-dimensional model of test section.

3.3. Laser Scanner

Although commercial 3D laser scanners are available, cost was prohibitive for the purpose of the current study and an in-house system was developed.

The Laser Scanner profilometer utilizes a S80-MH-5 Data Sensor Laser Distance Sensor to measure the profile of the terrain from a vertical distance of 2m. The Data Sensor is mounted in a purposely build gimball which is mounted on a tripod. The gimball enables the Laser Distance Sensor to rotate about two perpendicular axes. The rotation is controlled by two 9438iupf 1.8˚/step Stepper motors. A PC 104 data acquisitioning system controls the stepper motors, measures and saves the angles of the rotations of the stepper

motors and the distance measured by the Laser Distance Sensor from the sensor to the terrain. Figure 50 shows the Laser Distance Sensor and stepper motors mounted on the gimball.

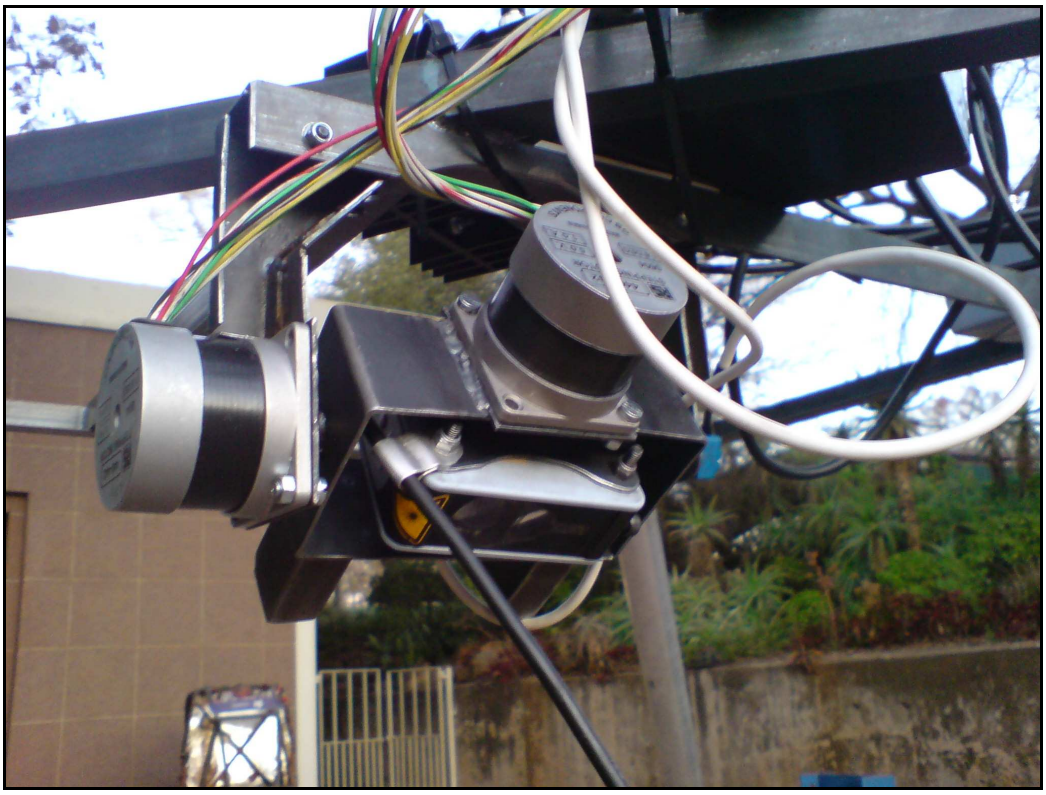

Figure 50: Gimball containing two stepper motors and a DM-80 Laser Distance Sensor.

The Laser Distance Sensor can measure a distance from 300 mm up to 4000 mm (on a surface which is from 90% white to 18% grey) with 5 mm accuracy. It is found that the Laser Distance Sensor is very sensitive to the surface to which the measurement is taken. The Laser Distance Sensor has a class 2 laser and the sensitivity on the measured surface is due to the laser only being a 1 milliWatt laser (mW), thus if most of the light is absorbed by the measured surface the laser is incapable of measuring the distance from the lens of the laser to the surface of the terrain. Tests done with and without uv-filters shows that the Laser Distance Sensor does not read any measurement on asphalt terrain whether the asphalt is in a shaded area or in direct sunlight. The Laser Distance Sensor does on the other hand measure on a shaded concrete surface. This means that measurements had to be taken in the dark.

The Laser Scanner profiles a 2.4 x 2.4 m terrain section at a time. If the terrain is viewed from the top, the Laser Scanner starts the profile by saving the angles of the stepper motors and the distance from the Laser Distance Sensor to the terrain, with the Laser Scanner in the centre of the profiled square and on three different corners of the profiled square. The laser is centred by suspending a pendulum from the base of the Laser Distance Sensor. This information is used as the reference from which the rest of the profile is

calculated. The Laser Scanner then moves towards the bottom left corner of the profiled square. Next the Laser Scanner profiles 32 points (referred to as the fast steps) in the positive longitudinal direction (from left to right if viewed from the top) after which the Scanner moves one step in the lateral direction (from the bottom to the top, referred to as the slow steps) and then again scans 32 points in the negative longitudinal direction (right to left).

A 10 second long-exposure photograph captured the movement of the laser and is shown in Figure 51. Figure 52 shows each channel of data as it is recorded. The top graph shows the longitudinal movement of the Laser Distance Sensor and the middle graph the lateral movement. The distance measured from the Laser Distance Sensor to a flat surface is displayed in the bottom graph. The angle of the rotation about both axes is measured with single turn potentiometers on each axis.

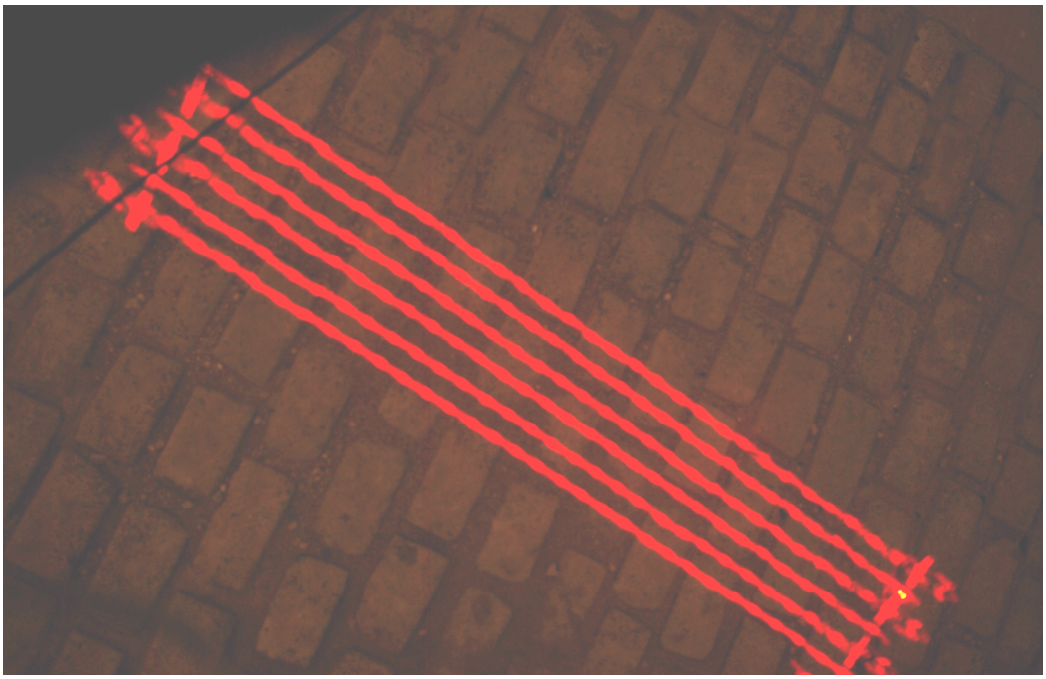

Figure 51: Top view of the laser movement.

Figure 53 shows the coordinate system used in calculating the scanned profile. The variables in blue are the measured variables (ϑ, γ, L) and the red variables (x, y, C, H, β) are calculated.

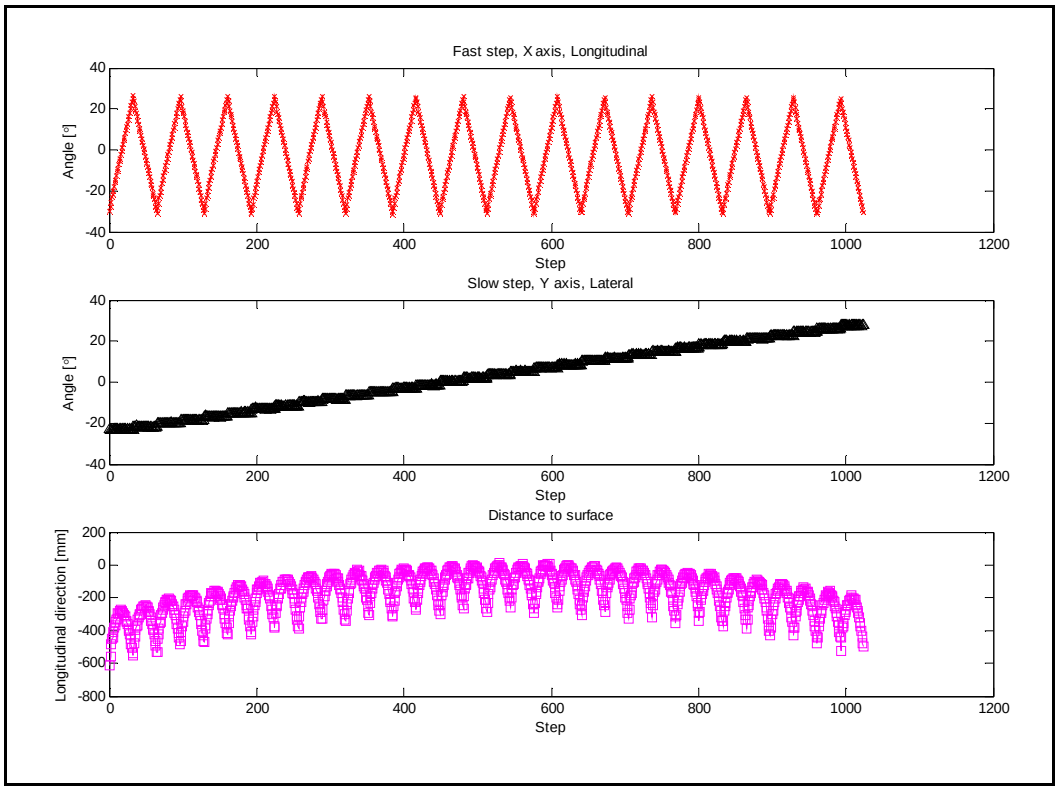

Figure 52: Measured data of a flat surface.

The profile of the measured terrain is calculated as follows:

$$\tan\gamma = \frac{y}{H}$$

$$\tan\vartheta = \frac{x}{H}$$

$$\tan\beta = \frac{C}{H}$$

and

$$C = \sqrt{x^2 + y^2}$$

Substituting gives

$$C = \sqrt{\tan^2\vartheta + \tan^2\gamma}$$

and

$$\beta = \arctan\left(\frac{C}{H}\right)$$

C, x and y can be calculated independently of H if the angles are known.

$$H = L\cos\beta$$
$$x = H\tan\vartheta$$
$$y = H\tan\gamma$$

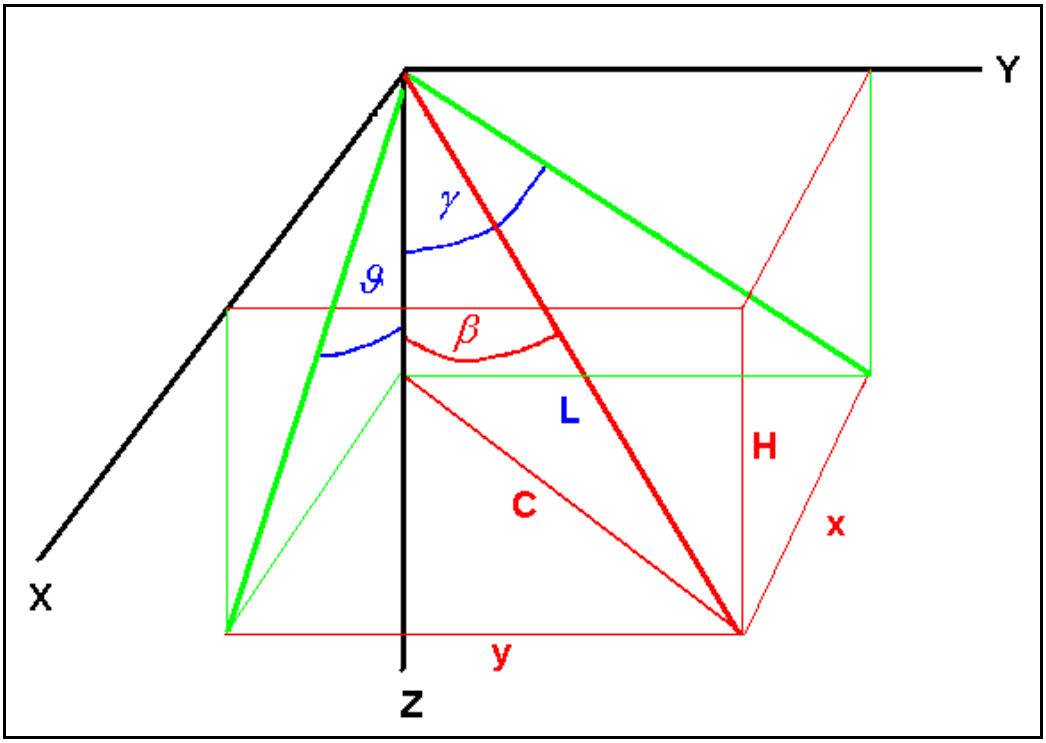

Figure 53: Description of coordinate system used for Laser Scanner calculations.

3.3.1. Test section for Laser Scanner

A test was performed on a concrete surface with a 500 x 360 x 58 mm concrete block on it. Figure 54 shows the concrete block on the larger concrete surface.

The surface was profiled at night to ensure that the Laser Distance Sensor was actually measuring correctly. Figure 55 shows the surface as profiled with the Laser Scanner. It can be seen that the profiled surface is slightly convex where the actual surface is flat. This is due to the construction of the gimball. The axis on which the Laser Distance Sensor rotates, goes through the centre of mass and not through the centre of the lens. Thus the lens is moving around instead of remaining in one position and just rotating on the axis. The difference in the position of the axes is added when the profile is determined. The profile is adjusted but some concavity remains. The error is accepted due

to the fact that the profilometer is still a prototype and will be improved in a revised design.

The surface is slightly rougher than the actual terrain because a mesh with an average block size of 60 x 60 mm is obtained with the use of a single step on the stepper motors. The mesh is not equally sized all over because the Laser Distance Sensor is rotated at a constant angle (a single step on the stepper motors). Thus the points neighbouring the centre has a smaller mesh block size and the points near the edge have a larger mesh block size. A smaller mesh may be obtained if reduction gearboxes are integrated onto the stepper motors which will reduce the step to each point.

The accuracy of the Laser Scanner is limited by the gimball, however a revision of the design is required in which the gimball may be revised and reduction gearboxes on the stepper motors incorporated.

The Laser Scanner is used to profile a section of the Belgian paving and is compared with the profiles of the Can-Can Machine and the Photogrammetry in paragraph 5.

Figure 54: Test block for Laser Scanner with 500 x 360 x 58 mm concrete block on a flat surface.

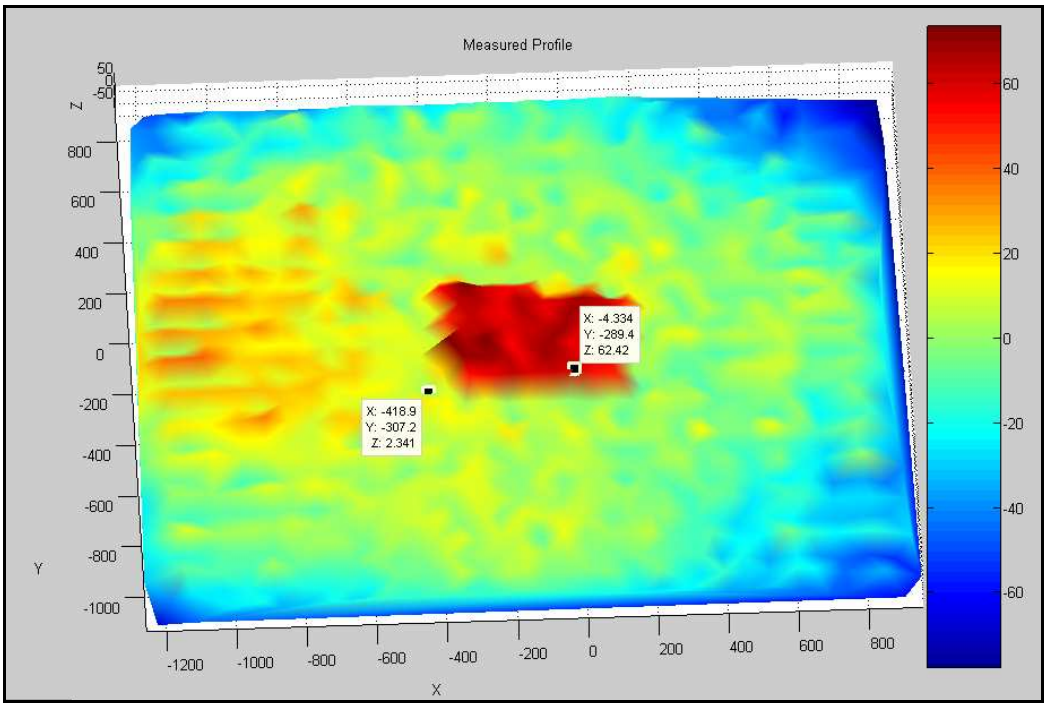

Figure 55: Measure profile of a flat concrete surface with a concrete block on top.

3.4. Summary of the three profiling methods

In this paragraph each of the three proposed profilometers were reviewed and the operational functions of each were examined. Test sections were profiled with each of the proposed profilometers and the results were evaluated.

It was found that the Can-Can Machine is a simple and effective profilometer with the ability to profile rough terrain. The Can-Can Machine can profile a terrain with an overall accuracy of < 5 mm. The maximum profiling speed of the Can-Can Machine is 0.98 km/h and produces a profile with a grid size of 100 mm in the lateral direction and 10.18 mm in the longitudinal direction. The width of a Can-Can Machine profile is 3 m.

The Photogrammetric profiling method is a valid and accurate profiling method with an accuracy of 5 mm, however it remains extremely slow and resource intensive. The profiling speed of the Photogrammetric profiling method is in the order of 8 hours/m^2.

The Laser Scanner is a time consuming Profilometer, however it remains a prospective profilometer still in the development phase. The Laser Distance Sensor has an accuracy of 5 mm but the accuracy of the total system is limited by the gimball. The Laser Scanner profiles with an average longitudinal and lateral resolution of 60 mm and with a total profile width of 2,4 m at a profiling speed of 8 m/hour. The accuracy of the profiler may be improved using a higher quality laser.

4. Profiling simple obstacles with the Can-Can

In this paragraph, obstacles with know dimensions and shapes will be profiled with the Can-Can Machine. These obstacles will be profiled to determine the level of accuracy obtainable with the use of the Can-Can Machine. The accuracy of the Can-Can was determined by comparing the Can-Can profile of an obstacle with the actual profile.

4.1. Discrete bumps

Discrete bumps and holes were profiled with the Can-Can Machine at the Gerotek test facilities. These obstacles are permanent and offer repeatability.

4.1.1. 100 mm semi-circular bump

The 100 mm semi-circle bump is a bump constructed out of steel and is used in the testing of suspensions on military vehicles or any all-terrain vehicle. The semi-circle bump is mounted on a 12 mm base plate so that it may be bolted to the ground. The base plate also strengthens the semi-circle. Handles were placed on the side of the bump for easy movement. Figure 56 shows the 100 mm bump.

Figure 56: 100 mm semi-circular bump.

Figure 57 shows the difference between the profiled bump and the actual bump. The profiled bump shows a small distortion in the profile. The distortion was caused due to part of the arm coming into contact with the bump and moving over the bump. Due to the contact between the arm and the bump the arm was raised instead of the arm being elevated by the wheel as the wheel travelled over the bump.

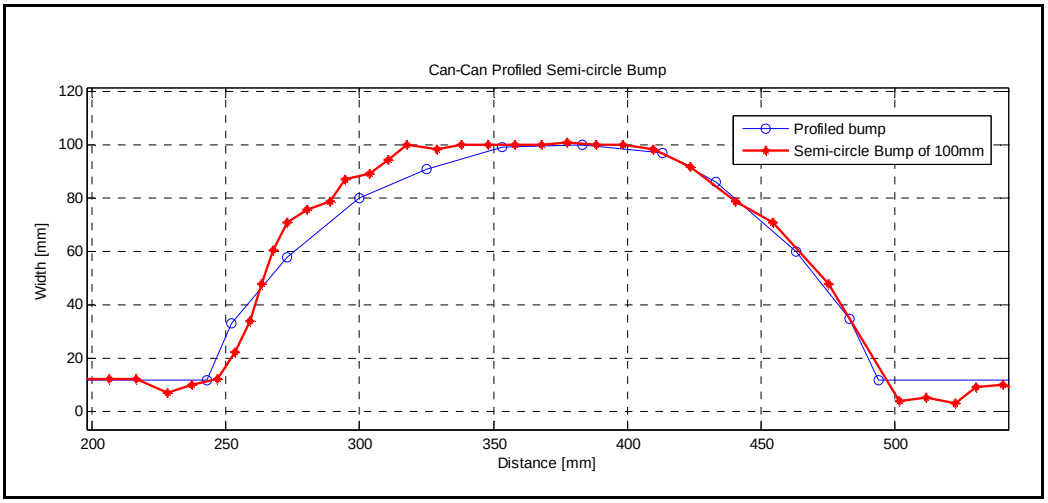

Figure 57: Profiled and actual 100 mm bump.

Although measurements are taken at constant horizontal intervals of 10.18 mm, the horizontal (X) data points are not equally spaced due to the effect of the arm's angle described in Figure 27. The horizontal distance between data points are therefore compressed as the arm rotates upward and again expands as the arm moves down after the crown of the obstacle.

The calculated RMS value of the vertical height of the bump was 55.42 mm and the RMS value of the profile was equal to 52.48 mm. The RMSE between the actual profile and the Can-Can profile was calculated to be 8.96 mm. The RMSE was higher than expected due to the contact between the middle of the arm and the obstacle as previously described. The RMSE and overall correlation obtained between the profiled bump and the actual bump was satisfactory. The error between the profiled bump and the actual bump in Figure 57 is exaggerated due to the difference in the x and y axis scaling.

4.1.2. Parallel and angled corrugations

The parallel and angled corrugations are used in simulating a corrugated gravel road with 25 mm bumps. The corrugation tracks are set in concrete to provide repeatability in any weather without the surface changing or deteriorating. The corrugation tracks are 4 m wide and 100 m in length. The Can-Can Machine profiled the terrain without any of its wheels on the profiled terrain. This increased the accuracy of the profile due to the fact that there was no vertical movement of the profilometer. The profiles of the corrugations were very representative of the actual bump and a profile of a single corrugation bump is shown in Figure 58.

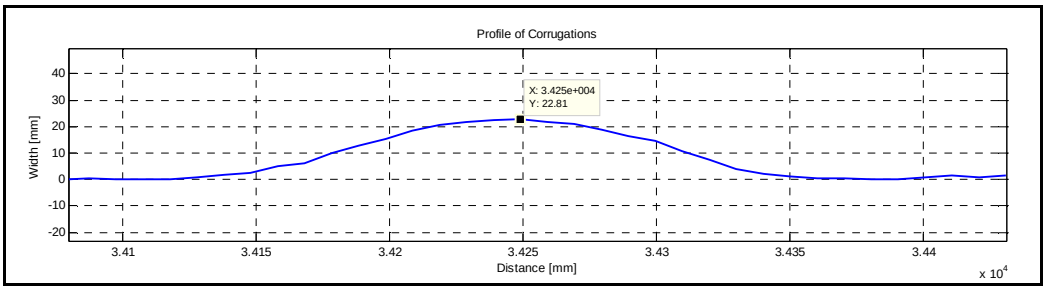

Figure 58: Profile of a corrugation bump.

The vertical RMS values of the actual bump and the profiled bumps could not be compared as the actual dimensions of each bump varied to some extent and were not constant. The profiled height of the corrugations were profiled at 20-26 mm where as the actual corrugations were alleged to be 25 mm.

The actual parallel and angled corrugations are shown in Figure 59 and Figure 61 respectively. Sections of the full profiles of the parallel and angled corrugations are shown in Figure 60 and Figure 62 respectively. The corrugation tracks were built at a slight sideways slant to facilitate water drainage as seen in the profiles.

The profiles of the corrugations were satisfactory as they were visually very representative of the actual tracks and the profiled bumps were within a tolerance of 5 mm of the alleged 25 mm. The deviations in the height of the bumps were as a result of years of testing large military vehicles on the track.

Figure 59: Parallel corrugations at Gerotek.

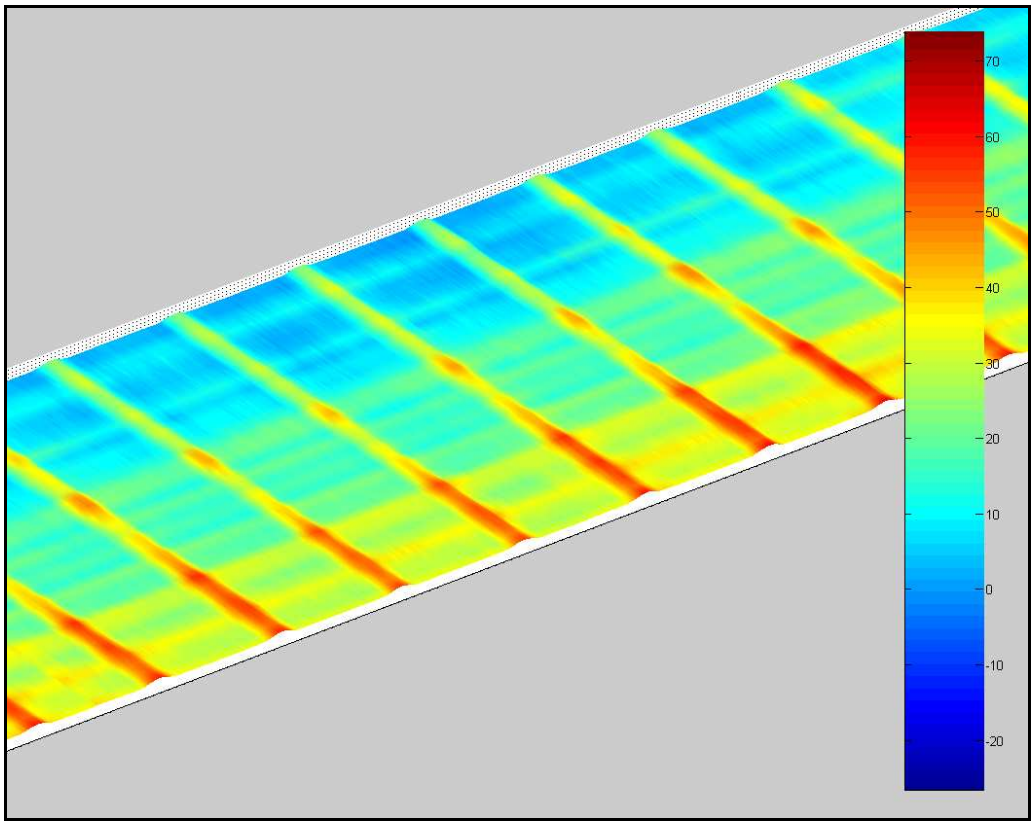

Figure 60: Profiled parallel corrugations.

Figure 61: Angled corrugations at Gerotek.

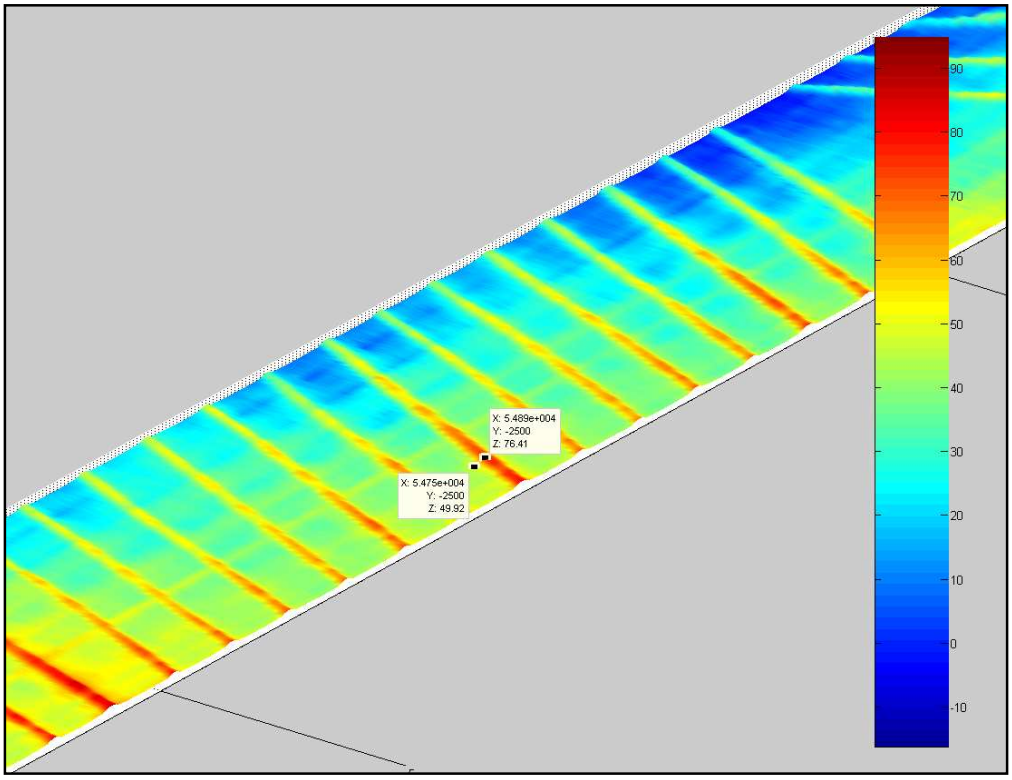

Figure 62: Profiled angled corrugations.

4.1.3. Pot-Holes

The pothole track at the Gerotek test facilities is used for testing the capability of a military vehicle's suspension and steering links in withstanding the input forces into the suspension by driving through 80 mm deep potholes in the road. The profile's accuracy was confirmed in Figure 63, where the actual profile was evaluated and compared with the profiled pothole.

The profile appears rough due to the scale of the graph. The rounded edge in the Can-Can profile is cause by the motion of the small wheels at the end of the arms, which provide a smoother transition over the edge.

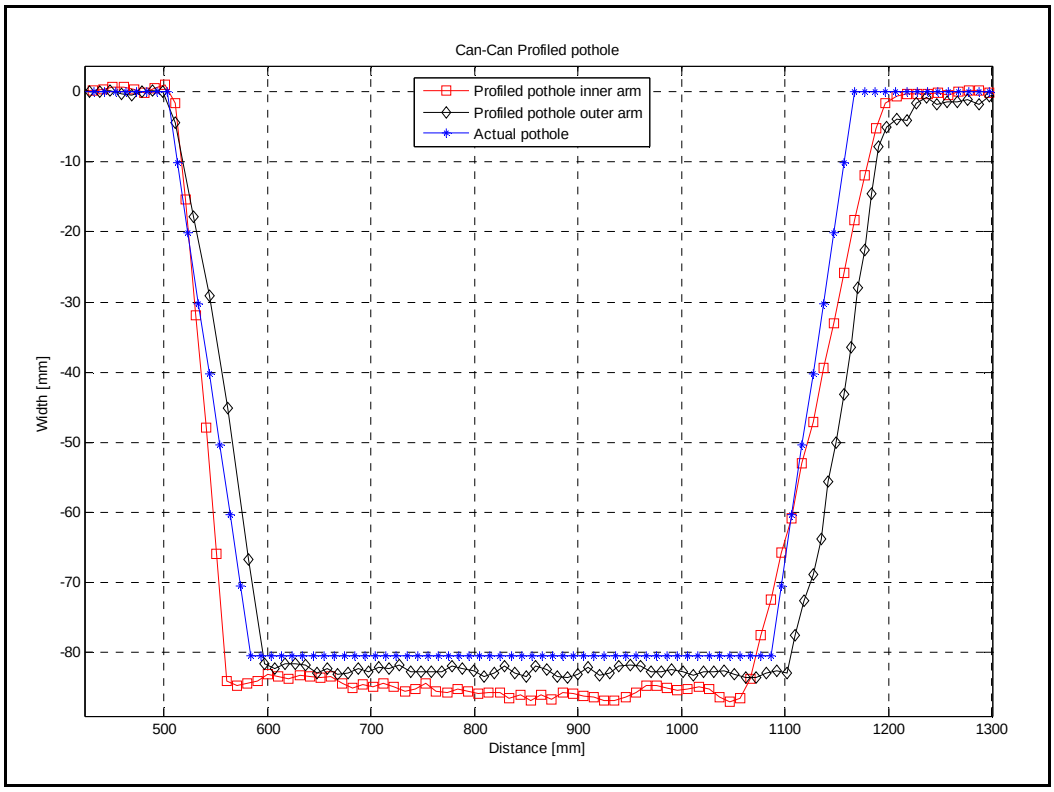

Figure 63: The actual profile and the Can-Can profile of the pothole.

The rounded top edge on the profile of the pothole is also due to wear on the actual pothole. The RMS value of the actual pothole is 46.344 mm and the RMS value of the inner and outer arms is 41.291 mm and 39.497 mm respectively. The RMSE of the profiles is 7.43 mm for the inner arm and 4.28 mm for the outer arm. The profile from the inner arm is deeper as each pothole is sloped towards the inside of the track to assist water drainage. This slope caused the higher RMSE calculated for the inner pothole profile. The difference in the slope of the walls of the inner and outer pothole profiles were due to the construction of the pothole. The profiles of the base of the pothole are rough due to sand and small stones in the actual pothole during profiling. Figure 64 and Figure 65 shows the actual pothole and the profiled pothole tracks respectively. The profile obtained from the Can-Can Machine is accurate and is a good representation of the pothole track. The 35X35 mm mesh grid covering the drain in the pothole is visible in Figure 65.

Figure 64: Pothole track at Gerotek.

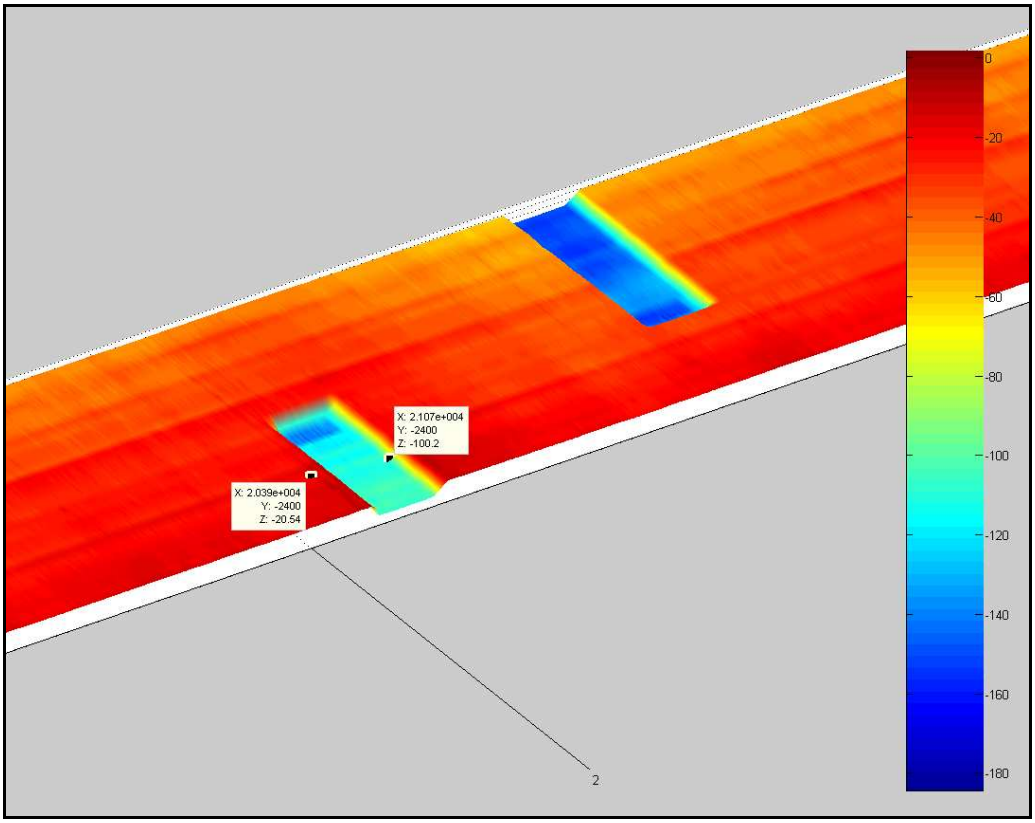

Figure 65: Profiled pothole track.

4.2. Summary on discrete bumps

The discrete bumps were profiled in an attempt to validate the accuracy of the Can-Can Machine. The so called actual bumps used in the graphs were theoretically representative of the bumps used during the tests. The theoretical bumps were generated with the information supplied by the test facility. Due to years of constant testing of large military vehicles at the test facilities deviations between the actual and theoretical bumps were expected.

Deviations in the profile of the 100 mm semi-circle bump were due to the arms making contact with the obstacle. This may be avoided with the adjustment of the curve and angle of the arms. Deviations in the profile of the pothole and corrugations were caused by wear on the concrete surface as well as deviations in the actual profile during construction of the potholes.

The results obtained with the profiling of the Can-Can Machine indicated that the Can-Can Machine can profile a terrain with an accuracy in the order of 5 mm.

5. Profiling 3-Dimensional rough road

The Gerotek Test Facilities was established to satisfy an urgent need for an all-encompassing test facility at which vehicle design and development could be monitored in a typical South African environment (Gerotek, 2007). This first class test facility offers unique heat and altitude test conditions. Figure 66 shows an aerial photograph of Gerotek (Google Earth, 2007).

Figure 66: Gerotek Test Facility (Google Earth, 2007).

The tracks on the Suspension track at Gerotek are used to perform repeatable and comparative suspension tests under simulated conditions. These tracks are used to test the body structure, body mountings, suspension, axles, steering, chassis, driveline durability and ride comfort. The parallel corrugations, angled corrugations and potholes on the Gerotek suspension track were profiled in paragraph 4, where the ability of the Can-Can Machine to profile simple obstacles was investigated. In this paragraph, profiling of 3-dimensional rough roads is performed.

The Belgian paving on the suspension track was profiled using all three methods proposed in paragraph 3. The fatigue track, Ride and Handling track as well as the rough track was profiled using only the Can-Can Machine due to the time consuming nature of the Photogrammetry and Laser scanner methods which make them unfeasible for profiling large sections of terrain.

5.1. Suspension Track - Belgian Paving

The Belgian paving is mainly used for testing ride comfort and durability of a vehicle. Figure 67 shows the Belgian paving at the Gerotek Test Facility. The Belgian paving was profiled with the Can-Can Machine, Photogrammetry and the Laser Scanner. The profiles obtained with the three methods are compared with each other by comparing the Displacement Spectral Densities.

Figure 67: Belgian paving at Gerotek.

5.1.1. Can-Can Machine

The Can-Can Machine was the first profilometer used to profile the full 100 m of the Belgian paving. The profile of the terrain is available as soon as the data is downloaded from the data acquisitioning system and run in a pre-written Matlab program. Figure 68 shows the Can-Can Machine in the process of profiling the Belgian paving. A section of the profile is shown in Figure 69. This is an excellent representation of the Belgian paving in colour. The Belgian paving was profiled with an accuracy of better than 5 mm and the Displacement Spectral Density of the profile is calculated, compared and examined in paragraph 5.5.

The Can-Can Machine profiled the Belgian paving at a speed of 0.98 km/h. The full 100 m of the Belgian paving was profiled in 12 minutes and the data reduction only required a few minutes.

Figure 68: Can-Can Machine profiling Belgian paving.

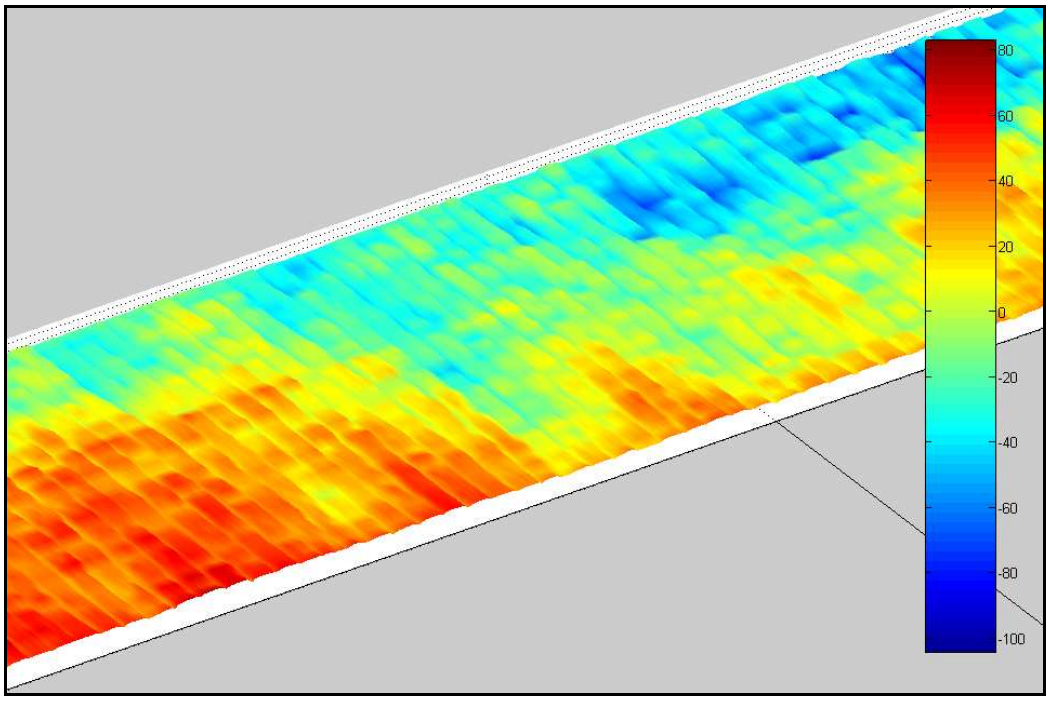

Figure 69: Can-Can profile of Belgian paving.

5.1.2. Photogrammetry

A Pentax K10D Digital camera with a PH-RBA 18-55 mm lens was used to photograph the Belgian paving. The Pentax K10D Digital camera has a stabilized ten mega pixel CCD. The PH-RBA 18-55 mm lens has an angle of view of 76 degrees at 18 mm and the focus distance was locked at the widest angle of view at 18 mm.

The photographs of the Belgian paving were taken with the use of a purposely build tripod with 6m long legs (see Figure 70). The tripod elevated the digital camera to a height of 4 m. With the camera positioned at 4 meters above the ground it was possible to capture the entire 4 m width of the Belgian paving. A 50 m section of the Belgian paving was profiled with the use of photogrammetry.

Figure 70: Tripod used to capture photographs.

The calibration certificate of the Pentax K10 camera is given in Appendix A. Figure 71 gives an example of the photographs used in the photogrammetry. The white squares in the photograph are the surveyed control points as described in paragraph 3.2.2.

Figure 71: Sample photograph used for photogrammetry.

Photographs of the 50 m section of the Belgian paving were captured with a 60 % overlap, after the control points were surveyed. The procedure as described in paragraph 3.2 was completed and a profile of the Belgian paving was produced. Figure 72 is a graphical representation of the Belgian paving as profiled with Photogrammetry. This profiling method has 3 mm accuracy but requires a great deal of time and funding to produce when compared with the Can-Can Machine. Figure 73 shows the Belgian paving profiled with Photogrammetry as plotted in Matlab.

Profiling a 50 m section of the Belgian paving with the use of the Photogrammetric method required 15 min/m to survey the control points and to capture the photographs. The mapping and processing of the photographs required in the order of 8 hours/m^2. This required time scale to profile 1 m^2 of terrain made the photogrammetric profiling method unfeasible to profile large sections of a terrain.

More terrain detail is apparent in Figure 72 and Figure 73 if compared with the profile obtained with the Can-Can Machine in Figure 69. A curvature effect on the individual photographed models can be seen on the 3-D model generated with Photogrammetry in Figure 72. This was a direct effect of an inconsistent lens calibration. It is also normal to get some distortion with the very wide angle lens (18 mm) used.

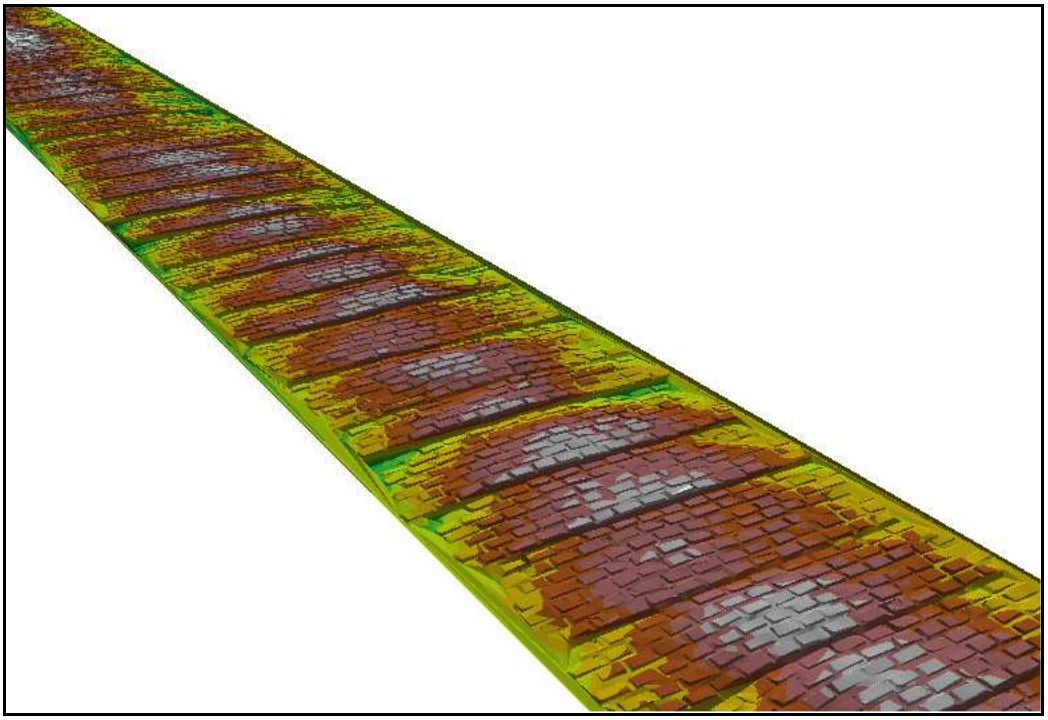

Figure 72: Belgian paving profile from Photogrammetry.

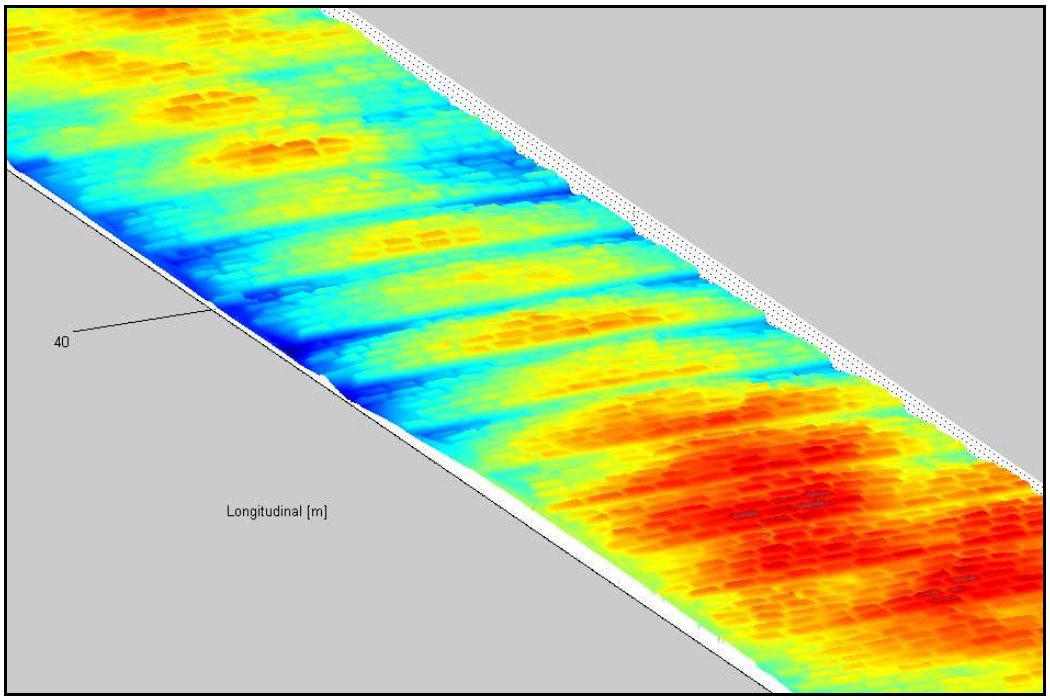

Figure 73: Belgian paving profile from Photogrammetry, plotted with Matlab.

The camera used to photograph the Belgian paving was a Pentax K10D Digital Camera with a standard 18-55 mm zoom lens locked in the 18 mm zoom setting. Off-the-shelf cameras are fitted with mass produced wide angle lenses in which the distortion is not significantly small enough for a photogrammetric application. The molds used to shape the mass production lenses are only calibrated at intervals of approximately 10 000 lenses produced. On photogrammetric assignments in practice, a professional medium format camera is used, these camera lenses are produced with minimum distortion and every lens is tested for inconsistencies. Every time a lens is made the lens mold is calibrated for optimum radial results. The medium format camera lens can be calibrated and the distortions are small enough to apply in a photogrammetric project. The radial distortion graphs in Figure 74 and Figure 75 show the different distortion results of the above mentioned lenses.

Pentax lens

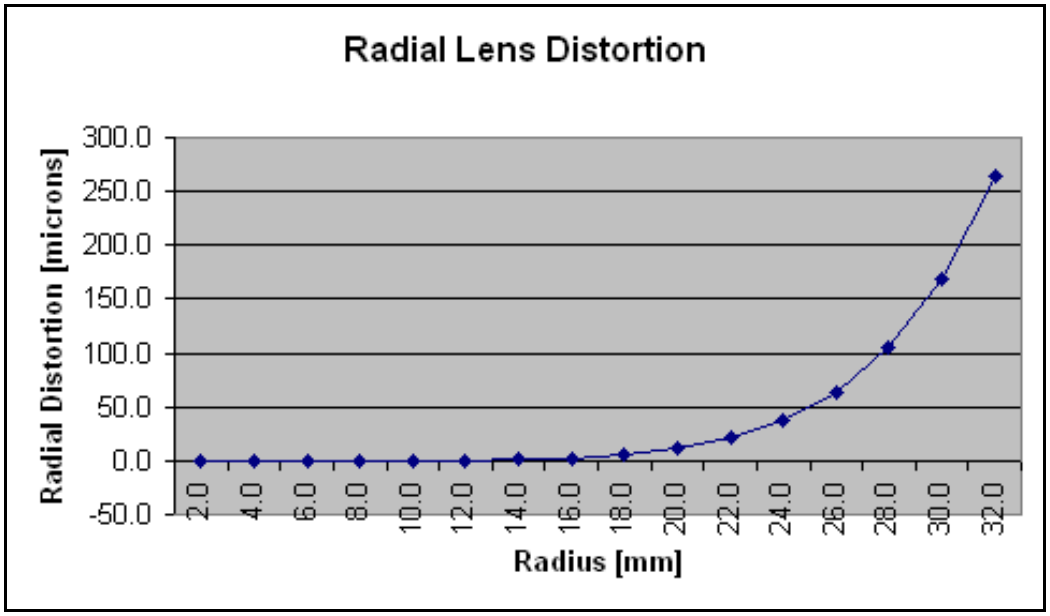

Figure 74: Lens distortion of the Pentax lens.

The Pentax lens yielded a distortion of up to 270 microns at the edge of the lens. In comparison the Hasselblad lens yielded a distortion of only 1.1 microns at the edge of the lens. The dome effect on the final 3-D model for the Belgian paving profiled with Photogrammetry was thus a direct result of this distortion in the lens. The distortions in the lens were exaggerated with the use of the colour representation in Figure 72 and Figure 73.

This project could not be executed with a Hasselblad camera since the lens used on the Hasselblad camera was a fixed lens with a longer focal length. A minimum of 8 meters was required between the lens and the target for optimal results. In addition the longer focal length on the Hasselblad camera reduces the distortion in the lens.

Medium format Hasselblad lens

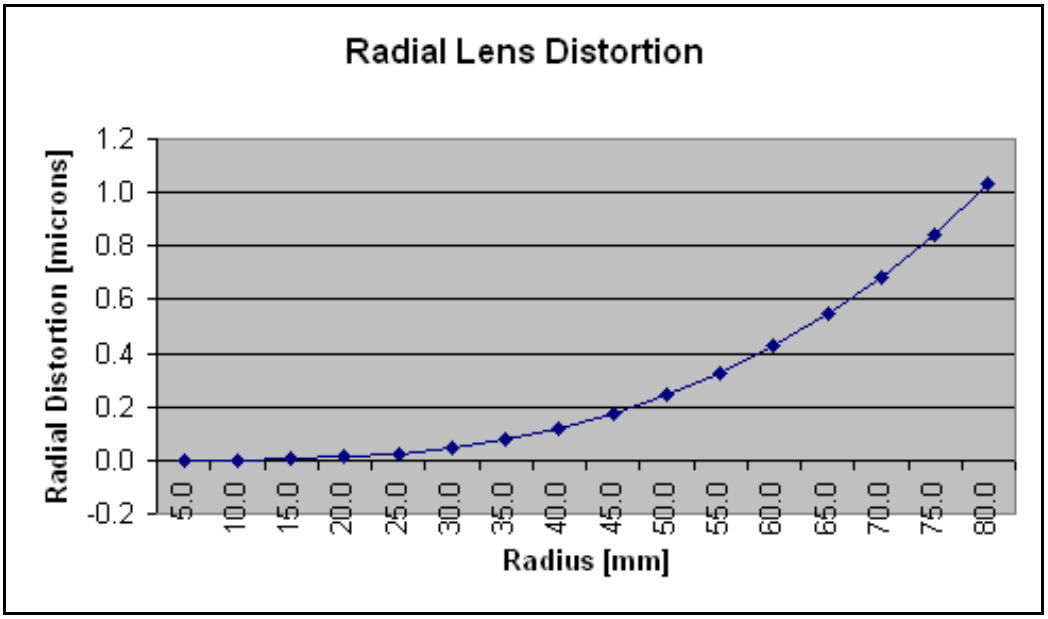

Figure 75: Lens distortions of the medium format Hasselblad lens.

It has been documented that some off-the-shelf 35 mm base digital cameras have been successfully calibrated to meet photogrammetric standards. The calibration software applied for this result was still in a development phase and not available in South Africa (Swart 2008).

The Displacement Spectral Density of the profile is calculated, compared and examined in paragraph 5.5.

5.1.3. Laser scanner

The Laser Scanner was also used for profiling a 40 m section of the Belgian paving. The profiled section was only 40 m due to bad weather on the night of profiling. The profiling proceeded at night due to the laser's ability of only measuring on a concrete surface at night. A 10 second long-exposure photograph shown in Figure 76 shows the set-up and operation of the Laser Scanner.

Figure 76: Laser scanner in operation on the Belgian paving at night.

The Laser Scanner can only profile a 2,4 x 2,4 m square at a time, thus the following procedure is performed to profile a 40 m section of the Belgian paving. The three points on the corners of the profiled square, measured at the beginning of the profiling procedure, was marked and surveyed in a local coordinate system. The following profiled square, which was next to the previous square, was profiled with the three measured starting points in line with the previous square. This was done sequentially and was used to place all of the profiled squares in sequence.

The profiled squares were added together and plotted in Matlab. Figure 77 shows the Laser Scanner profile of the Belgian paving.

The Laser Scanner profiles at 8 m/hour and requires in the order of 1 min/m for the processing of the measured data.

The resolution of the Laser Scanner profiled Belgian paving is lower when compared to the Can-Can and Photogrammetry profiles. This is due to the larger mesh size of the Laser Scanner profile. The comparison of the Displacement Spectral Densities will provide a good indication on the effect the mesh size has on the frequencies generated by the Belgian paving. The Displacement Spectral Densities are calculated and compared to the profiles of the Can-Can and Photogrammetry profilometers in paragraph 5.5.

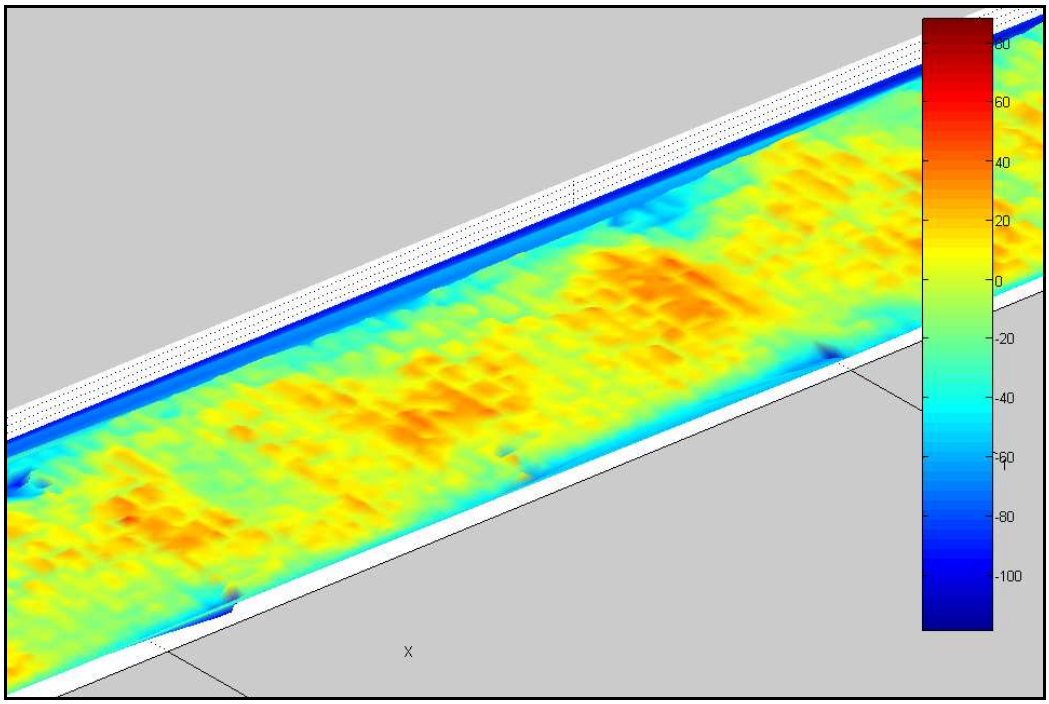

Figure 77: Laser Scanner profile of Belgian paving.

5.2. Fatigue track

The Fatigue section on the Suspension track at Gerotek accelerates the fatigue life of a vehicle's suspension by performing repeatable and comparative suspension tests under simulated conditions. The Fatigue track may appear smoother; however the RMS value of the Fatigue track is higher than the RMS value of the Belgian paving. Thus the Fatigue track tests the durability of the vehicle's suspension. The Can-Can Machine profiling the Fatigue track at Gerotek is shown in Figure 78. A full length 3-D profile of the Fatigue track was profiled and as a result a 3 x 100 m profile was obtained. A section of the Can-Can profile of the Fatigue track is shown in Figure 79.

Figure 78: The Can-Can Machine profiling the Fatigue track.

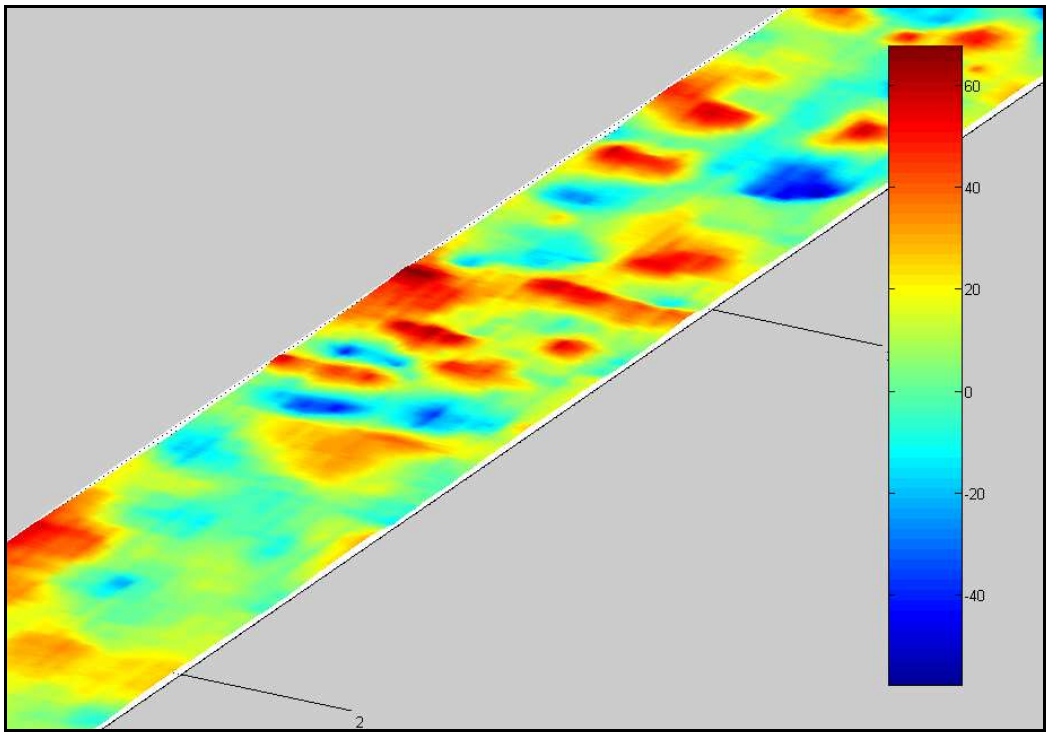

Figure 79: Can-Can profile of the Fatigue track.

The Displacement Spectral Density of the Fatigue track is calculated, compared and examined in paragraph 5.5.

5.3. Ride and Handling track

The Ride and Handling track at Gerotek is 4.2 km in length and is used for testing the ride comfort, driveline endurance and handling characteristics of a vehicle. The track consists of up and down hills, constant radius and decreasing radius turns, positive camber and negative camber corners and low speed as well as high speed corners. In addition the track also includes sections for low mobility vehicles and high mobility vehicles. For the purpose of this study only the low mobility vehicle sections were profiled with the use of the Can-Can Machine. This was done due to the fact that the high mobility vehicles sections were used only for large military vehicles. Figure 80 shows an aerial photograph of the Ride and Handling track with the Can-Can Machine profiled section in green. The surface of the Ride and Handling track is transversely tined concrete (see Figure 81).

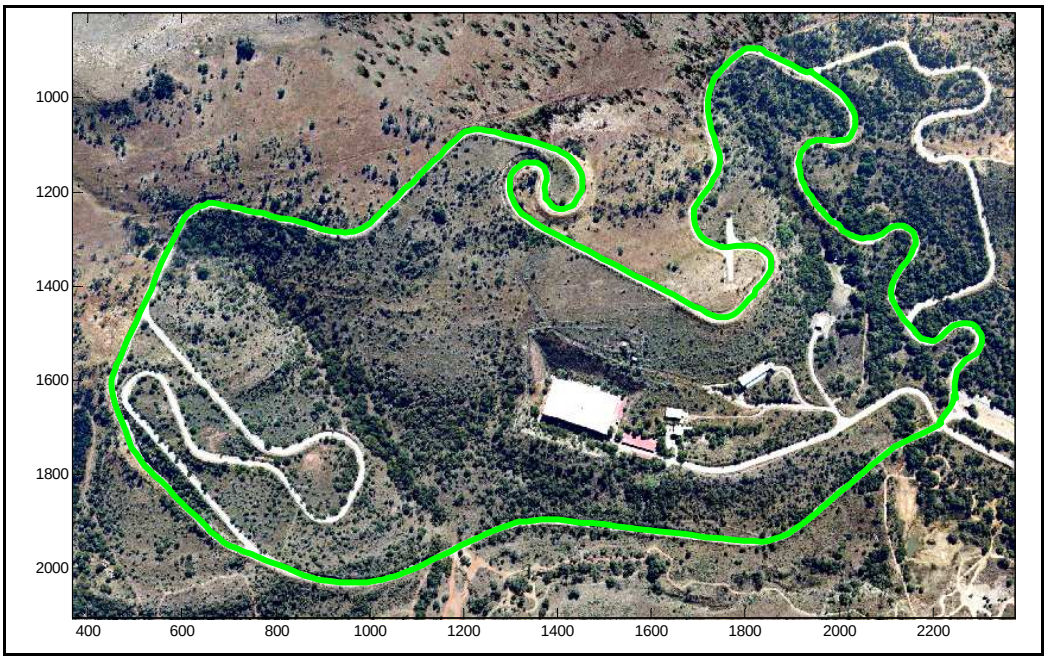

Figure 80: The profiled section of the Ride and Handling track at Gerotek.

The Ride and Handling track was profiled with the Can-Can Machine by marking control points on the concrete terrain with a spray can at 10 m intervals. The spray can was triggered with a trigger mechanism which was built in-house. The trigger mechanism used a 12 volt SANJI central locking actuator which presses on a trigger which in turn allows the spray can to release paint onto the terrain. The trigger mechanism is shown in Figure 81.

Pro Mapping cc surveyed the control points with a DGPS and was used in placing the profile recorded by the Can-Can Machine in a global coordinate system. A spline was fitted through the surveyed control points and the Rodrigues' rotation formula (Rodrigues' rotation formula 2008) was applied in

orientating the profile of the track with the spline. This gave the global position and orientation of the Can-Can Machine frame on which the profile measured by the arms could be superimposed after correction using the tilt sensor data. An exceptional 3-D profile of the Ride and Handling track was generated with this method. The Can-Can profiled Ride and Handling track is shown in Figure 82 and Figure 83.

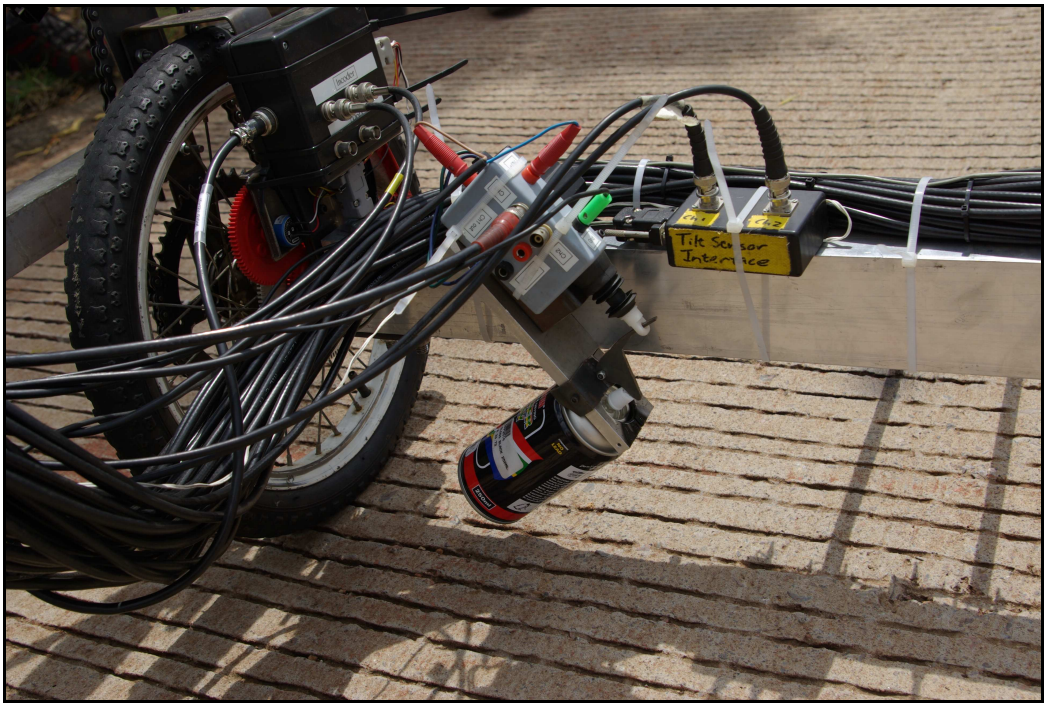

Figure 81: Trigger mechanism on Can-Can Machine.

The concrete surface of the Ride and Handling track appears smooth on the close-up of the profile shown in Figure 83. This is due to the fact that the concrete surface is fairly smooth, as shown in Figure 81 and also because the colour interpolation in the profile was done over the complete vertical displacement of the profiled terrain. The total vertical displacement on the profile was 60 m, thus the colour's resolution was not sensitive enough to detect a 10 – 20 mm change in height on the profile. Figure 84 is a close-up of a section the Ride and Handling track's profile with the colour interpolation performed over the close-up section.

The result of the profiled Ride and Handling track was very representative of the actual Ride and Handling track. A lot of detail was captured in the profile and the profile proved that the Can-Can Machine was capable of profiling a 4.2 km section of a terrain relatively quickly.

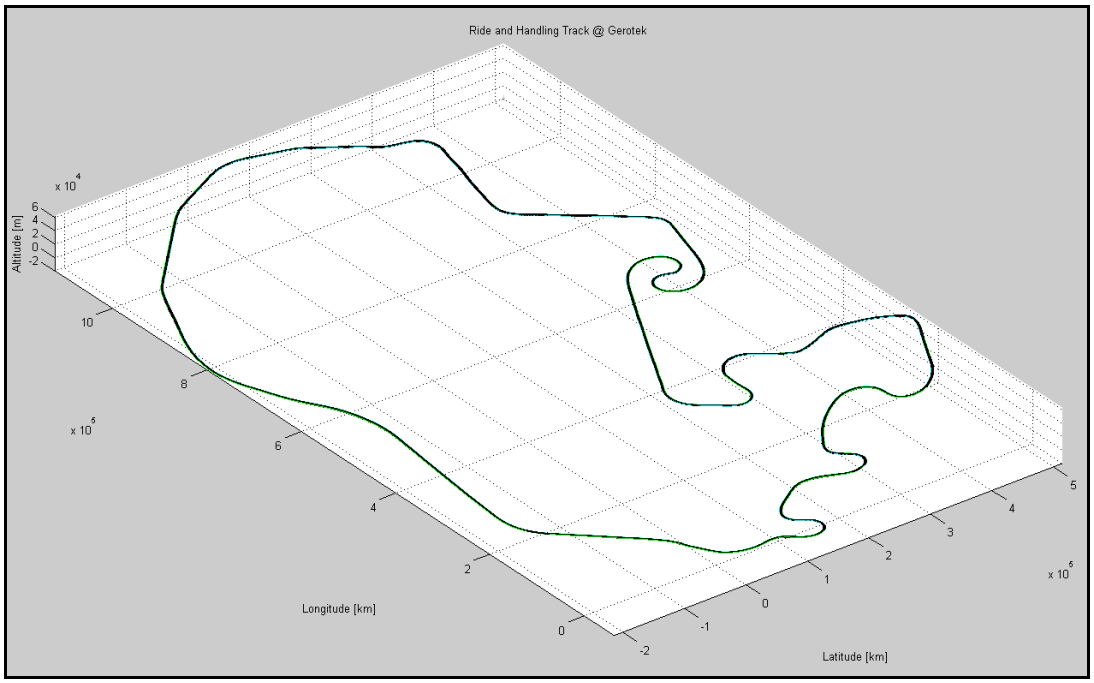

Figure 82: Ride and Handling track profiled with Can-Can Machine.

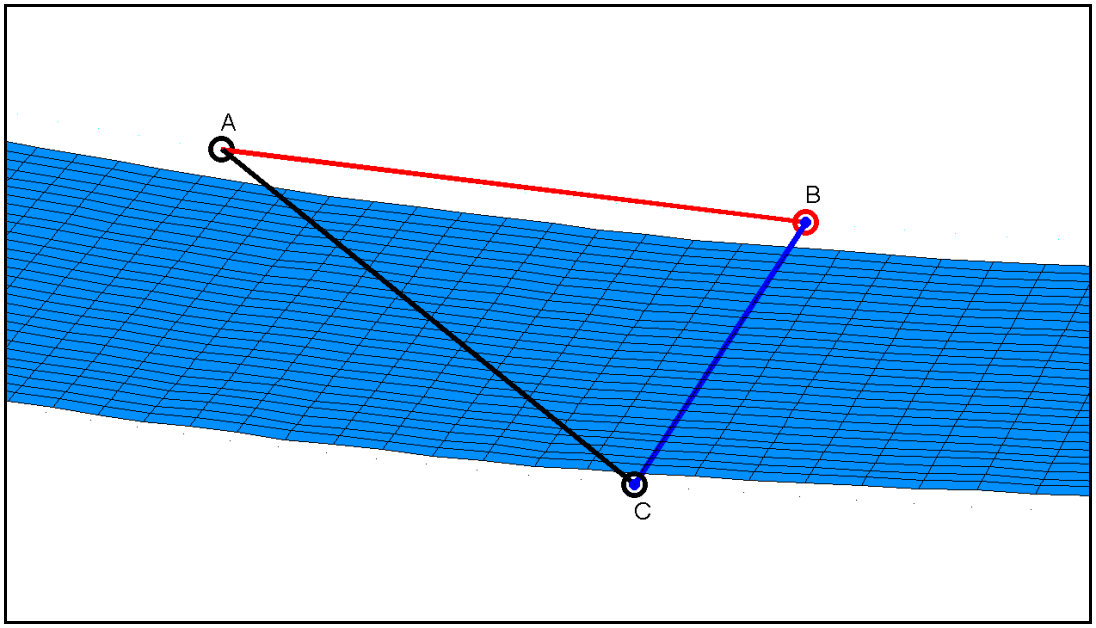

Figure 83: Close-up of Ride and Handling track with model Can-Can Machine.

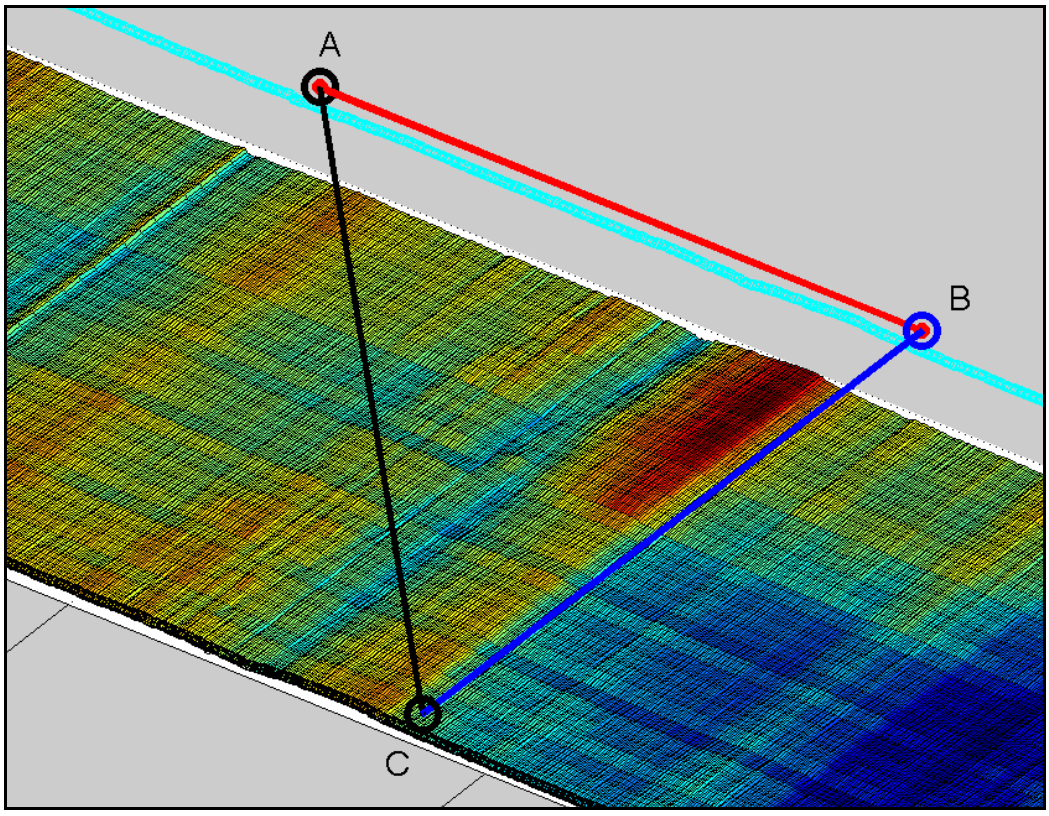

Figure 84: Close-up of the Ride and Handling track profile.

The Ride and Handling track was profiled at 0.98 km/h and the data processing required was 500 m/hour which was more time required than previous Can-Can profiled terrains due to the length of the Ride and Handling track.

The Displacement Spectral Density of the Ride and Handling track is calculated, compared and examined in paragraph 5.5.

5.4. Rough track

The Rough track at Gerotek is used for evaluating the rough terrain mobility and structural endurance of all-terrain vehicles. The track tests vehicle durability under accelerated conditions, including: chassis, body, suspension, steering, axles, differential locks, mountings, etc. Relative movement between body and cabin, chassis and wheels are also evaluated together with ride comfort and interior noise levels. The layout and surface varies with hills, ditches, chassis twisters, bumps and rocks all embedded in concrete to maintain a permanent profile. The concrete surface is fairly coarse to provide sufficient traction. The track is extremely rough and vehicle speeds above 20 km/h are seldom achieved.

For the purpose of this study an 800 m section of the track was profiled. This is a section of the track most frequently used for ride comfort assessment on extreme terrains. The profiled section is shown in Figure 85.

Figure 85: Profiled section of Rough track.

Tests completed, with the Can-Can Machine moving over large obstacles while profiling, indicated that the structural stiffness of the profilometer was too low for the profiling of the Rough track and will affect the accuracy of the Can-Can Machine. The low structural stiffness was due to the size of the profilometer and the requirement for the profilometer's weight to be as low as possible.

To reduce the vertical movement and input to the structure of the Can-Can Machine, a 9 m long mobile track was manufactured from lip channel. One side of the Can-Can Machine runs on a mobile track when profiling the Rough track at Gerotek. The side of the Can-Can Machine running on the mobile track was the driver wheel and the front wheel used for steering. Guides were made that guided the wheels on the beam and prevented them from falling off the beams. The mobile track supplied the Can-Can Machine with a straight line reference between surveyed points which simplified processing the profile of the Rough track. This mobile track consisted of two 4.5 m lip channel beams, each placed on three scissor jacks. The scissor jacks were used to stabilize the beams and adjust the height in order to maintain the horizontal reference set for the rear beam of the Can-Can Machine. This simplified the movement of the Can-Can Machine over the very rough terrain due to the fact that only one wheel of the profilometer was in direct contact with the terrain.

The beams were placed end-on-end with one another on the edge of the Rough track (to follow the course of the Rough track) and the Can-Can Machine started on one beam and moved along the beam onto the following beam, after which the rear beam was placed in front of the beam on which the Can-Can Machine was moving. This procedure was followed for the length of the profiled terrain (see Figure 87).

The front point of each beam had a reflective target that was surveyed with a total station at each placement of the beam as the Can-Can Machine was moving over the beams. The reflective targets on each beam also triggered a retro reflective optical speed sensor (Turck-Banner QS18VP6LP) that recorded the position of each surveyed point in the data file. The optical sensor was mounted next to the driver wheel which enabled it to be triggered by the reflective targets on the beams.

As with the profiling of the Ride and Handling track, the surveyed points were used in generating a spline which was placed in a global coordinate system. Rodrigues' rotation formula (Rodrigues' rotation formula 2008) was applied in orientating the profile of the track with the spline. The spline was linearly interpolated between the surveyed points with the correct amount of data points as required between each trigger.

Figure 86 shows a section of the Rough track and Figure 87 shows the Can-Can Machine crossing from one beam to another. Figure 88 shows the full Can-Can profiled Rough track and Figure 89 is a close up of a section of the Rough track.

Figure 86: A section of the Rough track at Gerotek.

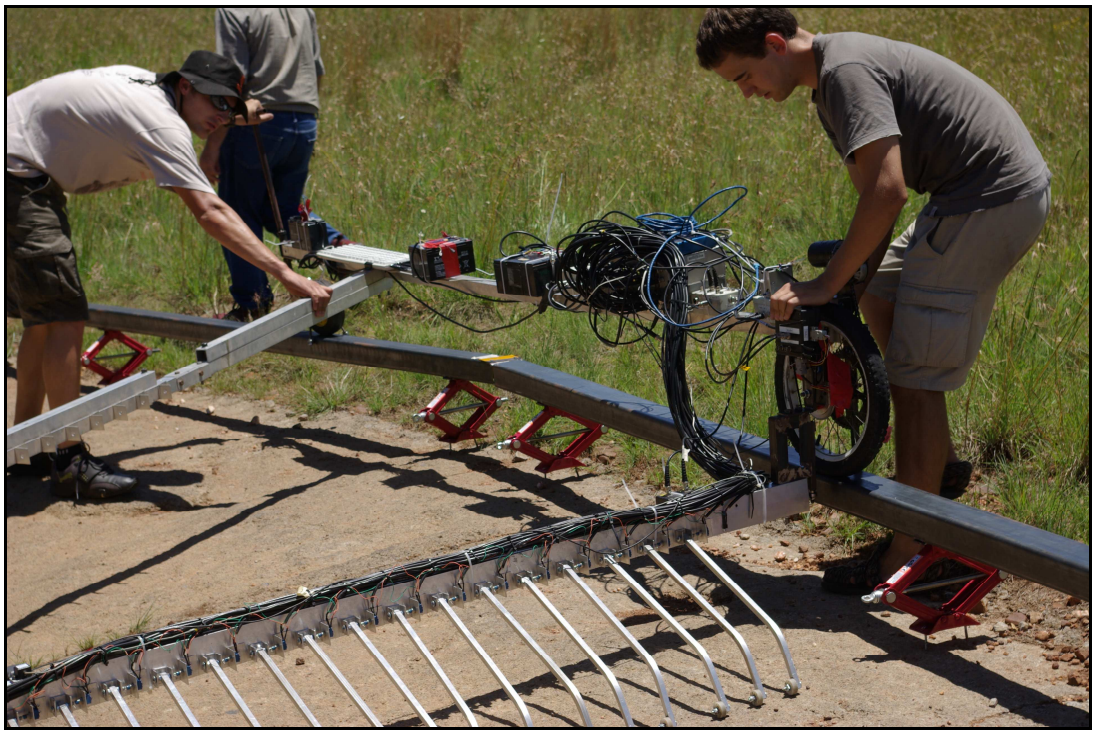

Figure 87: Can-Can Machine crossing from one beam to another.

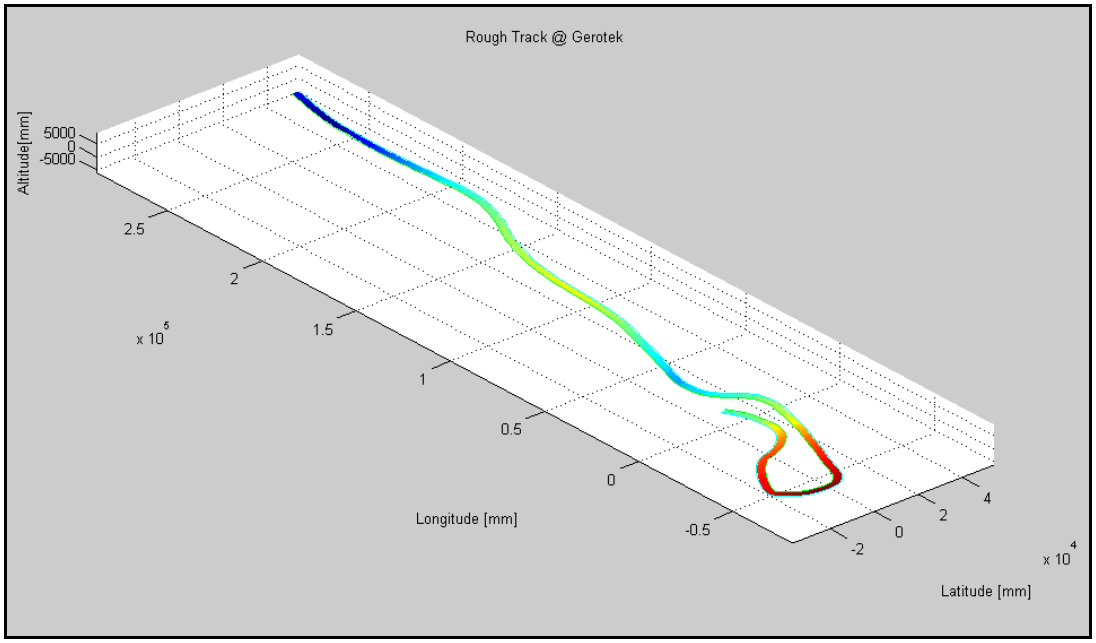

Figure 88: Profile of the Rough Track at Gerotek.

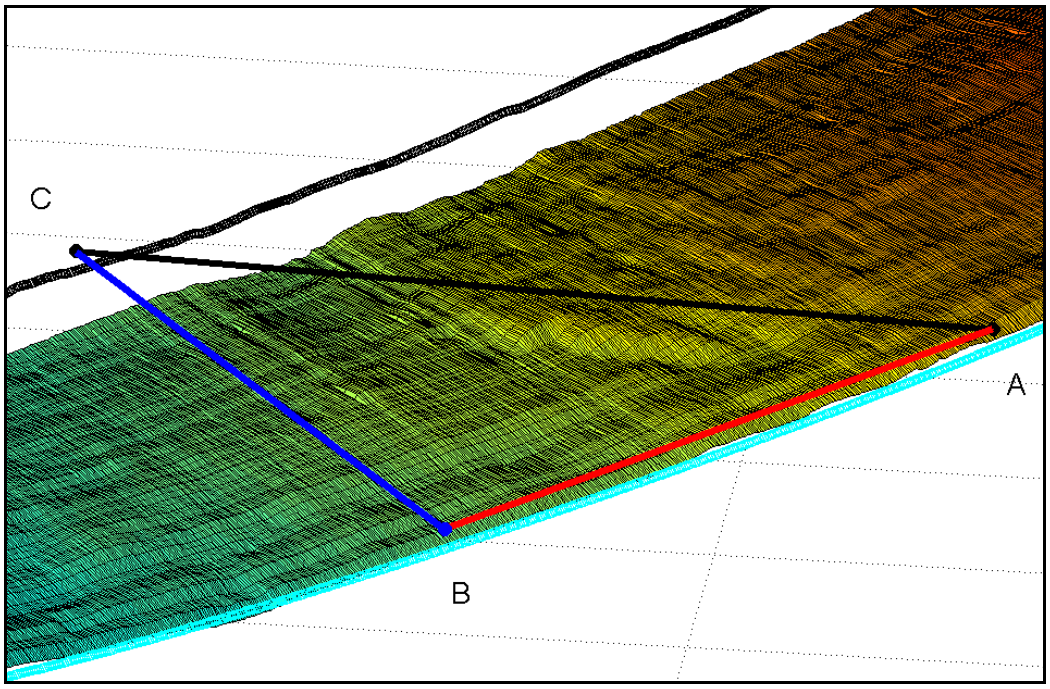

Figure 89: Close-up of the Rough track profile.

The result of the profiled Rough track was very representative of the actual Rough track. A lot of detail was captured in the profile and the profile proved that the Can-Can Machine was capable of profiling a very rough terrain in a relatively short space of time.

The Rough track was profiled at 0.1 km/h due to the roughness and profiling method used for the Rough track. The data processing required was 500 m/hour, which was more time required than previous Can-Can profiled terrains due to the length of the Rough track.

The Displacement Spectral Density of the Rough track is calculated, compared and examined in paragraph 5.5.

5.5. Displacement Spectral Densities of profiled tracks (DSD)

Although the main purpose of the present study is to obtain 3-D profiles of specific terrains for the use in vehicle dynamic simulations, the Displacement Spectral Density was also used to characterize the roughness of each profiled terrain. The following formula, as described in paragraph 2.8, is used for calculating the Displacement Spectral Densities.

$$S_{xx}(F) = \frac{\left|X_{\delta}(F)\right|^2}{2\Delta F}$$

The roughness of each track is compared with a class-A road to a class-H road, according to ISO 8606 road classification (ISO, 1995), which is a comparison from a smooth to a very rough terrain.

5.5.1. Belgian paving

The Displacement Spectral Density of the Belgian paving profiled with the Can-Can Machine was calculated for each arm after which the average of all 30 arms together was determined. Figure 90 shows the Displacement Spectral Densities of the Can-Can profiled Belgian paving. The green lines are the Displacement Spectral Densities from the 30 arms and the black line is the average Displacement Spectral Density of all 30 arms.

The peak at 6.066 cycles/m represents an average brick size of 164 mm where the actual average brick size was close to 130 mm. This difference in brick size is due to the shape of the bricks. The discrete obstacles profiled with the Can-Can Machine did not have 90 degree steps in them. The 90 degree direction change in a step was smoothed out by the small wheels at the end of the arms on the Can-Can Machine and resulted in a larger brick size. The correct brick size was obtained when the diameter of the small wheels was subtracted from the average brick size and resulted in a brick size of 134 mm. This is acceptable for the reason that the wheel on the actual vehicle is much larger and will not see the sharp 90 degree direction changes in the profile. The peak at 22.58 cycles/m represents the average gap size of 44 mm between the bricks.

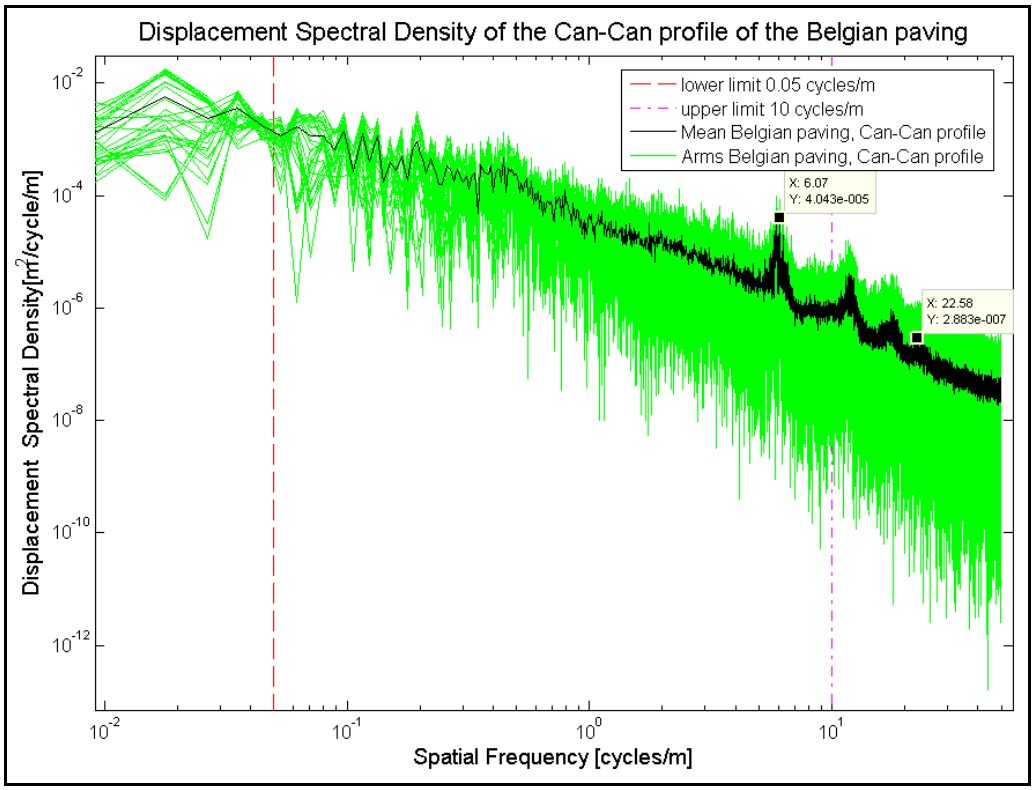

Figure 90: Displacement Spectral Density of the Can-Can profile of the Belgian paving.

The Photogrammetry profile data was determined for a 10 x 10 mm grid. The Displacement Spectral Density determined by calculating a Displacement Spectral Density for each longitudinal gridline, thus 300 Displacement Spectral Densities was calculated from the 3 x 50 m profile. Figure 91 shows the Displacement Spectral Densities of the Photogrammetry profiled Belgian paving with the blue lines each of the 300 Displacement Spectral Densities and the green line the average Displacement Spectral Density.

In Figure 91, the peak at 1 cycle/m was the result of the impurities and distortions in the lens as described in paragraph 5.1.2. This spatial frequency was evident in the Photogrammetry profile of the Belgian paving, as seen in Figure 72 and Figure 73 in paragraph 5.1.2. The average brick size is represented by the peak at 6.14 cycles/m which results in a 160 mm brick size. The larger brick size was due to the mapping procedure in which a break line around the base of the brick was mapped. The mapped break line was not always at the intersection of the brick and the ground since it was not always possible to see the intersection of the brick and the ground. A gap size of 36 mm was detected at 27.18 cycles/m and was also affected by the mapping procedure.

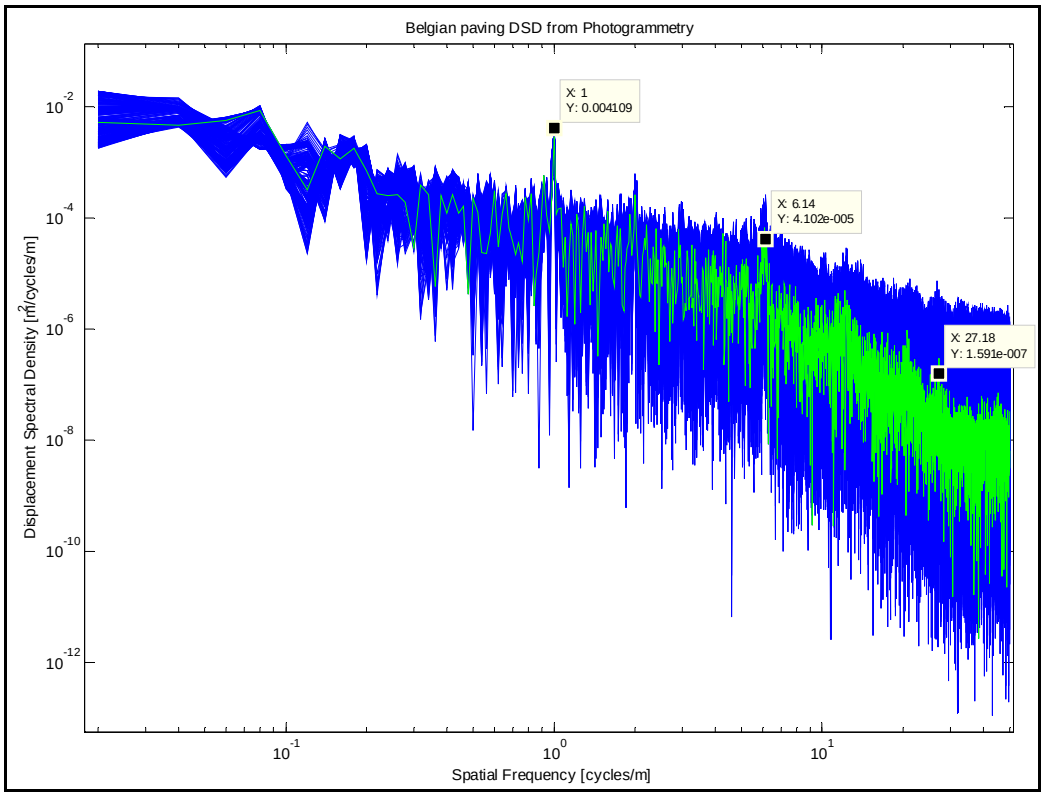

Figure 91: Belgian paving DSD from Photogrammetry profile.

Each 2,4 x 2,4 m block of the Laser Scanner resulted in a mesh with 32 perpendicular gridlines in both the longitudinal and lateral directions. The profile of a terrain profiled with the Laser Scanner was constructed as described in paragraph 5.1.3. The Displacement Spectral Density of each longitudinal gridline of the total profile as well as the average of the 32 Displacement Spectral Densities was calculated. Figure 92 shows the Displacement Spectral Density of the Laser Scanner profiled Belgian paving. The blue lines are the Displacement Spectral Densities from the 32 gridlines and the red line is the average Displacement Spectral Density of the 32 gridlines.

In Figure 92, the peak at 0.3877 cycles/m is caused by the convex shape of each individual profile as described in paragraph 3.3.1. Where as the peak seen at 4.837 cycles/m indicate that an average brick size of 206 mm are detected by the Laser Scanner. The larger recorded brick size was caused by the mesh size which was just larger than half of the actual brick size. The gaps between the bricks were not detected by the Laser Scanner due to the fact that the gaps between the bricks were smaller than the mesh size of the Laser Scanner.

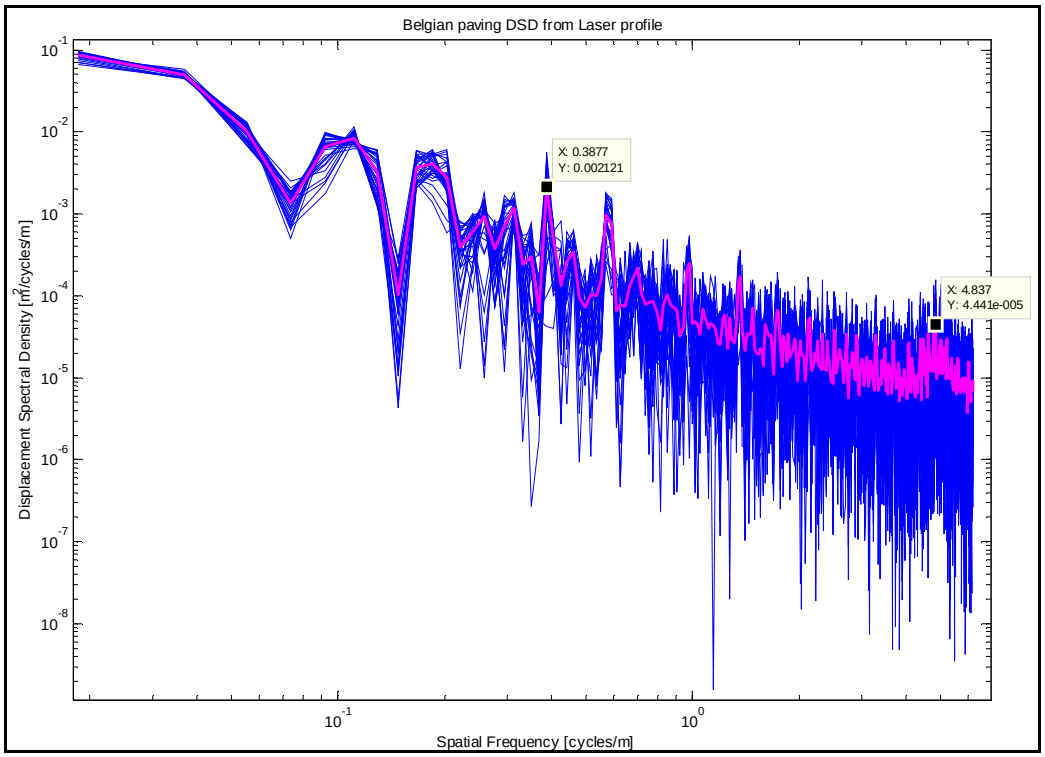

Figure 92: Displacement Spectral Density of the Belgian paving profiled with the Laser profile.

Figure 93 compares the Displacement Spectral Densities from all three profiles of the Belgian paving with Displacement Spectral Densities from class-A, class-D and class-H roads. The Displacement Spectral Densities of the class-A, D and H roads are plotted for special frequency range, 0.007 to 4 cycles/m, according to ISO 8608 (1995). The three profiling methods produced nearly equivalent Displacement Spectral Densities of the Belgian paving and indicated that the Belgian paving was a touch rougher than a class-D road. Figure 93 illustrates that the Laser profile has the lowest resolution and the Photogrammetry profile the highest resolution as expected.

From the results discussed above the following conclusions are made.
The Can-Can Machine is to be used of profiling terrains due to:

- The high profiling speed and efficiency of the Can-can Machine,
- The ease of data processing,
- The accuracy of the profilometer
- And the low operating costs of the Can-Can Machine.

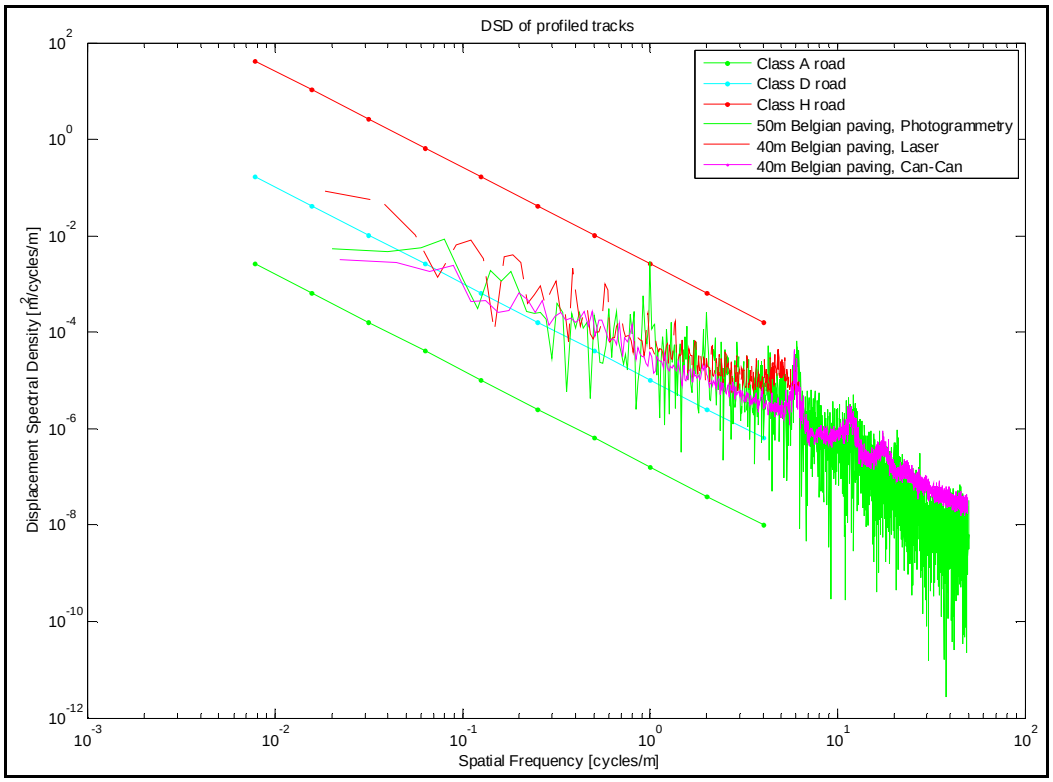

Figure 93: DSD's of all three Belgian paving profiles together with a class-A, class-D and class-H road.

5.5.2. Fatigue track

The Fatigue track was profiled only with the Can-Can Machine. The average Displacement Spectral Density in Figure 94 indicates that, compared to the class D-road, the Fatigue track generates higher amplitude inputs at spatial frequencies between 0.5 and 10 cycles/m (points A and B), but is significantly smoother below 0.5 (point A) and above 10 cycles/m (point B).

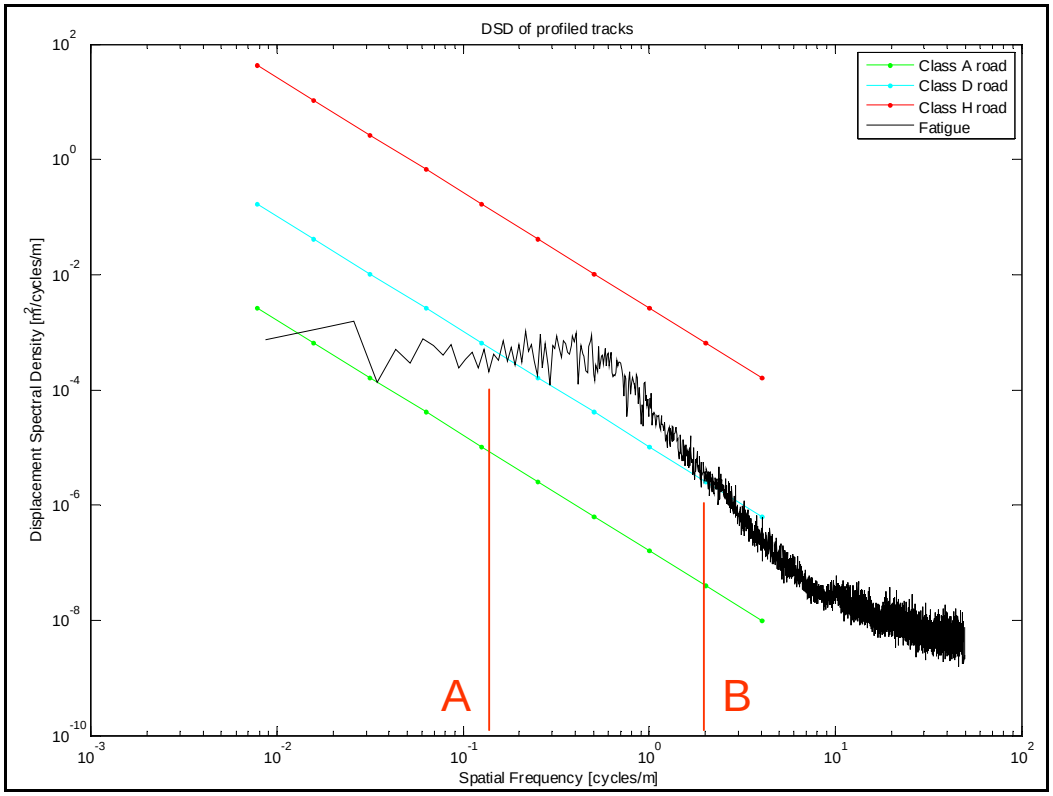

Figure 94: DSD of the fatigue track.

5.5.3. Parallel and angled corrugations

The parallel and angled corrugation track's were profiled with the Can-Can Machine and the Displacement Spectral Densities are compared to a class-A, class-D and a class-H road in Figure 95. An average distance of 760 mm between the 25 mm bumps is represented by the peak at a spatial frequency of 1.316 cycles/m. This illustrates the accuracy of the profilometer and the calculation of the Displacement Spectral Density since the actual distance between each 25 mm bump on these tracks is reported to be 750 mm. The other peaks in the Displacement Spectral Densities are fractions of the distance between the bumps.

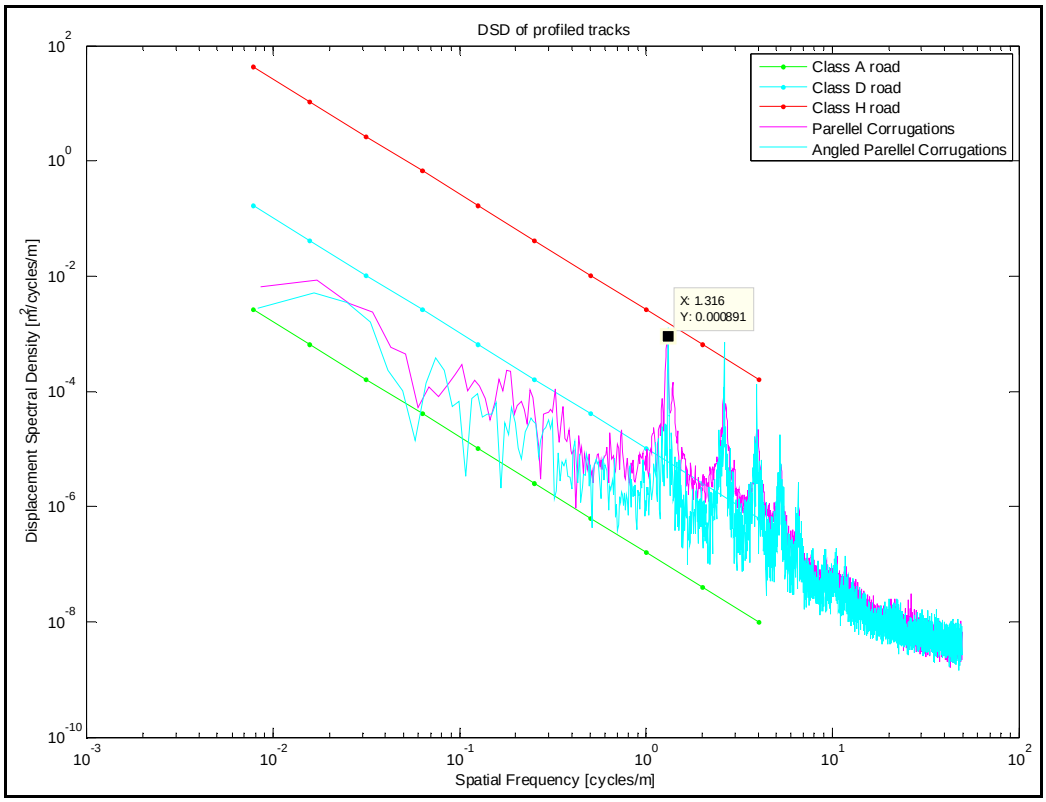

Figure 95: DSD of the parallel and angled corrugations tracks.

5.5.4. Pothole track

The Pothole track was profiled with the Can-Can Machine as described in paragraph 4.1.3. The Pothole track has 25 potholes spaced at different distances ranging from 3 m to 12 m apart and each pothole is 660 mm long at the top, 500 mm long at the bottom and 80 mm deep (see Figure 63, Figure 64 and Figure 65). The average Displacement Spectral Density of the Pothole track is presented in Figure 96. The valley at 1.782 cycles/m detects the average length of the potholes as 561 mm.

5.5.5. Ride and Handling track

The Ride and Handling track was profiled with the Can-Can Machine as described in paragraph 5.3. The Displacement Spectral Density of the Ride and Handling track, shown in Figure 97, indicates that the surface of the track is rather rough. The Displacement Spectral Density of the Ride and Handling track was calculated without the global surveyed coordinates.

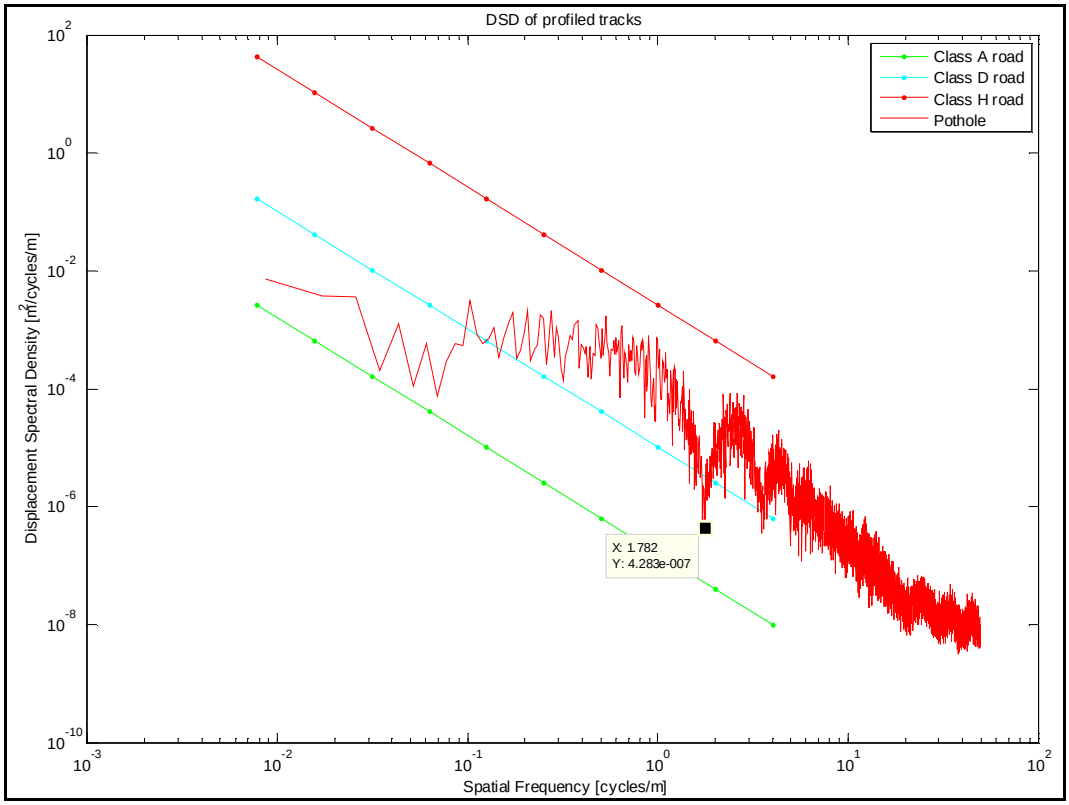

Figure 96: DSD of the pothole track.

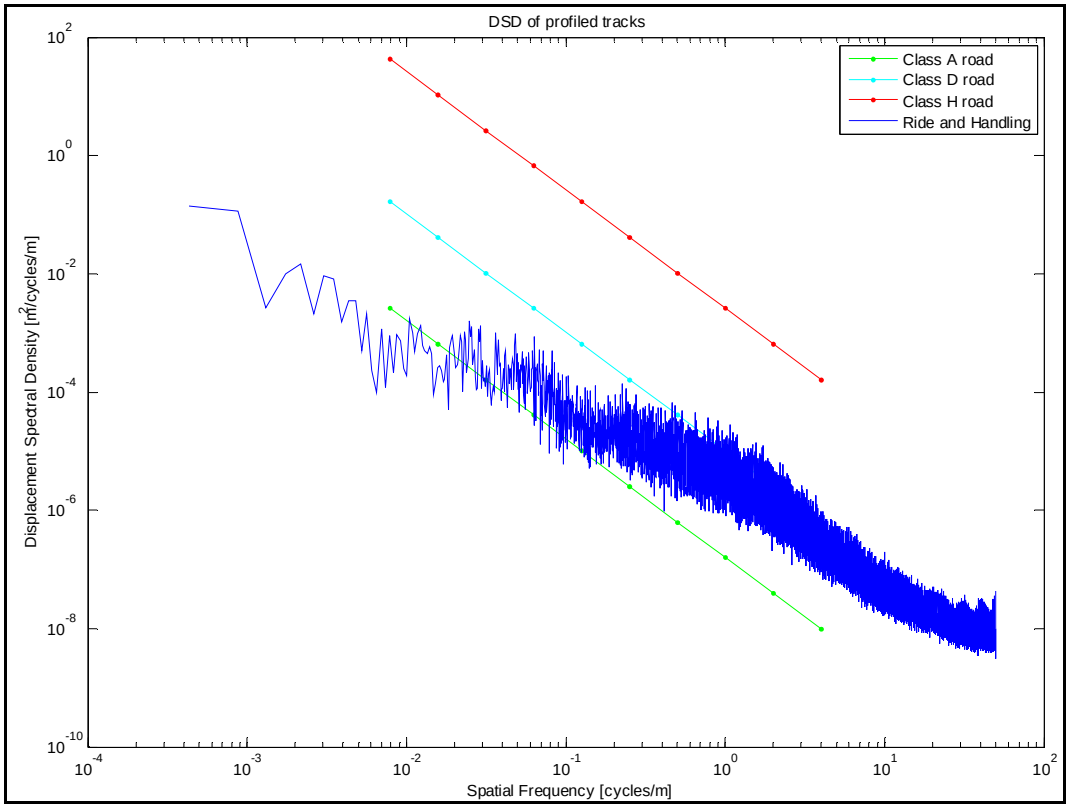

Figure 97: DSD of the Ride and Handling track.

5.5.6. Rough track

The Rough track was extremely rough and was profiled with the Can-Can Machine as described in paragraph 5.4. The Displacement Spectral Density of the Rough track is shown in Figure 98 and as expected it is classified as a class-H road. The graph also indicates that the surface roughness of the terrain was also high. This was indicated by the amplitude of the right hand side of the graph. The roughness of the terrain surface is high to increase the available traction on the terrain. Note that the log scale makes the “noise” appear smaller. The Displacement Spectral Density of the Rough track was calculated without the global surveyed coordinates.

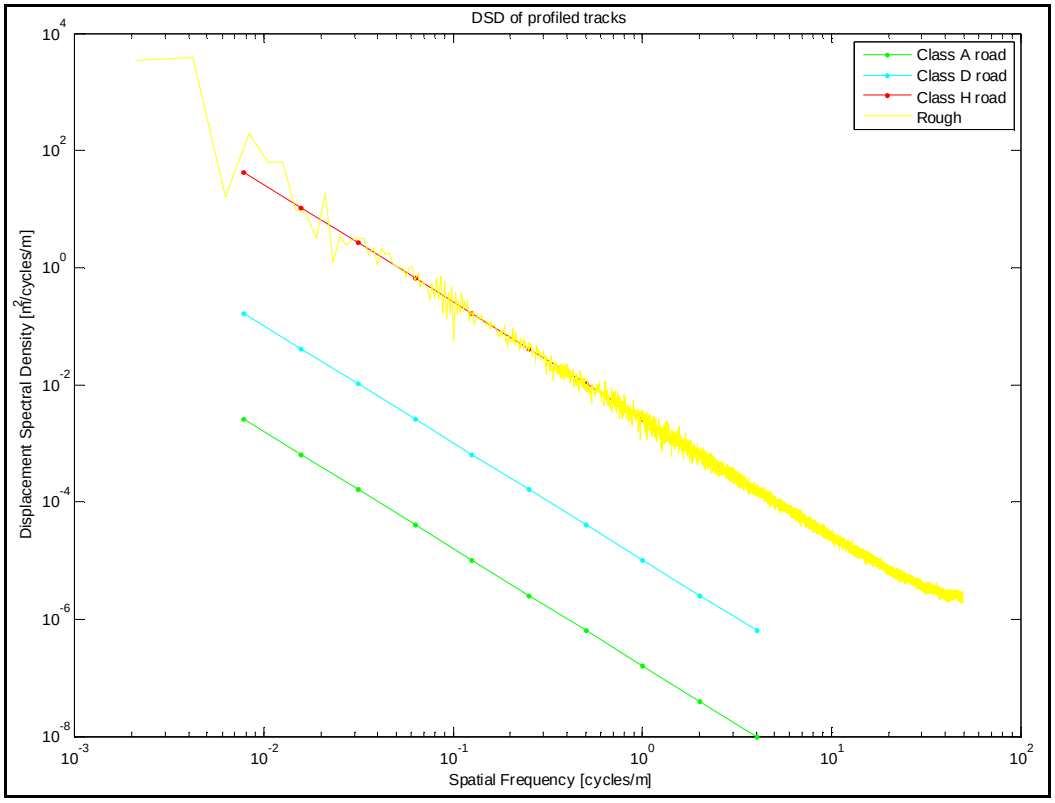

Figure 98: DSD of the Rough track.

5.5.7. Determining Roughness coefficient

The approximate linear shape of the Displacement Spectral Density when plotted on log-log coordinates is a consequence of the fact that long wavelength features in the terrain tend to have large amplitudes and short wavelengths features tend to have small amplitudes if a random terrain is

considered. The Displacement Spectral Density of a paved road surface profile normally has a more linear graph than an off-road terrain profile.

The Displacement Spectral Density is one method used in describing the roughness of a terrain. Other methods used are the route mean square (RMS) of the vertical displacement, which is equivalent to the square root of the area underneath the Displacement Spectral Density, a Power function or Inverse Power Law is often applied to DSD's of random roads using an equation of the following form:

$$S_z = A\varphi^{-n}$$

This approximation offers a very simple way of defining the characteristics of a random terrain. The terrains can only be compared to one another with the use of these methods if the same spatial frequency range is used for each terrain. For off-road profiles the reported spatial frequency range for φ should be from 0.05 cycles/m (wavelength = 20m) to 10 cycles/m (wavelength = 0.1m), ISO 8608 (1995).

The lower value of φ = 0.05 cycles/m is acceptable since the vehicle speed over off-road or rough terrain is normally much lower than the case for road. The upper spatial frequency limit of φ = 10 cycles/m is consistent with the length of the tyre contact patch, ISO 8608 (1995). Figure 99 presents an example of the Displacement Spectral Density of the Belgian paving, profiled with the Can-Can Machine, as well as an Inverse Power Law fit on the Displacement Spectral Density. The upper and lower limits of the spatial frequency window used in calculating the Inverse Power Law coefficients are also shown.

Table 2 presents results of the inverse power law approximation of each terrain, which consists of the roughness coefficient A and the road index n to describe different terrains. The first six terrains are described by Hall (1998). The roughness coefficients and road indexes of the terrains profiled with the Can-Can Machine is also presented as well as the profiles of the Belgian paving as profiled with Photogrammetry and the Laser Scanner.

This kind of approximation is not very satisfactory for most of the terrain under consideration for the present study due to the existence of definite peaks and valleys in the DSD's of most of the profiled terrains.

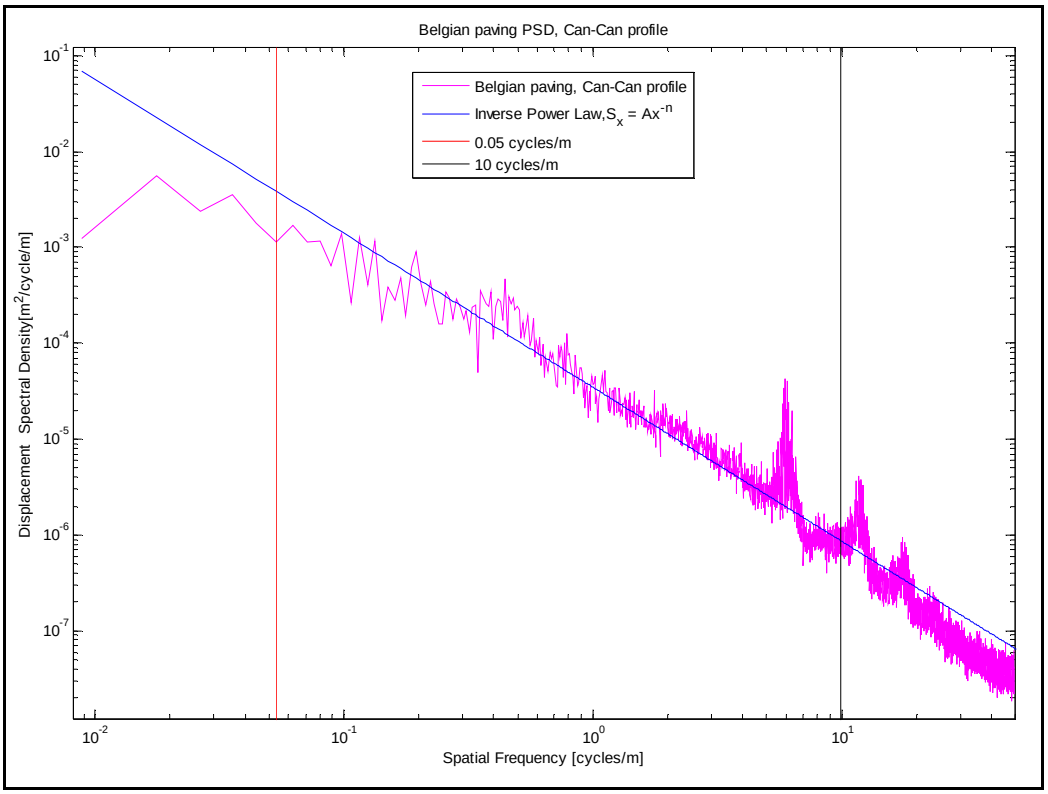

Figure 99: Inverse Power Law plot on Belgian paving.

Terrain	Roughness coefficient. A (m^2/cycles/m)	Road index, n
Smooth runway*	4.30E-11	3.8
Rough runway*	8.01E-04	2.1
Smooth highway*	4.80E-07	2.1
Highway with gravel*	4.40E-07	2.1
Pasture*	3.00E-04	1.6
Ploughed field*	6.50E-04	1.6
Belgian paving, Can-Can	3.48E-05	1.6
Belgian paving, Photogrammetry	5.72E-05	1.8
Belgian paving, Laser scanner	4.87E-05	1.0
Fatigue track, Can-Can	3.42E-05	2.9
Parallel Corrugations, Can-Can	2.20E-06	1.6
Angled Corrugations, Can-Can	7.67E-06	1.9
Pothole track, Can-Can	5.30E-05	2.2
Rough track, Can-Can	2.46E-03	1.9
Ride and Handling track, Can-Can	2.27E-06	1.8

* Hall (1998)

Table 2: Inverse Power Law values.

The roughness coefficient is the value of the Displacement Spectral Density at 1 cycle/m and the road index parameter is calculated with a spatial frequency window from 0.05 cycles/m to 10 cycles/m as indicated in Figure 99. The inverse power law approximation of each of the profiled terrains were calculated by fitting a straight line to the Displacement Spectral Density, with the use of a least squares fit and calculating the Roughness coefficient and the Road index of the straight line.

The road index of the Belgian paving profiled with the Laser Scanner is lower due to the fact that the upper limit of the spatial frequency window used in calculating the road index was used as 6.6 cycles/m and not 10 cycles/m. This was done because of the coarse resolution of the Laser Scanner profile.

The road index of the Belgian paving profiled with Photogrammetry is higher than the Can-Can Machine's due to the fact that the Photogrammetry profile had a higher resolution which contained more detail of the Belgian paving.

5.6. International Roughness Index (IRI)

The International Roughness Index was calculated as described in paragraph 2.9. A quarter-car model was created in Simulink which represented the Golden Car Model with the spring and damper characteristics as specified by Sayers and Karamihas (1998).

The quarter-car parameters are specified as part of the IRI statistic and the simulated travel speed is specified as 80 km/h. the Golden Car parameters are:

$$\frac{k_s}{m_s} = 63.3 \qquad \frac{k_t}{m_s} = 653 \qquad \frac{c}{m_s} = 6 \qquad \frac{m_u}{m_s} = 0.15$$

where k_s is the spring rate, m_s is the sprung mass, k_t is the tyre spring rate, c is the damper rate and m_u is the unsprung mass.

A single 2-D line from each of the 3-D profiled terrains were used as an input to the quarter-car model for all of the profiled terrains on the Suspension track as well as the profiled section of the Rough track.

The total suspension travel, as calculated from the quarter-car model, was divided by the distance travelled in order to obtain the International Roughness Index for each specific terrain. Figure 100 shows an example of the IRI vs. the distance travelled over the Belgian paving. The IRI vs. the distance travelled plots for all of the profiled terrains are available in Appendix D.

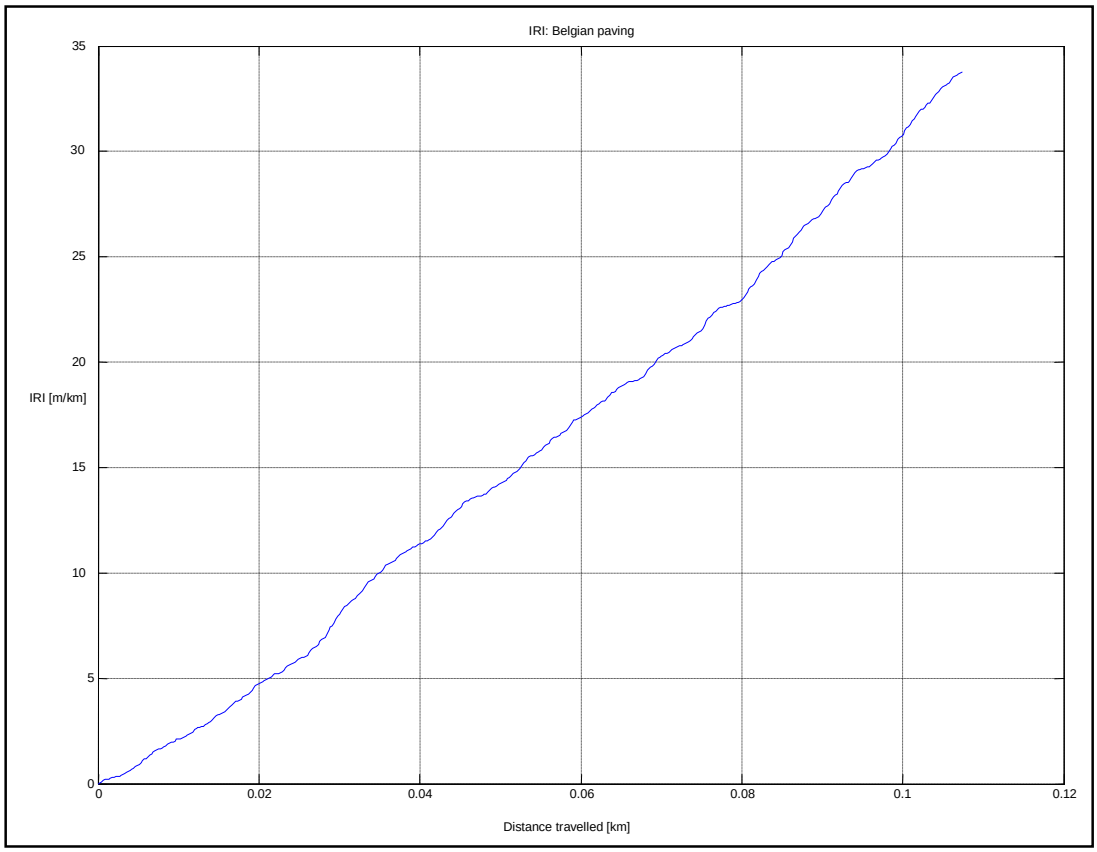

Figure 100: IRI vs. the distance travelled over the Belgian paving.

The calculated IRI for all of the profiled terrains are graphically shown in Figure 101 together with the upper and lower limits for the different road classes. Most of the roads profiled in the current study are significantly rougher than the “rough unpaved roads” presented by Sayers and Karamihas (1998).

This is an indication that the trends supplied by the International Roughness Index are only valid for smoother terrains. These smoother terrains are typically asphalt or concrete roads. This is expected as the International Roughness Index was designed for the characterization of asphalt and concrete roads. These asphalt and concrete roads are drastically smoother than the terrains which the present study concentrated on. The IRI uses a linear quarter-car model and is not compatible to the suspensions of most off-road vehicles. As a result it is recommended to use the profile of actual off-road terrains in simulations instead of statistically generated profiles.

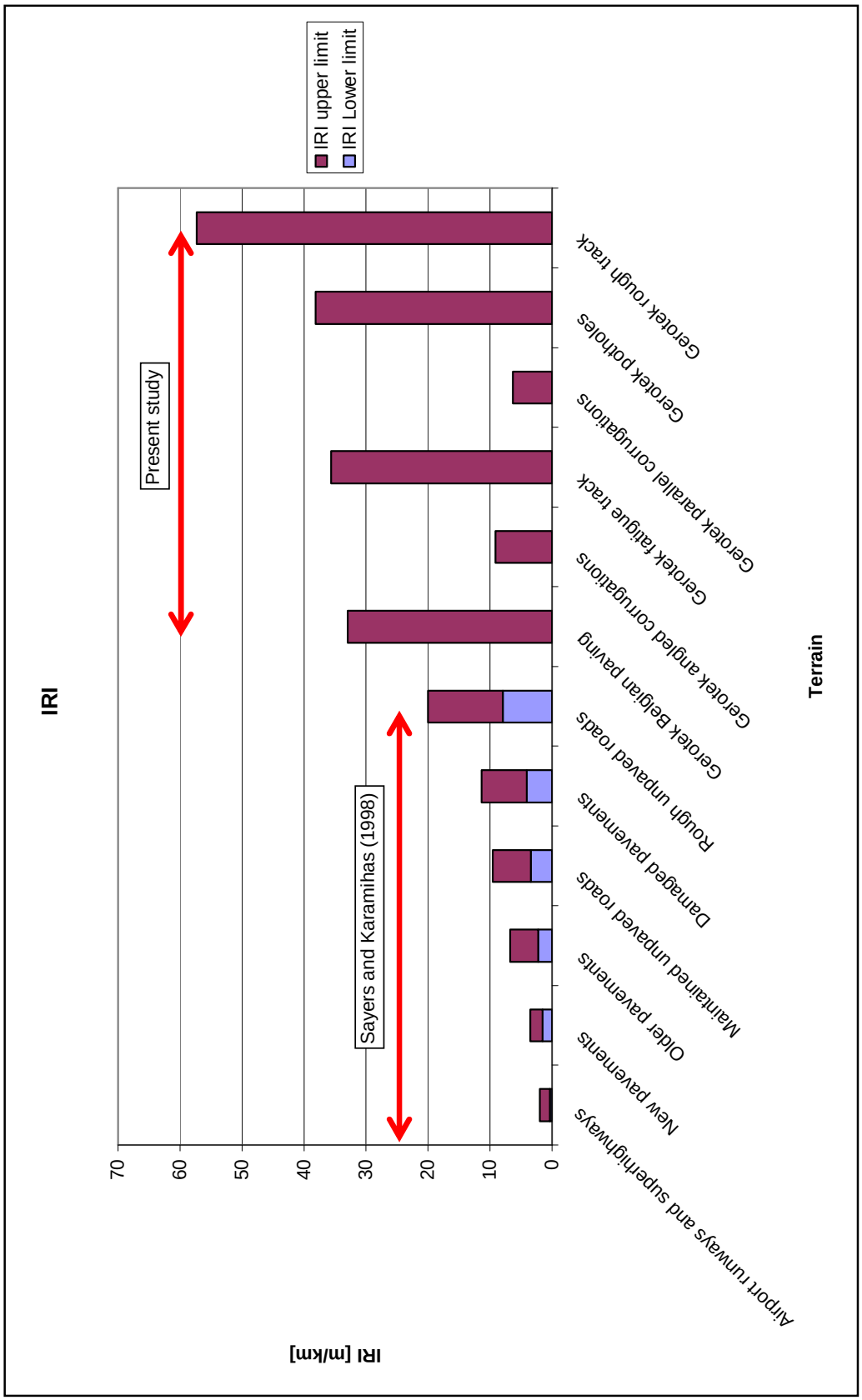

Figure 101: International Roughness Index

5.7. Summary on rough road profiling

The terrain profiles obtained with the three methods under consideration were visually very representative of the actual terrain. Although the resolution of the Laser Scanner was lower than the resolution of the Can-Can Machine and Photogrammetry a valid profile was still produced by the Laser Scanner. The resolution of the Belgian paving profile as profiled with Photogrammetry was very high and contained a high amount of detail, but remained time consuming and resource intensive. The Can-Can Machine produced profiles of the profiled terrains quickly and effectively. The Displacement Spectral Densities of the terrains profiled with the Can-Can Machine indicated that the resolution of the Can-Can Machine was high enough to obtain valuable information about the terrains. The conclusion is made that the Can-Can Machine is an accurate profilometer which profiles any terrain fast and cost effective.

The Displacement Spectral Densities of the profiled terrain are representative of the profiled terrain. The Displacement Spectral Density of each of the profiled terrains provided information about the terrains in the form of the Roughness Coefficient and the Road Index as well as the dominant frequencies generated when driving on the track. The Displacement Spectral Densities indicate that a straight line fit approximation on the Gerotek tracks does not include all of the track's characteristics.

The International Roughness Index was calculated for each of the profiled terrains and it indicated that the International Roughness Index was a valid method for characterizing smoother terrains.

6. 3-D road profiles in multi-body simulation models

The primary goal of this study was to obtain accurate 3-D profiles of actual test terrains used by the University of Pretoria. These profiles were required for the validation of mathematical models used in vehicle simulations. The MSC ADAMS simulation package is used by the University of Pretoria and thus the profiles were required to be described in terms of a MSC ADAMS Road Definition Files, also referred to as RDF files.

The ADAMS/3-D road models enable one to define an arbitrary three-dimensional smooth road surface, such as parking structures, racetracks and so forth. In addition, Adams/3-D Road lets you model three-dimensional road obstacles, which are placed on top of the underlying smooth road surface.

Road definition files can be created by defining the file type, file version and file format. Then the units of length, force, angle, mass and time are defined and the definition of the model method is set to 3-D after which the number of nodes is stated. The data points in the profile are known as nodes and presented by placing each node number followed by the x-value, y-value and z-value. Three nodes are used in defining each element in the road profile. The connectivity of the three nodes which define the element is defined in a clockwise direction. This is done to ensure that the orientation of each element is consistent. The definition of the road mesh is shown in Figure 102 and a blank example of the layout for a road definition file is supplied in Appendix C.

Road definition files were created with a program written in Matlab and were used for creating road definition files of the Belgian paving, fatigue track, parallel and angled corrugation tracks and the pothole track. All of these tracks were profiled with the use of the Can-Can Machine.

Road definition files were not created for the rough track and also not for the Ride and Handling track as these profiles were too large for the simulation programme to work with.

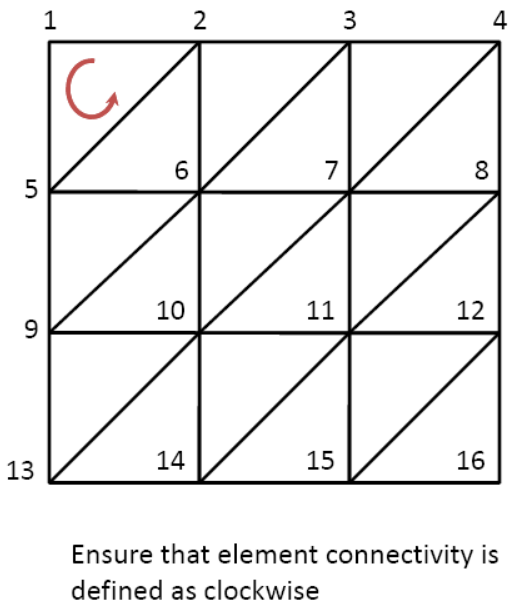

Element	Nodes		
1	1	5	2
2	2	5	6
3	2	6	3
4	3	6	7
5	3	7	4
6	4	7	8
7	5	9	6
8	6	9	10
9	6	10	7
10	7	10	11
11	7	11	8
12	8	11	12
13	9	13	10
14	10	13	14
15	10	14	11
16	11	14	15
17	11	15	12
18	12	15	16

Figure 102: Definition of Road Mesh used in MSC ADAMS, (MSC Software, 2007).

6.1. Simulation and data verification

Proving ground test surfaces have been modelled as Finite Element models. The Finite Element models are modelled as shell elements with rigid material properties. The modelling of the road surface is important as the analysis duration depends on the contact simulation between the road surfaces and tyres. The road is often modelled as separate left and right surfaces to reduce the number of elements in contact with the tyre, as it reduces the solving time.

While generating a road surface for a simulation, sufficient length of smooth road surface needs to be provided at the start of the simulation. This enables the vehicle to stabilize before entering onto the proving ground, Edara (2005).

3-D contact analyses are useful for generating road load histories and stress and fatigue studies that require component force and acceleration calculation. These studies can help one calculate the effects of road profiles, such as potholes, curbs, or Belgian blocks.

Previous road surfaces used for vehicle simulations at the University of Pretoria was road surfaces modelled as separate left and right surfaces (Thoresson (2003), Els (2006) and Uys (2007)). With the availability of the ADAMS/3-D Road the requirement of full 3-D road surfaces increased. The accuracy of the Can-Can Machine has been established by the actual measurement and profiling of discrete obstacles. The following step was to

validate the road definition files created from the Can-Can profiled terrains. The validation of the simulation with the road definition file was done by comparing the measured response of the modelled Land Rover Defender 110 in the simulation, in the form of vertical accelerations, with the actual response of the Land Rover Defender 110 driving over the profiled terrain. The profiled terrain used in the validation was the Belgian paving.

The response of the actual Land Rover Defender 110 was measured with the use of accelerometers. An accelerometer was positioned inside on the body of the vehicle, below each of the rear passengers, as shown in Figure 103. Another accelerometer was located on the chassis, 300 mm in front of the front axle, as shown in Figure 104.

Figure 103: Placement of rear accelerometers in Land Rover Defender 110.

The response of the Land Rover was measured while driving over the Belgian paving at five different velocities namely, 15km/h, 26km/h, 40km/h, 57km/h and 73km/h. The velocity of the Land Rover was kept constant by driving against the governor in different gears.

Figure 104: Placement of front accelerometer on chassis of Land Rover Defender 110.

6.1.1. Simulations on the Belgian paving

Simulations were conducted at the required velocities in MSC.ADAMS/VIEW with the use of the previously validated model of the baseline Land Rover Defender 110. The validation of the model was conducted by Thoresson (2003).

Figure 105 indicates the layout of the front suspension system. The rigid axle is located longitudinally by leading arms connected to the vehicle body with rubber bushes. The stiffness of these bushes was measured and included in the ADAMS model. Lateral location of the axle is via a Panhard rod. The baseline vehicle is fitted with coil springs, translational dampers concentric with the coil springs and rubber bump stops. A steering angle driver is applied directly to the kingpin with a steering link connecting the left and right wheels. All other steering geometry is ignored in the model. The connections between the different components are indicated in Figure 106. To take the torsional stiffness of the ladder chassis into account, the vehicle body is modelled as two bodies connected to each other with a revolute joint along the roll axis and a torsional spring.

The rear suspension consists of a rigid axle with trailing arms, an A-arm, coil springs, translational dampers mounted at an angle outside coil springs and rubber bump stops. The basic layout is indicated in Figure 107. An anti-roll bar

is fitted to the rear suspension. The stiffness of the trailing arm rubber bushes is included in the ADAMS model. The schematic layout of the rear suspension is indicated in Figure 108.

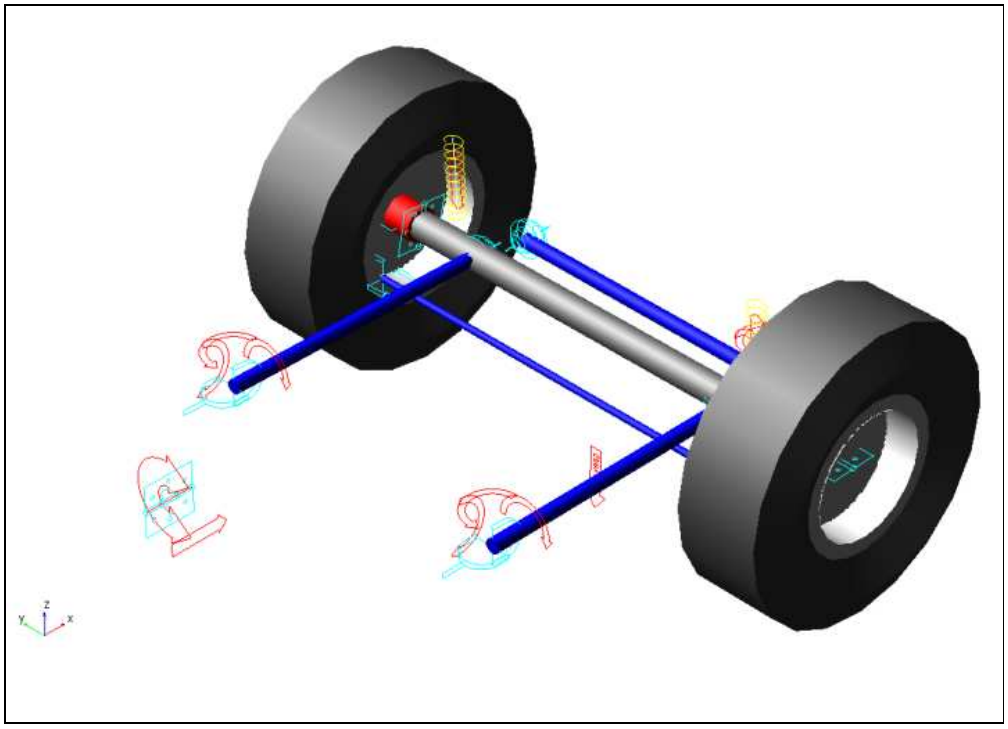

Figure 105: Front suspension layout.

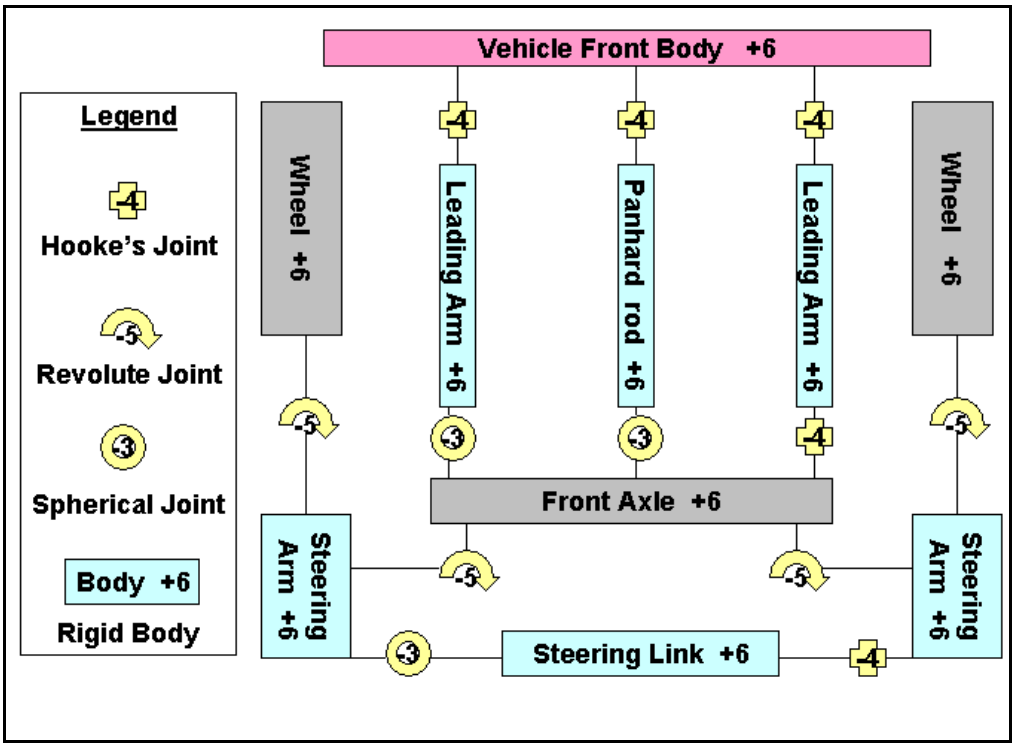

Figure 106: Front suspension schematic.

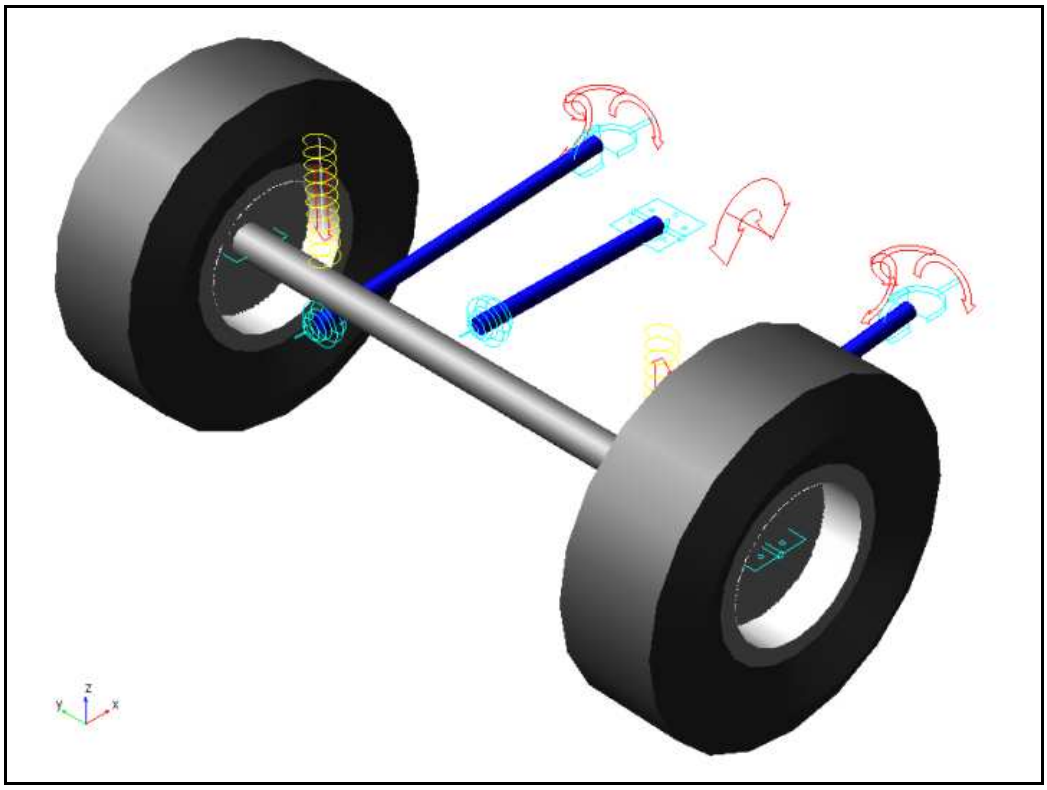

Figure 107: Rear suspension layout.

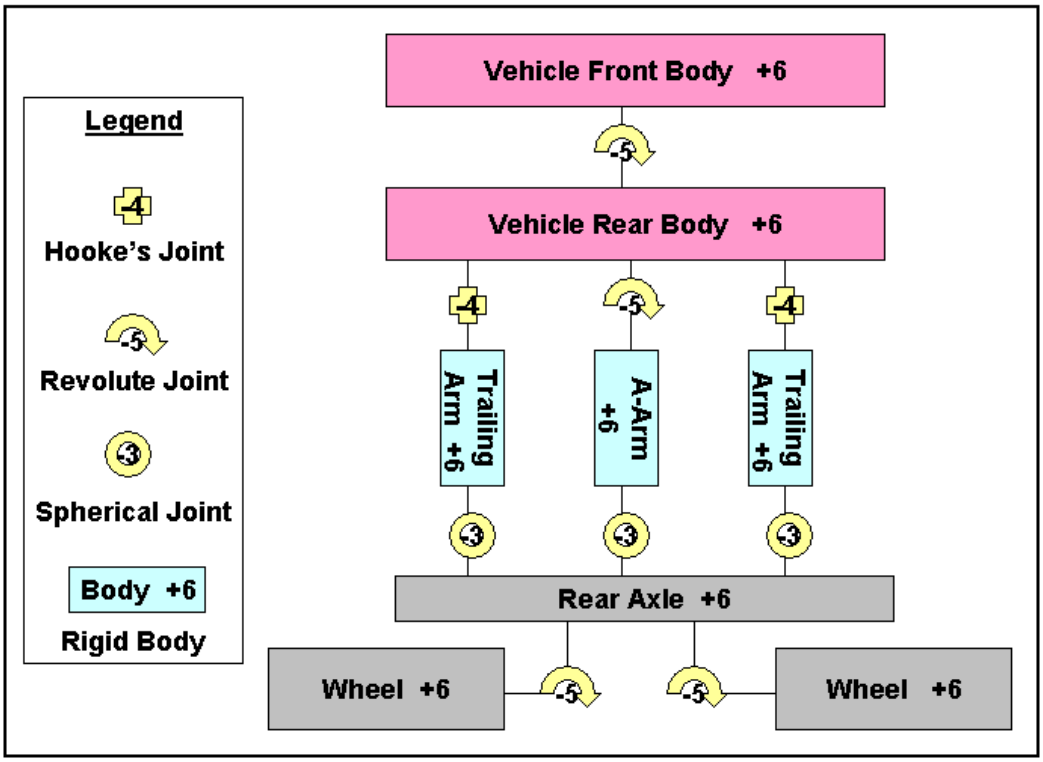

Figure 108: Rear suspension schematic.

Tyre side-force *vs.* slip angle characteristics were obtained from measurements using a two-wheeled tyre tester towed behind a vehicle. The measured data was converted to the coefficients required for the MSC ADAMS Pacjeka '89 tyre model. The tyre side-force vs. slip angle characteristics is indicated in Figure 109.

A Land Rover Defender 110 SUV was obtained locally for testing purposes. The aim of the baseline vehicle tests was to validate the ADAMS model of the vehicle and the tests were performed at the Gerotek Vehicle Test Facility.

The instrumentation used for the baseline tests, as well as measurement positions, is indicated in Table 3.

To validate the ADAMS model, simulation results were compared to measured results over a trapezoidal bump test. The vehicle driving over the trapezoidal bump is shown in Figure 110.

Test procedure and obstacle was chosen to ensure repeatability. Vehicle speed was kept constant by driving the diesel engine against its governor.

The vertical acceleration from the actual tests as well as the simulation results were weighted using the British Standard BS 6841, BS (1987), W_b weighting filter.

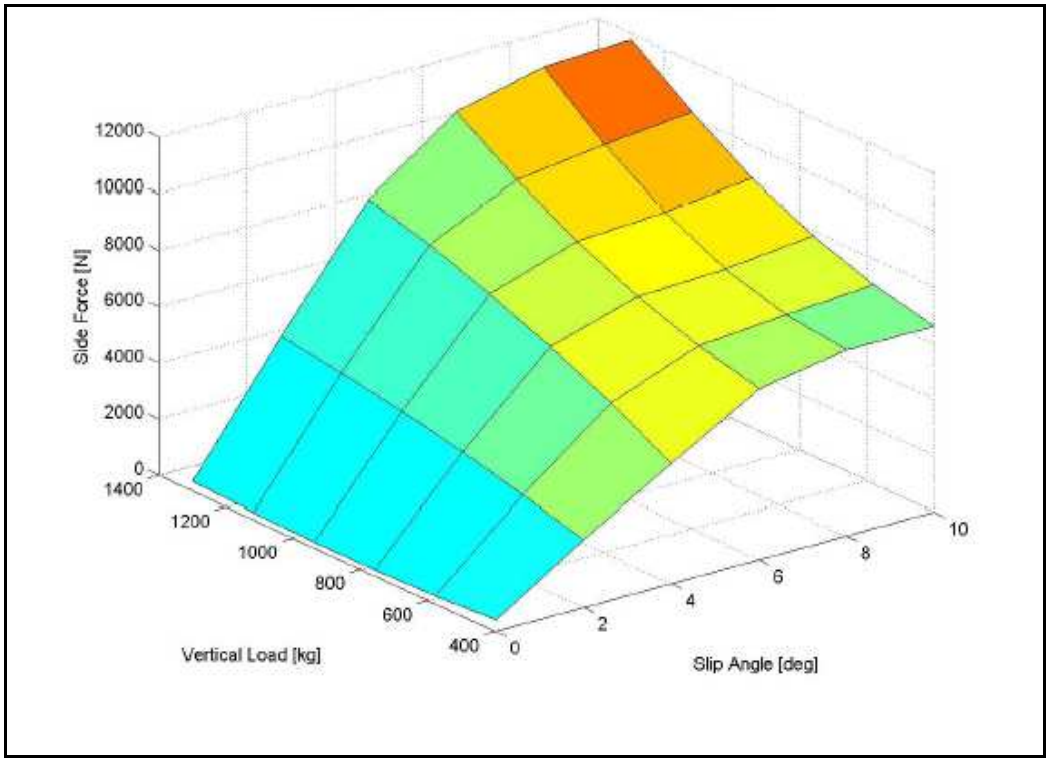

Figure 109: Tyre side-force vs. slip angle characteristic.

No	Parameter	Position	Equipment
1	Vehicle speed	Roof	VBOX GPS
2	Relative displacement	Left front suspension	Penny&Giles rope displacement transducer
3	Relative displacement	Right front suspension	Penny&Giles rope displacement transducer
4	Relative displacement	Left rear suspension	DWT rope displacement transducer
5	Relative displacement	Right rear suspension	DWT rope displacement transducer
6	Roll velocity	Vehicle body between front seats	Solid state gyro
7	Yaw velocity	Vehicle body between front seats (close to cg)	Solid state gyro
8	Relative displacement	Steering arm between axle and body	Penny&Giles rope displacement transducer
9	Acceleration	Left front lateral	Solid state accelerometer ±4g range
10	Acceleration	Right rear vertical	Solid state accelerometer ±4g range
11	Acceleration	Left rear lateral	Solid state accelerometer ±4g range
12	Acceleration	Left rear vertical	Solid state accelerometer ±4g range
13	Pitch velocity	Vehicle body between front seats	Solid state gyro
14	Kingpin steer angle	Kingpin	Potentiometer
15	Wheel speed	Left rear wheel	Turck Banner optical speed sensor
16	Driveshaft speed	Gearbox output rear	Turck Banner optical speed sensor

Table 3: Instrumentation used for baseline vehicle tests.

Figure 110: Trapezoidal Bump.

The trapezoidal bump was chosen to validate the vertical and pitch dynamics of the vehicle. The road input profile is easily measured and included in a

simulation model. Figure 111 indicates the correlation obtained between the measured and simulated results. Correlation is indicated for pitch velocity, spring displacement right front (rf), spring displacement rear left (rl), steering displacement as well as front and rear vertical accelerations. Correlation for vertical accelerations is especially good which is important because vertical acceleration is a direct measure of ride comfort. The model is thus considered validated for ride comfort simulation.

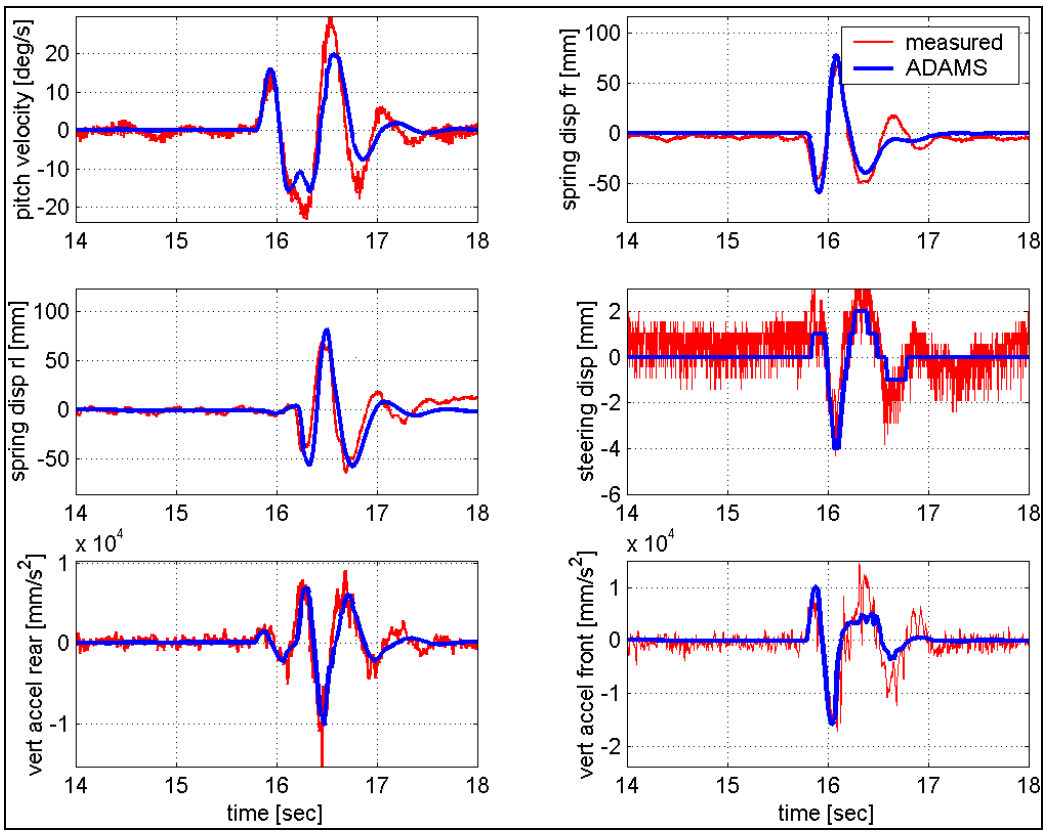

Figure 111: Model validation results for passing over 100 mm trapezoidal bump at 25 km/h.

The only adjustments made to the model, used for the simulations with the terrain profiles from the current study, were the addition of the 3-D Road Definition File and a steering driver was added which allowed the Land Rover to drive in a straight line over the terrain.

When simulating vehicle dynamics, the tyre model used is very important. ADAMS/Tire has a selection of tyre models which may be used of handling, ride, chassis control or durability simulations. Each tyre model is valid in a specific area and using a tyre model outside the specified area may result in non-realistic analysis. Table 4 indicates the preferred tyre model(s) to be used for a number of applications. In general the ADAMS/Tire Handling models are valid on rather smooth roads only. The wavelength of the road obstacles should not be smaller than the tyre circumference. If the wavelengths are shorter, the FTire model should be used which is able to cope with the non-linear tyre enveloping effects at high excitation frequencies.

Table 4: Typical applications for each tyre model (ADAMS/Tire, 2007).

MD Adams	Event / Maneuver	ADAMS/ Handling Tire							Specific Models	
		PAC2002[1]	PAC-TIME[1]	PAC89[1]	PAC94[1]	FIALA[1]	5.2.1.[1]	UA Tire[1]	PAC-MC[1]	FTire
Handling	Stand still and start	+	o/+	o/+	o/+	o/+	o/+	o/+	o/+	+
	Parking (standing steering effort)	+	-	-	-	-	-	-	-	+
	Standing on tilt table	+	+	+	+	+	+	+	+	+
	Steady state cornering	+	+	o/+	+	o	o	o/+	+	o/+
	Lane change	+	+	o/+	+	o	o	o/+	+	o/+
	ABS braking distance	+	o/+	o/+	o/+	o	o	o/+	o/+	+
	Braking/power-off in a turn	+	+	o	o	o	o	o	+	o/+
	Vehicle Roll-over	+	o	o	o	o	o	o	o	+
	On-line scaling tire properties	+	-	-	-	-	-	-	-	o
Ride	Cornering over uneven roads *	o/+	o	o	o	o	o	o	o	o/+
	Braking on uneven road *	o/+	o	o	o	o	o	o	o	+
	Crossing cleats / obstacles	-	-	-	-	-	-	-	-	+
	Driving over uneven road	-	-	-	-	-	-	-	-	+
	4 post rig (A/Ride)	+	o/+	o/+	o/+	o/+	o/+	o/+	o/+	o/+
Chassis Control	ABS braking control	o/+	o	o	o	o	o	o	o	+
	Shimmy[2]	o/+	o	o	o	o	o	o	o	+
	Steering system vibrations	o/+	o	o	o	o	o	o	o	+
	Real-time	+	-	-	-	-	-	-	-	-
	Chassis control systems > 8 Hz	o/+	-	-	-	-	-	-	-	+
	Chassis control with ride	-	-	-	-	-	-	-	-	+
Dura-bility	Driving over curb	-	-	-	-	-	o	o	-	o/+
	Driving over curb with rim impact	o	-	-	-	-	o	o	-	o/+
	Passing pothole	-	-	-	-	-	o	o	-	o/+
	Load cases	-	-	-	-	-	o	o	-	o/+

* wavelength road obstacles > tire diameter

[1] use_mode on transient and combined slip

[2] wheel yawing vibration due to supension flexibility and tire dynamic response

-	Not possible/Not realistic
o	Possible
o/+	Better
+	Best to use

Some Handling Tyre models can describe the first order response of the tyre, but do not take the eigen frequencies of the tyre into account. This causes the Handling Tyre models to be valid up to approximately 8 Hz.

The Land Rover model used in ADAMS used the PAC89 ADAMS/Tire model which is a point follower together with the Pacejka '89 Magic Tyre Formula which calculates the forces in the tyre. The PAC89 tyre model was used for the validation of the Belgian paving Road Definition File since the model was previously validated with the Double Lane Change manoeuvre, (Thoresson, 2003), as well as for Vehicle Roll-over manoeuvres, (Uys, 2007). Table 4 indicates that with the use of the PAC89 tyre model, non-realistic analysis may be obtained. The Ftire model is the preferred tyre model to use for driving over uneven roads, however at the time an Ftire model and license was not available for the Land Rover Defender 110 model.

The model of the Land Rover driving over the Belgian paving is shown in Figure 112. In the figure the front wheels of the model are on the Belgian paving and the rear wheels are still on the smooth section of the terrain.

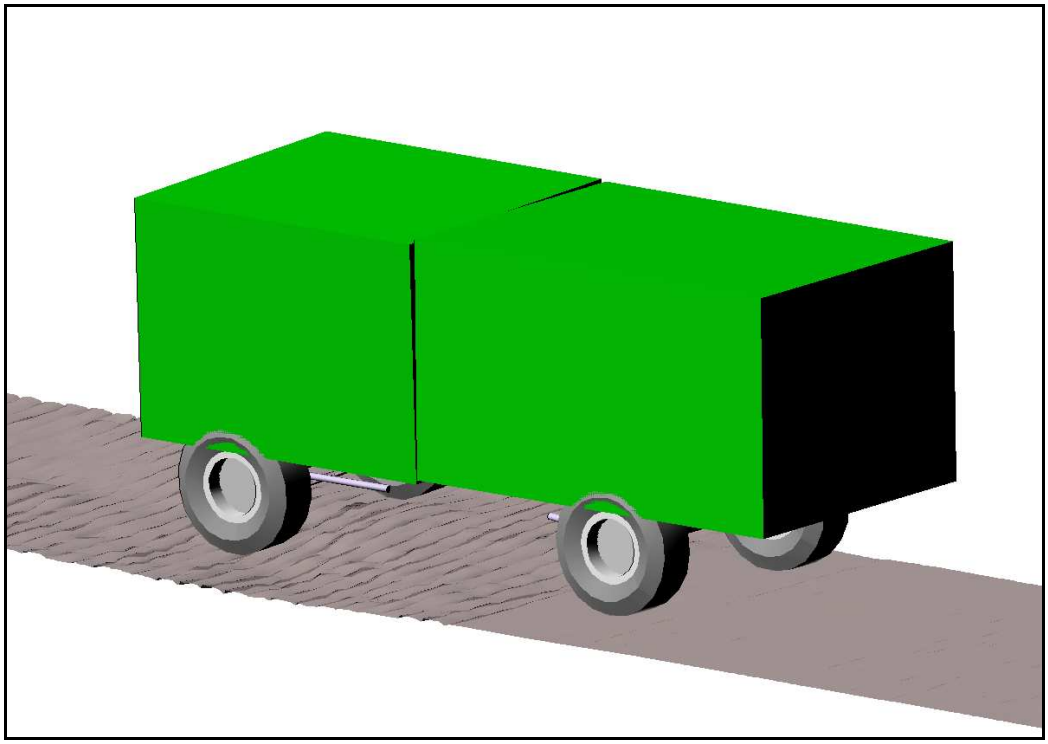

Figure 112: Model of Land Rover Defender 110 on the Belgian paving in ADAMS.

A close-up of the wire frame representing the wheel of the Land Rover and the mesh of the Belgian paving in ADAMS is shown in Figure 113. This figure illustrates the resolution of the terrain obtained with the use of the Can-Can Machine.

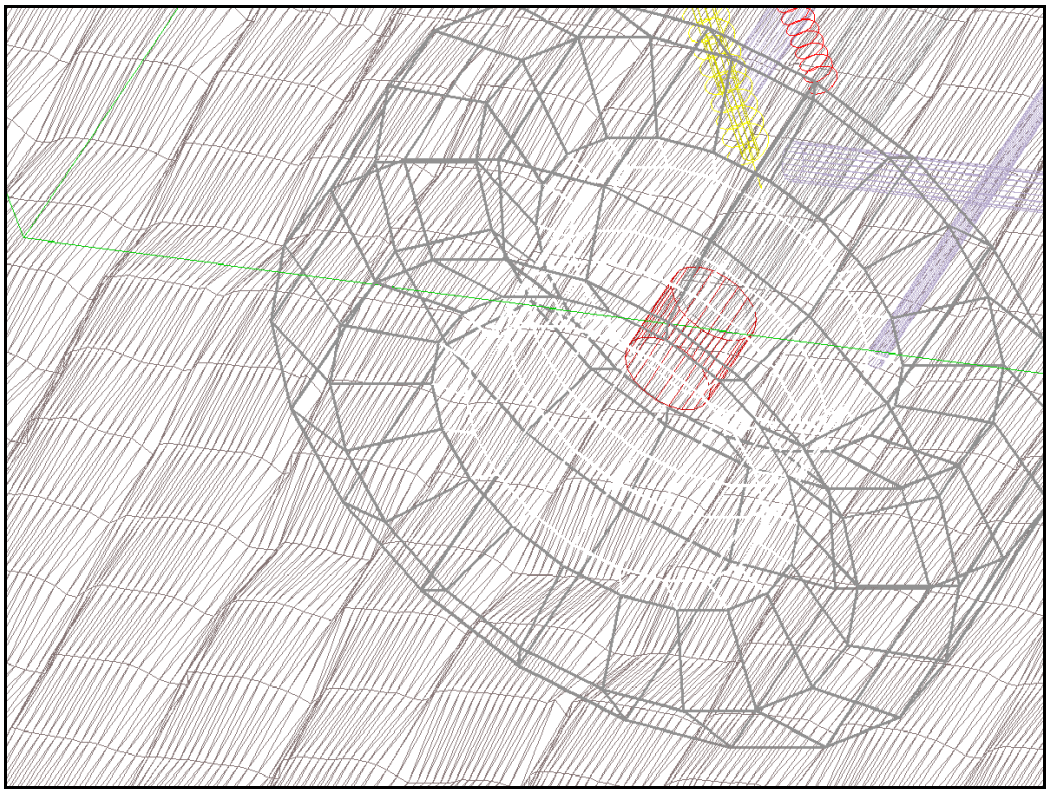

Figure 113: Close-up of the wire frame of the wheel on the Belgian paving mesh.

6.1.2. Simulation of Land Rover ride comfort

The ride comfort of the Land Rover was simulated over the Belgian paving road. Vertical accelerations at the three positions on the vehicle body were weighted using the BS 6841, BS, (1987) filter indicated in Figure 114. The BS 6841 standard is the British Standard Guide to measurement and evaluation of human exposure to whole-body mechanical vibration and repeated shock.

The Fast Fourier Transforms were calculated for the vertical accelerations of the three points of interest in the simulations as well as the vertical accelerations from the actual Land Rover measurements. The Fast Fourier Transforms were filtered with the weighting function prescribed by the BS 6841 standard (BS, 1987). An example of the weighted Fast Fourier Transform from the simulation and Land Rover data @ 40 km/h is shown in Figure 115. The weighted Fast Fourier Transform plots for all of the simulations and Land Rover data are available in Appendix E.

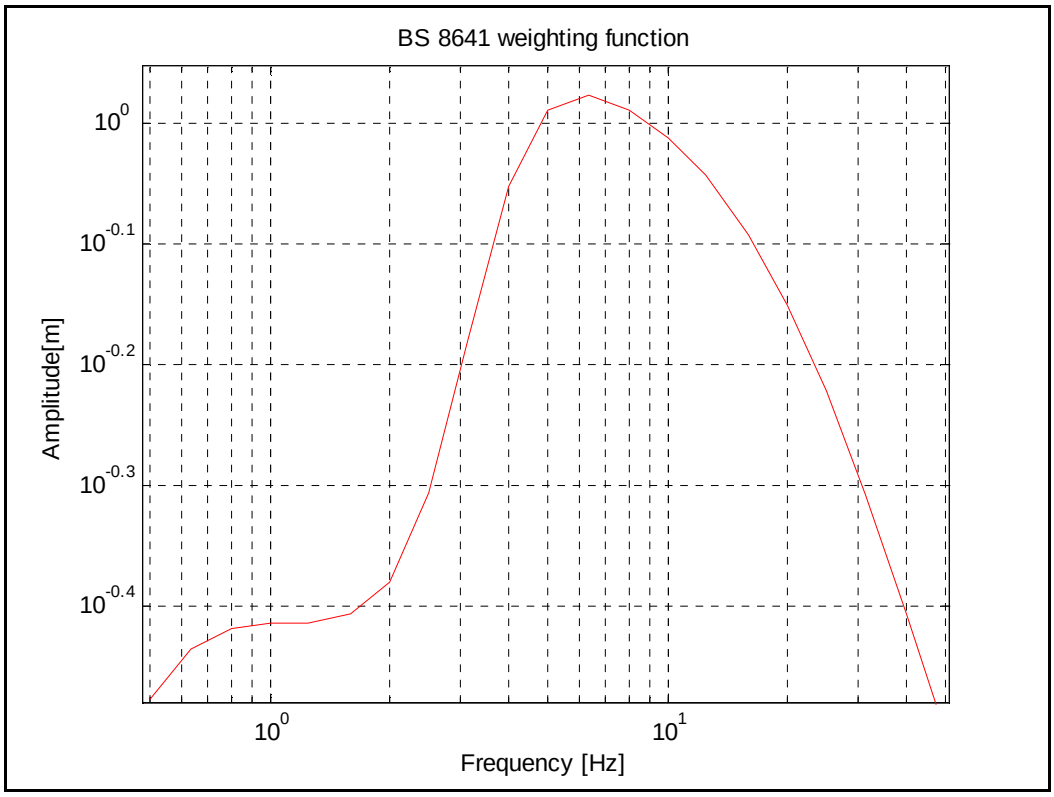

Figure 114: BS 6841 weighting function.

It can be seen in Figure 115 that there is good correlation between the simulation and Land Rover data up to approximately 8 Hz. This is expected due to the fact that the PAC89 Tyre model is valid up to approximately 8 Hz (see Table 4). Both measured and simulated data was subsequently filtered with an 8 Hz low pass filter and the resultant Fast Fourier Transform is shown in Figure 116. The 8Hz low pass filtered Fast Fourier Transform plots for all of the simulations and Land Rover data are available in Appendix E.

The Fast Fourier Transforms from the Simulations and the Actual Land Rover test data correlate very well. The trends and magnitudes of the Fast Fourier Transforms was the same and the peaks and valleys were found at the same frequencies.

The 8 Hz low pass filtered Fast Fourier Transforms were transformed back to the vertical accelerations in the time domain. The filtered vertical accelerations of the right rear body of the simulations and the actual Land Rover data @ 40 km/h is shown in Figure 117. The filtered vertical accelerations measured at the points of interest also correlate very well and it can be seen in Figure 117 that the trend of the accelerations were the same and the acceleration peaks were recorded at the same time. The filtered vertical accelerations of the three points of interest in the simulations and the Actual Land Rover data are presented in Appendix E. Direct comparison in the time domain is not possible because the chance that the vehicle followed exactly the same path (lateral position) during the simulation and actual tests are very slim.

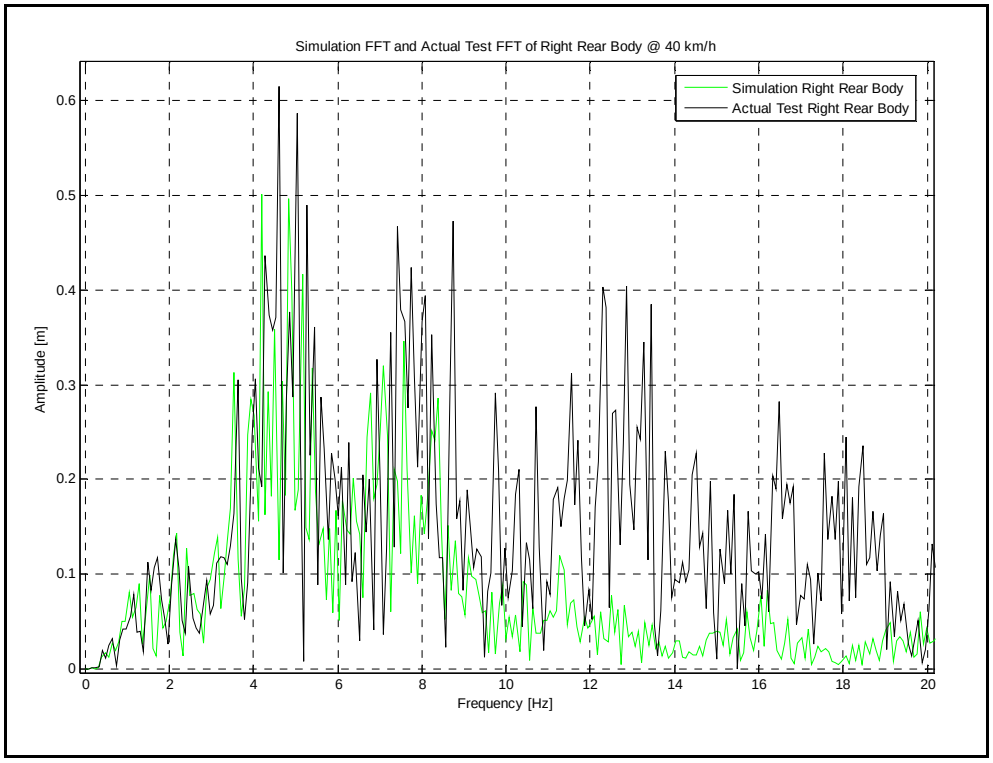

Figure 115: Weighted Fast Fourier Transforms of the Simulation and Land Rover data @ 40 km/h.

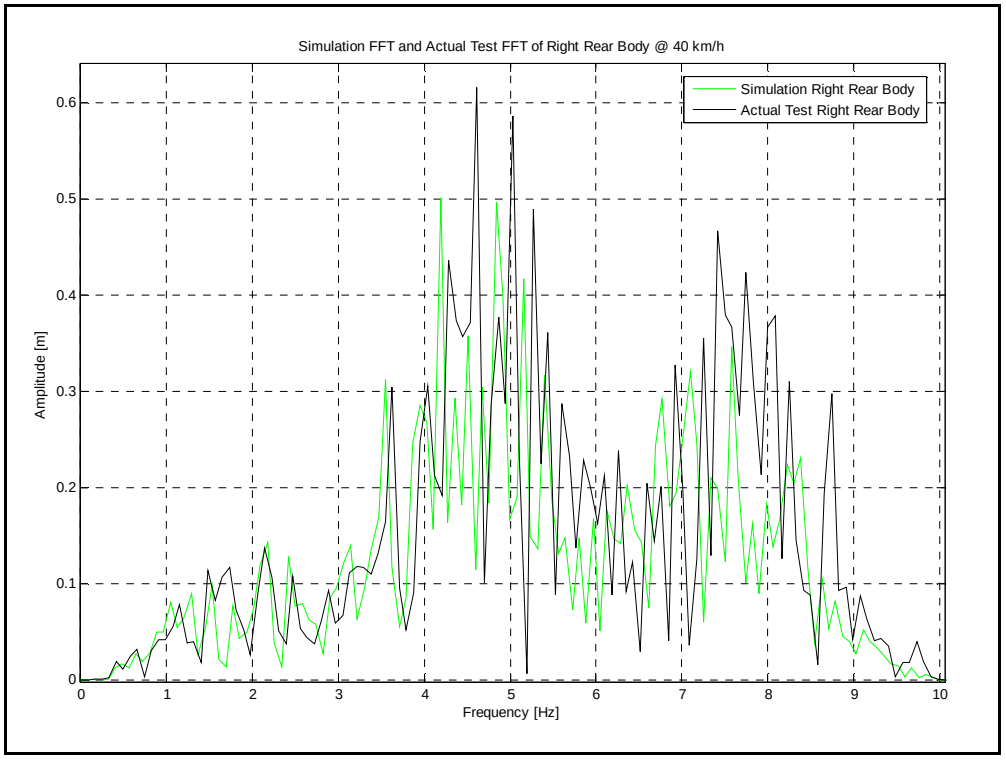

Figure 116: 8 Hz Low Pass Filtered FFT of the simulation and Land Rover data @ 40km/h.

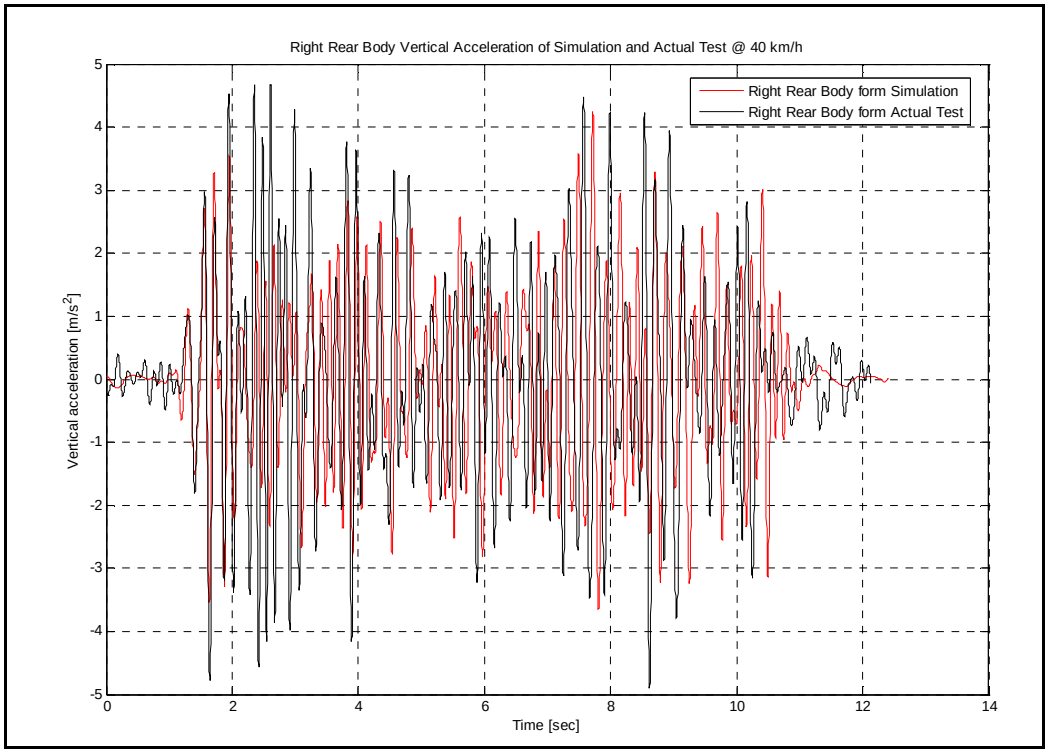

Figure 117: Filtered Right Rear Body vertical accelerations from simulation and Land Rover @ 40km/h.

The ride comfort of the occupants was therefore determined by calculating the Root Mean Square (RMS) value of the vertical acceleration. The Root Mean Square measures of acceleration may be used when the crest factor does not exceed 6. The crest factor of the motion is to be determined from the peak and RMS value of the acceleration after it has been frequency weighted.

$$\text{Crest factor} = \frac{\text{weighted peak acceleration}}{\text{weighted RMS acceleration}}$$

The peak and RMS values were determined over the full period of vibration exposure.

The RMS values of the three points of interest were calculated for the different speeds travelled in the simulations and the actual Land Rover. These values are graphically shown in Figure 118. It can be seen that the Left Front (LF) position in the simulation tends to measure higher accelerations than the same position on the actual Land Rover where as the Right Rear and Left Rear (RR and LR) positions of the actual Land Rover tend to measure higher accelerations than the same positions in the simulations.

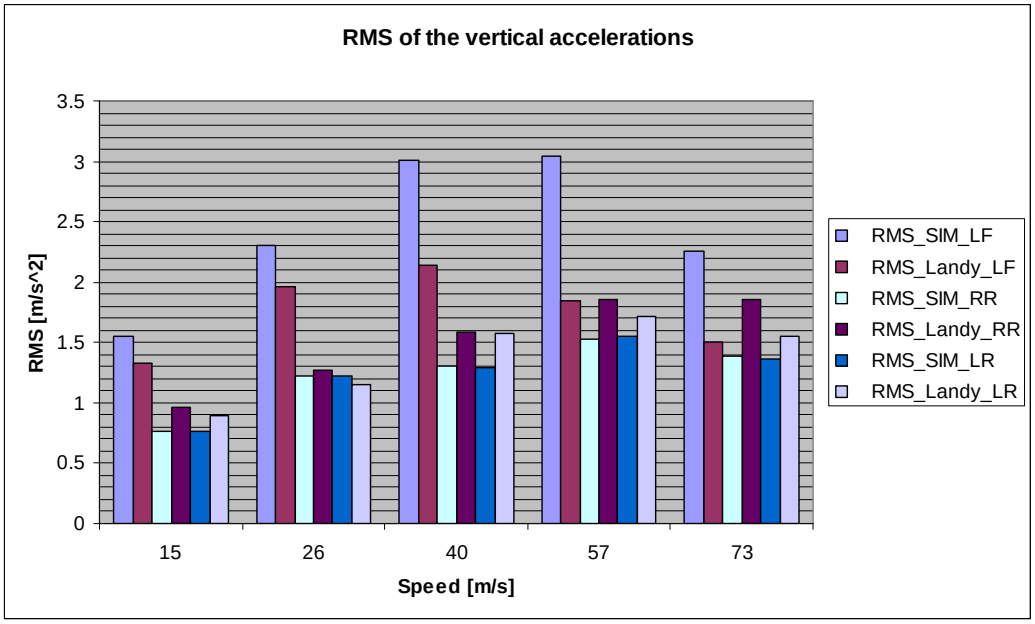

Figure 118: RMS values from Simulations and measured Land Rover data.

The higher accelerations and RMS values of the LF position in the actual Land Rover measurements was expected due to the fact that the accelerometer was placed on the chassis of the vehicle which in turn was exposed to additional accelerations caused by engine and driveline vibrations.

The higher accelerations and RMS values of the LF position in the simulations may have been due to the fact that the placement was 300 mm in front of the front axle which may be exposed to higher accelerations as the position was very close to the front of the vehicle.

The difference between the RMS values calculated from the vertical accelerations measured in the simulations and the vertical accelerations from the actual Land Rover is shown in Figure 119. It can be seen in Figure 119 that the best correlation between the simulations and the actual Land Rover is obtained at 26 km/h.

Simulated RMS values for LR and RR correlate well with the actual measurements and are generally within 20%. Correlation becomes worse as vehicle speed increases. This is attributed to the tyre model that only allows acceptable results up to 8 Hz, which excludes tyre hop. As vehicle speed increases, the terrain excitation moves to higher frequencies and the tyre model deficiencies become more pronounced.

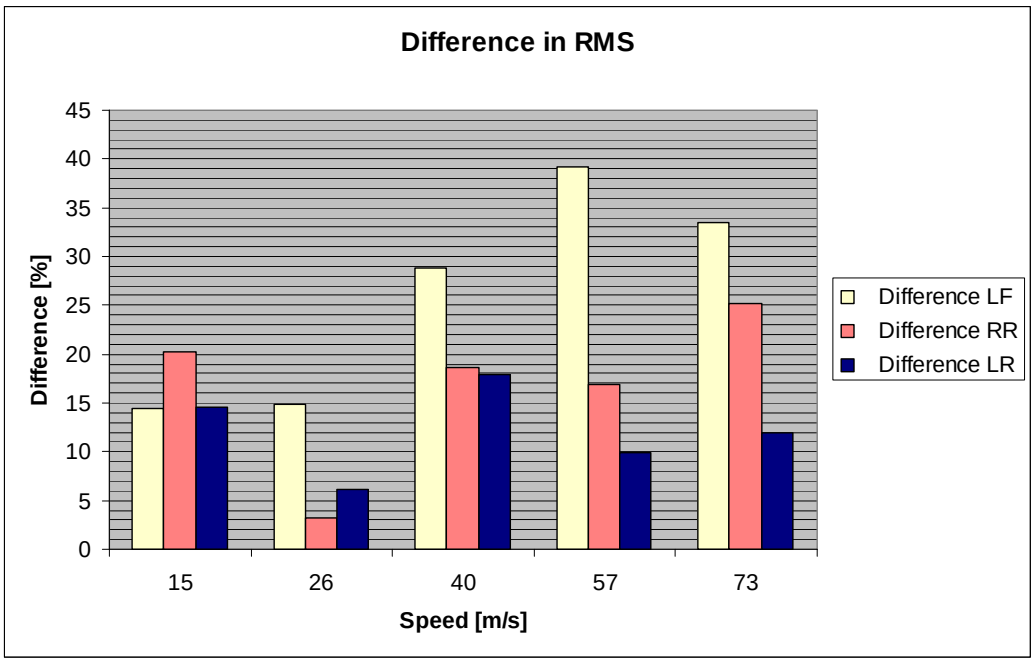

Figure 119: Difference in Simulations RMS values and Land Rover RMS values.

When compared to the RMS values in the BS code, the occupants' measured ride is very uncomfortable (1.25 – 2.5 m/s^2) when driving over the Belgian paving, which is indeed the case.

6.2. Simulation and data verification

The conclusion is made that the 3-D profile of a terrain, profiled with the Can-Can Machine, was successfully implemented in a 3-D simulation of a Land Rover Defender 110 driving over the Belgian paving.

Good correlation between the response of the two rear points of interest in the simulation model and on the actual Land Rover indicates that the 3-D profile of the terrain is a valid and accurate profile of the actual terrain. The tyre model used in the simulations limited the results of the simulation. This limit was in the form of accurate and realistic analysis up to approximately 8 Hz. Improved analyses is possible with the use of an Ftire model. The Ftire model is fully nonlinear and provides accurate and realistic analysis in the frequency domain up to 120 Hz. The Ftire model was not used during this analysis due to the fact that an Ftire model for the Land Rover used in the simulations was not available.

The RMS values presented in Figure 118 and the difference in the RMS values from the simulations and the actual Land Rover shown in Figure 119 indicate that the correlation between the simulation and the actual Land Rover decreases as the speed of the vehicle increases. This is a direct result from

the PAC89 tyre model used in the simulations. This result is due to the fact that the PAC89 tyre model can only supply realistic analysis results up to approximately 8 Hz.

When the vehicle is travelling at 73 km/h and a realistic analysis can only be conducted at 8 Hz, very important data is lost between data points. This is the case because at 73 km/h the distance between data points is 2.5 m. It is also concluded that 73 km/h may also be too fast when calculating the RMS values for ride comfort on rough terrain. The calculation of the RMS value is very dependent on the correct travelling speed.

The best correlation between the simulation and the actual Land Rover was at 26 km/h where the difference in the RMS values at the three points of interest was 15% and lower.

Improved correlation may be obtained between the LF position in both the simulation model and the actual Land Rover if the LF position is moved to a position inside the vehicle and not directly on the chassis of the vehicle. This will reduce the effect of engine and drive train vibration on the measurement.

7. Conclusions and recommendations

7.1. Conclusions

To obtain an accurate profile of a terrain it is important to know the orientation of the profilometer when a terrain is profiled. Most of the terrains used for testing by the University of Pretoria have a known fixed reference around the terrain. The fixed reference is in the form of a flat surface around each terrain. Three profilometers were designed and built with the known flat reference in mind. The first profilometer was a mechanical profilometer (Can-Can Machine) on three wheels, each moving on the flat reference. The second profilometer profiled a terrain with the use of Photogrammetry. The third profilometer used a laser displacement sensor which was mounted in a gimball and positioned with stepper motors.

Photogrammetry and stereo techniques with aerial imagery is a possible option in profiling rough terrains. Although no literature was obtained where actual rough terrains were profiled with the use of Photogrammetry it remains a feasible option in the profiling rough terrains.

Laser scanning platforms are very accurate systems but the accuracy is compromised by the Global Positioning System when the 3-D model is placed in a global coordinate system. These systems have colossal raw data bundles and require state of the art computers for effective data processing. The laser scanning platforms are highly-priced and way beyond the resources for this study. The Laser scanning platforms are widely available however the vertical height required in order to profile a 100 m section of a terrain may compromise the obtainable resolution of the profile.

The proposed profilometers were reviewed and the operational functions of each were examined. Test sections were profiled with each of the proposed profilometers and the results were evaluated.

It was found that the Can-Can Machine is a simple and effective profilometer with the ability to profile rough terrain. The Can-Can Machine can profile a rough terrain with an accuracy of < 5 mm. The Photogrammetry profiling method is a valid and accurate profiling method with an accuracy of < 5 mm, however it remains time consuming and resource intensive. The Laser Scanner is a time consuming profilometer but remains a prospective profilometer still in the development phase. The Laser Distance Sensor has an accuracy of 5 mm but the accuracy of the total system is limited by the gimball.

The profiles obtained of the profiled terrains were accurate and visually very representative of the actual terrain. Although the resolution of the Laser Scanner was lower than the resolution of the Can-Can Machine a valid profile was still produced by the Laser Scanner. The resolution of the Belgian paving profile as profiled with Photogrammetry was very high and contained a high

amount of detail, but remained time consuming and resource intensive. The Can-Can Machine produced profiles of the terrains quickly and effectively. The Displacement Spectral Densities of the terrains profiled with the Can-Can Machine indicated that the resolution of the Can-Can Machine was high enough to obtain valuable information about the terrains.

The conclusion is made that the Displacement Spectral Densities of the profiled terrain were representative of the profiled terrain. The Displacement Spectral Density of each of the profiled terrains provided information about the terrains in the form of the Roughness Coefficient and the Road Index as well as the dominant frequencies generated when driving on the track. The values of the Roughness Coefficient and the Road Index were high as expected.

The International Roughness Index was calculated for each of the profiled terrains and it indicated that the International Roughness Index was a valid method for characterizing smoother terrains. The International Roughness Index of the rough terrains on which this present study were concentrating on indicated that the Displacement Spectral Density of the profiles were the superior method used in characterizing rough terrains.

When a 3-D tyre model is used in a simulation the mesh size of the road profile used for the simulation may not be larger than half the contact patch of the tyre. Thus one is able to use a road profile with a mesh size smaller or equal to 100 mm in the direction of travel.

Good correlation between the response of the two rear points of interest in the simulation model and on the actual Land Rover indicated that the 3-D profile of the terrain (as profiled with the Can-Can Machine) was a valid and accurate profile of the actual terrain. The tyre model used in the simulations limited the results of the simulation. This limit was in the form of accurate and realistic analysis up to approximately 8 Hz. Improved simulation analyses is possible with the use of an Ftire model. The Ftire model is fully nonlinear and provides accurate and realistic analysis in the frequency domain up to 120 Hz. The Ftire model was not used during this analysis due to the fact that an Ftire model for the Land Rover used in the simulations was not available.

The best correlation between the simulation and the actual Land Rover was at 26 km/h where the difference in the RMS values at the three points of interest was 15% and lower.

7.2. Recommendations for future work

It has been established that the Can-Can Machine is a fast, cost effective and accurate profilometer, however the following is suggested to improve the accuracy and operation of the Can-Can Machine:

I. The use of multiple tilt sensors, one on the front and one on the rear of the Can-Can Machine, to determine the orientation of the structure of the profilometer. The multiple tilt sensors can be used to evaluate the front and rear movement of the structure.

II. Stiffening the structure of the profilometer to enable the profilometer to move over rough terrain with ease.

III. Increase the power delivered on the drive wheel to allow the profilometer to move over large obstacles without additional assistance.

IV. A revision on the shape of the arms on the rear beam, which will allow the profilometer to profile large obstacles without the arms coming into contact with the obstacle.

V. The accuracy of the Can-Can Machine in a global coordinate system can be increased with the addition of a RTK DGPS and an IMU to the Can-Can system.

Improved simulation analyses are possible with the use of an Ftire model. The Ftire model is fully nonlinear and provides accurate and realistic analysis in the frequency domain up to 120 Hz.

Improved correlation may be obtained between the LF position in both the simulation model and the actual Land Rover if the LF position is moved to a position inside the vehicle and not directly on the chassis of the vehicle. This will reduce the effect of engine and drivetrain vibration on the measurement.

References

A

Andren, P., 2006, **Power spectral density approximations of longitudinal road profiles**, International Journal of Vehicle Design, 40, (1/2/3), pp. 2-14.

Anon, 2005, **High Speed Profilometer**, Surveillance Services, CSIR website, World Wide Web, www.csir.co.ca, Assessed 2005-03-10.

Antone, M.E., and Teller, S., 2000, **Automatic recovery of relative camera positions in urban scenes**, Computer Vision and Pattern Recognition, 2, pp 282-289.

ASTM E1364, 2005, **Standard Test Method for Measuring Road Roughness by Static Level Method**, ASTM E1364 – 95(2005), American Society for Testing and Materials (ASTM).

B

British Standards Institution, 1987, **British Standard Guide to Measurement and Evaluation of Human Exposure to Whole Body Mechanical Vibration and Repeated Shock**, BS 6841, 1987.

C

Canny, J., 1986, **A computational approach to edge detection**, IEEE Trans. Patt. Anal, Machine Intelli, vol. 8, pp 679-698.

D

Davis, B.R. and Thompson, A.G., 2001, **Power spectral density of road profiles**, Vehicle System Dynamics, Vol. 35, pp. 409-415.

E

Edara, R., Shih, S., Tamini, N., Palmer, T. and Tang, A., 2005, **Heavy Vehicle Suspension Frame Durability Analysis Using Virtual Proving Ground**, SAE 2005-01-3609.

Els, P.S., 2006, **The ride comfort vs. handling compromise for off-road vehicles**, Unpublished PhD.Eng Thesis, University of Pretoria, Pretoria, South Africa.

G

Gerotek Test Facilities, 2007, www.gerotek.co.za, Accessed 2007/02/27.

Google earth, 2007 , **Gerotek Test Facility**, Pretoria, South Africa, 25° 45' 30.19" S 28° 00' 27.82" E, Accessed 2007/09/13.

Gorsich, D.J., Chaika, M., Gunter, D., Karlsen, R., Haueisen, B., Sun, T. and Ferris, J., 2003, **Terrain Roughness Standards for Mobility and Ultra-Reliability Prediction**, SAE 2003-01-0218.

Grinstead, B., Koschan, A.,Page, D., Gribok, A. and Abidi, M.A., 2005, **Vehicle-borne Scanning for Detailed 3D Terrain Model Generation**, SAE(Society of Automotive Engineers) Commercial Vehicle Engineering Congress, Chicago, IL, November, 2005, SAE Technical Paper 2005-01-3557.

H

Hall, L.C, 1998, **Terrain Profile Characteristics**, Fundamentals of Terramechanics & Soil Vehicle Interaction.

I

Imine, H., M'Sirdi, N.K. and Delanne, Y., 2003, **Adaptive Observers and Estimation of the Road Profile**, SAE 2003-01-1282.

Imine, H. and Delanne, Y., 2005, **Triangular Observers for Road Profiles Inputs Estimation and Vehicle Dynamics Analysis**, International Conference on Robotics and Automation, Barcelona, Spain.

International Organization for Standardization, 1995, **International Organization for Standardization ISO 8606: Mechanical vibration - Road surface profiles - Reporting of measured data**, ISO 8608:1995(E).

K

Karamihas, S.M. and Gillespie, T.D., 2002, **Assessment of Profilometer Performance for Construction Quality Control**, University of Michigan, December 2002.

Kern, J.V, 2007, **The Development of Measurement and Characterization Techniques of Road Profiles**, Master of Science in Engineering, Virginia Polytechnic Institute and State University, Danville, USA, June 2007.

Kulakoski, B.T., Henry, J.J. and Wambold, J.C., 1986, **Relative Influence of Accelerometer and Displacement Transducer Signals in Road Profilometry**, Transportation Research Record, January 1986.

M

MSC Software web page, 2007, **MSC.Software\MSC.ADAMS\2007r1\help**, **Defenition of Road Mesh in MSC>ADAMS**, accessed on 2007/7/20.

MSC Sotfware web page, 2007, **MSC.Software\MSC.ADAMS\2007r1\help, Contens, Which Tyre Model Should You Use?**, accessed on 2007/11/10.

McDonald, A.J., Crossley, S., Bennett, J.C., Brown, S.C.M., Cookmartin, G., Morrison, K. and Quegan, S., 2000, **Stereo vision measurements of soil surface characteristics and their use in model validation**, European Space Agency, pp. 575-580.

P

Pollard, S.B., Pridmore, T.P., Porril, J., Mayhew, J.E.W. and Frisby, J.P., 1989, **Geometrical modeling from multiple stereo views**, Int. J. Robot. Res., vol. 8 pp. 3-32.

R

Ritchie, W., Wood, M., Wright, R. and Tait, D., 1991, **Surveying and mapping for field scientists**, USA, Chapter 3.

Rodrigues' rotation formula, 2008, Wikipedia, **Rodrigues' rotation formula**, www.wikipedia.org/Rodigues'_rotation_formula, Accessed 2008/01/10.

Rouillard, V., Sek, M.A. and Bruscella, B., 2001, **Simulation of road surface profiles**, Journal of Transportation Engineering, May/June, pp 247-253.

S

Sayers, M.W. and Karamihas, S.M., 1998, **The Little Book of Profiling**, University of Michigan.

Shoop, S., Coutermarsh, B. and Reid, A., 2004, **All-Season Virtual Test Site for a Real-Time Vehicle Simulator**, SAE 2004-01-2644.

Spangler, E.B., 1964, **Road Profilometer Method for Measuring Road Profile**, General Motors Research Publication, GMR-452.

Sun, L., 2001, **Simulation of pavement roughness and IRI based on power spectral density**, The University of Texas at Austin.

Sun, T.C., Alyass, K., Wei, J., Gorsich, D., Chaika, M. and Ferris, J., 2005, **Time Series Modeling of Terrain Profiles**, SAE 2005-01-3561.

Swart, B., 2008, ***Photogrammetry profile of Belgian paving report***, unpublished report, CAD Mapping.

T

Thoresson, M.J., 2003, **Mathematical optimisation of the suspension system of an off-road vehicle for ride comfort and handling**, Unpublished M.Eng Thesis, University of Pretoria, Pretoria, South Africa.

U

Uys, B.P., 2007, **Rollover of off-road vehicle**, Unpublished M.Eng Thesis, University of Pretoria, Pretoria, South Africa.

Uys, P.E., Els, P.S. and THoresson, M., 2007, **Suspension settings for optimal ride comfort of off-road vehicles traveling on roads with different roughness and speeds**, Journal of Terramechanics, vol. 44, pp. 163-175.

Z

Zaayman, O.C.D., 1988, **Terrain profile roughness measurement and characterization***,* Unpublished M.Eng Thesis, University of Pretoria, Pretoria, South Africa.

Appendix A:

- ***Certificate of Conformance for Crossbow Tilt Sensor***

- ***Calibration certificate of Sony Cyber Shot 5 mega pixel Digital Camera***

- ***Calibration certificate of Pentax K10D Digital Camera***

Certificate of Conformance for Crossbow Tilt Sensor

Certificate of Conformance **Crossbow** 2.12

calibration date: 09/11/2002

Calibration Data: Room Temperature

	X Axis	Y Axis
Zero-Angle Voltage	2.527	2.492
Sensitivity	35.003	35.116

Part Number	CXTA02
Serial Number	124759

Options: Regulator

Wiring Diagram:

Color	Function
Red	8 - 30 Vdc
Black	Ground
White	X-Axis
Yellow	Y-Axis

Thank you for choosing a Crossbow sensor. This worksheet is designed to help you get started. Refer to the product data sheet for more complete information.

Definitions

Zero - Angle Voltage : This number is the output voltage (in V) of the sensor on a level surface (zero tilt) measured at the factory on the day of the calibration.

Sensitivity : This number is the sensor's sensitivity in mV per degree.

Technical Support

For further technical assistance, contact Crossbow Technology.

Crossbow Technology, Inc.
41 East Daggett Drive
San Jose, CA 95134
Phone : 408.965.3300
Fax : 408.324.4840
URL : http://www.xbow.com
Email : info@xbow.com

Calibration certificate of Sony Cyber Shot 5 mega pixel Digital Camera

Status Report Tree

PhotoModeler Version: 5.1.0

Project Name: *** Rough Road Profiling ***

Problems and Suggestions (0)
  Project Problems (0)
  Problems related to most recent processing (0)

Information from most recent processing
  Last Processing Attempt: Wed Aug 31 14:39:30 2005
  Status: successful
  Processing Options
    Orientation: off
    Global Optimization: on
    Calibration: on (full calibration)
    Constraints: off
  Total Error
    Number of Processing Iterations: 4
    Number of Processing Stages: 2
    First Error: 0.019
    Last Error: 0.008
  Precisions / Standard Deviations
    Camera Calibration Standard Deviations
      Camera1: SONY
        Focal Length
          Value: 6.118036 mm
          Deviation: Focal: 0.002 mm
        Xp - principal point x
          Value: 2.640445 mm
          Deviation: Xp: 0.001 mm
        Yp - principal point y
          Value: 1.939080 mm
          Deviation: Yp: 0.001 mm
        Fw - format width
          Value: 5.312163 mm
          Deviation: Fw: 2.1e-004 mm
        K1 - radial distortion 1
          Value: 2.806e-003
          Deviation: K1: 4.7e-005
        K2 - radial distortion 2
          Value: 1.253e-004
          Deviation: K2: 5.3e-006
        K3 - radial distortion 3
          Value: 0.000e+000
        P1 - decentering distortion 1
          Value: 1.973e-004
          Deviation: P1: 8.8e-006
        P2 - decentering distortion 2
          Value: 1.761e-004
          Deviation: P2: 9.1e-006

Quality
- Photographs
  - Total Number: 11
    - Bad Photos: 0
    - Weak Photos: 0
    - OK Photos: 11
  - Number Oriented: 11
  - Number with inverse camera flags set: 0
- Cameras
  - Camera1: SONY
    - Calibration: yes
    - Number of photos using camera: 11
- Point Marking Residuals
  - Overall RMS: 0.045 pixels
  - Maximum: 0.389 pixels
    - Point 10 on Photo 1
  - Minimum: 0.040 pixels
    - Point 22 on Photo 11
  - Maximum RMS: 0.189 pixels
    - Point 10
  - Minimum RMS: 0.024 pixels
    - Point 71
- Point Tightness
  - Maximum: 0.00088 m
    - Point 10
  - Minimum: 0.0001 m
    - Point 71
- Point Precisions
  - Overall RMS Vector Length: 0.000151 m
  - Maximum Vector Length: 0.000176 m
    - Point 10
  - Minimum Vector Length: 0.000149 m
    - Point 48
  - Maximum X: 7.23e-005 m
  - Maximum Y: 7.42e-005 m
  - Maximum Z: 0.000144 m
  - Minimum X: 5.17e-005 m
  - Minimum Y: 5.17e-005 m
  - Minimum Z: 0.000127 m

Calibration certificate of Pentax K10D Digital Camera

Status Report Tree

PhotoModeler Version: 5.1.0

Project Name: *** Project has not yet been saved ***

Problems and Suggestions (1)
  Project Problems (1)
    Problem: A large percentage of your points are sub-pixel marked so it is assumed you are striving for a high accuracy result. The largest residual (Point10 - 3.902977) is greater than 1.00 pixels.
      Suggestion: In high accuracy projects, strive to get all point residuals under 1.00 pixels. If you have just a few high residual points, study them on each photo to ensure they are marked and referenced correctly. If many of your points have high residuals then make sure the camera stations are solving correctly. Ensure that you are using the best calibrated camera possible. Remove points that have been manually marked unless you need them.
  Problems related to most recent processing (0)

Information from most recent processing
  Last Processing Attempt: Tue Jan 15 08:01:21 2008
  Status: successful
  Processing Options
    Orientation: off
    Global Optimization: on
    Calibration: on (full calibration)
    Constraints: off
  Total Error
    Number of Processing Iterations: 4
    Number of Processing Stages: 2
    First Error: 0.119
    Last Error: 0.119
  Precisions / Standard Deviations
    Camera Calibration Standard Deviations
      Camera1: carl pentax
        Focal Length
          Value: 17.314739 mm
          Deviation: Focal: 0.001 mm
        Xp - principal point x
          Value: 11.002161 mm
          Deviation: Xp: 9.4e-004 mm
        Yp - principal point y
          Value: 7.737493 mm
          Deviation: Yp: 9.2e-004 mm
        Fw - format width
          Value: 21.914795 mm
          Deviation: Fw: 2.9e-004 mm
        K1 - radial distortion 1
          Value: 3.605e-004
          Deviation: K1: 1.3e-006
        K2 - radial distortion 2
          Value: -6.221e-007
          Deviation: K2: 9.3e-009
        K3 - radial distortion 3
          Value: 0.000e+000
        P1 - decentering distortion 1
          Value: -1.572e-005

Deviation: P1: 9.5e-007
P2 - decentering distortion 2
Value: 1.153e-005
Deviation: P2: 9.1e-007

Quality
Photographs
Total Number: 12
Bad Photos: 0
Weak Photos: 0
OK Photos: 12
Number Oriented: 12
Number with inverse camera flags set: 0
Cameras
Camera1: carl pentax
Calibration: yes
Number of photos using camera: 12
Point Marking Residuals
Overall RMS: 0.686 pixels
Maximum: 3.903 pixels
Point 10 on Photo 1
Minimum: 0.414 pixels
Point 14 on Photo 12
Maximum RMS: 1.924 pixels
Point 57
Minimum RMS: 0.266 pixels
Point 58
Point Tightness
Maximum: 0.0039 m
Point 10
Minimum: 0.00039 m
Point 58
Point Precisions
Overall RMS Vector Length: 4.67e-005 m
Maximum Vector Length: 5.11e-005 m
Point 2
Minimum Vector Length: 4.54e-005 m
Point 8
Maximum X: 2.58e-005 m
Maximum Y: 2.29e-005 m
Maximum Z: 3.97e-005 m
Minimum X: 1.75e-005 m
Minimum Y: 1.82e-005 m
Minimum Z: 3.62e-005 m

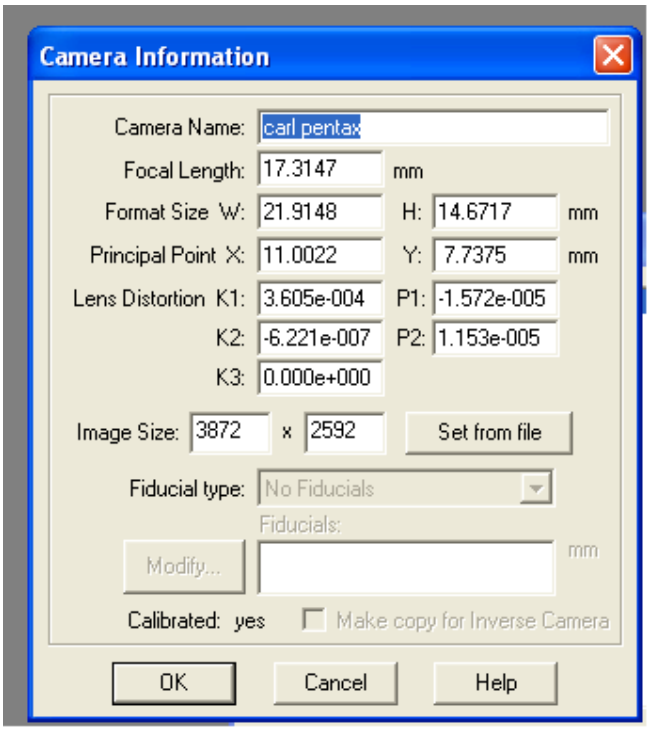
Camera Information
Camera Name: carl pentax
Focal Length: 17.3147 mm
Format Size W: 21.9148 H: 14.6717 mm
Principal Point X: 11.0022 Y: 7.7375 mm
Lens Distortion K1: 3.605e-004 P1: -1.572e-005
K2: -6.221e-007 P2: 1.153e-005
K3: 0.000e+000
Image Size: 3872 x 2592 Set from file
Fiducial type: No Fiducials
Fiducials:
Modify...
mm
Calibrated: yes
Make copy for Inverse Camera
OK
Cancel
Help

Appendix B: Datasheet on S80-MH-5 Data sensor

DATASENSOR

S80L-Y

Distance sensor with laser emission and time of flight measurement

INSTRUCTION MANUAL

CLASS 2 EN 60825-1 (1994)
LASER PRODUCT

CONTROLS

FRONT INDICATORS LED

OUTPUT LED
The yellow LED ON indicates the OR function of the OUT1 and OUT2 outputs (one of the 2 outputs is active).

ALARM LED
The red LED ON indicates the absence of signal.

COMMAND PANEL AND DISPLAY

OUTPUT LED
The yellow LED ON indicates the logic OR function of the two OUT1 and OUT2 outputs (one of the 2 outputs is active).

DISPLAY (4-digit green coloured display)
In the normal mode, the display indicates the detected distance, in millimetres.

OUT1, OUT2 LEDs
The n.1 and n.2 green LEDs ON indicate the activation of the OUT1 and OUT2 outputs.

FAST LED
The n.3 green LED ON indicates the activation of the FAST reading mode (500 Hz).

SET PUSHBUTTON
A pressure on the pushbutton activates the self-setting procedure.
A long pressure on the pushbutton allows the user to access into the mode (FAST or NORM) and delay setting menu.

+/- PUSHBUTTONS
A light pressure on these pushbuttons allows the user to run through the menu of the sensor parameters and setting menu.
Moreover, a long pressure allows to change the switching threshold value, as indicated in the "SWITCHING THRESHOLD ADJUSTMENT" paragraph.

INSTALLATION

The sensor can be positioned by means of the three housing's holes using screws (M5x40 or longer) with nuts and washers.
Various orientable fixing brackets to ease the sensor positioning are available (please refer to the accessories listed in the catalogue).
The operating distance is measured from the front surface of the sensor optics.
The M12 connector can be oriented at two different positions (refer to figure).

CONNECTIONS

M12 CONNECTOR

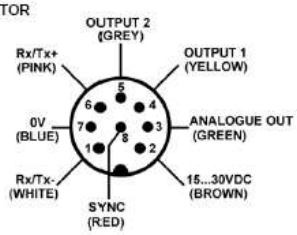

NOTE: the wire colours are referred to the cables manufactured according to the European standard.

TECHNICAL DATA

Power supply:	15 ... 30 Vdc limit values
Ripple:	2 Vpp max.
Consumption (output current excluded):	170 mA max (110 mA @ 24 V)
Outputs:	2 PNP or NPN outputs 30 Vdc max. (short-circuit protection) analogue output with 4-20 mA
Serial interface:	RS485, 9600Bd, 8N1
SYNC input:	PNP
Measurement range:	300 ... 4000 mm (from 90% white to 18% grey) 400 ... 2600 mm (6% black)
Linearity:	0.3% (24Vdc, 25°C, with 90% white target)
Digital resolution:	0.9 mm
Hysteresis:	5 mm (NORM) ; 10 mm (FAST)
Temperature drift:	< 0.6 mm/°C
Output current:	100 mA max.
Output saturation voltage:	≤ 2 V
Response time:	5 ms (NORM) ; 1 ms (FAST)
Switching frequency:	100 HZ (NORM) ; 500 Hz (FAST)
Indicators:	*command panel:* 4-digit display (GREEN), OUTPUT LED (YELLOW) 2 OUT1, OUT2 LEDs (GREEN) FAST LED (GREEN). *indicators LED:* OUTPUT LED (YELLOW) / ALARM LED (RED)
Setting:	SET, +, - pushbuttons
Data retention:	non volatile EEPROM memory
Operating temperature:	-10 ... 50 °C
Storage temperature:	-20 ... 70 °C
Electrical shock protection:	Class 2
Typical spot dimension:	Ø 12 mm at 2 m Ø 20 mm at 4 m
Emission type:	Red laser (665 nm) Class 2 (λ 665 nm) EN 60825-1 (1994)
Ambient light rejection:	According to EN 60947-5-2
Vibrations:	0.5 mm amplitude, 10 ... 55 Hz frequency, for every axis (EN60068-2-6)
Shock resistance:	11 ms (30 G) 6 shock for every axis (EN60068-2-27)
Housing material:	aluminium
Lens material:	Window and lenses in glass
Mechanical protection:	IP67
Connections:	M12-8 pole connector
Weight:	330 g. max.

DIMENSIONS

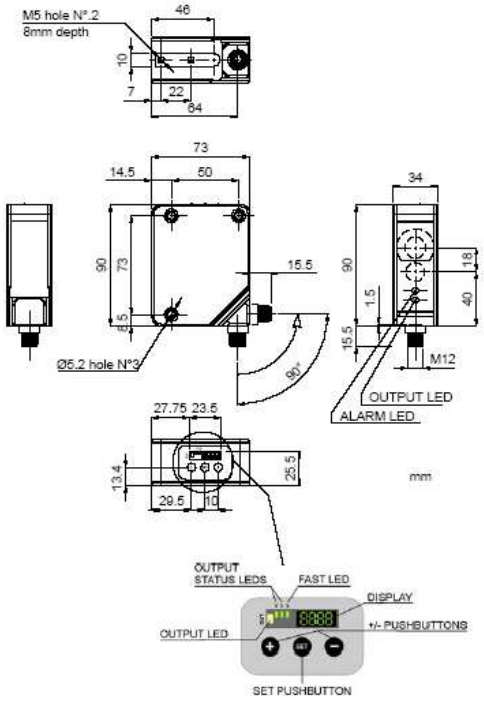

COMMAND PANEL AND DISPLAY

Appendix C: Blank example of a Road Definition File

```
$-----------------------------------------------------------------MDI_HEADER
[MDI_HEADER]
FILE_TYPE  =  'rdf'
FILE_VERSION  =  5.00
FILE_FORMAT  =  'ASCII'
$-------------------------------------------------------------------------units
[UNITS]
 LENGTH            = 'mm'
 FORCE             = 'newton'
 ANGLE             = 'radians'
 MASS              = 'kg'
 TIME              = 'sec'
$-----------------------------------------------------------------definition
[MODEL]
 METHOD            = '3D'
$-------------------------------------------------------------------------nodes
[NODES]
 NUMBER_OF_NODES    =
{ node   x_value   y_value   z_value }


$-----------------------------------------------------------------offset
[ELEMENTS]
 NUMBER_OF_ELEMENTS    =
{ node_1   node_2  node_3   mu }
```

Appendix D: International Roughness Index plots of profiled terrains

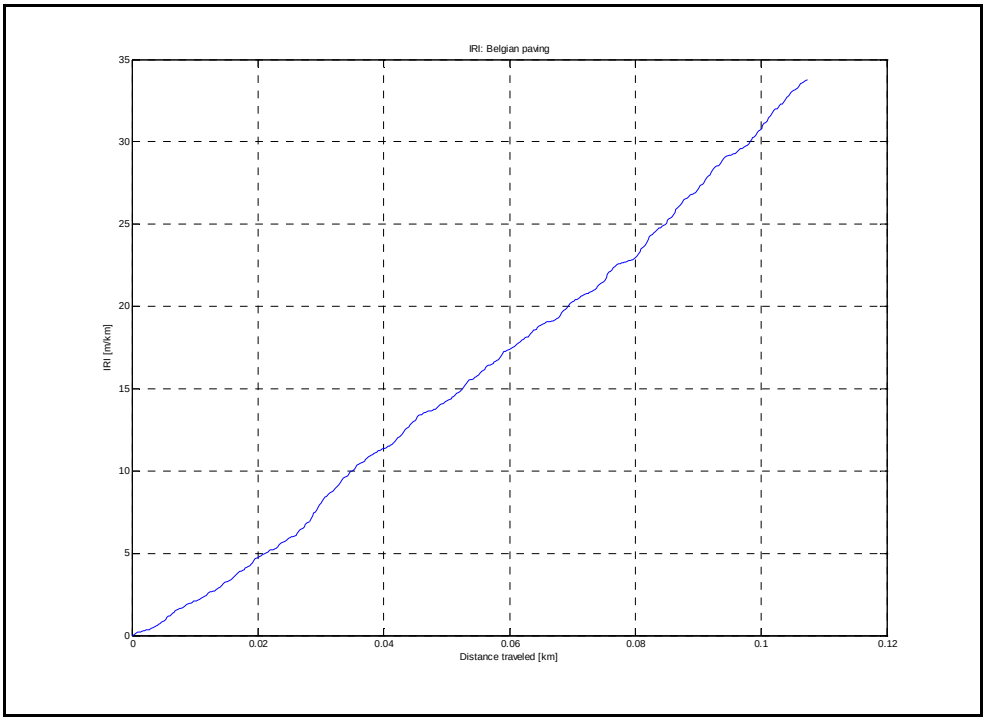

Figure 120: IRI Belgian paving.

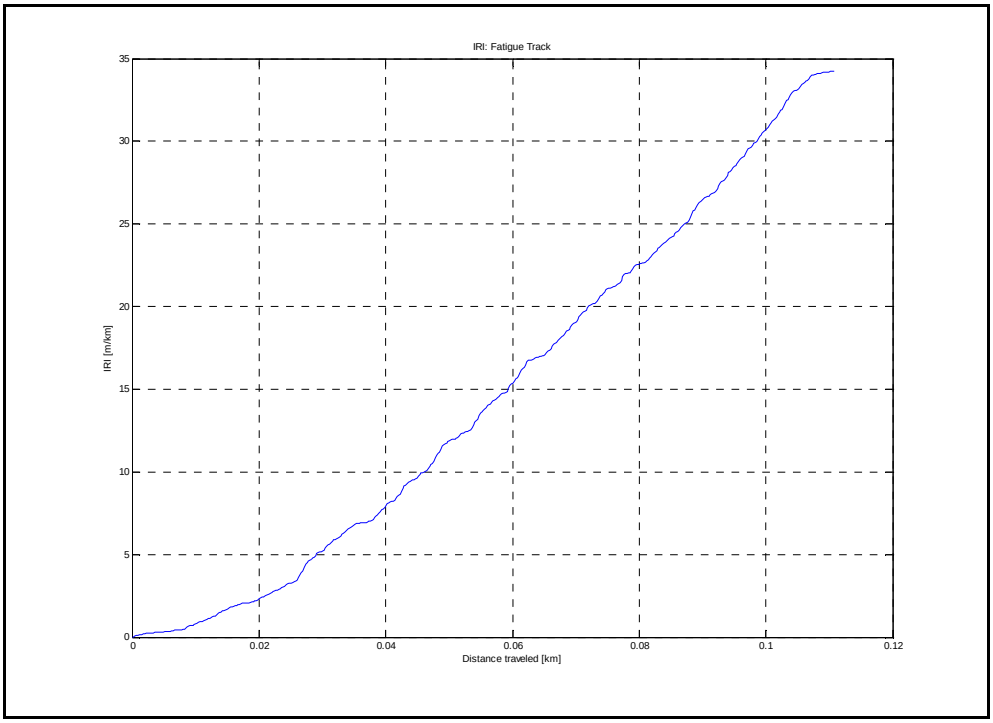

Figure 121: IRI Fatigue Track.

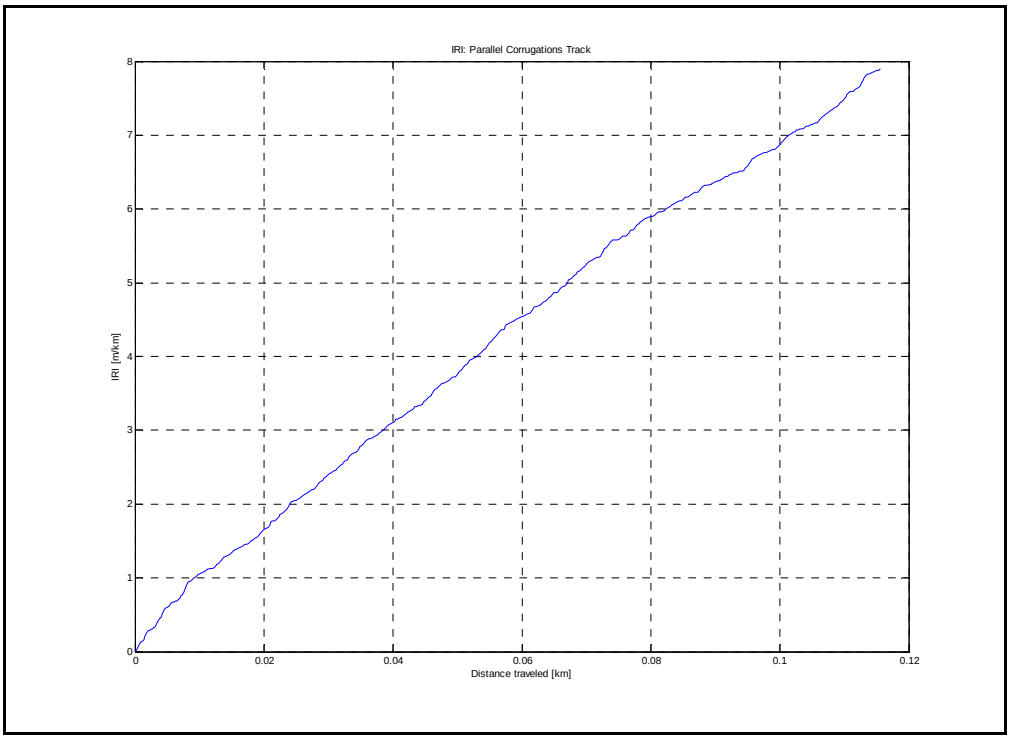

Figure 122: IRI Parallel Corrugations Track.

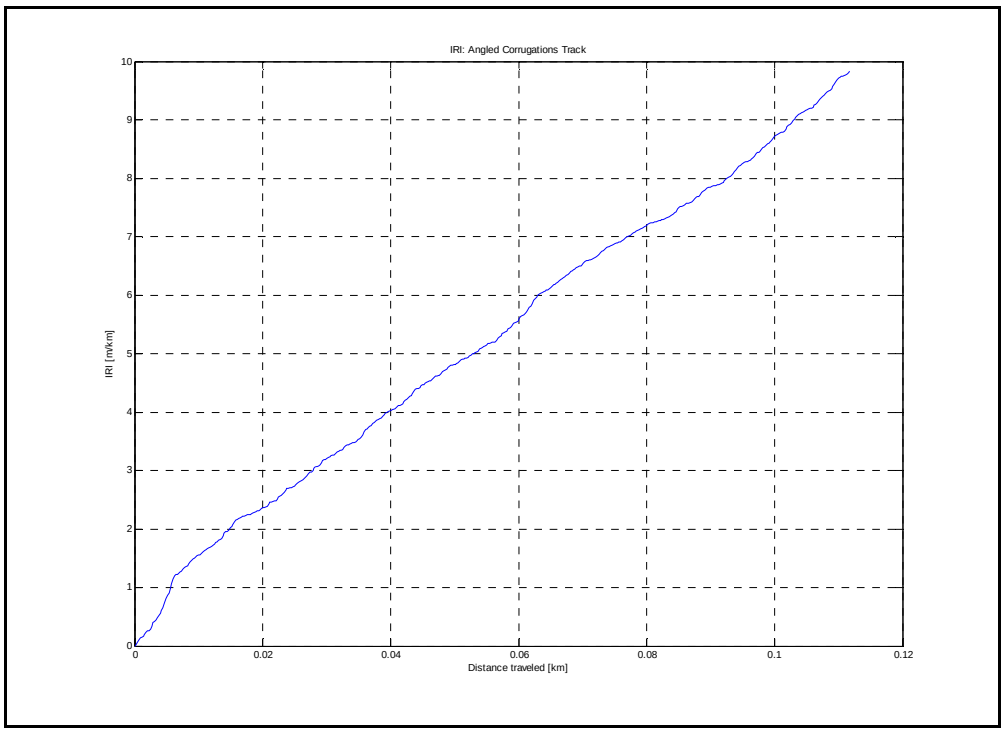

Figure 123: IRI Angled Corrugations Track.

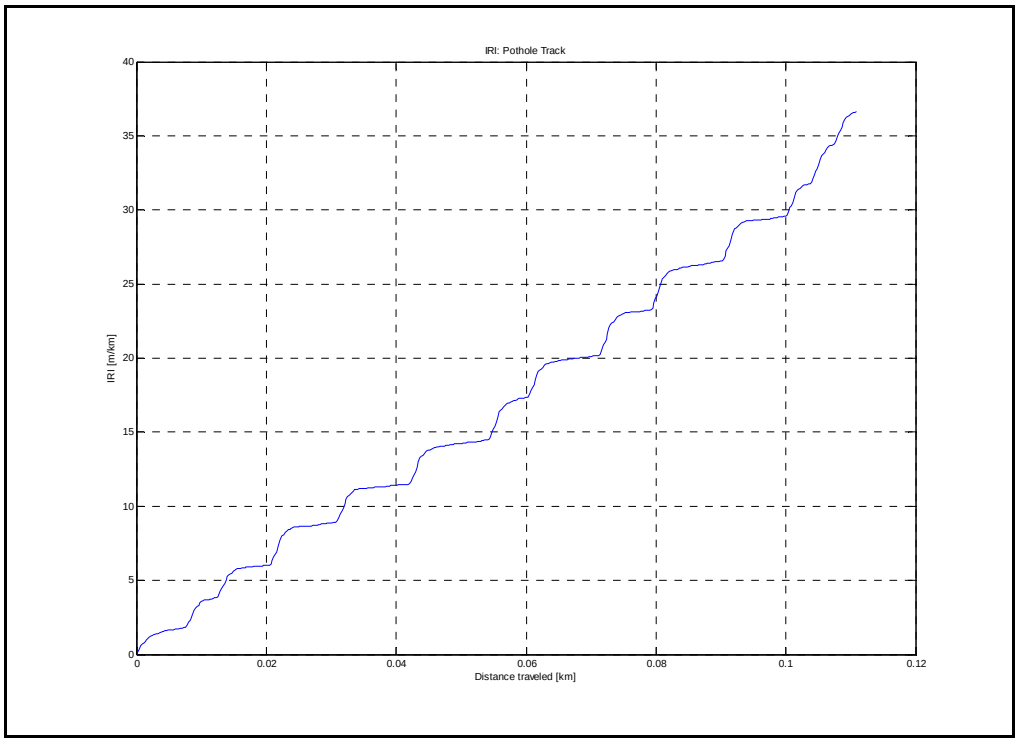

Figure 124: IRI Pothole Track.

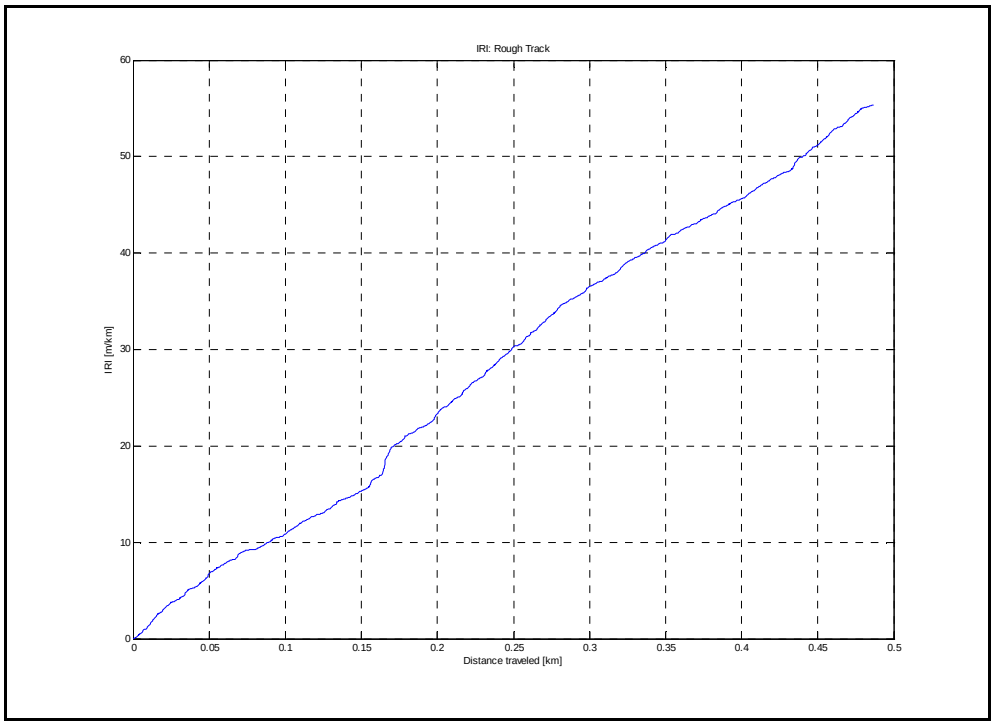

Figure 125: IRI Rough Track.

Appendix E: Weighted FFT from the Simulation and Land Rover data

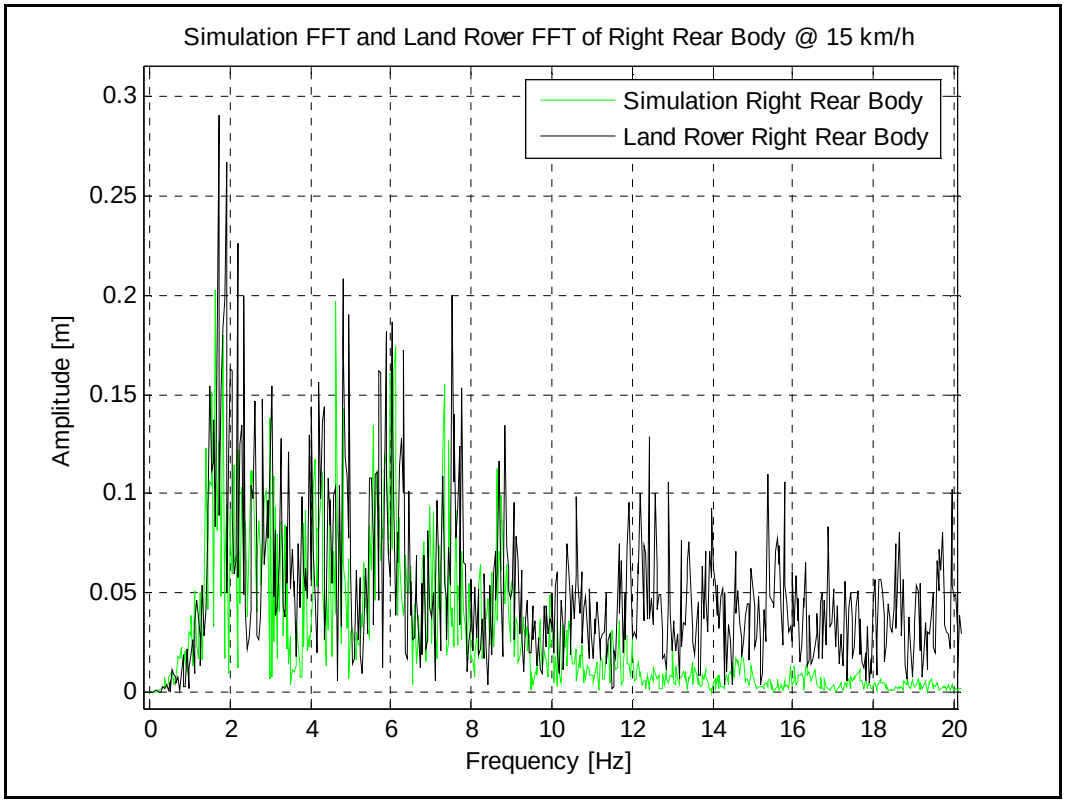

Figure 126: Weighted FFT from the Simulation and Land Rover data @ 15km/h.

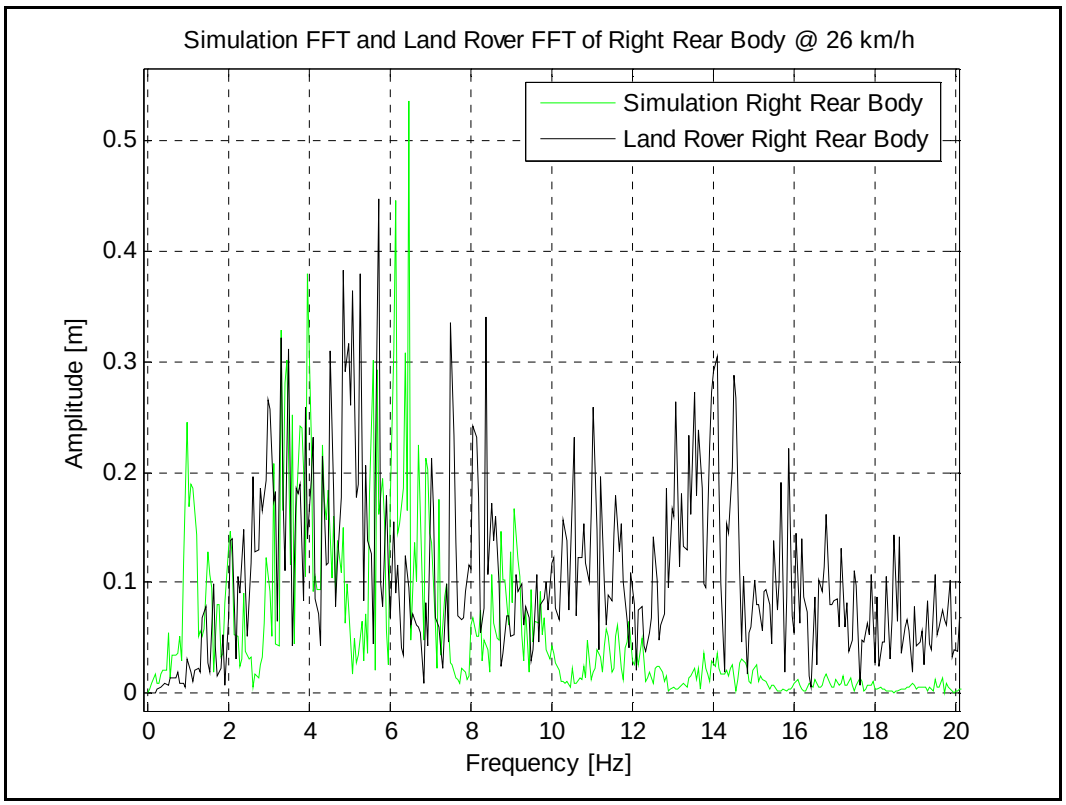

Figure 127: Weighted FFT from the Simulation and Land Rover data @ 26km/h.

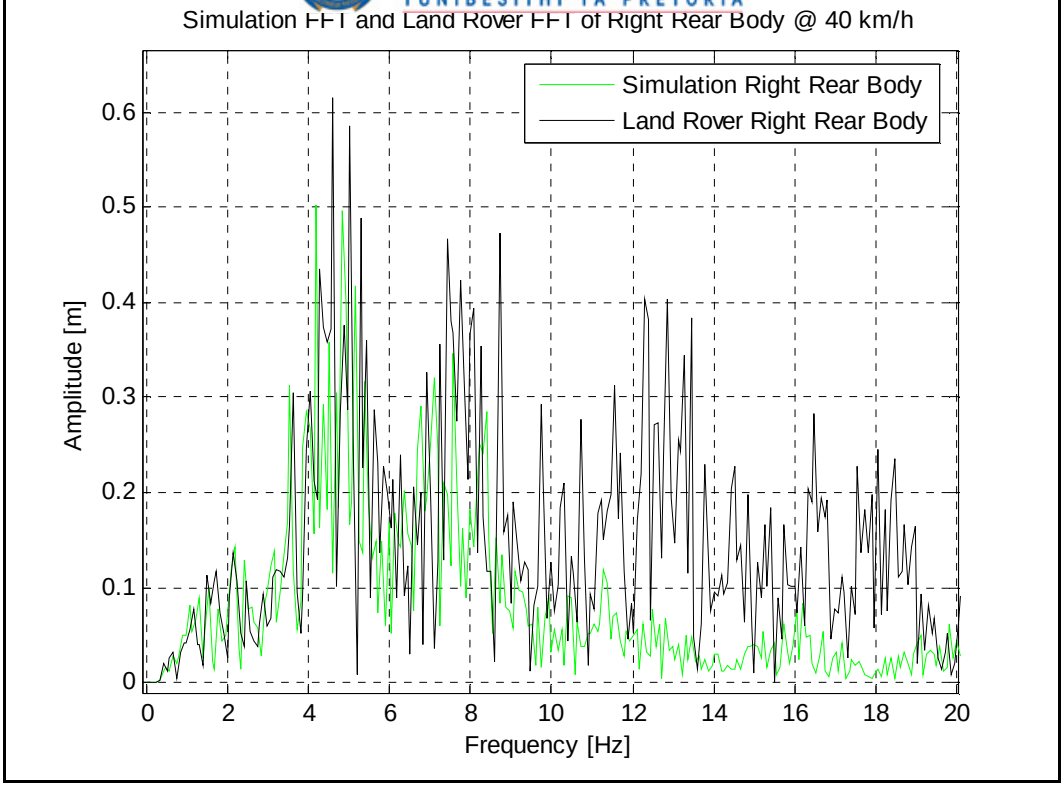

Figure 128: Weighted FFT from the Simulation and Land Rover data @ 40km/h.

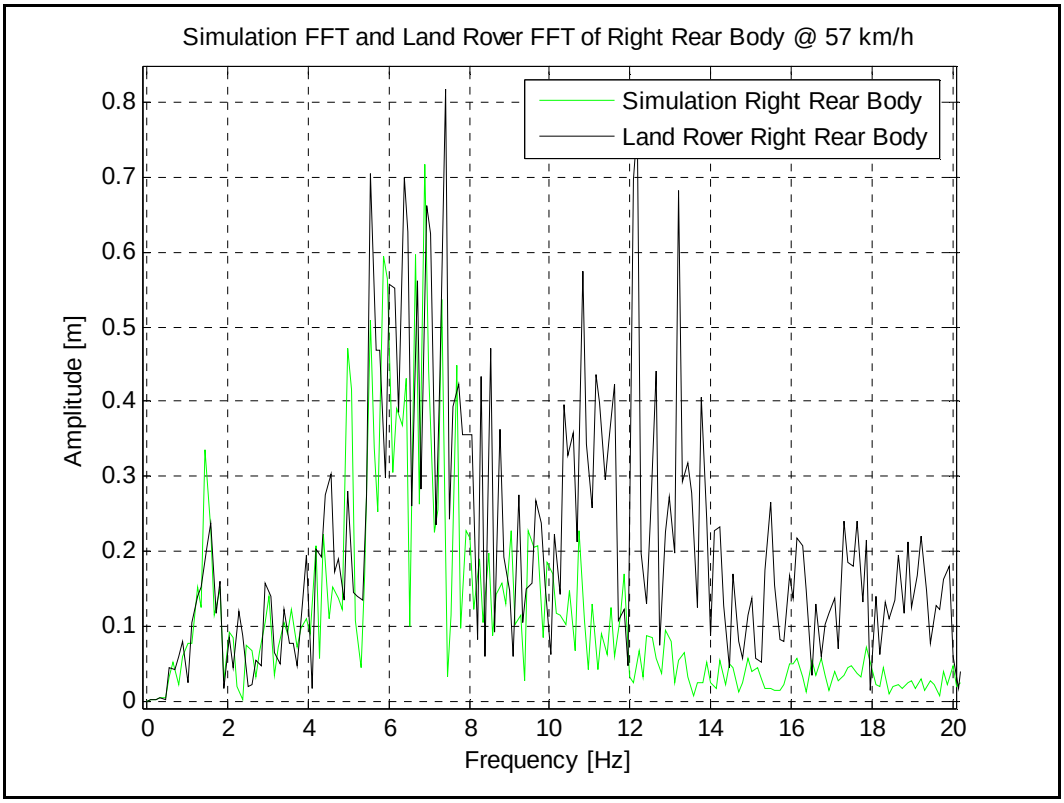

Figure 129: Weighted FFT from the Simulation and Land Rover data @ 57km/h.

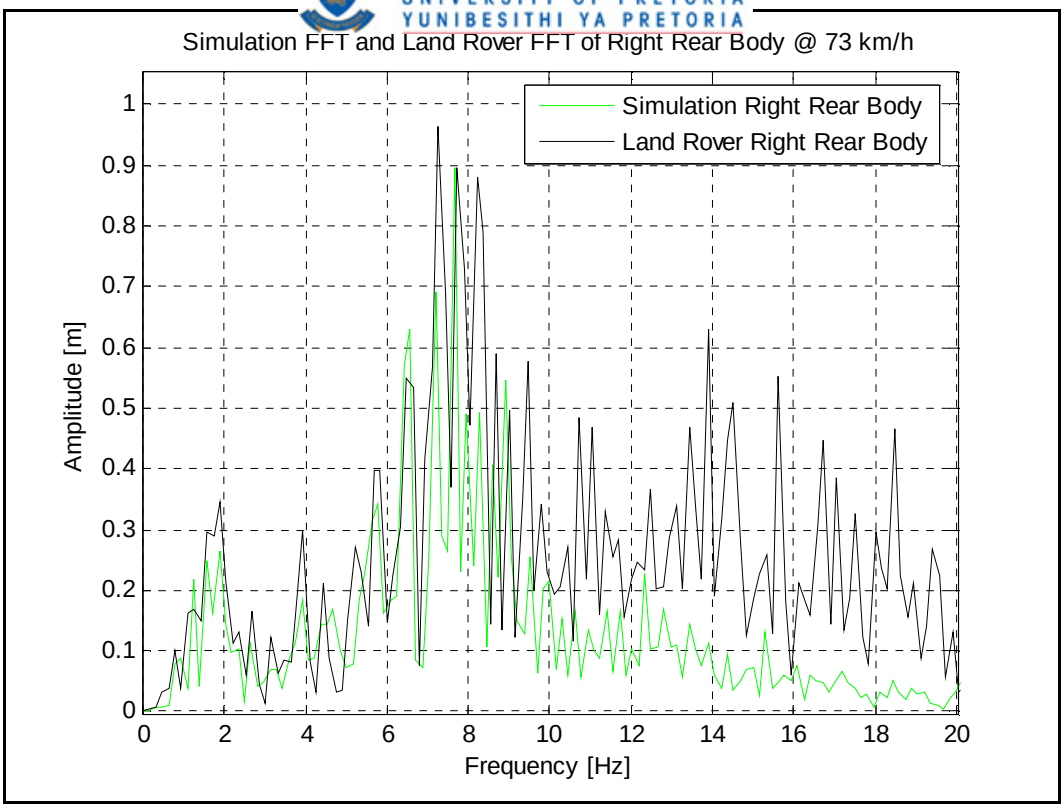

Figure 130: Weighted FFT from the Simulation and Land Rover data @ 73km/h.

Appendix F: Filtered vertical accelerations from simulations and Land Rover data

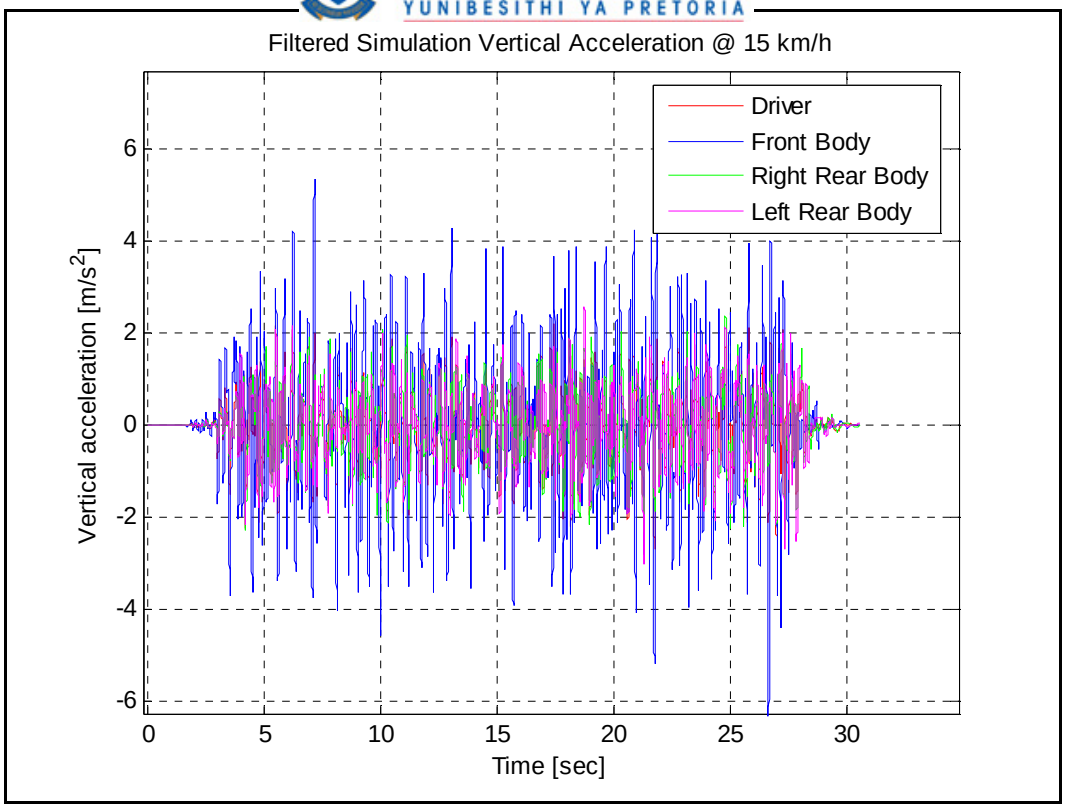

Figure 131: Simulation vertical accelerations @ 15km/h.

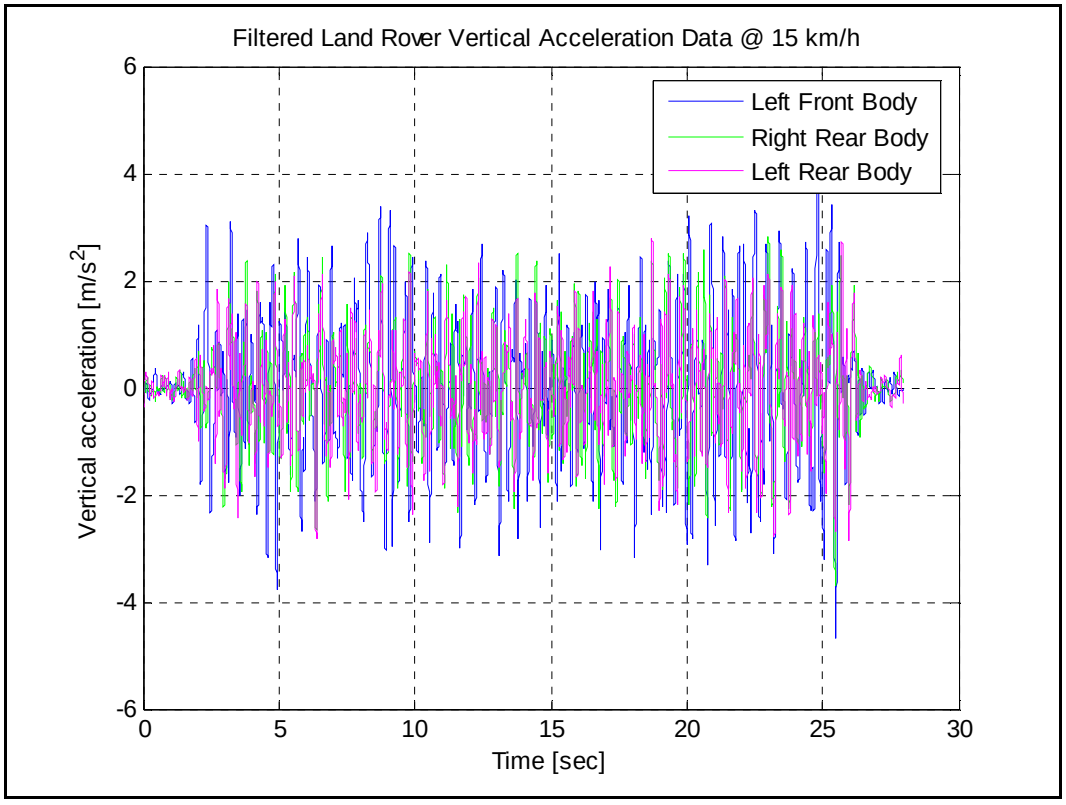

Figure 132: Land Rover vertical accelerations @ 15km/h.

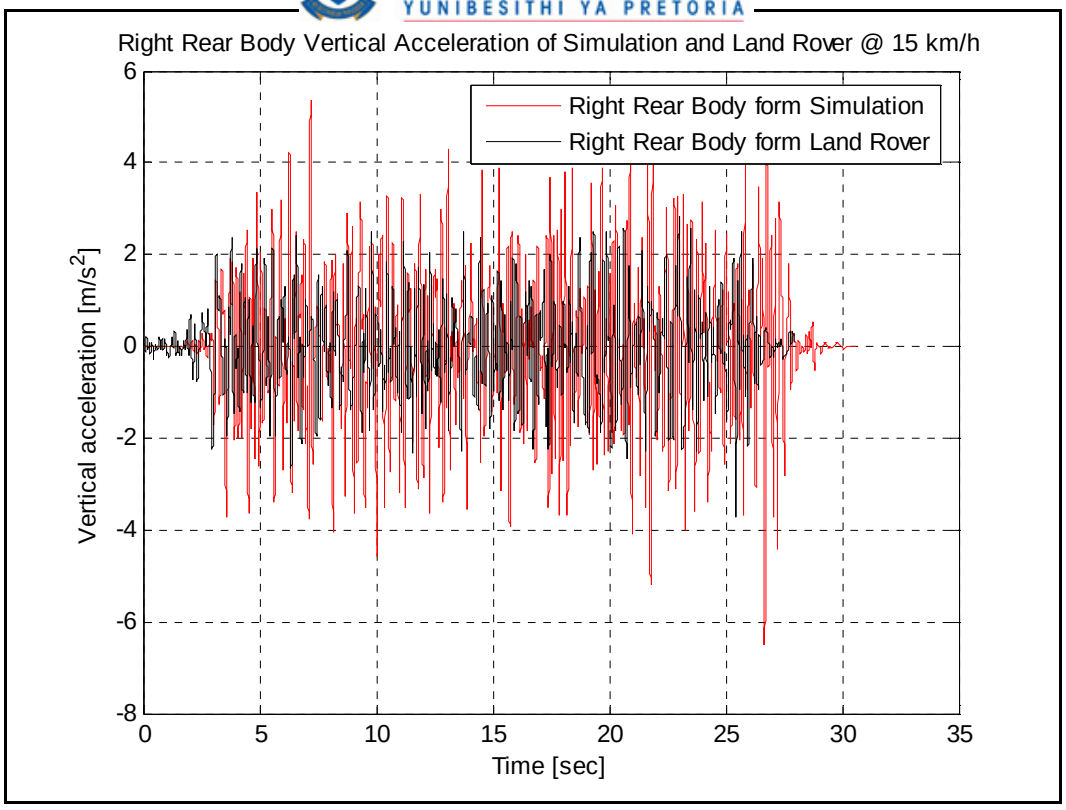

Figure 133: Right Rear Body vertical accelerations from Simulation and Land Rover @ 15km/h.

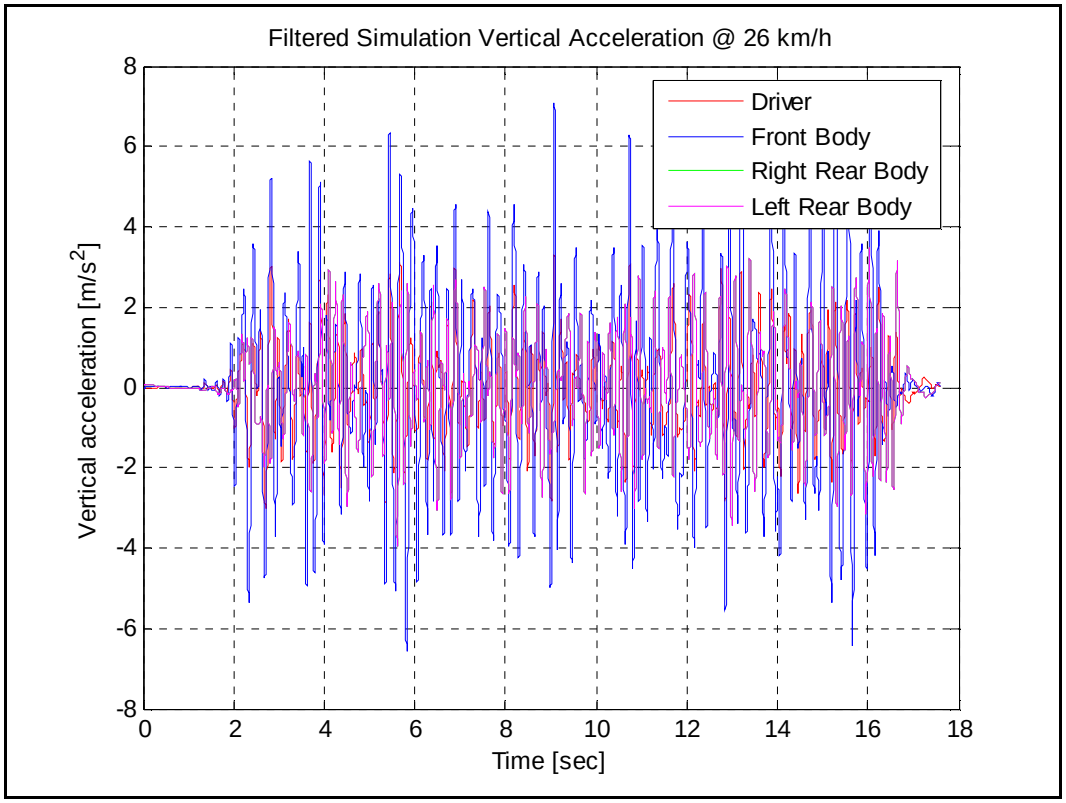

Figure 134: Simulation vertical accelerations @ 26km/h.

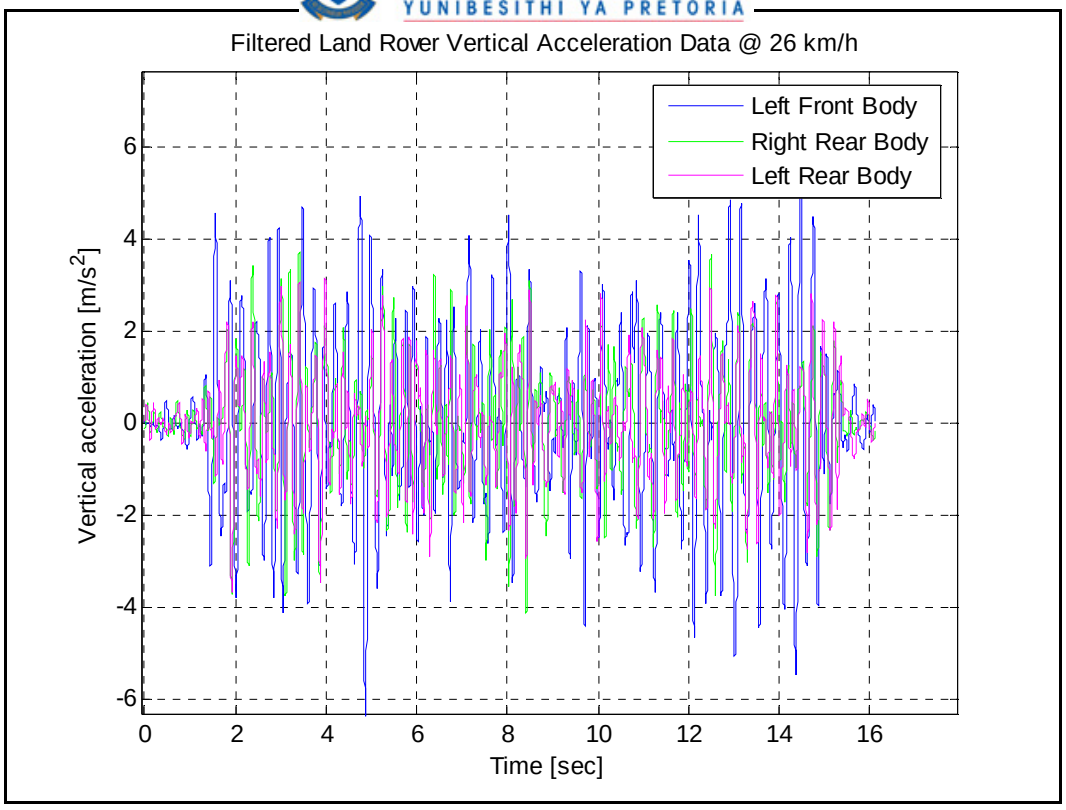

Figure 135: Land Rover vertical accelerations @ 26km/h.

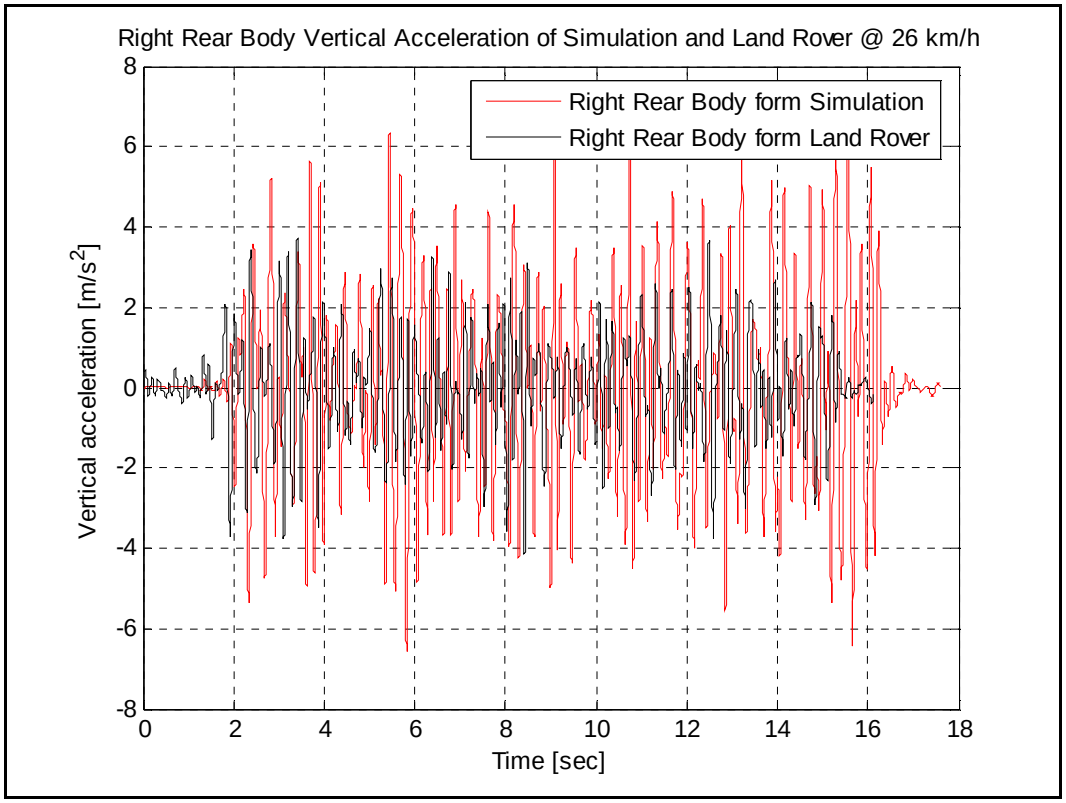

Figure 136: Right Rear Body vertical accelerations from simulation and Land Rover @ 26km/h.

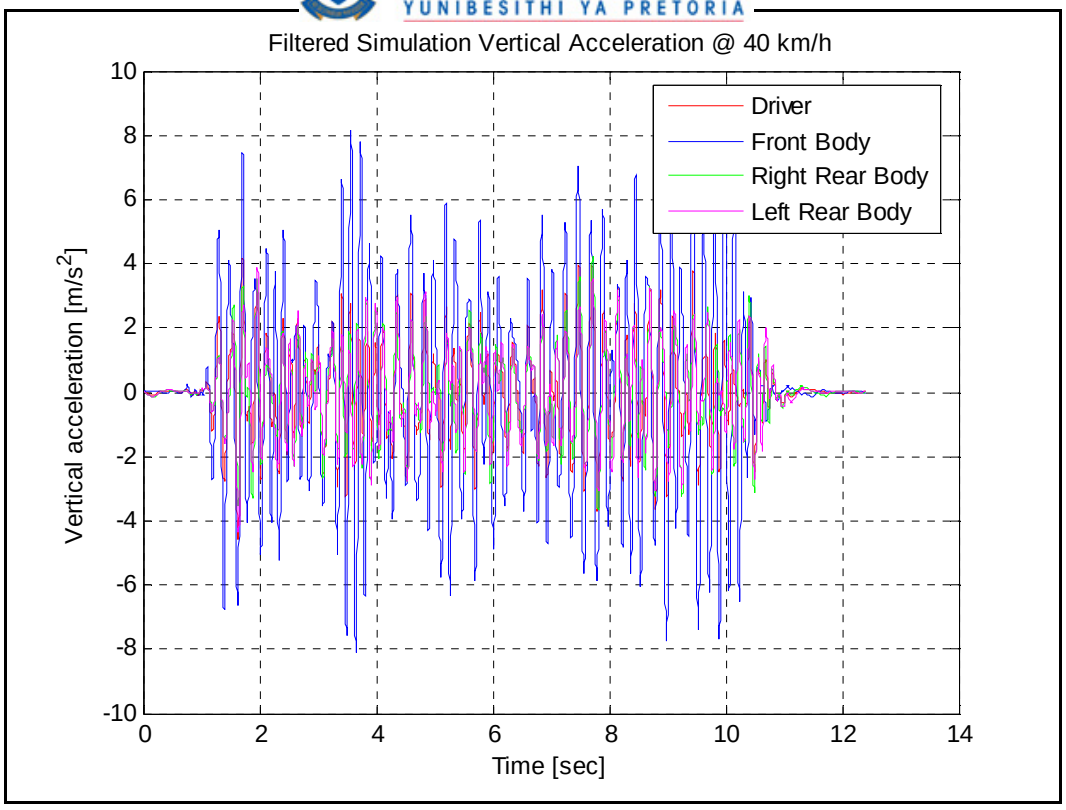

Figure 137: Simulation vertical accelerations @ 40km/h.

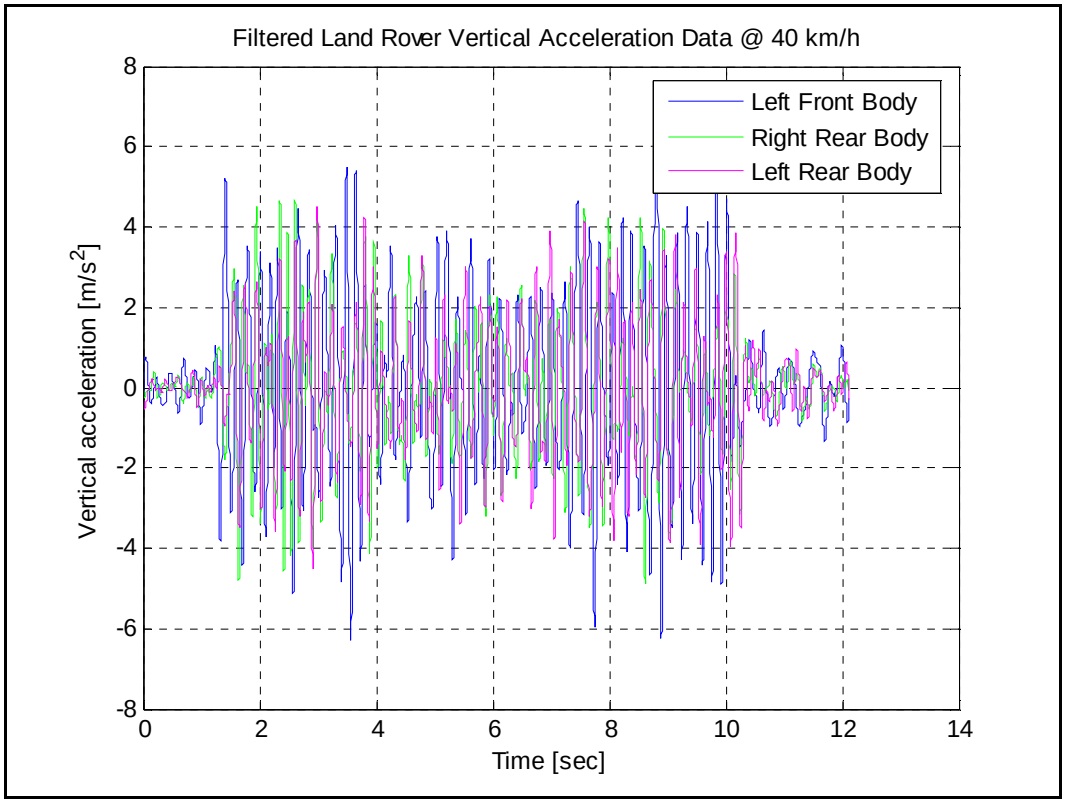

Figure 138: Land Rover vertical accelerations @ 40km/h.

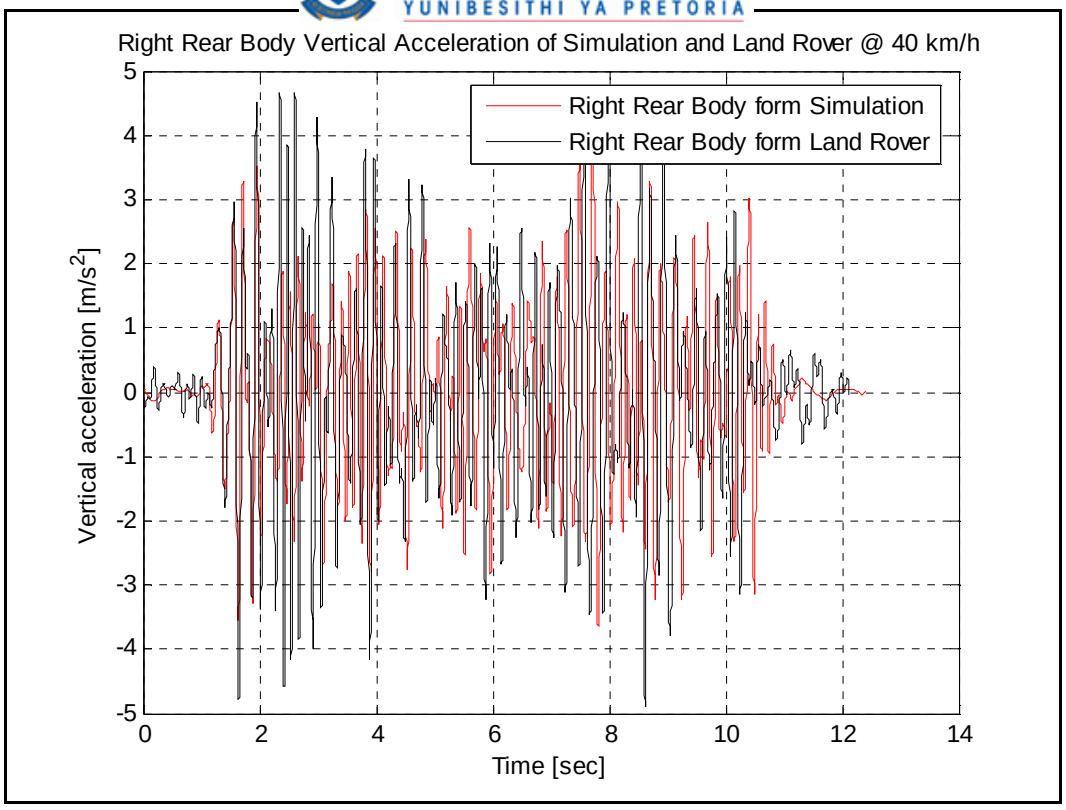

Figure 139: Right Rear Body vertical accelerations from simulation and Land Rover @ 40km/h.

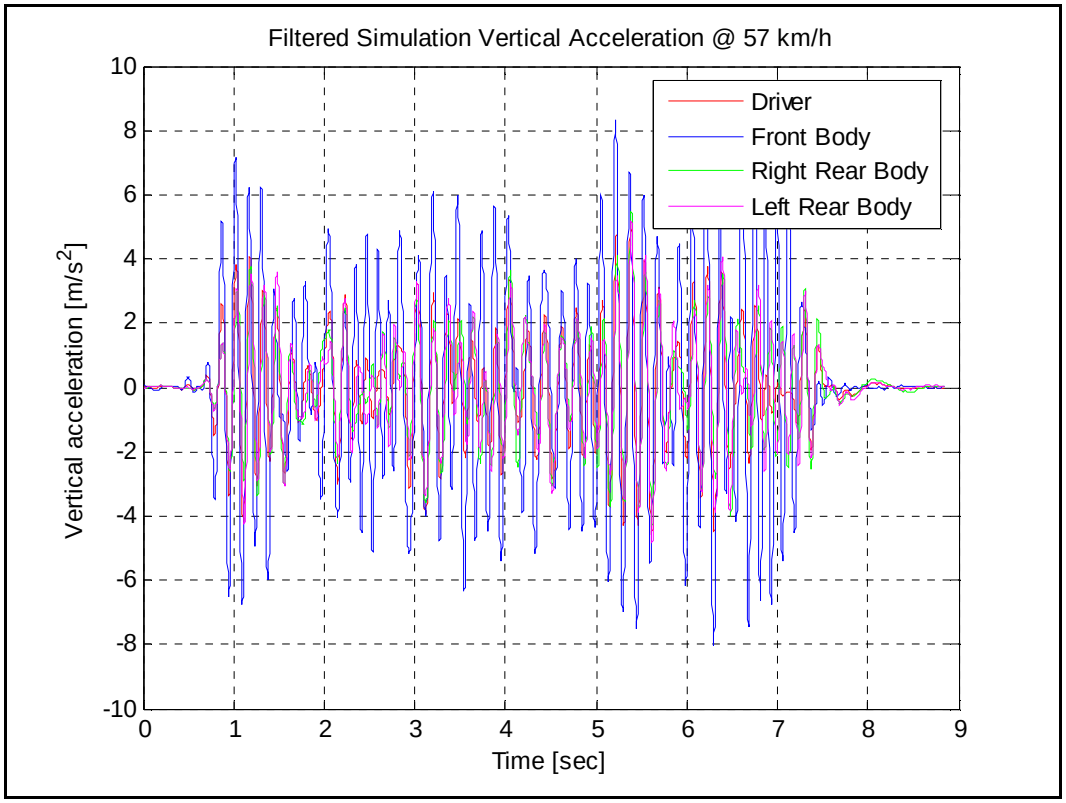

Figure 140: Simulation vertical accelerations @ 57km/h.

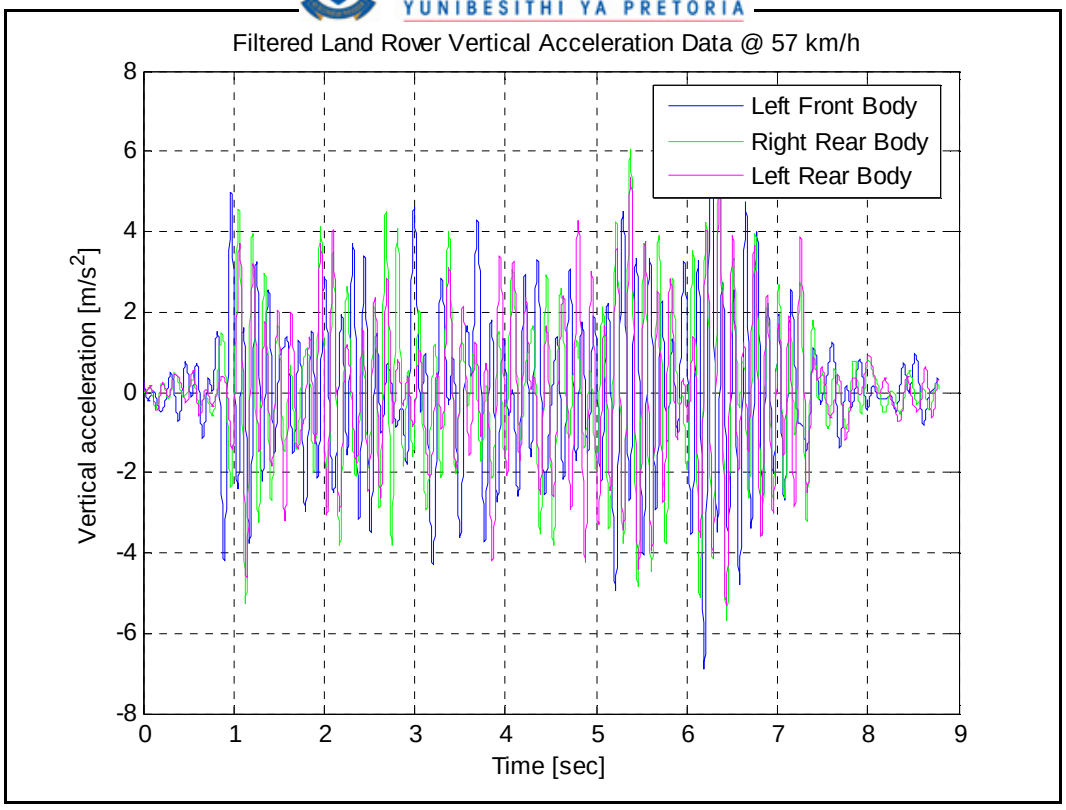

Figure 141: Land Rover vertical accelerations @ 57km/h.

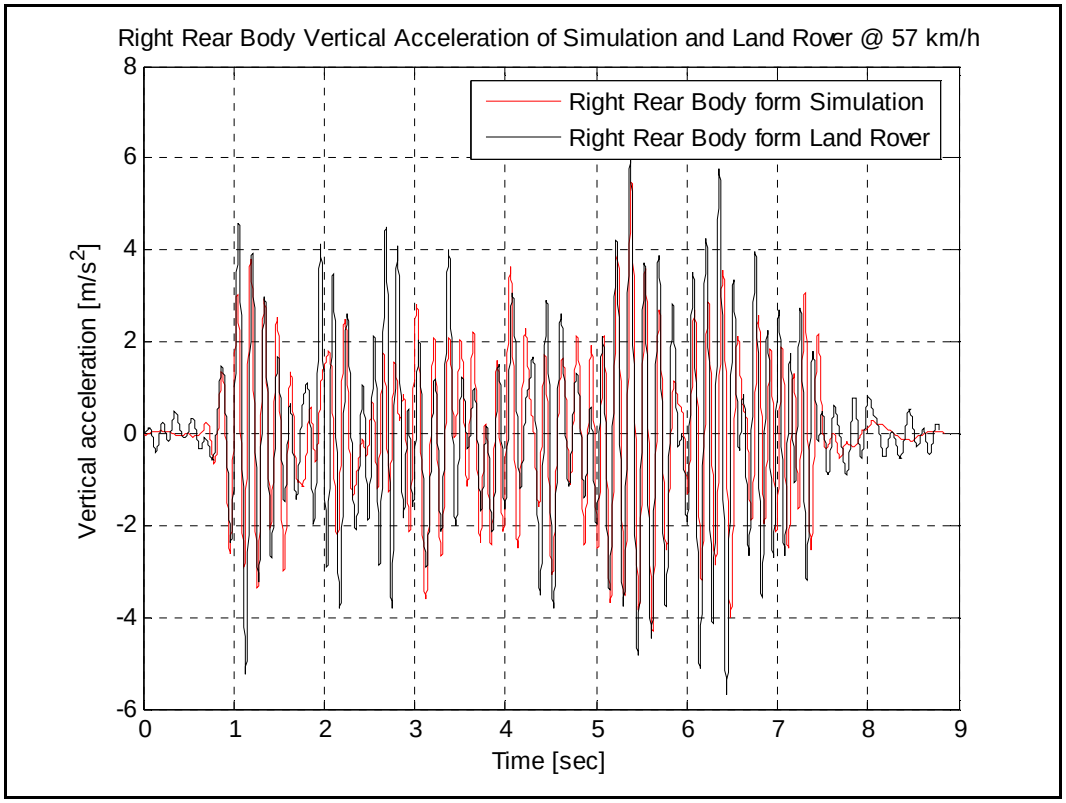

Figure 142: Right Rear Body vertical accelerations from simulation and Land Rover @ 57km/h.

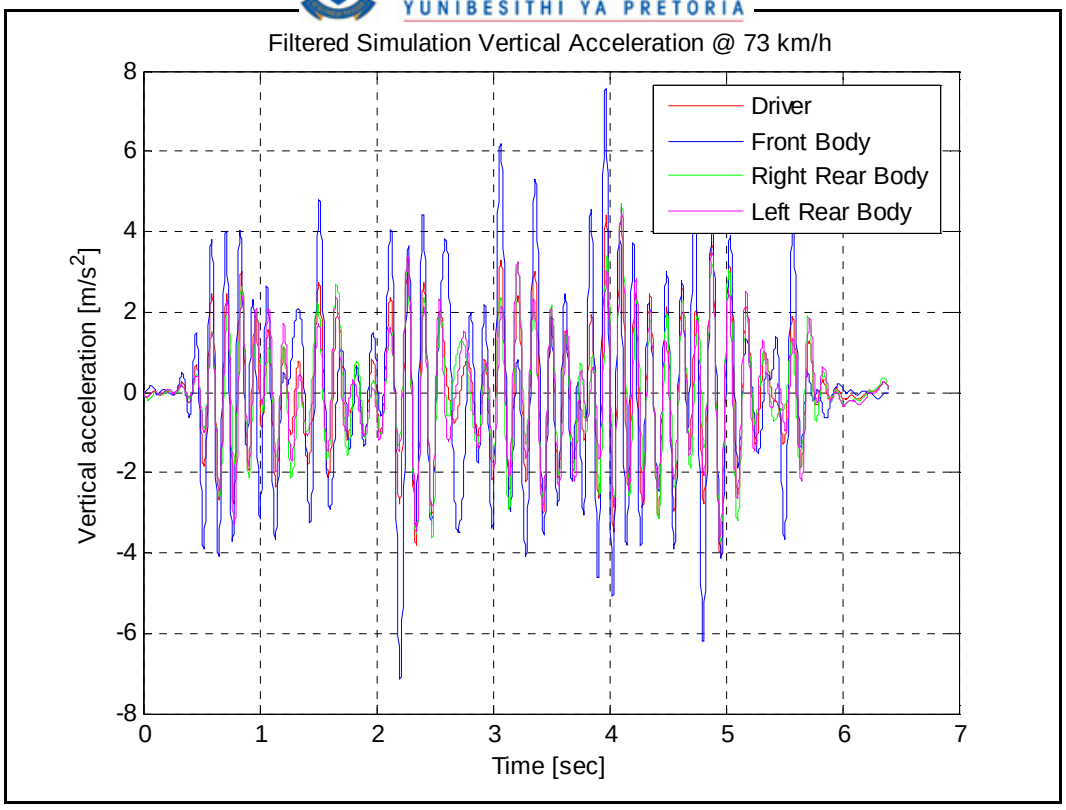

Figure 143: Simulation vertical accelerations @ 73km/h.

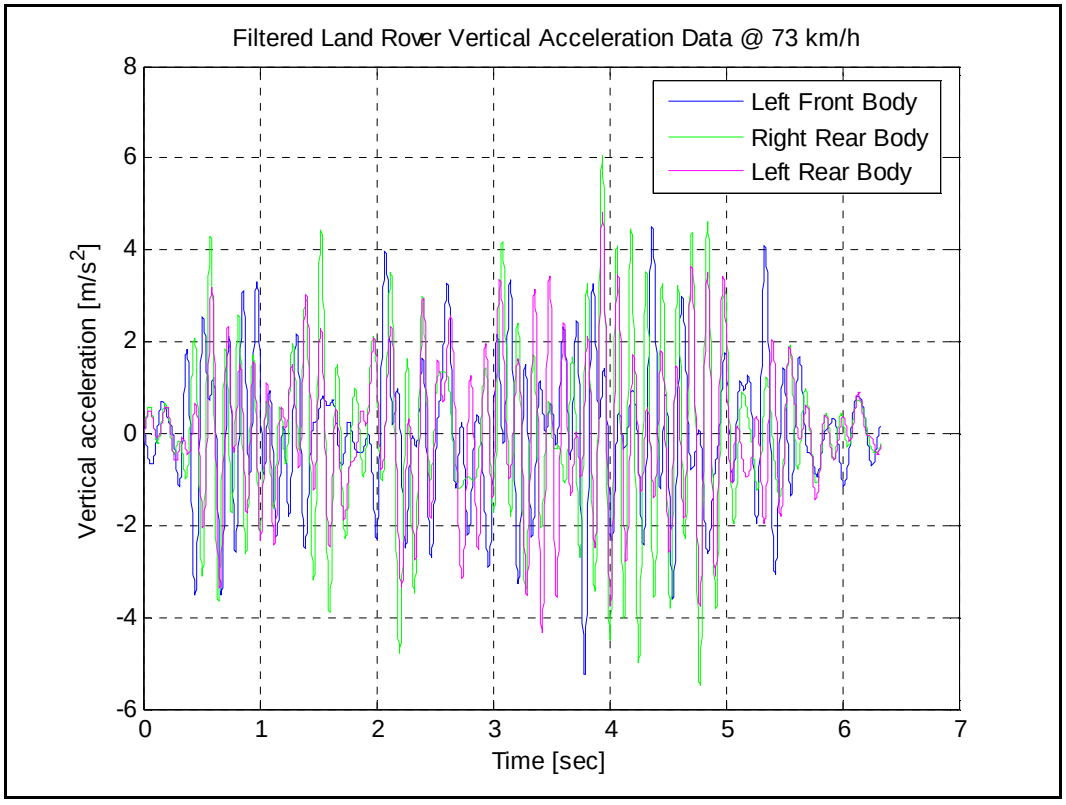

Figure 144: Land Rover vertical accelerations @ 73km/h.

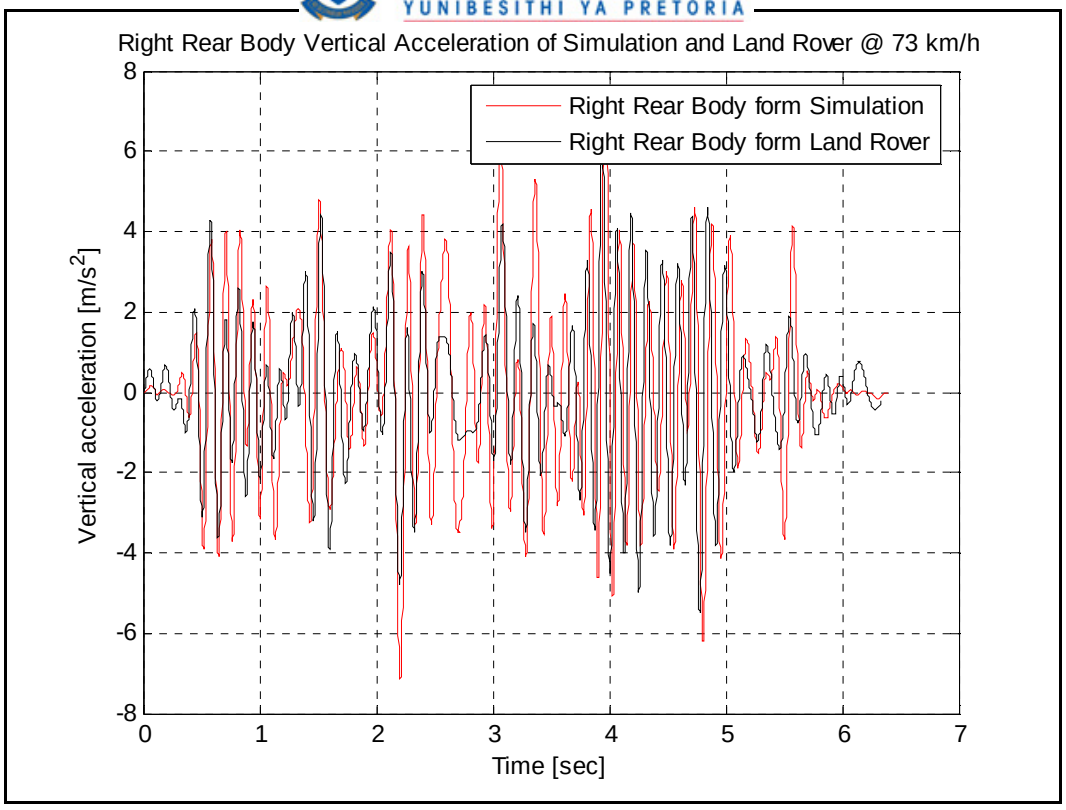

Figure 145: Right Rear Body vertical accelerations from simulation and Land Rover @ 73km.

Appendix G: 8 Hz Low Pass Filtered Fast Fourier Transforms of Simulations and Land Rover Vertical Accelerations

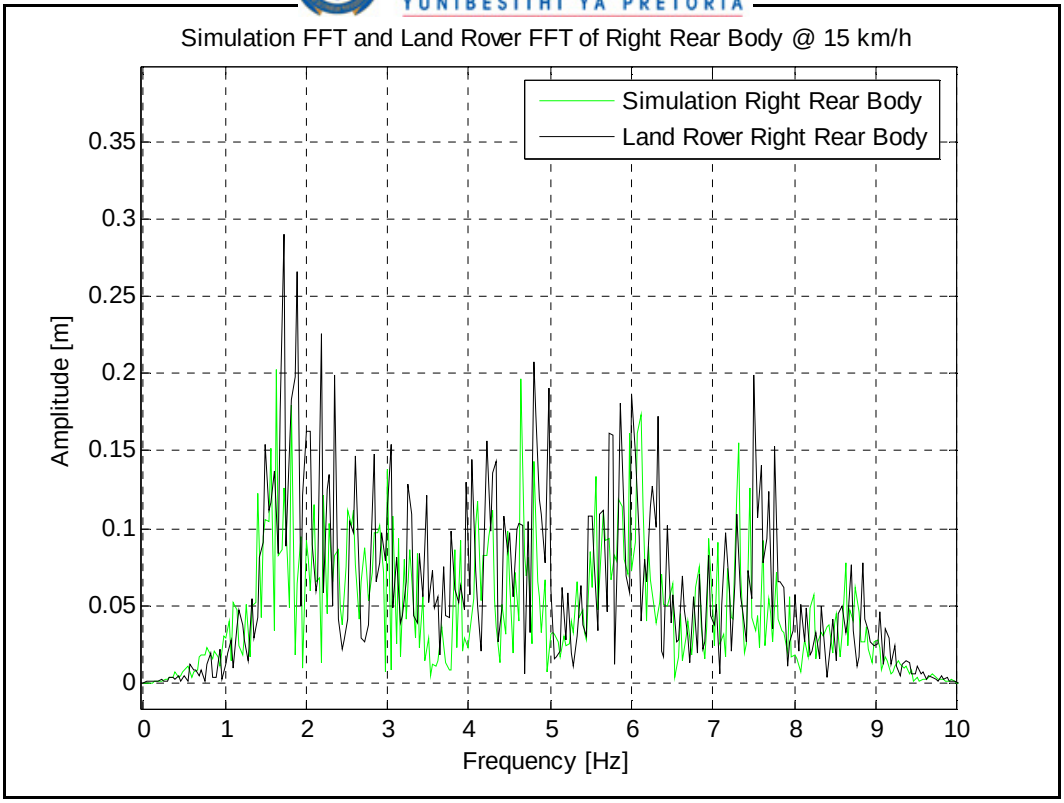

Figure 146: Filtered FFT of vertical accelerations @ 15km/h

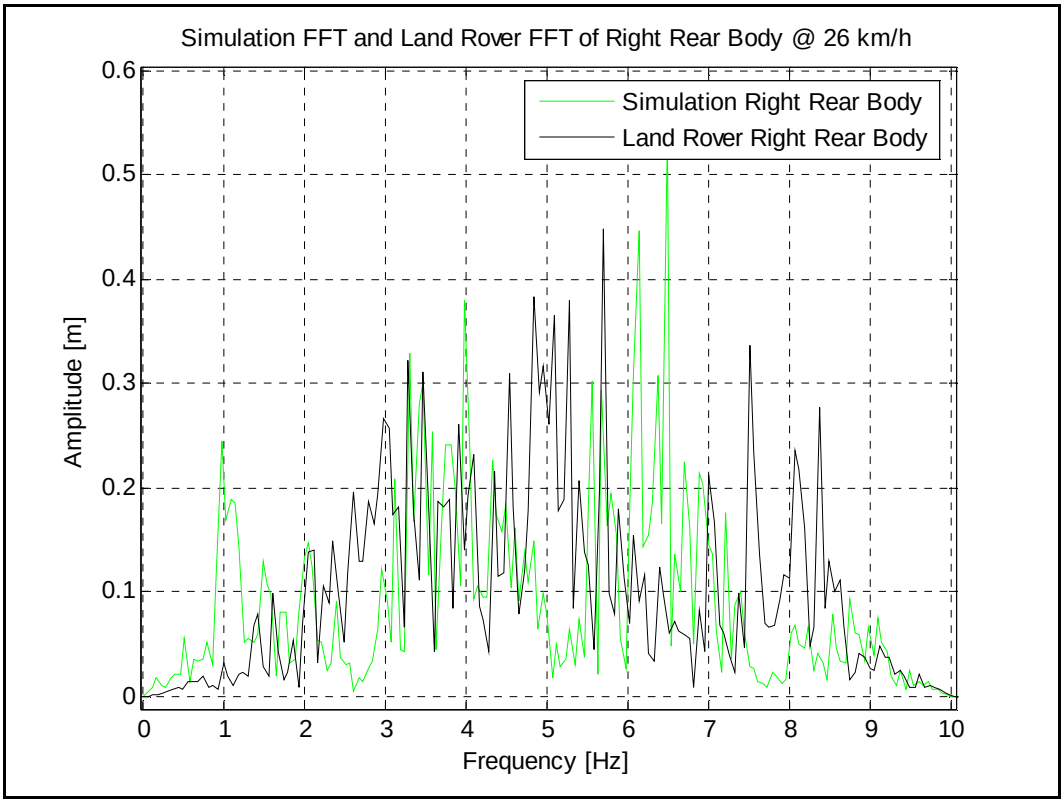

Figure 147: Filtered FFT of vertical accelerations @ 26km/h.

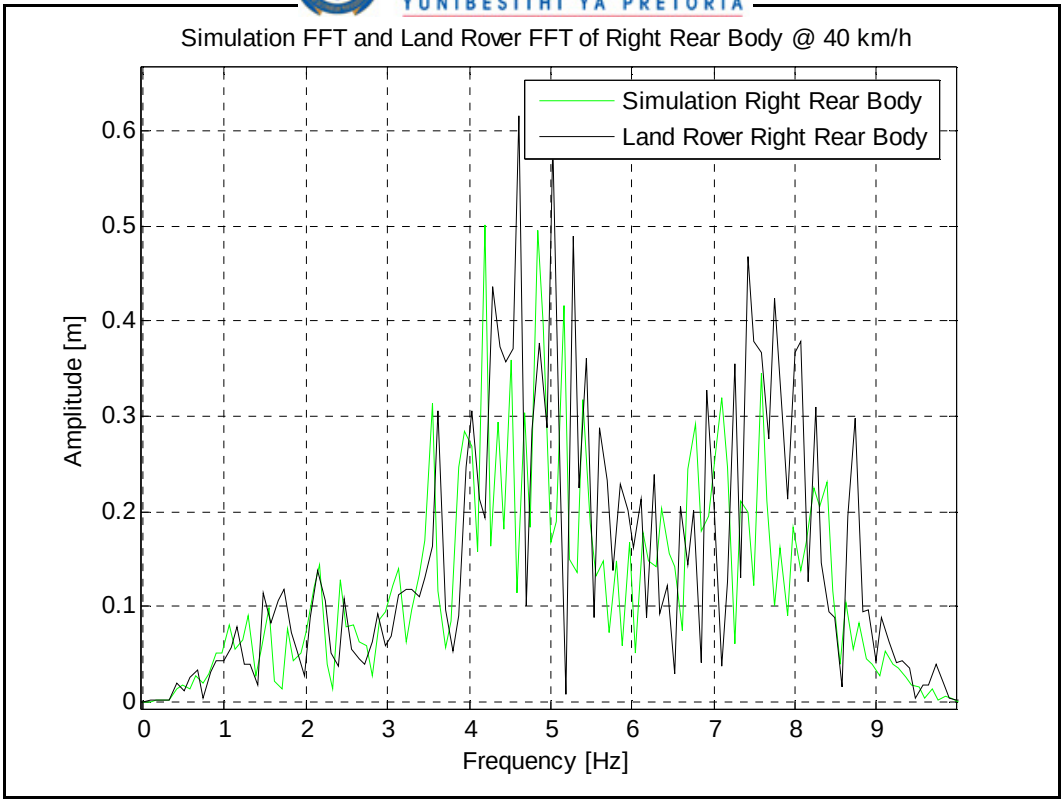

Figure 148: Filtered FFT of vertical accelerations @ 40km/h.

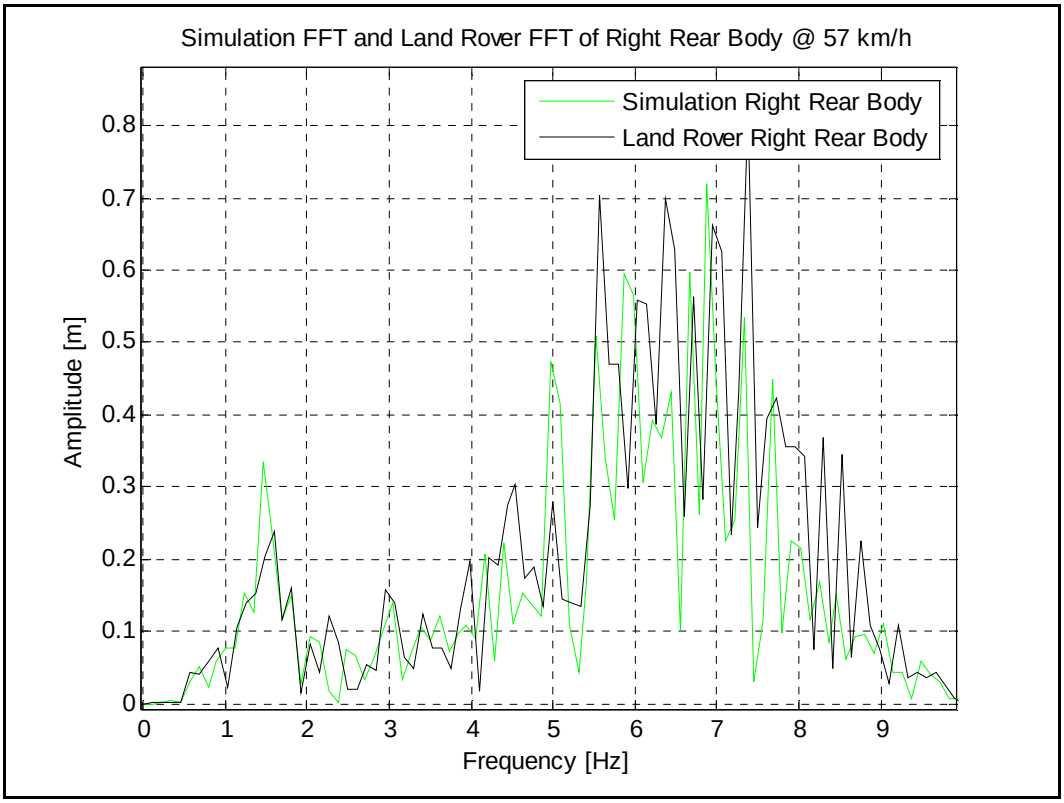

Figure 149: Filtered FFT of vertical accelerations @ 56km/h.

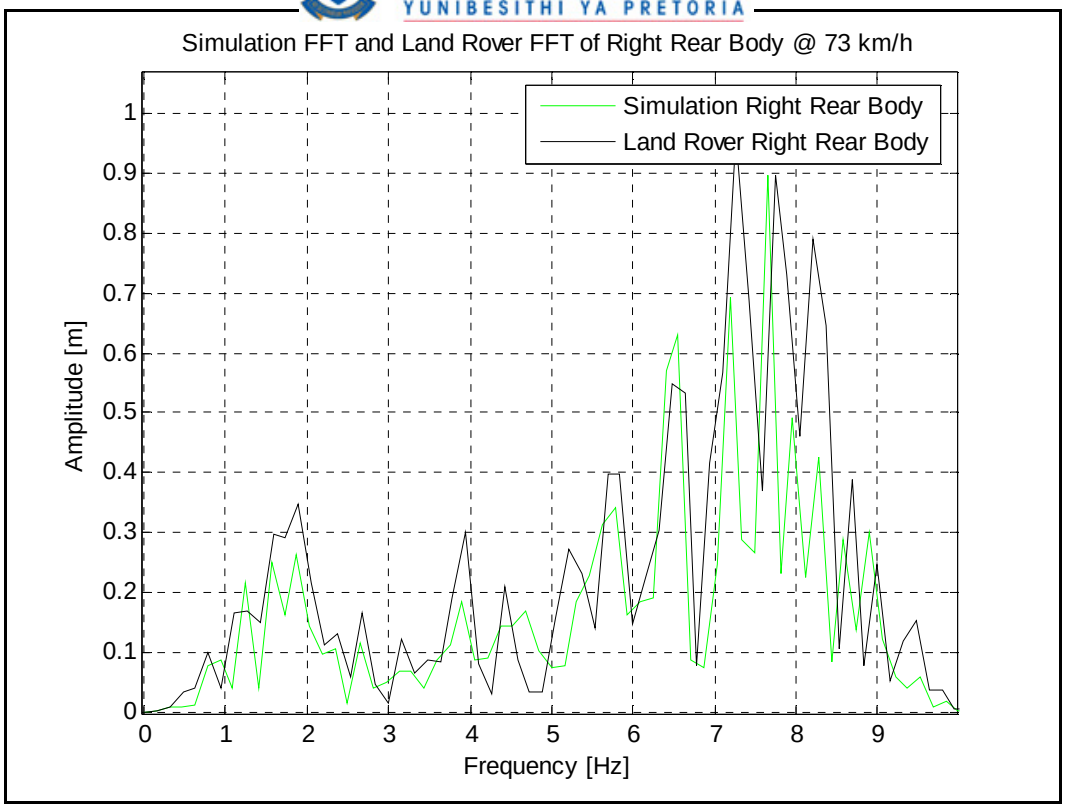

Figure 150: Filtered FFT of vertical accelerations @ 73km/h.